

Tampereen teknillinen korkeakoulu  
Julkaisuja 304



Tampere University of Technology  
Publications 304

Tarja Shakespeare

**Colorant Modelling for On-Line Paper Coloring:  
Evaluations of Models and an Extension to Kubelka-  
Munk Model**

Tampere 2000

**Tampereen teknillinen korkeakoulu  
Julkaisuja 304**

**Tampere University of Technology  
Publications 304**



**Tarja Shakespeare**

## **Colorant Modelling for On-Line Paper Coloring: Evaluations of Models and an Extension to Kubelka- Munk Model**

Dissertation for the degree of Doctor of Philosophy to be presented with due permission for public examination and criticism in Auditorium RG202 at Tampere University of Technology, on the 27th of October 2000 at 12 o'clock noon.

**Tampere 2000**

---

**Colorant Modelling for On-Line Paper Coloring: Evaluations of Models and an Extension to Kubelka-Munk Model.**

**Copyright © 2000 by Tarja Shakespeare**

**ISBN 952-15-0474-9**

**ISSN 0356-4940**

**ISBN 978-952-03-2662-3 (verkkojulkaisu)**

**TTKK-PAINO  
Tampere 2000**

# Abstract

Traditionally, single constant Kubelka-Munk type colorant formulation algorithms have been used for color control in the paper industry. Tuning data is derived from colored handsheets representing dyeing of a particular color grade, applicable to a substrate of similar properties. Due to furnish variation and changes in the chemical environment, such tuning data is of limited accuracy in practice. Kubelka-Munk approaches have numerous other limitations, in part due to their physically unrealistic assumptions. In particular, they neglect fluorescence phenomena, the interdependence of absorption and scattering, and nonlinearities due to colorant interactions. This thesis addresses those problems.

A set of colored handsheets was made, employing several anionic direct dyes and fluorescent colorants, individually and in various combinations. Both a spectrophotometer and a spectrofluorimeter were used for measuring color properties. An extended Langmuir adsorption isotherm was used in modelling the dye-on-fiber in each dyeing. Kubelka-Munk absorption and scattering coefficients were then modelled based on dye-on-fiber, and a number of the limitations of the Kubelka-Munk approach were clearly demonstrated.

An extended phenomenological model was derived, incorporating fluorescence and interdependence of absorption and scattering. This model predicts illuminator-independent radiance transfer factors based on dye-on-fiber, from which total radiance factor responses under arbitrary illumination can be computed. It requires spectrofluorometric measurements to characterize the coloring process.

A new reflectance factor model, based on the same adsorption isotherm approach, was derived for non-fluorescent colorants. A corresponding total radiance factor model, which is illuminator-dependent, was derived for fluorescent colorants. These models have provision for phenomena such as broadening of absorption and scattering bands, which are encountered in practice. Being based on spectrophotometric measurements, they are directly applicable in industrial settings, and predict colorant responses reliably under wider ranges of conditions than the Kubelka-Munk approach.



# Acknowledgements

This research was supported in part by Neles Automation and in part by the Finnish Academy's Paper Making Graduate School Program, which together made it possible for me to complete the research and to write the thesis. I am grateful for the favourable and supportive spirit of my colleagues and managers in Neles Automation.

I thank the Paper Technology Unit at Tampere Polytechnic and the Paper Converting Institute at Tampere University of Technology for allowing me to use their laboratory facilities, and Metsä-Serla's Kyröskoski and Tako board mills for supplying pulp. I thank Mitaten Finland Oy for lending me the Minolta Spectrophotometer CM-3700 for an extended period. I also thank BASF Finland, Ciba Specialty Chemicals and Clariant UK for their assistance and supply of colorants.

I also thank my brothers Markku and Seppo, for constructing the heat bath used throughout the experimental program and the sheet former and sheet dryer used during the later stages. I also thank my parents Heimo and Martta, for support from a distance, of other kinds.

Above all, I want to thank my husband, John, and my 4 years old daughter, Cliona, for their patience, support and encouragement during these more than three years. For John also, thanks for comprehensive discussions and guidance.

Nokia, October 2000

Tarja Shakespeare



# Contents

<b>1</b>	<b>Introduction</b>	<b>1</b>
<b>2</b>	<b>Paper Coloring Process</b>	<b>7</b>
2.1	Introduction to Coloring Terminology . . . . .	7
2.2	Paper Color . . . . .	8
2.2.1	Effect of Sheet Structure . . . . .	9
2.2.2	Physical Basis of Color . . . . .	11
2.2.3	Factors Affecting Colorants' efficiency . . . . .	15
2.3	Classification of Colorants . . . . .	26
2.4	Fiber Coloring . . . . .	29
2.5	Paper Coloring . . . . .	34
2.5.1	Stock Coloring . . . . .	34
<b>3</b>	<b>Color Measurement</b>	<b>41</b>
3.1	Illuminating and Viewing conditions . . . . .	41
3.2	Color stimulus . . . . .	43
3.3	Radiance Factors . . . . .	44
3.3.1	Spectrophotometer . . . . .	45
3.3.2	Spectrofluorimeter . . . . .	48
3.4	Color Specification . . . . .	51
3.5	Color Difference Formulas . . . . .	53
3.6	Accuracy . . . . .	54
<b>4</b>	<b>Experimental Work</b>	<b>57</b>
4.1	Colored Handsheets . . . . .	57
4.2	Measurements . . . . .	61
4.2.1	Used Instruments . . . . .	62
4.2.2	Measurement Uncertainty . . . . .	63
4.3	Coloring Method Analysis . . . . .	71
4.3.1	Coloring Uncertainty . . . . .	74
4.3.2	Conclusions . . . . .	79

---

<b>5</b>	<b>Colorant Modelling</b>	<b>81</b>
5.1	Adsorption isotherm analysis . . . . .	81
5.2	Importance of Colorant Modelling . . . . .	85
5.2.1	Colorant Formulation with Dyes . . . . .	88
5.2.2	Optimizing Color Controller . . . . .	90
5.3	Two-Flux Model . . . . .	91
5.3.1	Surface Reflection Correction . . . . .	95
5.3.2	Interdependence of the Coefficients . . . . .	96
5.3.3	Single Constant Kubelka-Munk Model . . . . .	97
5.4	Absorption Band Broadening and Non-Linear Extension to Kubelka-Munk Model . . . . .	108
5.5	Two-Flux Model with Fluorescence . . . . .	111
5.5.1	Extended Kubelka-Munk Model for Fluorescence, Polychromatic Illumination . . . . .	114
5.5.2	Extended Kubelka-Munk Model for Fluorescence, Monochromatic Illumination . . . . .	117
5.6	Absorption Band Broadening and Non-Linear Total Radiance Factor Model . . . . .	123
5.7	Colorant Responses . . . . .	132
<b>6</b>	<b>Conclusions</b>	<b>135</b>

# Table of Symbols

Since several symbols are assigned specific meaning by standards, some symbols must perform multiple duties. Where several meanings exist for a symbol, the context should make it clear which meaning is intended. The following table is organized into five groups: operators, lowercase and uppercase of Greek symbols, and lowercase and uppercase of Latin symbols.

## Operators

$\partial$	Partial differential
$\nabla$	Gradient
$\nabla\nabla$	Hessian matrix
$F$	Convolution operator for monochromator (illumination).
$G$	Convolution operator for monochromator (detector).

## Lowercase Greek Symbols

$\alpha_{\beta_T(\lambda S)}$	Scalar weighting factor for the total radiance factor optimization objective $P_{\beta_T(\lambda S)}$ .
$\alpha_j$	A self-tuning scalar term to adjust the absorption coefficient $a_j(\lambda)$ of the colorant $j$ to current process steady-state.
$\alpha_{XYZ(S,k)}$	Scalar weighting factor for the CIE tristimulus optimization objective $P_{XYZ(S,k)}$ .
$\beta(\zeta, \lambda)$	Radiance transfer function, defined in Section 3.3.2.
$\beta_L(\lambda S)$	Luminescent radiance factor of a fluorescent specimen for a known illuminant $S$ . Ratio of the radiance due to fluorescence of the specimen to that of the perfect reflecting diffuser identically irradiated, after [Gru80].
$\beta_L(\lambda)_{\infty*}, \beta_L(\lambda)_{\infty*,a}$	Luminescent radiance factor of the colored substrate and the green-ing effect in principle at adsorption saturation. In practice measured at a high enough adsorption level. Defined in Section 5.6.

$\beta_L(\lambda)_c, \beta_L(\lambda)_s$	Luminescent radiance factor of colored substrate and the base substrate.
$\beta_R(\lambda)$	Reflected radiance factor. The ratio of the radiance due to reflection of the specimen to that of a perfect reflecting diffuser identically irradiated [Gru80].
$\beta_T(\lambda S)$	Total radiance factor of a specimen for a known illuminant $S$ , equal to radiance factor $\beta$ . Ratio of the radiance of the surface element in the given direction to that of the perfect reflecting diffuser identically irradiated. Note, for photoluminescent media, the radiance factor is the sum of two portions, the reflected radiance factor $\beta_R(\lambda)$ and the luminescent radiance factor $\beta_L(\lambda S)$ [CIE87].
$\beta_T(\lambda)_{\infty*}, \beta_T(\lambda)_{\infty*,a}$	Total radiance factor of the colored substrate and absorption band broadening and the greening effect in principle at adsorption saturation. In practice measured at a high enough adsorption level that the difference from saturation is not significant. Defined in Section 5.6.
$\beta_T(\lambda)_c, \beta_T(\lambda)_s$	Total radiance factor of colored substrate and the base substrate.
$\delta\lambda, \delta\zeta$	Instrumental wavelength intervals of the instrument. Unit: nm.
$\varepsilon(\lambda)$	Spectral absorption coefficient in the used cell. Unit: $\text{l g}^{-1} \text{cm}^{-1}$ .
$\zeta$	Wavelength. Unit: nm.
$\eta_j$	Fraction of total adsorption sites within homogeneous region $j$ for an inhomogeneous substrate.
$\kappa(\lambda)$	Absorption index of the material.
$\lambda$	Wavelength. Unit: nm.
$\mu$	Wavelength. Unit: nm.
$\nu$	Frequency. Unit: Hz.
$\rho(\lambda), \rho(\mu)$	Reflectance. Ratio of the reflected radiance to the incident flux in the given conditions.
$\tau$	A constant.

### Uppercase Greek Symbols

$\Delta\lambda, \Delta\zeta$	The spectral bandpass of the monochromator. Unit: nm.
$\Delta a^*, \Delta b^*, \Delta L^*$	Difference (specimen minus reference) of color coordinates of CIE 1976 ( $L^*a^*b^*$ ) color space.
$\Delta c$	Change in the colorant concentration $c$ .

---

$\Delta C_{ab}^*$	CIE 1976 chroma difference.
$\Delta E$	Energy difference between ground state and excited state of molecule. Unit: eV.
$\Delta E_{ab}^*$	CIE 1976 total color difference.
$\Delta E_{94}^*$	CIE 1994 total color difference.
$\Delta G$	Change in Gibbs free energy of a reaction. Unit: J mol <sup>-1</sup> .
$\Delta X, \Delta Y, \Delta Z$	CIE tristimulus value error, the difference between target and measured values.
$\Phi_0^+(\lambda), \Phi_0^-(\lambda)$	Diffuse spectral radiant flux at wavelength $\lambda$ on the illuminated surface, radiance travelled back to the illuminated surface. Unit: W nm <sup>-1</sup> .
$\Phi_z^+(\lambda), \Phi_z^-(\lambda)$	Diffuse spectral radiant flux at wavelength $\lambda$ travelling inside a plane-parallel light scattering specimen towards its unilluminated and illuminated surface at position $z$ . Unit: W nm <sup>-1</sup> .
$\Phi(\lambda S)$	Steady-state spectral radiant flux leaving from a specimen under stable illumination conditions $S$ . Unit: W nm <sup>-1</sup> . The spectral irradiance of an illuminator $S$ can be polychromatic $E(\lambda)$ or monochromatic $E(\zeta) d\zeta$ at wavelength $\zeta$ . Note, for fluorescent media, the steady-state spectral radiant flux is the sum of two proportions, the reflected spectral radiant flux $\Phi_R(\lambda S)$ and the luminescent spectral radiant flux $\Phi_L(\lambda S)$ . In principle, $\Phi(\lambda S)$ is the same as the color stimulus function.
$\Phi_R(\lambda S)$	Reflected spectral radiant flux leaving from a specimen under stable illumination conditions $S$ . Unit: W nm <sup>-1</sup> .
$\Phi_R(\lambda S)_{PRD}$	Reflected spectral radiant flux from the perfect reflecting diffuser. Unit: W nm <sup>-1</sup> .
$\Phi_R(\lambda S)_{Std-White}$	Reflected spectral radiant flux from a white standard calibrated relative to a perfect reflecting diffuser. Unit: W nm <sup>-1</sup> .
$\Phi_R(\lambda S)_{Std-Black}$	Reflected spectral radiant flux from a black standard calibrated relative to the perfect light trap. Unit: W nm <sup>-1</sup> .
$\Phi_T(\lambda S)$	Transmitted spectral radiant flux through a specimen under stable illumination conditions $S$ . Unit: W nm <sup>-1</sup> .
$\Phi_T(\lambda S)_{Std}$	Transmitted radiant flux through a standard solution under stable illumination conditions $S$ . Unit: W nm <sup>-1</sup> .
$\Psi_{S,\lambda}$	Finite estimation of $\Phi(\lambda S) d\lambda$ . Unit: W nm <sup>-1</sup> .

$\Psi_{S,\lambda_{PRD}}$	Finite estimation of $\Phi_R(\lambda S)_{PRD} d\lambda$ . Unit: $\text{W nm}^{-1}$ .
$\Psi_{\zeta,\lambda}$	Finite estimation of $M(\lambda E(\zeta) d\zeta) d\lambda$ . Unit: $\text{W m}^{-2} \text{nm}^{-1}$ .

### Lowercase Latin Symbols

$a_j(\lambda), a(\lambda)$	Wavelength dependent absorption coefficient for a specific colorant $j$ . Unit: $\text{T kg}^{-1}$ .
$b$	Equilibrium constant of a reaction.
$b_j$	Adsorption affinity constant of the Langmuir isotherm at region $j$ .
$a^*, b^*, L^*$	Color coordinates of CIE 1976 ( $L^*a^*b^*$ ) color space.
$c, c_j$	A colorant and the $j^{\text{th}}$ colorant concentration in dyebath, defined as the mass ratio of pure colorant to total dry mass of solids, $\text{kg T}^{-1}$ .
$c_0$	Speed of light in vacuum. Value: $2.99792458 \cdot 10^8 \text{ m s}^{-1}$ .
$d\lambda, d\zeta$	Infinitesimal wavelength band. Unit: nm.
$f_\lambda(\mu)$	Slit-scattering function of the monochromator at nominal wavelength $\lambda$ , zero outside $-L < \mu < L$ .
$f_z(\beta, \lambda)$	Radiance of fluorescent light produced in an infinitesimal layer at depth $z$ .
$g_\zeta(\xi)$	Slit-scattering function of the monochromator at nominal wavelength $\zeta$ , zero outside $-Z < \mu < Z$ .
$h$	Planck's constant. Value: $4.135669 \cdot 10^{-15} \text{ eVs}$ .
$k$	Normalization factor for CIE tristimulus calculation.
$k_{ads}, k_{des}$	Adsorption and desorption rate constant for the particular set of dyeing conditions. Units: $\text{L g}^{-1} \text{ s}^{-1}$ and $\text{s}^{-1}$ .
$n(\lambda)$	Refractive index of the material.
$p$	Power term.
$r_0(\lambda), r_2(\lambda)$	Specular reflection, and internal reflection.
$r_{ads}, r_{des}$	Adsorption and desorption rate for the particular set of dyeing conditions. Unit: $\text{L g}^{-1} \text{ s}^{-1}$ .
$r^f(\lambda)$	Responsivity factor of an instrument.
$u(x_i)$	Standard uncertainty. Defined in Section 4.2.2.
$u(R(\lambda)_{col})$	Nominal standard uncertainty of the colorings. Defined in Section 4.3.1.

---

$u(R(\lambda)_{tot})$	Nominal total standard uncertainty. Defined in Section 4.3.1.
$w$	Grammage of the sheet. Unit: $\text{g m}^{-2}$ .
$w_X, w_Y, w_Z$	Scalar weighting factors for CIE tristimulus errors.
$\bar{x}(\lambda), \bar{y}(\lambda), \bar{z}(\lambda)$	CIE 1931 standard colorimetric observer. Color-matching functions for $2^\circ$ field of view.
$\bar{x}_{10}(\lambda), \bar{y}_{10}(\lambda), \bar{z}_{10}(\lambda)$	CIE 1964 supplementary standard colorimetric observer. Color-matching functions for $10^\circ$ field of view.
$z$	Position of coordinate from illuminated surface. Unit: m.

### Uppercase Latin Symbols

$A$	CIE standard illuminant $A$ . Colorimetric illuminant representing daylight with an absolute temperature of 2856 K, defined by the CIE in terms of a relative spectral power distribution
$A(\lambda)$	Spectral absorbance.
$A_{ads}, A_{des}$	Arrhenius frequency factors of adsorption and desorption. Units: $\text{L g}^{-1} \text{s}^{-1}$ and $\text{s}^{-1}$ .
$B(\zeta, \lambda)$	Radiance transfer factor, also called bispectral radiance factor. Discrete approximation of $\beta(\zeta, \lambda)$ for particular $\delta\zeta$ and $\delta\lambda$ , defined in Section 3.3.2.
$C$	CIE standard illuminant $C$ . Colorimetric illuminant representing daylight with a correlated color temperature of 6774 K, defined by the CIE in terms of a relative spectral power distribution [CIE86].
$C_{ab,1}^*, C_{ab,2}^*$	CIE 1976 a,b chroma of specimens 1 and 2.
$[D]_f$	Dye-on-fibre concentration, defined as the mass ratio of pure colorant to total dry mass of solids, $\text{kg T}^{-1}$ .
$[D]_s$	Dye-in-dyebath concentration, defined as the mass per unit volume, $\text{g L}^{-1}$ .
$[D_1]_f, [D_2]_f, \dots$	Dye-on-fiber in successive layers.
$[D_{mono}]_f$	Dye-on-fiber in monolayer, bound only to substrate.
$[D_{multi}]_f$	Dye-on-fiber in multilayer, bound to other colorant molecules.
$[D_{sub}]_f$	Dye-on-fiber in sublayer, bound both to substrate and to other colorant molecules.
$[D_{super}]_f$	Dye-on-fiber in superlayer, bound only to other colorant molecules.

$D_{65}$	CIE standard illuminant $D_{65}$ . Colorimetric illuminant representing daylight with a correlated color temperature of 6504 K, defined by the CIE in terms of a relative spectral power distribution [CIE86].
$E_0, E_1, E_2, \dots$	Successive energy levels of a molecule or ion. Unit: eV.
$E_{ads}, E_{des}$	Activation energies for adsorption and desorption processes. Unit: $\text{J mol}^{-1}$ .
$K(\lambda), K(\zeta)$	Kubelka-Munk absorption coefficient. Unit: $\text{m}^2 \text{kg}^{-1}$ . For a thin layer within an isotropic scattering and absorbing material over a black backing, the limit as the layer thickness approaches zero of the fraction of the incident radiation absorbed by the layer, divided by its thickness [AST95b].
$K_{\infty}(\lambda), K_{\infty,a}(\lambda)$	Kubelka-Munk absorption coefficient of the colored substrate and absorption band broadening effect in principle at adsorption saturation. In practice measured at a high enough adsorption level. Defined in Section 5.4. Unit: $\text{m}^2 \text{kg}^{-1}$
$K_c(\lambda), K_s(\lambda), K_t(\lambda)$	Kubelka-Munk absorption coefficient for a colored substrate, base substrate and target colored specimen. Unit: $\text{m}^2 \text{kg}^{-1}$
$K_f(\lambda), K_{fs}(\lambda)$	Kubelka-Munk absorption coefficient for the filler, a filled sheet by filler. Unit: $\text{m}^2 \text{kg}^{-1}$ .
$K_F(\zeta)$	Effective Kubelka-Munk absorption coefficient of a colored specimen, equal to $K_c(\zeta) - K_s(\zeta)$ . Unit: $\text{m}^2 \text{kg}^{-1}$
$M(\lambda S)$	Steady-state spectral radiant exitance leaving from a specimen under stable illumination conditions $S$ . Unit: $\text{W m}^{-2} \text{nm}^{-1}$ . The spectral irradiance of an illuminator $S$ can be polychromatic $E(\lambda)$ or monochromatic $E(\zeta) d\zeta$ at wavelength $\zeta$ . Note, for fluorescent media, the spectral radiant exitance is the sum of two proportions, the reflected spectral radiant exitance $M_R(\lambda S)$ and the luminescent spectral radiant exitance $M_L(\lambda S)$ . In principle, $M(\lambda S)$ is the same as the color stimulus function.
$M_L(\lambda S)$	Luminescent spectral radiant exitance leaving from a specimen under stable illumination conditions $S$ . Unit: $\text{W m}^{-2} \text{nm}^{-1}$ .
$M_R(\lambda S)$	Reflected spectral radiant exitance leaving from a specimen under stable illumination conditions $S$ . Unit: $\text{W m}^{-2} \text{nm}^{-1}$ .
$M_{\zeta=\lambda}(\lambda S)_{PRD}$	Reflected spectral radiant exitance from the perfect reflecting diffuser, when $\zeta = \lambda$ . Unit: $\text{W m}^{-2} \text{nm}^{-1}$ .
$P_{\beta_T}(\lambda S)$	Optimization objective for total radiance factors, where specimen is irradiated with the illuminant $S$ .

---

$P_{XYZ(S,k)}$	Optimization objective for CIE tristimulus values, evaluated from the total radiance factor using illuminant $S$ and field of view $k$ .
$Q$	Total luminescence quantum yield of fluorescent colorant.
$Q(\zeta, \lambda)$	Luminescence quantum yield per unit at emission wavelength $\lambda$ .
$R$	The universal gas constant. Value: $8.3145 \text{ J mol}^{-1} \text{ K}^{-1}$ .
$R(\lambda)$	Reflectance factor, values $[0,1]$ . Ratio of the radiant flux reflected in the directions delimited by the given cone to that reflected in the same directions by the perfect reflecting diffuser identically irradiated or illuminated [CIE87].
$R(\lambda)_{\infty}, R(\lambda)_{\infty,a}$	Reflectance factor of the colored substrate and absorption band broadening effect in principle at adsorption saturation. In practice measured at a high enough adsorption level. Defined in Section 5.6.
$R(\lambda)_k$	Calculated reflectance factor based on colorant model at given concentration.
$R(\lambda)_c, R(\lambda)_s, R(\lambda)_t$	Reflectance factor of the colored substrate, the base substrate and the target specimen.
$R(\lambda)_{Std-Black}$	Reflectance factor of the black standard calibrated relative to a perfect light trap with a reflectance equal to zero.
$R(\lambda)_{Std-White}$	Reflectance factor of the white standard calibrated relative to a perfect reflecting diffuser with a reflectance equal to unity.
$R_0(\lambda)$	Reflectance factor of a single sheet of material with a black cavity as backing.
$R_{\infty}(\lambda)$	Reflectance factor of a layer of material of such a thickness that there is no change of reflectance factor if it is doubled in thickness.
$R_*(\lambda)$	Saunderson corrected reflectance factor.
$R'(\lambda S)$	Apparent reflectance factor for a illuminator realizing the known illuminant $S$ , values $[0, \infty]$ . Ratio of the sum of reflected and emitted flux from the fluorescent specimen to the flux reflected from the perfect reflecting diffuser, when both are irradiated by the same known heterochromatic flux under the same geometric and spectral conditions of measurement, after [Gru80].
$S$	CIE standard illuminant or an illuminator which realizes it. The illuminator $S$ is understood to specify the relative spectral power distribution $S(\lambda)$ as well as the spectral irradiance $E(\lambda)$ used to irradiate the specimen.

$[S]_f$	Concentration of dye on fiber when all adsorption sites are occupied defined as the mass ratio of pure colorant to total dry mass of solids, $\text{kg T}^{-1}$ .
$S(\lambda), S(\zeta)$	Relative spectral power distribution of a known illuminant or spectral irradiance of an illuminator with unit: $\text{W m}^{-2} \text{nm}^{-1}$ . First defined as ratio of the spectral distribution $X_\lambda(\lambda)$ of the quantity $X(\lambda)$ to a fixed reference value $R$ which can be an average value, a maximum value or an arbitrarily chosen value of this distribution [CIE87].
$S_\infty(\lambda), S_{\infty,a}(\lambda)$	Kubelka-Munk scattering coefficient of the colored substrate and absorption band broadening effect in principle at adsorption saturation. In practice measured at a high enough adsorption level. Defined in Section 5.4. Unit: $\text{m}^2 \text{kg}^{-1}$ .
$S(\lambda), S(\zeta)$	Kubelka-Munk scattering coefficient. Unit: $\text{m}^2 \text{kg}^{-1}$ . For a thin layer within an isotropic scattering and absorbing material over a black backing, the limit as the layer thickness approaches zero of the fraction of the incident radiation scattered (reflected) by the layer, divided by its thickness [AST95b].
$S_c(\lambda), S_s(\lambda), S_t(\lambda)$	Kubelka-Munk scattering coefficient for a colored substrate, a base substrate and a target specimen. Unit: $\text{m}^2 \text{kg}^{-1}$ .
$S_f(\lambda), S_{fs}(\lambda)$	Kubelka-Munk scattering coefficient for the filler, a filled sheet by filler. Unit: $\text{m}^2 \text{kg}^{-1}$ .
$T$	Absolute temperature. Unit: K
$T(\lambda)$	Transmittance factor. Ratio of the flux transmitted by the specimen to the flux transmitted by the perfect transmitting diffuser under the same geometric and spectral conditions of measurement [AST95b].
$T_1, T_2, \dots$	Successive energy levels of triplet states of a molecule or ion. Unit: eV.
$X, Y, Z$	CIE tristimulus values calculated for the 1931 standard colorimetric observer.
$X_{10}, Y_{10}, Z_{10}$	CIE tristimulus values calculated for the 1964 supplementary standard colorimetric observer.
$X_n, Y_n, Z_n$	CIE tristimulus values of a perfect reflecting diffuser with respect to specified standard illuminant and standard colorimetric observer.
$X_s, Y_s, Z_s$	CIE tristimulus values of the base substrate.
$X_t, Y_t, Z_t$	CIE tristimulus values of the target specimen.
$X_{S,k}, Y_{S,k}, Z_{S,k}$	CIE tristimulus values calculated based on illuminant $S$ and field of view $k$ .

# Glossary

ASTM	The American Society of Testing and Materials
BET	Brunauer-Emmett-Teller (isotherm)
CD	Cross-machine direction
CIE	La Commission Internationale de l'Éclairage
FBA	Fluorescent brightening agent
FWA	Fluorescent whitening agent. Synonym for FBA.
GCC	Ground calcium carbonate
ISO	Internal Organization for Standardization
KCL	The Finnish Pulp and Paper Research Institute, Espoo
MD	Machine direction
NRC	National Research Council of Canada
OBA	Optical brightening agent. Synonym for FBA.
PCC	Precipitated calcium carbonate
PRD	Perfect reflecting diffuser
RBA	Relative bonding area
SCE	Specular component excluded in sphere measurement
SCI	Specular component included in sphere measurement
SPD	Spectral powerdistribution of an illuminator
TAPPI	Technical Association of the Pulp and Paper Industry
UV	Ultraviolet light



# Chapter 1

## Introduction

Today, color is an issue on almost every paper, board, and tissue grade from brilliant white and near-white shades to pastel and deeply-colored shades. Continuous progress in several technologies, such as dye chemistry, printing, and paper manufacture, coupled with end-user demands and preferences is causing progressively tighter specifications in paper color and a widening range of used colors, which are leading to smaller single orders and consequently shorter color grade runs for many mills [SS98b, She00]. Customers now demand continuous, batchless quality for ordered paper. As a result, the importance of color measurement and control is increasing to the papermaker.

The function of color control is to minimize specified color errors by governing the available colorants' dosage. To perform well, an on-line color control requires a good optimization algorithm and a reliable colorant response model derived from the colorant model, whose relationship is shown in Figure 1.1. The external influences (such as variations in furnish quality and coloring conditions) affect the perceived coloring results, which may cause erroneous colorant models and disturbances into coloring process.

Traditionally, Kubelka-Munk based colorant formulation algorithms [KM31, McD97b] originating from the textile industry have also been used for on-line color control in the paper industry [CMS96, She99], despite their limitations, of which the neglect of fluorescence is the most serious. In a commercial color control, an approach was taken in 1993 to control paper coloring directly in total radiance factor domain, using a non-linearized colorant response model, and to regulate the colorants' dosage to minimize for example CIE  $L^*$   $a^*$   $b^*$  errors for a particular standard illuminant and field of view [SS98a, SS98b]. The research work leading to this thesis evolved from studying methods to improve the colorant response model used in the optimizing color controller [SS98a, SS98b], which was initiated by the present author in 1997.

To properly formulate a colorant modelling problem, the challenges in controlling paper color must be understood. It was stated almost twenty years ago that "The science of paper coloring is a knowledge which is least understood by its users, neglected by dyestuff manufacturers and often, completely ignored by paper manufacturers" [Lat81]. Today, successful coloring of paper

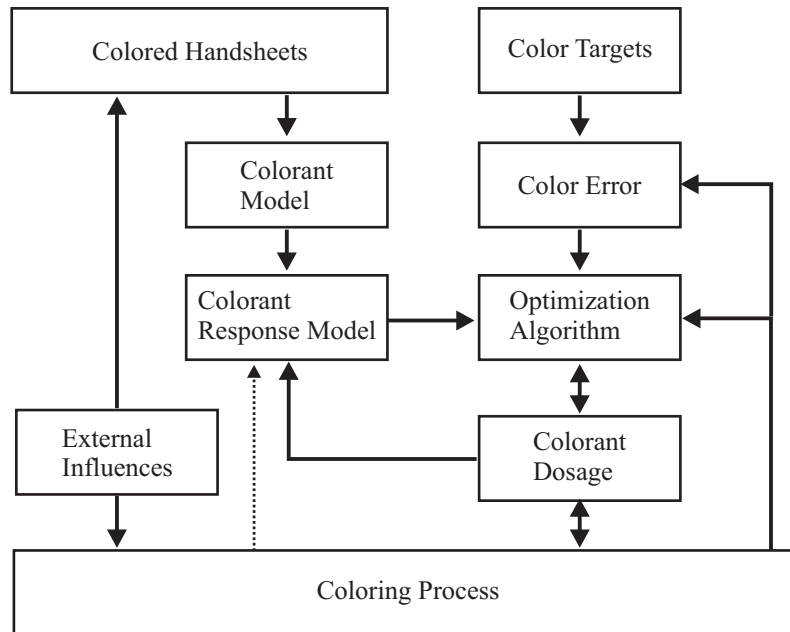


Figure 1.1: Block diagram of an on-line color control system.

is still a mixture of scientific facts from several fields (chemistry, paper physics, phenomenological theory, colorimetry) and practical observation. The prevalent use – intended or not – of fluorescent brightening agents in papermaking and their effects on color have confused many papermakers even more. This means, that the nature of the coloring process and paper color must be known, and these are the main themes of the supporting material in this thesis.

In contrast to the paper industry, coloring research has long traditions in the textile industry. Unfortunately, the research made by commercial organizations is not usually published for competitive reasons. However, it seems that most colorant models used for non-fluorescent dyes are based on a single constant version of the Kubelka-Munk two-flux model approach [KM31, McD97a] or simple extensions of it [LOG65, McK76], even though real colorants do not respond ideally in the way suggested by the phenomenological theory [Hof89]. This model is also usually used for the excitation band of fluorescent dyes [McK76, Bon86].

With non-fluorescent dyes, the fundamental relationship between the increase of the concentration of a dye in the substrate and an increase in incident radiation absorption at absorption wavelength band of the dye is undisputed [BS94, §5]. This is also true at the excitation band of the fluorescent brightening agents (FBAs) and fluorescent dyes, because the absorption of ultraviolet and visible light does not differ in respect to the mechanism of light absorption by colorants [Zol91, §2.3]. However, colorant modelling in the emission band of the fluorescent brighteners and fluorescent dyes is more complicated. The quality and quantity of fluorescent emission depends on the concentration of fluorescent dye on fiber, the colorant's quantum yield of

fluorescence, the substrate's absorption properties at the colorant's excitation band, the spectral power distribution of the used illumination especially at the colorant's excitation band, extent of intermolecular interaction [Pue96], and at the level of photodegradation in the fluorescent sample [WW99, §6.5]. Firstly, this causes a measurement problem for total radiance factor of fluorescent papers under a specific standard illuminant utilizing spectrophotometers with a monochromator in the viewing beam. The second problem is to define the reflectance factor of the fluorescent paper. Both problems relating to spectrophotometers have been studied extensively since 1970's [Sim72, All73, AB77, GC77, BC80, Alg87, CIE90, IIKM97], providing various approximate solutions for these problems. Notwithstanding these problems, several colorant models for fluorescent dyes utilizing traditional spectrophotometric measurement or their modifications which attempt to approximate spectrofluorimeters have been developed.

Ganz formally treats fluorescence in his extension to a single constant version of the Kubelka-Munk two-flux model as negative absorption by using the sign-function [Gan77]. This is an attractive method, because no additional constant is needed. However it is suitable only for the case of a single fluorescent colorant, and it does not distinguish between reflected and emitted light being based on total radiance factors.

McKay separates total radiance factor into reflectance factor and luminescent radiance factor employing cut-off filters [McK76, McK81]. The relationship between reflectance factors and dye-on-fiber is explained with an extension to a single constant version of the Kubelka-Munk two-flux model, which takes a form similar to the Langmuir adsorption isotherm. The excitation band of the fluorescent dye is also modelled with this relation. In the emission band of the fluorescent dye, the luminescent radiance factor is defined for a single fluorescent dye as a function of wavelength dependent constants defining the generation of fluorescence in the dye and the fluorescent dye's self-absorption. This model can be extended to deal with mixtures of a single fluorescent and non-fluorescent dyes. McKay's approach is not practical for the paper industry. It has too many parameters to be estimated requiring usually a calibration set with twelve concentrations per colorant. Also the model for luminescence is based on spectrophotometric measurements, and hence depends on the instrument illuminator.

Funk employs a two-monochromator system based on a Match-Scan spectrophotometer equipped with the second monochromator to produce monochromatic illumination to separate the reflectance factor and the luminescent radiance factor from the total radiance factor [Fun80]. The reflectance factor relationship to concentration of a fluorescent dye is modelled traditionally using a single constant version of the Kubelka-Munk two-flux model in the excitation band. The developed set of equations is based on two assumptions, (i) the distribution of fluorescence emission has a constant shape at the molecular level, (ii) the intensity of fluorescence produced is directly proportional to the quantity of excitation energy absorbed by the fluorescing molecule. Thus the amount of fluorescence produced is estimated based on the difference in the reflectance factor of the dyed substrate to the base substrate's one, the incident radiation, and the colorant's quantum yield of fluorescence. Funk concludes that the results obtained are comparable to those obtained when formulations using nonfluorescent colorants were first developed. However, no

investigation was made to determine the effect of experimental variability.

Bonham's model is an extended single constant version of the Kubelka-Munk two-flux model with fluorescence for polychromatic illumination [Bon86]. The reflectance factor relationship to concentration of a fluorescent dye in the excitation band is modelled traditionally using a single constant version of the Kubelka-Munk two-flux model. The amount of fluorescence produced is estimated based on the difference in absorption coefficient of the dyed substrate to the base substrate's one, the colorant's quantum yield of fluorescence, and the incident radiation. The model is discussed in more detail in Section 5.5.1, since it is used as the base to derive a colorant model for fluorescent dyes and FBAs in this thesis. The derived model is supported by radiance transfer factor measurements using a commercially available spectrofluorimeter providing an illuminator independent colorant model.

## Research Objectives

As stated, the main intention of this research was to create steady-state colorant models for dyes and for fluorescent dyes including FBAs to cope with the gamut from bright fluorescent shades to nearly saturated shades. These models are needed in the optimizing color controller to improve the currently used colorant response model. Common requirements for such models are to minimize the number of parameters for easy and fast color control tuning, and the models must describe the process reliably. Since spectrofluorimeters intended for colorimetry have recently become commercially available, it was planned to use the additional measurement information they provide in quantifying a model, especially the excitation-emission relationships of fluorescent colorants.

Methods of colorant formulation or color control by themselves are beyond the scope of the thesis, because their efficacy depends strongly on their optimization algorithm and its constraint handling. Moreover specification of color targets and acceptable limits for deviation from the targets varies widely among papermakers. However, to understand the requirements for and use of the colorant models an overview of colorant formulation and an optimizing color controller is given in Section 5.2.

The chemistry of color and colorants is not studied in detail in this thesis, although relevant photochemical and physicochemical effects are briefly surveyed. Also the psychophysical basis for perception of color is outside the scope of this thesis.

The research work was divided into the following objectives:

- To study factors affecting paper color in stock coloring and methods of fluorescent color measurement.
- To quantify linearity and additivity of a single constant version of Kubelka-Munk two-flux model, in stock colored sheet with anionic direct dyes.
- To study differences in colorant responses used in colorimetric color formulation and used in the optimizing color controller.

- 
- To quantify a common well-behaved colorant model for dyes as a function of their concentration on dry-solids for stock dyeing based on reflectance factors measured using a commercially available spectrofluorimeter and spectrophotometer.
  - To quantify a common well-behaved colorant model for fluorescent dyes and FBAs as a function of their concentration on dry-solids for stock dyeing based on radiance transfer factors and reflectance factors measured using a commercially available spectrofluorimeter and spectrophotometer.

A rather traditional experimental program was carried out to study the objectives by making colored handsheets with anionic direct dyes, fluorescent dyes and FBAs, which are most used in wood-free publishing and fine papers. The substrate for coloring was bleached cellulose with and without fillers.

## Structure and Contributions

In this thesis knowledge from several fields such as stock coloring, colorimetry and on-line color control is collected together to form a firm base for colorant modelling. This thesis comprises six chapters, whose contents are outlined below.

In Chapter 2 the theory of stock coloring of paper is discussed with qualitative examples. Anionic direct dyes, FBAs and fluorescent dyes were used to show how colorants' interactions influence their coloring efficiency. A commercial spectrofluorimeter was used to study interactions between fluorescent and other dyes. This set of spectrofluorimetric measurements has a novel nature. This chapter also contains discussions of the physical basis of color, the nature of different colorant classes and fundamental aspects of fiber coloring process, all relevant in formulating colorant models.

In Chapter 3 the principles of radiance factor measurement and methods used within spectrophotometers and spectrofluorimeters are reviewed. This provides the base for defining color targets and describing colorant models. Sources of errors in colorimetry caused by the measuring instruments are shortly discussed. Based on the present author's observations, the issues in fluorescent color measurement are not widely known in the paper industry, leading to opinions such as "Color too true can be too expensive to be good" [JW75, p.461].

In Chapter 4 the experimental work is described. Furnish properties and preparation of the colored handsheets used in this study are described. Also the magnitude and origins of variation in quantities of interest are discussed based on two sets of repeated colorings. The measurement instruments, spectrophotometer and spectrofluorimeter, are introduced and their uncertainty is studied. These studies give a basis for estimating the goodness of the developed colorant models.

In Chapter 5 an overview of colorant responses used in color control algorithms is given, to illustrate the need for and importance of colorant models in control. Also, the fundamental bases of phenomenological models are explained, including extension for fluorescence, and colorant models are derived. These models can incorporate known changes in scattering and absorption due to variation in the substrate (fiber types, furnish blends, fillers, pigments), but they do not

predict such changes. Rather, they model the effect of dyes and fluorescent dyes including FBAs on absorption and scattering characteristics of the substrate. This chapter contains the following contributions :

- Based on a linearity study of a single constant version of Kubelka-Munk two-flux model the main source of observed non-linearity is identified as a missing relation in the way the scattering and the absorption are affected at the absorption band of the dye by the dyeing.
- An improved method is proposed for off-line tuning of color controllers using handsheets produced with mixed colorants as used in the mill.
- The knowledge of Langmuir-type adsorption isotherm process is utilized in the development of colorant models. This includes a term for absorption band broadening to account for phenomena at high dosage rates. This approach was used to model Kubelka-Munk absorption and scattering coefficient instead of their ratio, and hence also to model total radiance factor versus dye-on-fiber.
- A colorant model is developed for emission due to fluorescent dyes and FBAs based on an extended single constant version of the Kubelka-Munk two-flux model. Fluorescence is quantified and modelled for monochromatic illumination based on radiance transfer factors. This gives the possibility to calculate colorant model in total radiance factors for each fluorescent dye under several illumination conditions at once, which is a requirement for minimization of illuminator metamerism.

Finally, Chapter 6 draws the final conclusions from the results presented in the thesis and presents suggestions for further work in this area.

## Chapter 2

# Paper Coloring Process

Paper can be colored using three methods: stock coloring, surface coloring, or a combination of the two. In stock coloring, the paper – more precisely the base paper – is dyed throughout, with dyes either added in batches or metered continuously in furnish with good mixing. The most common surface coloring method is coloration at the size press. Other methods in use are coating coloring, calender dyeing, spray dyeing, and dip dyeing mainly for decorative grades. These processes produce surface dyeings of greater or lesser penetration. Only stock coloring will be discussed here. Figure 2.16 contains an example of a stock coloring process.

### 2.1 Introduction to Coloring Terminology

The vocabulary for describing color, colorants, and coloration includes many common terms which are given precise definitions in a technical context. Unfortunately, even professionals sometimes use these terms ambiguously, so that it can be unclear whether the technical or a looser vernacular meaning is intended.

What is color? “Colour is a physical experience in the mind of an observer and as such is impossible to measure” [Bat97]. This also helps to explain why there are so many different terms used to describe perceived color, and why color measurement and colorimetric calculations describe only approximately what people see.

Any material which can be added or applied to a substrate to give it color may be referred to as a colorant, and the process of application can be referred to as coloration or coloring [Asp97, §23.2]. Generally, it is agreed that dyes and pigments are colorants.

Dyeing is the collective name for the processes whereby dyes are dissolved, transported to the fiber surface and, as individual molecules or ions, adsorbed onto the fibers for which they have some substantivity [Asp97, §23.2]. Dyes are highly colored, aromatic-organic molecules of modest size. They may be anionic, cationic or electrically neutral (including zwitterions). They are either intrinsically soluble in water (with a wide range of solubilities) or can be made soluble in the medium in which dyeing is conducted [Asp97, §23.2].

Based on this definition fluorescent brightening agents (FBAs) and dyes which fluoresce are also dyes. However, FBAs and fluorescent dyes are commonly separated from the absorptive dyes due to their different optical behavior. That is also the case in this thesis.

The definitions of substantivity and affinity seem to vary in the literature. Substantivity has been defined as “the attraction between a substrate and a dye or other substance under the conditions of test whereby the latter is selectively extracted from the application medium by the substrate” [Sum89]. Extraction, sorption, can be understood to contain one or all of following processes:

- Adsorption is usually analogous to a condensation of gas molecules, or to crystallization from the liquid. It is most pronounced as a monomolecular layer next to the solid surface, but at times may persist to a height of three or four molecules [PC73, §16].
- Absorption, penetration of one substance into another [Zum98, §15.9].
- Entrainment, to draw in and transport (as solid particles or gas) by the flow of a fluid [Mer94].

Affinity is the quantitative expression of substantivity [DS89, Appendix A]. It is the difference between the chemical potential of the dye in its standard state in fiber and the corresponding chemical potential in its standard state in the dyebath [Sum89].

Pigments may be white as well as colored, and they are not soluble in their application medium and contain no available water solubilizing groups [Asp97, §23.2]. Note, fillers used in papermaking are not classed as pigments in the meaning of paper coloring even though they do affect the perceived color. In pigmenting or pigmentation, any pigments applied to fibers from an external medium will require the additional use of polymeric materials, known as fixatives, to encapsulate the particles deposited on the fiber surfaces and hold them on the surface by virtue of the adhesion between fiber and fixative [Asp97, §23.2].

In papermaking, the terms tinting and shading are often used instead of dyeing when referring to the application of dyes to white shade paper grades. At present, dyes and FBAs are mostly used in this application, but pigments are slowly supplanting dyes. In time, this will doubtless introduce yet another ambiguity in terminology. A solution would be to use only the term paper coloring, and always to define the types of used colorants.

## 2.2 Paper Color

The color of a paper sheet can be modified either by affecting the light absorption or light scattering within paper using colorants and bleaching additives or controlling sheet density and filler loading. With fluorescent colorants the light absorption and emission can be affected. By contrast, the gloss of a paper sheet depends on the specular reflection at the first surface of the sheet, which is affected by fiber smoothness, the degree of calendering, and smoothness of coatings.

The portion of the electromagnetic spectrum which affects appearance of paper is approximately from 240 to 780 nm in wavelength, of which the human eye is sensitive to approximately

the range 360 to 830 nm [CIE87]. The incident radiation required for excitation of commonly used fluorescent brightening agents in paper is in the near ultraviolet (UV) to violet region circa 240 to 420 nm, which is typically re-emitted as violet-blue visible light, mainly 380 to 500 nm, causing paper to look less yellow.

### 2.2.1 Effect of Sheet Structure

The interaction of light with paper is complex, since a typical A4 sheet of fine paper contains millions of fibers, filler particles and fine material, which are usually packed nonuniformly in the sheet structure. This nonuniformity is particularly evident in the direction perpendicular to the plane of the sheet (the  $z$ -direction) producing structural two-sidedness, but most papers also differ in their light interaction in machine direction (MD) and cross-machine direction (CD), mainly due to the nonuniform distribution of planar fiber orientation angles and surface topography due to wire and felt weave patterns or roll grooves [Sha98]. The main interaction processes are specular reflection (associated with gloss, where incident light is redirected at the specular angle without diffusion), scattering within the material (associated with diffuse reflection or diffuse transmission), where the spatial distribution of a beam of radiation is changed when it is dispersed in many directions by a surface or by a medium, without change of frequency or of its monochromatic components [McC94, §6.7.2], absorption within a material (associated with color, where incident light is converted into heat or other radiation of longer wavelengths when incident on or passing through the material) and regular transmission directly through the object (associated with clarity, where incident light is transmitted through an object in a rectilinear manner without dispersion) [HH87, Glossary]. Colorants' light absorption diminishes both diffuse and directional radiant fluxes, while scattering converts directional to diffuse fluxes. If paper contains FBAs, some of the absorbed UV light will be emitted as bluish light contributing to diffuse fluxes. Diffusely reflected light with emitted light are predominantly responsible for the perceived color of the paper, and they are clearly functions of light absorption and scattering in the sheet.

Cellulosic fibers are translucent by nature and diffusely transmit light. Figure 2.1 shows the amount of diffusely reflected light from stacks of sheets and from single sheets over a black cavity, for 70 g/m<sup>2</sup> handsheets made from 100 % bleached cellulose fibers and 80 % bleached cellulose fibers with 10 % ground calcium carbonate (GCC) and 10 % kaolin. The Figure also shows the sum of diffusely and regularly transmitted light of single sheets. The measured sheets are from a set of customer handsheets made by KCL. As can be seen, a single sheet of paper is rarely opaque. This is often eliminated in colorimetric measurement such as color, brightness etc. by performing the measurement on a pad of paper of "infinite" thickness. In this case, "infinite" thickness is defined as a pad of sufficient thickness that no change in diffuse reflectance occurs when it is doubled in thickness. This is because colorimetric methods are based on comparing the amount of light diffusely reflected from a specimen to that for the ideal diffusor under identical illumination conditions for opaque matter. The ideal diffusor is, of course, opaque.

Paper scientists have tried to explain the scattering properties of the sheet based on properties

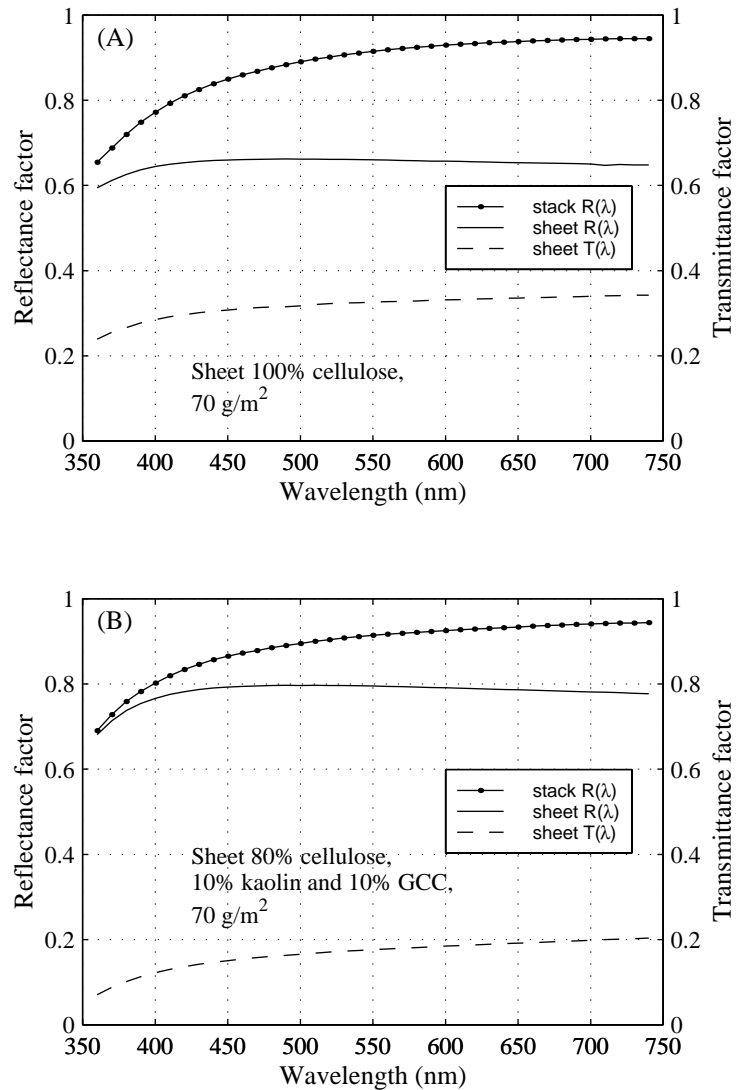


Figure 2.1: Amount of diffusely reflected light from stack of sheets and from single sheets over black cavity, and both diffusely and regularly transmitted light through single sheets for 70 g/m<sup>2</sup> handsheets made from (A) 100 % bleached cellulose fibers and (B) 80 % bleached cellulose fibers with 10 % GCC and 10 % kaolin. Measured from the customer handsheets made by KCL.

of its individual components typically using Kubelka-Munk theory [KM31], which unfortunately fails in that duty [Les97]. Kubelka-Munk theory will be reviewed in Section 5.3. The determining factors controlling the amount of scattering and thus having an effect on diffuse reflection are: specific surface area of fillers, fines and fibers, the number and size of voids, and the effect of fillers on interfiber bonding [Les97].

Part of fibers' surface area is occupied by interfiber bonding. This surface portion, which absorbs all entering light and thus does not participate in scattering, is described by relative bonding area (RBA). Light scattering can also occur in the internal surface areas of the fibers, since uncollapsed lumens of the fibers are large enough to scatter visible light [LL93]. It has been shown that increasing sheet density by wet pressing or beating, which indicates a change in the number and size of voids, will reduce light scattering and will change the way light is absorbed [Bur95], which is perceived as darker color. Also calendering generally increases the color depth of the paper. These and some other mechanical processes lead to collapse of the lumen, so that fibers become ribbon-like instead of tubular.

Fillers, such as titanium dioxide, clay and calcium carbonate, are added to pulp to increase opacity, whiteness and other properties of paper. Most fillers are colorants by nature, since they do not reflect light achromatically and thus may not be white. Thus they will typically contribute to the shade of the paper, for example by making it yellower. Fillers have a masking effect, which refers to the combination of substantivity of the dye to the filler, the filler retention itself and the change in scattering in the sheet. Often, their addition into the sheet will cause the depth of color to be weaker. To maintain the equivalent depth of dyeing an increase in colorant addition of 0-4 % may be required for each 1 % increase of filler load depending mainly on the affinity of the dye to filler and fiber and amount of dye-on-solids.

The specific surface area of fibers have values 1-2 m<sup>2</sup>/g, fines 8-10 m<sup>2</sup>/g and fillers 8-80 m<sup>2</sup>/g [Sco96, Glossary]. Thus an increase in filler amount in sheet structure increases the surface area where reflection can occur as can be seen in Figure 2.1. The maximum amount of scattering results when the diameters of the fillers and fines are roughly about 40-50 % of the wavelength of the visible light to be scattered [Kwo90] and void dimensions are also about half of the wavelength of visible light. However, filler agglomeration almost always leads to reduced scattering, which is common with filler loading above 10 % [Bie96, §24]. Also increasing moisture in the sheet lowers scattering, because water replaces many fiber-air interfaces with fiber-water interfaces [Ste69, p.200]. Only TiO<sub>2</sub> has a significantly greater refractive index than fibers, and can dominate the scattering effect. This can be seen especially in deeply colored papers, where a small increase in titanium dioxide loading will necessitate significant increases in dye addition to produce the same color appearance.

### 2.2.2 Physical Basis of Color

A light beam travelling within paper forms 'an optical path', where colorant molecules on fibers, fines and fillers can be described as colored filters with specific absorption and where fiber, fines and fillers as light redirectors and dispersers. The effect of colorant molecules is additive, so that the total absorption depends on the total number of colorant molecules the light has passed through. The light may be diffusely transmitted through the fiber walls. Existing colorant molecules on the surface of fibers and on walls of pores may selectively absorb light. Thus, light transmitted into the lumen can differ from incident light, and may be further modified if colorant molecules exist also within the lumen. This explains why fibers with colorant molecules dis-

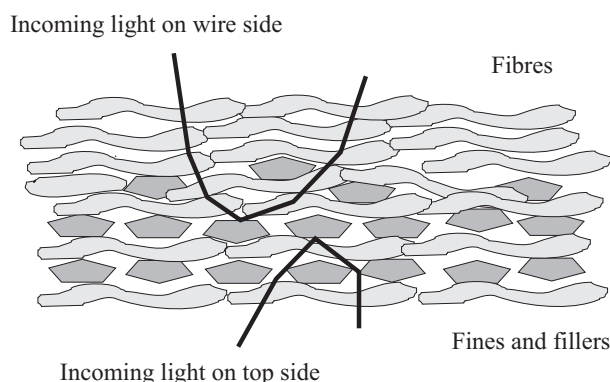


Figure 2.2: Light paths in structurally two-sided paper.

tributed uniformly through the fiber absorb more light and look darker than if the same amount of colorant were concentrated largely at the fiber surfaces [Asp97, §1.4.7]. In Figure 2.2 optical paths for fiber dominated and filler dominated sides of a sheet are shown. The length of these optical paths is different mainly due to higher scattering caused by fillers' greater specific surface area. Thus in terms of total absorption these optical paths are different, causing different perceived color being more intense in fiber side and lighter in filler side of sheet if the colorants' affinity for fillers is equal or lower than for fibers.

The coloring effect of colorants is based on their capability to absorb electromagnetic radiation, especially visible and ultraviolet light. The energy is absorbed by the colorant molecule as discrete quantities, photons, and is used to promote one of the electrons from the ground state  $E_0$  to a level of higher energy, an excited singlet state  $E_1$ ,  $E_2$  etc., Figure 2.3. This energy corresponds to 5.2 eV at 240 nm, 3.3 eV at 380 nm and down to 1.6 eV at 780 nm. In most cases, light of longer wavelengths, above 700 nm, is not sufficiently energetic to cause electronic promoting to a higher energy level, but stimulates molecular vibrations [Zol91, §2.3]. The energy differences  $\Delta E$  of ground states and excited states of the molecules and ions are directly proportional to the observed frequency  $\nu$ , and inversely proportional to the wavelength  $\lambda$  of the absorbed light, where  $h$  is Planck's constant and  $c_0$  speed of light:

$$\Delta E = h\nu = hc_0/\lambda \quad (2.1)$$

In contrast to isolated atoms or ions, large molecules and crystals have their energy bands split into many finely separated levels, through delocalization of electrons. The energy levels available to the molecule are further broadened by the range of vibrational and rotational modes geometrically possible. This quantized system can absorb light only at discrete frequencies determined in Equation 2.1. However, the resulting smooth shaped absorption spectrum of many liquids, solids and solutions is often as shown in Figure 2.4 and is determined by superposition of a large number of fine structured absorption or emission bands, each with absorption or emis-

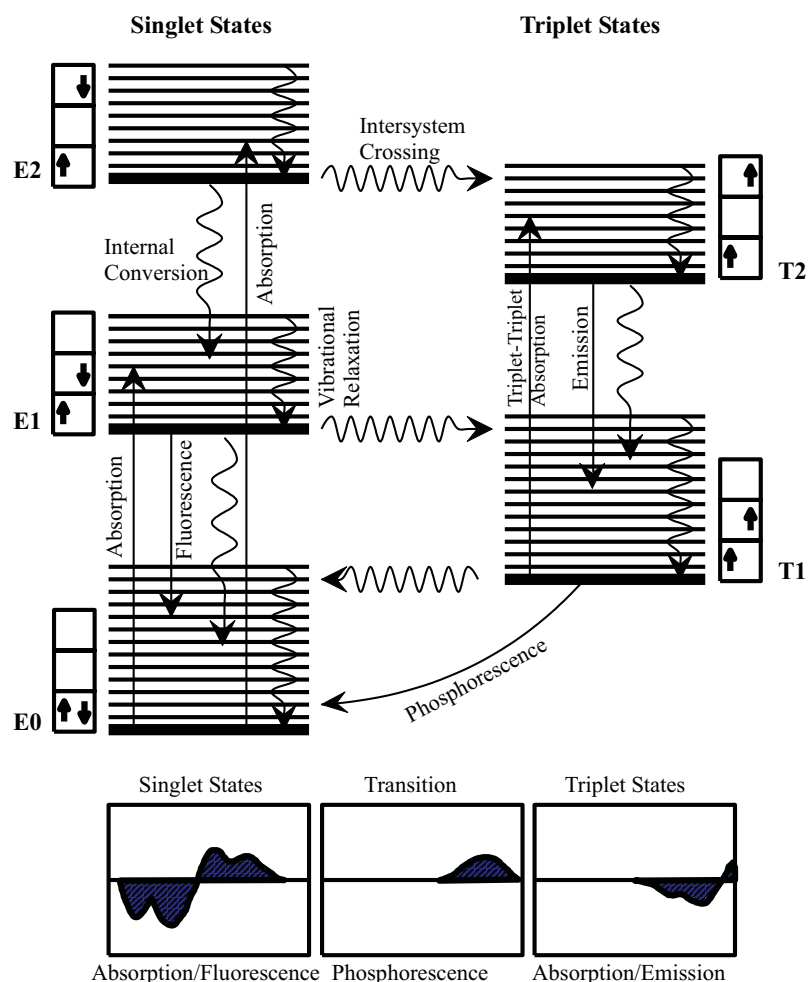


Figure 2.3: Jablonski diagram, after [Sin97].

sion intensity following a Gaussian distribution and whose fine structure due to rotational and vibrational modes may not be resolvable [Suz67, §1.1.2].

The energy emitted in returning to the ground state  $E_0$  cannot exceed the energy absorbed in reaching an excited singlet state  $E_1$ . Some or all of the absorbed energy may be dissipated by radiationless transitions, such as internal conversion or intersystem crossing. ‘Radiationless transition’ in this sense means that no visible or ultraviolet photon is absorbed or emitted; obviously many rotational and vibrational transitions are accompanied by emission of infra-red or microwave photons.

The time scale for singlet state transition processes have the following orders of magnitude: light absorption  $10^{-15}$  s, vibrational relaxation  $\geq 10^{-12}$  s, fluorescence  $10^{-9}$  to  $10^{-6}$  s, intersystem crossing  $10^{-5}$  to 10 s and phosphorescence  $10^{-4}$  to  $10^3$  s [Zol91, §2.4]. Radiationless transi-

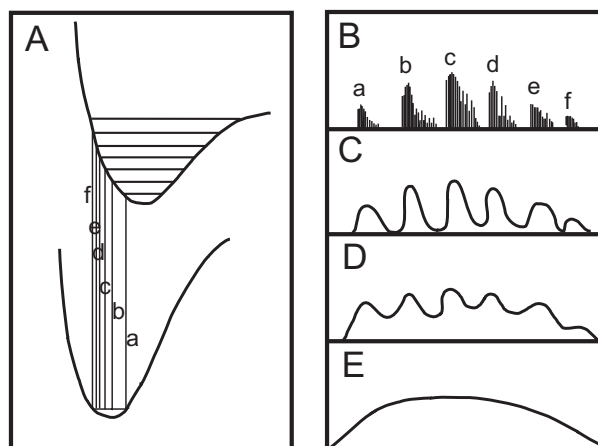


Figure 2.4: Effect of intermolecular forces on an idealized absorption band.

(A) Potential energy curves involved in the transition.

(B) Absorption spectrum of the dilute vapor.

(C) Absorption spectrum of the vapor at moderate pressures (rotational structure smeared out).

(D) Absorption spectrum in liquid with weak intermolecular forces (vibrational structure present, but less pronounced than in vapor and somewhat shifted in frequency).

(E) Absorption spectrum in liquid with strong intermolecular forces (vibrational structure smeared out), after [Kau57, p. 669].

tions are shown by wavy lines in Figure 2.3. Internal conversion leads to vibrational deactivation, i.e. relaxation of molecular rotational or vibrational modes at either  $E_0$  or  $E_1$  states, which may result in emission of infra-red or lower energy quanta. These mechanisms depend on the degrees of geometrical freedom available to the molecule, and are inhibited in rigid molecules. Intersystem crossing leads to triplet states, i.e. the electron in the singlet excited state  $E_1$  can undergo a spin change, resulting in a metastable triplet state  $T_1$ , where photochemical reactions generally occur, and which have lifetimes of 100 ns to 10 s [Zol91, §2.4]. Phosphorescent emission from triplet states (a return to the ground state,  $E_0$ ) is at lower energies than from the corresponding excited singlet states, with rate constants from milliseconds to hours. Triplet states can also be excited by absorbing photons, usually in a lower energy range than for singlet excitation from the ground state. Electrons in excited triplet states ( $T_2$ , etc.) may return to a lower triplet state or to an excited singlet state. Normally, very few molecules will exist in triplet states, except under intense ground state excitation, but for some substances triplet effects will dominate [Smi97].

Fluorescence generally takes place when emission of radiation from the lowest vibrational levels of the first excited state  $E_1$  to one of the vibrational levels of the ground state  $E_0$  happens. Thus, most fluorescent compounds are rigid in their structure to prevent the energy of the excited states from being lost by torsional vibrations of the molecule. Absorption in the visible or near ultra-violet ranges with re-emission at longer wavelengths in the visible range gives rise to the

visual property of fluorescence. Emitted radiant fluxes contribute to diffuse fluxes, since the direction of the emitted quantum is uncorrelated with that of the absorbed quantum (momentum is conserved by other molecular processes). An absorption band in which absorption stimulates a fluorescent emission is termed a fluorescent excitation band or just an excitation band. This distinction is only made for clarity of exposition in discussion which relates to fluorescent and non-fluorescent colorants.

Absorption in the visible range with re-emission at infra-red and longer wavelengths (including dissipation through molecular vibrational and rotational modes) results in absorptive coloration. This is the principal mechanism by which dyes impart color. Pigments impart color by scattering of some wavelength bands and sometimes by absorption as well. The light absorption and emission properties of a colorant molecule are determined by its chromophores, which are usually linear or cyclic systems of conjugated double bonds, in which valence electrons are delocalized [Zol91, §2.2]. These properties may be modified and increased in intensity by introduction of suitable electron donors, auxochromes. For the perceived color of a dyed substrate, the position of the maximum absorption with respect to wavelength and the shape of the absorption band of the colorant are both important. The absorption band location defines the perceived color, e.g. a dye with absorption band at 435 to 480 nm is perceived as yellow. The narrower the width and the steeper the slopes of a band, the brighter and purer the color. Figure 2.5 contains examples of absorption bands of yellow dyes, from the group A and B sheets, the latter containing 16 % retained chalk. The present author's measurement results from the colored handsheets, described in Section 4.1, are used from now on as qualitative examples to support the coloring theory.

By introducing other groups having no influence on the color of the molecule, but which change the insoluble molecule to a water-soluble dye, the solubility of the dye can be manipulated to suit different dyeing conditions. This is very important, since increasing dye concentration tends to lead to molecule grouping, aggregation. These aggregated molecules may be adsorbed on the surface of the fiber causing higher light absorption than single-layer molecule adsorption [Koo90], resulting in a duller color due to absorption band broadening as shown in Figure 2.6, see also Figure 2.13. The measured sheets are from the group B sheets containing 16 % retained chalk. Similarly, charged dyes from the same dye class may have both cationic and anionic groups on the molecule causing them to interact if applied together in the dyeing medium, possibly resulting in precipitation causing this complex to act as a colored pigment if entrained in the sheet. The produced shade will often be duller.

### 2.2.3 Factors Affecting Colorants' efficiency

Several factors can affect the final color of stock dyed base paper as will be discussed below.

For each dye, FBA and fluorescent dye, there is a distribution of excitation energies, with some wavelengths absorbing more strongly than others. For each absorption wavelength, the emitted radiant fluxes are distributed among a range of emission wavelengths, as described by its radiance transfer function  $\beta(\zeta, \lambda)$  from excitation wavelength  $\zeta$  to emission wavelength  $\lambda$ .

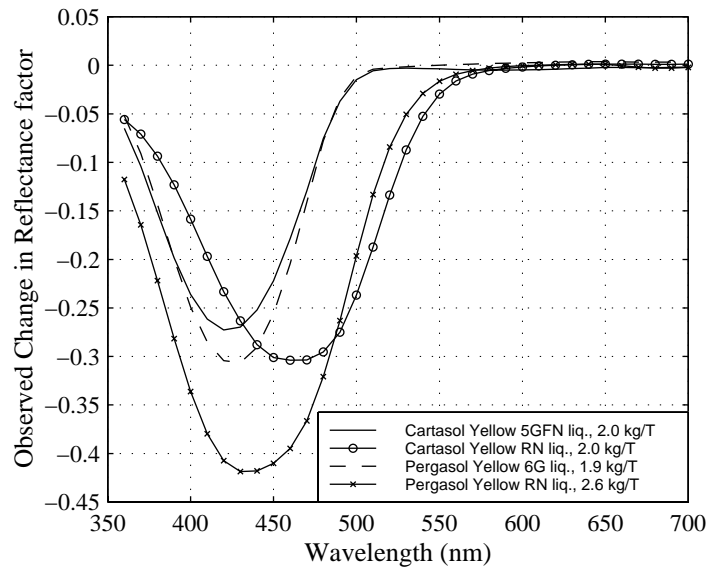


Figure 2.5: Absorption bands of yellow dyes based on measurements from the group A and B sheets, the latter containing 16 % retained chalk.

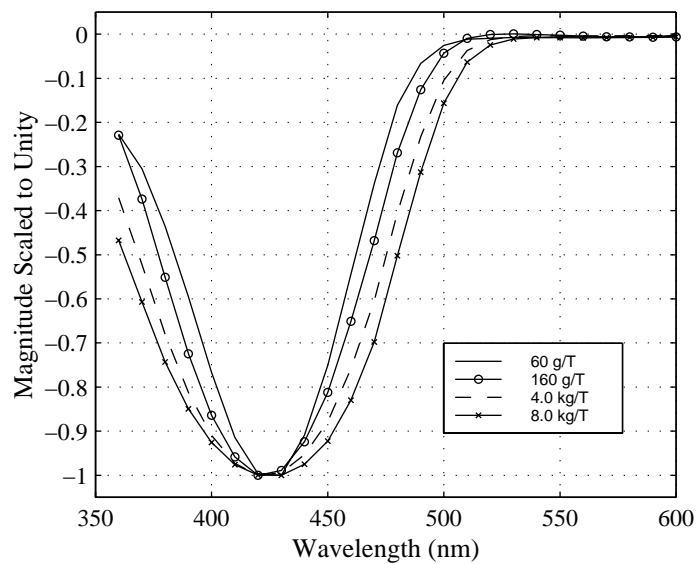


Figure 2.6: Absorption band broadening of Cartasol Yellow 5GFN liq. as function of dye-on-fiber, based on measurements from the group B sheets with 16 % of retained chalk.

This relationship is measurable as discrete radiance transfer factor  $\mathbf{B}(\zeta, \lambda)$  from each discrete excitation waveband  $\zeta, \delta\zeta$  to discrete emission waveband  $\lambda, \delta\lambda$  as shown for paper containing FBA in Figure 2.7. The radiance transfer factor  $\mathbf{B}(\lambda, \lambda)$  is the reflected radiance factor  $\beta_R(\lambda)$  and in principle is identical to the reflectance factor  $R(\lambda)$ .

In the case of fluorescent specimens, spectrophotometers actually measure apparent reflectance factor  $R'(\lambda|S)$ , which depends on the illumination  $S$  of the specimen, but often treat it as if it were an illumination-independent reflectance factor  $R(\lambda)$ . Spectrofluorimeters measure the discrete radiance transfer factor  $\mathbf{B}(\zeta, \lambda)$  from which total radiance factor  $\beta_T(\lambda|S)$  for any

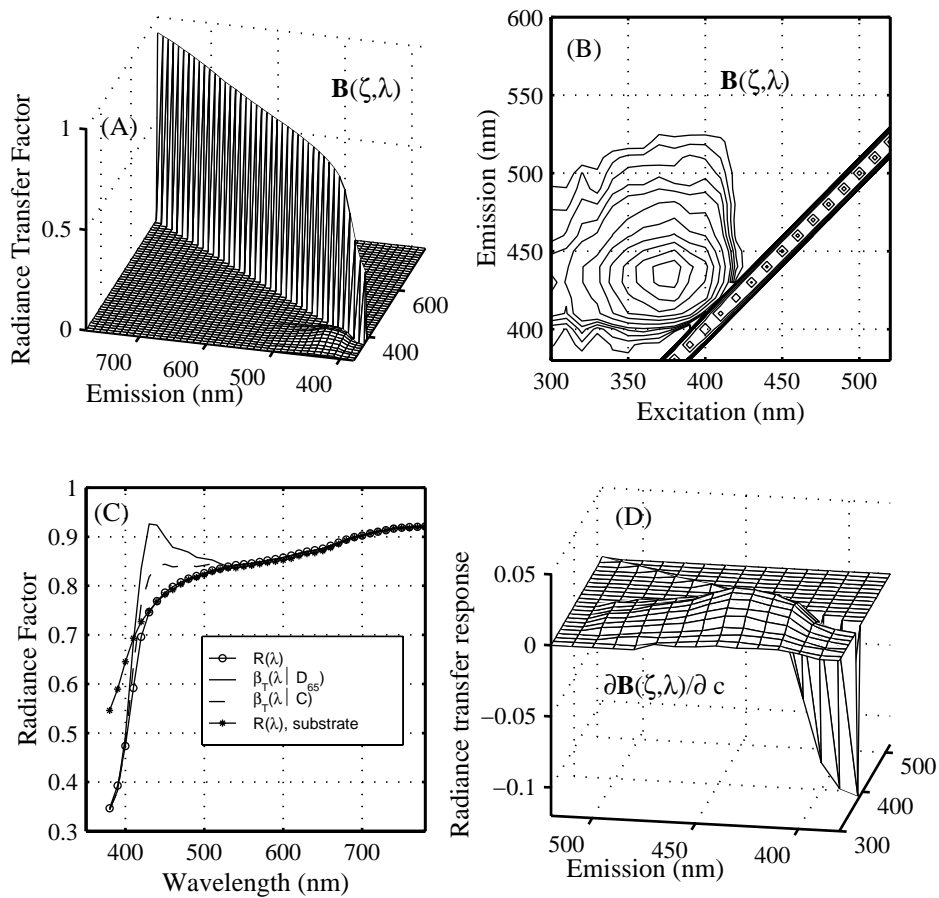


Figure 2.7: (A) Radiance transfer factor  $\mathbf{B}(\zeta, \lambda)$  of a handsheet containing 1.7 kg/T of Tinopal UP.

(B) Its  $\mathbf{B}(\zeta, \lambda)$  as contour map at levels [0.002:0.002:0.008 0.01:0.005:0.1 0.2 0.3 0.5 0.7].

(C) Its total radiance factors  $\beta_T(\lambda|S)$  under  $D_{65}$  and C illuminants, reflectance factor  $R(\lambda)$  and  $R(\lambda)$  of the substrate, all from the group A sheets.

(D) Its normalized radiance transfer factor response  $\partial\mathbf{B}(\zeta, \lambda)/\partial c$ .

illuminant  $S$  can be computed, and from which the reflected radiance factor  $\beta_R(\lambda)$  can be extracted. Spectrophotometric measurements will be discussed in more detail in Section 3.3. The radiance transfer factor response  $\partial \mathbf{B}(\zeta, \lambda)/\partial c$  describes the change in the radiance transfer factor  $\mathbf{B}(\zeta, \lambda)$  per unit change of colorant concentration  $c$  in paper, and is a very valuable quantity for modelling paper coloring. The apparent reflectance factor response  $\partial R'(\lambda|S)/\partial c$  can be computed directly from apparent reflectance factor measurements or the total radiance factor response  $\partial \beta_T(\lambda|S)/\partial c$  can be computed from the radiance transfer factor response [SS99].

The distribution of energy levels in both ground state and excitation bands is determined by the molecular electronic configuration, as explained earlier. However, those energy distributions are altered by the environment of the molecule, including effects of weak intermolecular forces (London and Van der Waals). In particular, the energy gaps and geometric relaxation modes available can differ subtly between a dye or FBA molecule adsorbed onto a cellulose fiber and the same molecule adsorbed onto a filler such as calcite. This causes the coloring effect of absorptive dyes, or the absorption-emission relations of fluorescent dyes including FBAs to differ correspondingly. Similarly, coloring effects may differ when adsorbed onto different types of fiber, or different adsorption sites in a particular fiber type. This is especially problematic with recycled fiber, whose type and quality is usually uncertain, and which usually contains unknown amounts of a range of contaminants such as residual ink, de-inking chemicals, fillers, starches, resins as well as colorants and FBA-quenchers. In principle the composition of broke is less uncertain, but good broke management is required [SS99, Bur95]. Pigments are not affected by fiber types or other properties of fibers [Car98, Pamphlet Wp8006e]. Starch, clays, resins and other fillers or strength modifiers also have an effect on the substantivity of dyes and FBAs, and can modify absorption and fluorescence processes [Sho90]. Modification of quantum relations can cause shifts on both  $\zeta$  and  $\lambda$  axes as well as shape changes to the radiance transfer factor response  $\partial \mathbf{B}(\zeta, \lambda)/\partial c$ .

Colorants can be reduced in effectiveness by three major physical mechanisms [WW99, §3.9]:

- Absorption and emission interaction without chemical interactions (involves either absorption of emitted light or reduction of light available to be absorbed by the colorant in its absorption band because of existence of another substrate or colorant)
- Intermolecular deactivation (involves modification of absorption and emission bands due to electronic orbital changes caused by chemical interaction between molecules, whether of the same or different species)
- Intramolecular deactivation (in which a new electronic state of the same molecule is populated, allowing internal conversion and/or intersystem crossing, and leading to modified absorption and emission bands)

Some examples of reduction in colorant efficiency will be discussed next. In the following analysis, the Ganz extension for  $\frac{K(\lambda)}{S(\lambda)}$  is used, where fluorescence producing an apparent reflectance factor greater than unity is treated as a negative absorption by using a sign-function [Gan77].

### Absorption and emission interaction

The phenomenon of absorption band competition, where another substrate or colorant reduces the amount of light available to be absorbed by the colorant in its absorption band, is essential in describing superposition of dye effects in dyeing combinations. The reduction in effectiveness depends on the extent to which the absorption bands overlap, and the relative absorptivity of the interfering agent and the base substrate compared to the dye.

An example of absorption band competition is shown in Figure 2.8, where Pergasol Yellow 6G is reduced in effectiveness when another absorbing agent, Levacell Violet BNN (which also absorbs in the Yellow dye's absorption band), is present in the stock, as the amount of light available for Yellow dye excitation is depleted. This statement is based on the failure of additivity of  $\frac{K(\lambda)}{S(\lambda)}$  as shown in subfigures (C) and (D), see Section 5.3.3, where the amplitude of the experimental curve for Yellow 6G and its estimated curve differ. The first experiments contain combinations of 67 g/T of Pergasol Yellow 6G and 140 g/T Levacell Violet BNN, subfigures (A) and (C). The second experiments contain combinations of 150 g/T of Pergasol Yellow 6G and 140 g/T Levacell Violet BNN, subfigures (B) and (D). The amount of the Yellow is the same in dyeings with and without the Violet in subfigure (A). This should have produced nearly identical  $\Delta \frac{K(\lambda)}{S(\lambda)} = \frac{K_c(\lambda)}{S_c(\lambda)} - \frac{K_s(\lambda)}{S_s(\lambda)}$  in subfigure (C), where  $K_c(\lambda)$  and  $S_c(\lambda)$  are the absorption and scattering coefficients for the dyeings containing the Yellow, and  $K_s(\lambda)$  and  $S_s(\lambda)$  are the absorption and scattering coefficients for corresponding dyeings with and without the Violet. An analogous situation also exists in subfigures (B) and (D). The experiment shows increasing reduction in absorptivity of Pergasol Yellow 6G, when amount of Levacell Violet BNN increases on-fiber. The measured handsheets belong to the group D sheets, and in all cases Pergasol Yellow 6G was dosed as first dye.

Another example of absorption band competition is given in Figure 2.9, where Fastusol Yellow 14L, an anionic fluorescent dye, is reduced in effectiveness when another agent which absorbs in its excitation band are present in the stock, in this case Pergasol Yellow 6G, as the amount of light available for excitation is depleted. Assuming additivity of  $\frac{K(\lambda)}{S(\lambda)}$ , the estimated  $\Delta \frac{K(\lambda)}{S(\lambda)}$  for the Yellow 14L is calculated based on the mixture of 0.35 kg/T of Fastusol Yellow 14L and 67 g/T of Pergasol Yellow 6G, subfigure (B). The calculated ratio of 'areas' on the excitation band with and without Yellow 6G is 0.98, when calculated as  $\sum_{380nm}^{490nm} \Delta \frac{K(\lambda)}{S(\lambda)}$ . Whereas the calculated ratio of 'areas' on the emission band with and without Yellow 6G is 0.88, based on  $\sum_{490nm}^{650nm} \Delta \frac{K(\lambda)}{S(\lambda)}$ . This simplified analysis shows a reduction in Yellow 14L's emission primarily caused by competing absorption of Yellow 6G in the excitation band of Yellow 14L. The effect of absorption by Yellow 6G in the emission band of Yellow 14L is small enough to be ignored in the analysis. The measured handsheets belong to the group D sheets, and in all cases Fastusol Yellow 14L was dosed first.

Many bivalent metallic cations have multiple absorption bands in ultra-violet [Dea79].  $Ca^{2+}$  and  $Mg^{2+}$  ions are common cations in paper mills, as they may be introduced in the water supply, or be present to varying extents in recycled fiber or coated broke.  $Cu^{2+}$ ,  $Zn^{2+}$  or  $Fe^{2+}$  ions may also be present due to corrosion and rust of the pipes and storage tanks. Substances

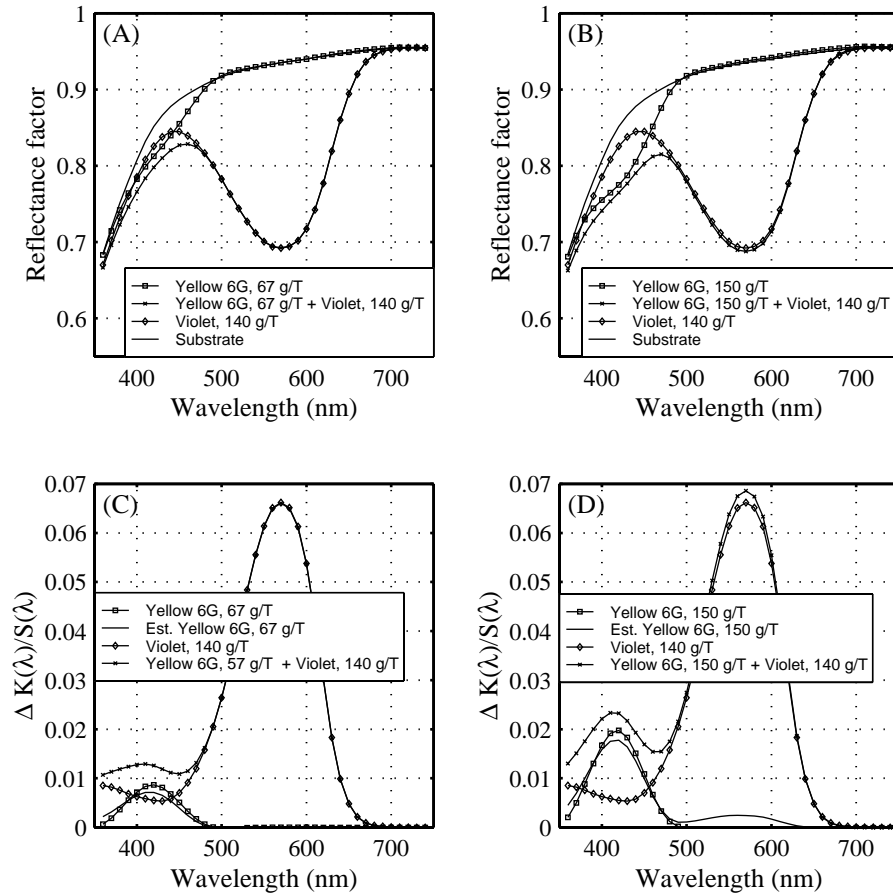


Figure 2.8: (A) Measured reflectance factors  $R(\lambda)$  of experiments containing combinations of 67 g/T of Pergasol Yellow 6G and 140 g/T Levacell Violet BNN, and substrate.

(B) Measured reflectance factors  $R(\lambda)$  of experiments containing combinations of 150 g/T of Pergasol Yellow 6G and 140 g/T Levacell Violet BNN, and substrate.

(C) Calculated  $\Delta \frac{K(\lambda)}{S(\lambda)}$  and estimated one based on additivity of dyeings in (A).

(D) Calculated  $\Delta \frac{K(\lambda)}{S(\lambda)}$  and estimated one based on additivity of dyeings in (B). Data from the group D sheets.

such as humic acid (in mill water), lignin (due to incomplete bleaching), alum (used as a sizing fixative), and  $\text{TiO}_2$  (used to improve opacity or whiteness) also absorb strongly in the ultra-violet. The anatase form of  $\text{TiO}_2$  absorbs ultra-violet less strongly than the rutile form, and is less problematic for FBAs [LK95]. These interfering substances can be present in varying amounts in recycled fiber. Due to the broad absorption bands of most dyes, almost any other dye will interfere to some extent with a fluorescent colorant including FBAs. Absorption band competition can be considered to have an effect equivalent to a reduction in  $\partial B(\zeta, \lambda)/\partial c$  for

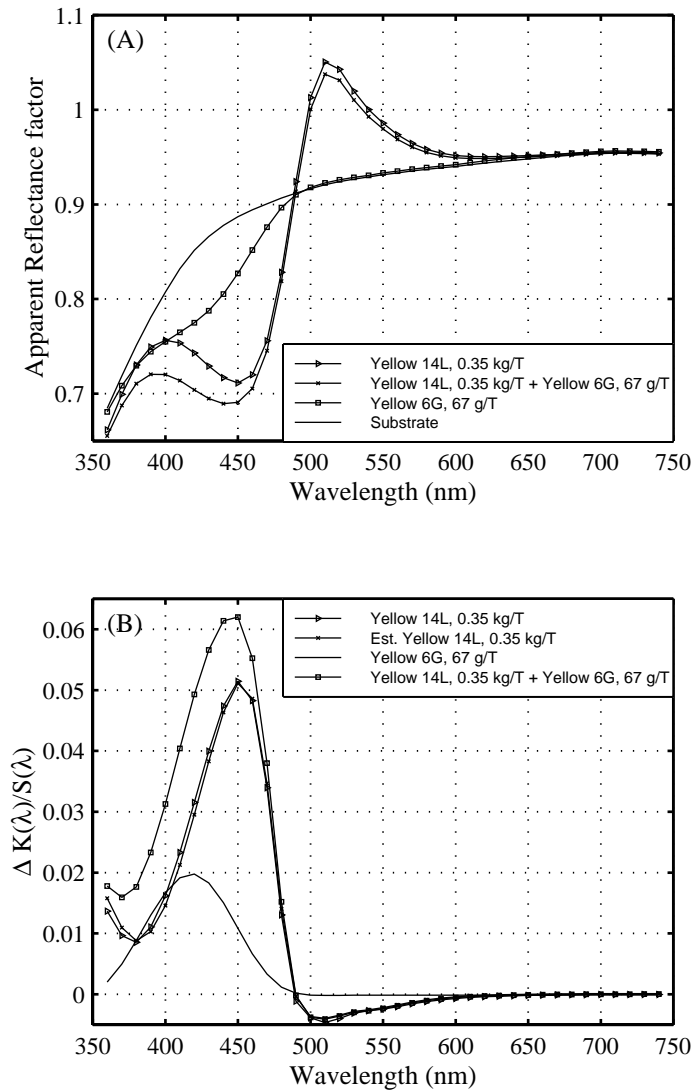


Figure 2.9: (A) Apparent reflectance factors  $R'(\lambda|D_{65})$  of the experiments containing combinations of 0.35 kg/T of Fastusol Yellow 14L and 67 g/T of Pergasol Yellow 6G, and substrate. (B) Calculated  $\Delta \frac{K(\lambda)}{S(\lambda)}$  and estimated one based on additivity of dyeings in (A).

some range of absorption wavelengths,  $\zeta$ , where  $B(\zeta, \lambda)$  is the effective radiance transfer from  $\zeta$  to  $\lambda$  and  $c$  is the colorant's concentration.

If the absorption band of a dye overlaps the emission band of a fluorescent agent, the coloring effects of both will be reduced or canceled. Thus, FBA occurring in broke or recycled fiber can partially cancel the effect of a yellow, orange, or red dye, as it will increase the amount of light in

the blue band. Similarly, a yellow, orange, or red dye in broke can partially cancel the effect of an FBA, as it will absorb some of the violet-blue light emitted by the FBA. However, combinations such as these are usually undesirable, as the cancellation is strongly illuminator dependent, so that metameric effects are likely.

An example of this phenomenon is given in Figure 2.10, where the absorption band of Lev-acell Violet BNN overlaps the emission band of Fastusol Yellow 14L. In subfigure (C),  $\Delta \frac{K(\lambda)}{S(\lambda)}$  values are calculated for combination dyeings of 0.35 kg/T of Yellow 14L and 65 g/T of the Violet using substrate as  $\frac{K_s(\lambda)}{S_s(\lambda)}$ . Recall that the Ganz extension to the Kubelka-Munk model is used for this analysis of linearity and additivity, since it is an attempt to preserve these features for fluorescence [Gan77], discussed above. The estimated  $\Delta \frac{K(\lambda)}{S(\lambda)}$  is also calculated based on the assumption of additivity for a combination dyeing of 0.35 kg/T of the Yellow 14L and 69 g/T of the Violet. Correspondingly in (D),  $\Delta \frac{K(\lambda)}{S(\lambda)}$  values are calculated and estimated based on additivity for combination dyeings of 0.35 kg/T of Yellow 14L and 140 g/T of the Violet using substrate as  $\frac{K_s(\lambda)}{S_s(\lambda)}$ . As can be seen, the existence of emission of a fluorescent dye in the absorption band of another dye affects its observed response and causes problems in additivity of  $\frac{K(\lambda)}{S(\lambda)}$ . Note, that the overlap of absorption band of Violet BNN with the excitation band of Yellow 14L is quite small, so that the effect of absorption band competition can be ignored in this simplified analysis. The measured handsheets belong to the group D sheets, and in all cases Fastusol Yellow 14L was dosed first. Absorption in the emission band of a fluorescent dye can be considered to have an effect equivalent to a reduction in  $\partial B(\zeta, \lambda)/\partial c$  for some range of emission wavelengths,  $\lambda$ .

When both FBAs and fluorescent colorants are present, fluorescent cascades can occur. If a fluorescent dye has an excitation band which overlaps the emission band of the FBA, then some of the light emitted by the FBA may in turn be absorbed by the fluorescent dye and re-emitted in the fluorescent dye's emission band. A fluorescent cascade changes  $\partial B(\zeta, \lambda)/\partial c$  in a complex way. In principle, a deliberate fluorescent cascade may be beneficial, in that the FBA is boosting the available light in the absorption band of the fluorescent dye. This averts saturation of fluorescence in the fluorescent dye, and allows higher concentrations to be used effectively. In practice, fluorescent cascades are problematic, and rarely intentional; their effect becomes dependent on absolute and relative power across a wide range of illuminator wavelengths. Current color measurement instruments can provide recognition of such effects, but do not provide a means of accurately measuring such effects, and hence coloring processes with fluorescent cascades are difficult to monitor and control.

### Intermolecular deactivation

Cationic chemicals such as cationic fixing agents, cationic auxiliary chemicals, synthetic wet strength agents and cationic retention agents and their residuals in general tend to dull and alter the shades of most dyes. In the case of anionic fluorescent dyes including FBAs, cationic agents may deactivate ("quench") it by intermolecular deactivation. This may cause a change in substantivity of the fluorescent dye as well as changes in geometric relaxation modes favouring internal conversion instead of photon emission

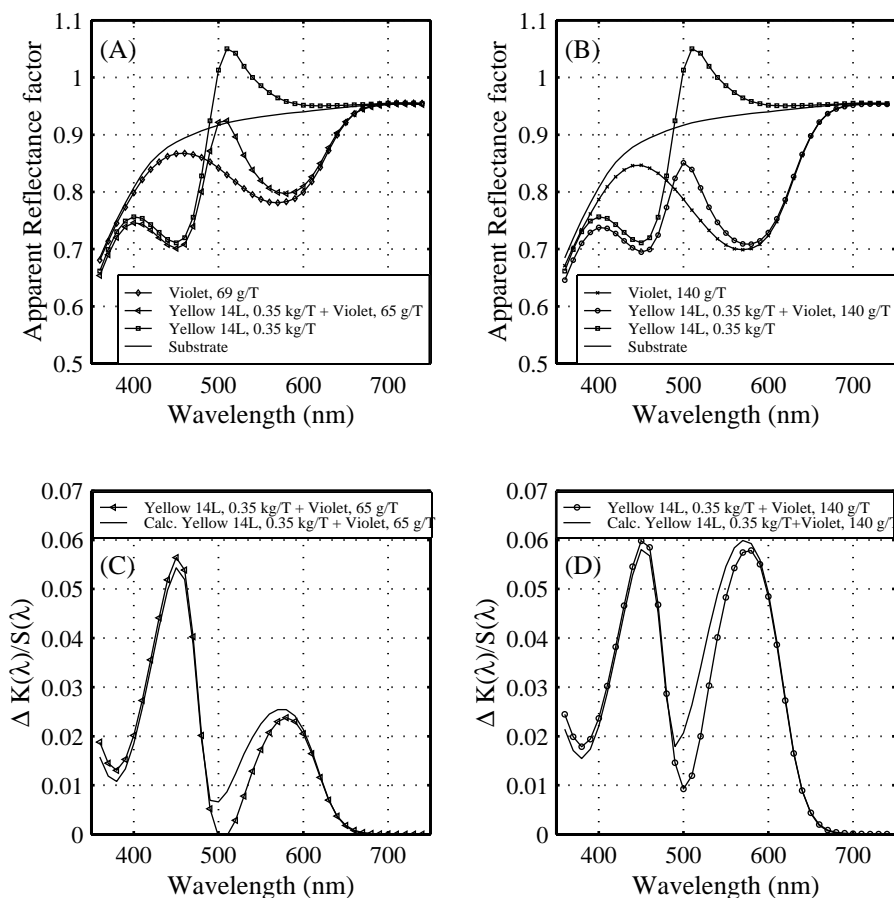


Figure 2.10: (A)-(B) Apparent reflectance factors  $R'(\lambda, D_{65})$  of experiments containing combinations of 69 g/T and 0.14 kg/T of Levacell Violet BNN, 0.35 kg/T of Fastusol Yellow 14L, and substrate.

(C) Calculated  $\Delta \frac{K(\lambda)}{S(\lambda)}$  and estimated one based on additivity of dyeings in (A).

(D) Calculated  $\Delta \frac{K(\lambda)}{S(\lambda)}$  and estimated one based on additivity of dyeings in (B).

An example of intermolecular deactivation is shown in Figure 2.11, which contains dyeings of 0.35 kg/T of Fastusol Yellow 14L, and a combination of 0.73 kg/T of Fastusol Yellow 14L with nominal 0.5 kg/T of Catiofast CS. Note, in the latter case the substantivity of Yellow 14L changed, while initial amount of dye-in-dyebath stayed the same. The calculated ratio of 'areas' on the excitation band with and without Catiofast CS is 2.3, based on  $\sum_{380nm}^{490nm} \Delta \frac{K(\lambda)}{S(\lambda)}$ . Whereas the calculated ratio of 'areas' of the emission band with and without Catiofast CS is 0.79, based on  $\sum_{490nm}^{650nm} \Delta \frac{K(\lambda)}{S(\lambda)}$ . Thus the estimated quantum efficiency of Yellow 14L decreased while the dye-on-fiber increased, indicating intermolecular deactivation. Data is derived from the group D

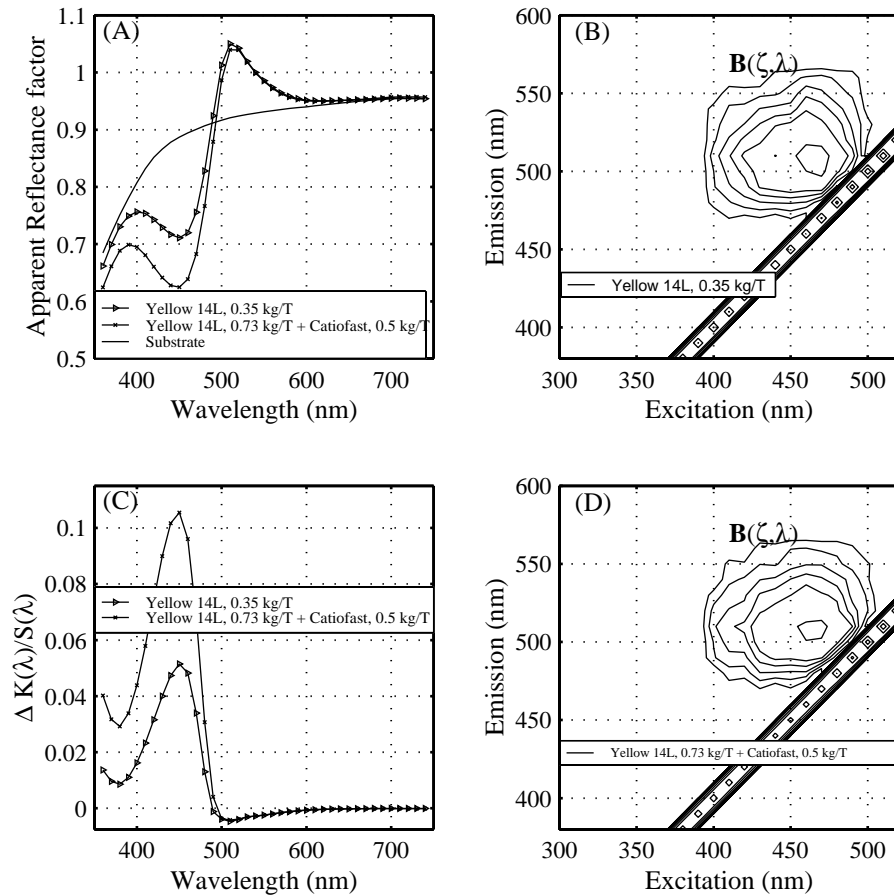


Figure 2.11: (A) Apparent radiance factors  $R'(\lambda|D_{65})$  of dyeings containing 0.35 kg/T of Fastusol Yellow 14L, combination of 0.73 kg/T of Fastusol Yellow 14L with nominal 0.5 kg/T of Catiofast CS, and substrate.

(B) and (D) Radiance transfer factor  $B(\zeta, \lambda)$  as contour map of dyeings in (A), contours at levels [0.002:0.002:0.008 0.01:0.005:0.1 0.2 0.3 0.5 0.7].

(C) Calculated  $\Delta \frac{K(\lambda)}{S(\lambda)}$  from (A). Data from the group D sheets.

sheets, and Fastusol Yellow 14L was dosed first.

Greening is a term used to describe the red-ward shift of both excitation and emission bands in dimers and aggregates compared to the spectra of single fluorescent dye molecules. When these aggregates occur in the presence of fluorescent dye monomers, there can be a significant overlap between the excitation band of the aggregate and the emission band of the monomer, leading to an increase in the apparent self-absorbance. A contribution of possible fluorescent dye molecule aggregation to apparent reflectance factor is presented in Figure 2.12 using Fastusol Yellow 14L. Based on the additivity of  $\frac{K(\lambda)}{S(\lambda)}$ , the  $\Delta \frac{K(\lambda)}{S(\lambda)}$  for Yellow 14L is calculated at 0.52 kg/T

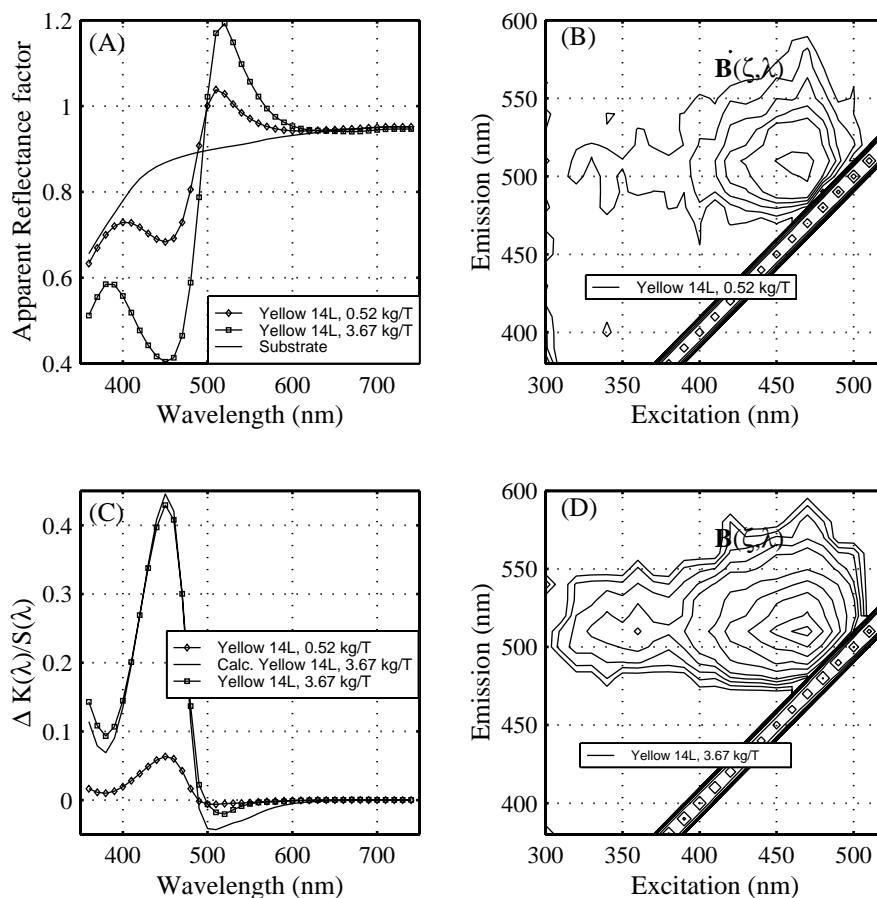


Figure 2.12: (A) Apparent reflectance factors  $R'(\lambda|D_{65})$  of the experiments containing 0.52 kg/T and 3.67 kg/T Fastusol Yellow 14L, and substrate.

(B) and (D) Radiance transfer factor  $B(\zeta, \lambda)$  as contour map of dyeings in (A), contours at levels [0.002:0.002:0.008 0.01:0.005:0.1 0.2 0.3 0.5 0.7].

(C) Calculated  $\Delta \frac{K(\lambda)}{S(\lambda)}$  for dyeings in (A). Data from the group D sheets.

and scaled for 3.67 kg/T of Yellow 14L. It is also calculated for dye-on-fiber at 3.67 kg/T of Yellow 14L, subfigure (B). As can be seen, additivity applies on the excitation band. However the observed emission as 'area' is 0.22 times smaller than estimated one indicating reduction in quantum efficiency, based on  $\sum_{490nm}^{650nm} \Delta \frac{K(\lambda)}{S(\lambda)}$ . A red-ward shift of the maximum of emission is observable in total radiance factor in subfigure (A), and in the Ganz negative absorption in subfigure (C). A red-ward shift for the maximum of excitation is not apparent. These colorings are from the group D sheets.

### Other forms of reduction

A partial reduction of fluorescence can occur if the intensity level of the incident light does not exceed the spectral absorptivity on the exciting wavelengths of a fluorescent colorant, so that the incident light in some exciting wavelengths of the fluorescent colorant becomes fully utilized before absorption is completed [Gru80, §XIII]. It can also occur at high usage rates of fluorescent colorant, even with strong illumination, and partial reduction may be difficult to distinguish from greening. When full reduction occurs, further addition of fluorescent colorant produces no increase in fluorescent emission.

In general the spectral distribution of the fluorescent emission depends only on the emission spectrum of the fluorescent species [Gru80, §X] at excitation wavelengths which do not overlap the emission band. At wavelengths where the excitation and emission bands overlap, the emission spectrum of the fluorescent species is dependent on the exciting wavelength. This is clearly illustrated in the radiance transfer factor measurements, such as in subfigure (D) of Figure 2.12. The intensity of emission depends on, (i) the quantum efficiency of the material, which may be a function of exciting wavelength, (ii) the total number of photons, adsorbed by the material, capable of exciting the fluorescence [Gru80, §X], and (iii) spectral absorption coefficient [Mie82b, §B].

Chemical decomposition of dyes and FBAs can also occur, if there is residual ozone or hypochlorite from bleaching or from water treatment. This may appear as shade and depth variations. Most dyes in use in the paper industry are bleachable with chlorine for deinking and broke bleaching purposes. Fluorescent colorants, and to a lesser extent dyes, are subject to gradual photodecomposition, especially when exposed to UV light.

Biocides, fungicides and defoamers may not be directly compatible with the colorants. They can sometimes lead to precipitation, aggregation or destruction of many colorants [Bur95]. Therefore, addition points for all wet end chemicals should be carefully selected to ensure the optimum efficiency of the individual components.

Some dyes have a few inconvenient properties, which may cause discrepancies in color measurement and visual matching of specimens, unless due care is taken. Photochromism is a reversible change in color of a specimen due to exposure to light (or other radiant flux) without appreciable heating of specimen [AST95b]. Thermochromism is a change in color with temperature change [AST95b].

## 2.3 Classification of Colorants

The selection of colorant class for each colored paper grade is greatly dependent on the furnish, the coloring method and intended use of the paper. They impose different requirements for light and bleed fastness (fastness for light and liquids), coloring economics and so on, but the primary colorants must have high affinity for used furnish.

Of dyes used in the paper industry, about 95 % of tonnage is applied to the stock and about 5 % at the size press [Mur92]. By dye class, the breakdown of tonnage is about 70 % anionic and

cationic direct dyes, about 25 % basic dyes and about 5 % acid dyes [CG88, §3]. Usage of FBAs is roughly evenly distributed between stock, sizing and coating applications, of which sizing may be slightly higher [Jok98]. The portion of pigments for stock and coating pigmentation is less than 5 % of the total colorant usage [CG88, §3].

There are many ways of classifying colorants which absorb visible light. The two most common ones are the Color Index [SDC96] system, which is followed here, and classification by chemical structure.

Acid dyes are suitable for dip and surface dyeing due to their high solubility in water. They are often azo dyes containing one or more water-solubilizing anionic groups which are almost invariably sulphonic acid groups or their sodium or ammonium salts ( $-\text{SO}_3^-$  in aqueous solution). They are quite small, often non-planar molecules. Their affinity for cellulose and other fibers is poor needing cationic fixing agents or aluminum sulfate, and their light fastness level is low, but better than basic dyes [Bur95]. The shade of some acid dyes is pH dependent. Ions of the acid dyes formed by electrolytic dissociation are anions. Anionic cellulose in water can attract these dyes with anionic charge only by means of hydrogen bonding or through Van der Waals forces, for which linearity and/or planarity of the molecule is required. They are quite bright dyes [Mur92]. They have a tendency to migrate during sheet drying due to particularly good solubility in hot water, leading to two-sidedness.

Basic dyes are suitable for stock dyeing of lignin containing pulps, and are mainly used in paper products not requiring good lightfastness, such as newsprint, packing and kraft papers. Their chemical structure may be triphenylmethane or azo dye with  $\text{N}^+(\text{R})_4$ -groups. The positive charge is associated with the chromophore, but it may be delocalised over the whole molecule. Their structure is neither planar nor large enough for sufficient affinity for cellulose. They dissociate in aqueous solution to give cations and react with the acid groups of lignin, resulting in good exhaustion properties on pulps containing lignin. They are bright, intense colors and quite economical [Mur92]. Their disadvantages are that sometimes aluminum sulfate or an anionic fixative such as tannic acid is required, and they can give silurian fibers when used with mixed fiber. 'Silurian' is a term used to sometimes to describe large differences in the dye adsorption onto individual fibers. Also mottling can occur especially in drying section, and they break down with hydrolysis. To avoid the latter two problems, it is advisable not to use dilute dye solutions. If dilution is forced, the dilution water should be pre-acidified with acetic acid to a pH of approximately 3.0 and protected from light [BD95].

Anionic direct dyes are suitable for stock dyeing of wood-free pulps and for surface dyeing. About 70 % of anionic direct dyes are polyazo dyes based on extended chains of conjugated double bonds [Mur92]. They are large, linear and/or planar molecules with an extensive, delocalised  $\pi$  electron system. This makes it possible for them to approach the cellulose chains more closely, participate in hydrogen bonding, and bind via Van der Waals forces and hydrophobic interactions. They have a good affinity for bleached cellulose fibers and are applicable over a wide pH range to give good all-round fastness properties. In aqueous solutions, direct dye molecules interact through hydrogen bonding to form very large aggregates (colloidal suspensions), which

reduces their solubility and facilitates their attachment to fibers. By joining two or more dye molecules together the properties of anionic direct dyes can be improved. This causes the molecular weight to increase, and consequently retention and bleed fastness properties are improved. Often, cationic fixatives are necessary in conjunction with the dye to improve its retention and bleed fastness, especially when high dye-on-fiber amounts are aimed. Depending on the dye and the dyeing process, better performance may be achieved when the cationic fixatives are added before or after the anionic direct dye.

Cationic direct dyes are suitable for stock dyeing of lignin and cellulose containing pulps and surface dyeing, and are extensively used in tissue dyeing. Cationic direct dyes appear in the Color Index as basic dyes, which is not strictly correct [Zol91, §7.9]. They differ from basic dyes in being larger and more linear and/or planar. Their positive charge may be pendant, or it may be delocalised. They form strong electrostatic attractions (salt links) in addition to hydrogen bonding, Van der Waals and hydrophobic interactions. Because of attached pendant cationic groups, the substantivity for cellulose and lignin is greatly increased [Mur92]. This substantivity to lignin may be further increased by a small addition of a cationic agent before dye addition to quench any anionic 'trash' which may be present in the system [Hin99]. Cationic direct dyes are less sensitive to variations in pH, temperature and water hardness than anionic ones [Mur92]. They tend to be expensive and generally exhibit variable light fastness.

Pigments are suitable for dyeing and shading via coating and stock, mainly used in products requiring good light fastness such as laminated papers or book covers. Pigments contain no solubilising groups and their charge is neutral, therefore they are insoluble in water. They are azo or phthalocyanine pigments in chemical structure. They do not have an affinity for furnish. They are deposited physically on the fiber via adhesion of the pigment particle, typically with the help of anionically charged dispersants, where adhesion is dependent on van der Waals forces and electrostatic effects. Advantages of pigments are high wet fastness and light fastness levels. Their disadvantages are a tendency to foaming, possible two-sidedness, and expense.

Fluorescent brightening agents are predominantly used in manufacture of white and high-white grades made from wood-free pulps. These chemicals are variously referred to as optical brightening agents (OBA), fluorescent brightening agents (FBA), or fluorescent whitening agents (FWA), which absorb in the ultra-violet (240 to 420 nm) with a maximum absorption at a wavelength between 340 and 380 nm and emit in the violet-blue range (mainly 380 to 500 nm) with a typical emission maximum between 425 and 450 nm [Mer90]. Almost all FBAs used in paper are derivatives of stilbene, and most are based on 4,4'-diaminostilbene-2,2' disulphonic acid. FBAs used in wet end, size press, and coating applications are chemically different, but all are anionic. Negative charge densities vary determined by the number of sulphonic acid groups ( $-\text{SO}_3\text{H}$ ) per molecule, being greatest for FBAs in the least aqueous environments. FBA molecules are adsorbed at suitable sites on the surface of fibers and fillers, and have different affinities for each substrate. Their bonding mechanism to fibers is similar to that of anionic direct dyes. However, cationic polymers cannot be used to increase anionic FBA exhaustion, since they are strong fluorescent quenchers. FBA light fastness is better when applied to the stock, which leaves most of

the added FBA embedded inside the paper compared to size press or coater application. The photodecomposition of FBA via formation of triplet states is a major reason for poor light fastness. Generally, light fastness decreases with increasing amounts of FBA. Specialty colored grades may also contain fluorescent dyes or pigments. These agents absorb and emit light at longer wavelength than FBAs, often with maximum excitation in blue or green and maximum emission in yellow or orange spectral regions.

## 2.4 Fiber Coloring

Cellulosic fibers have properties which fulfill the requirements of papermaking and dyeing: hydrophilic, able to absorb modifying additives, chemically stable, inherent bonding ability, water insoluble, relatively colorless and wide range of dimensions [Mur92, §1.7].

Dye sorption is influenced by the different accessibilities of the amorphous regions of the fiber during cellulosic fiber dyeing, and can be divided into four subprocesses [CBD<sup>+</sup>97]:

- dye in solution
- dye at fiber surface
- dye in the interior of the fiber
- dye-fiber bond

The diffusion rate of a dye from the solution to the fiber surface is enhanced by increasing dye concentration in the solution and solution temperature. Due to desirable substantivity of the dyes, they are more concentrated at interfaces of dyebath, including fiber surfaces.

The coloring properties of fibers and fines are determined not only by their chemical structure but also by their external and internal structure. Interfiber bonding can occur over most of the fiber surface, but dyeing or any other reaction can not take place within the crystalline regions of the fiber [Nev95, §1.10.1]. However, dyes are capable of hydrogen bonding to the inner fiber as well as the surface [Bur95]. Thus in principle, the hydroxyl groups in the fiber which are not involved with interfiber bonding are available for dye bonding, and will henceforth be referred to as dye bonding sites. These sites for dye molecules in broke and recycled fibers are often partly occupied by fillers and other chemicals so that they may not accept colorants to the same extent as virgin fibers.

A cellulose fiber is essentially a nonionic polymer [Asp97, §1.2.1]. However, when immersed in water it acquires a negative electrical potential in the immediate vicinity of the surface due to the ionization of surface groups associated with oxidized cellulose [Sco96, §3]. The surface charge of fibers and fines is a complex function of the chemical composition of the surfaces, the states of ionization which are influenced by the pH of the fiber-containing solution, and the nature and amounts of additional substances sorped mainly during pulping and bleaching, which commonly are anionic in nature and cause fibers to take a greater negative charge [Sco96, §3].

The negatively charged fiber or fine surface forms an electrical double layer when it is immersed in a solution containing ions. It attracts oppositely charged ions (counter-ions) and repels ions with the same charge (co-ions). In the classical coagulation theory, the total energy of interaction between two particles is a superposition of the electrostatic repulsive force and London-Van der Waals attractive force [Lin92]. Basically, there is a potential barrier which a particle must surmount in order to collide and unite with a second particle. The height of this barrier depends upon electrolyte concentration and counter-ion valency [Lin92]. This phenomenon is also referred to as an ion exchange capacity, and it has a great importance in coloring processes, especially with dye-fiber bonding by Van der Waals forces. Often more than one type of intermolecular force operates in the same dye-fiber bond. In any dye-fiber system the dominant force depends on the chemical character of the fiber and the chemical groups in the dye molecule. The relative strength of the intermolecular forces are in the following order (strongest to weakest) [Mur92, §9.5.1]:

- Electrostatic forces. Cationic dyes have an electrostatic attraction for anionic fibers and fines, while anionic dyes have an electrostatic repulsion.
- Hydrogen bonding. Dyes containing auxochromes for example hydroxyl, amino, azo, or amide groups can form hydrogen bonds with the hydroxyl groups present in cellulose [Mur92]. For hydrogen bonding to occur, the dye molecule must be oriented in a particular way relative to cellulose.
- Van der Waals forces are ineffective unless the dye and cellulose molecule are very close together. Thus dyes with large, delocalised, linear and/or planar structures are required. It is estimated, that the large, delocalised  $\pi$  electron system of the double bonds of direct dye molecules have an attraction for the nuclei of the atoms in the cellulose chains [Mur92].
- Hydrophobic interaction can be thought of as an attraction between the hydrophobic parts of a dye molecule and the hydrophobic parts of the cellulose chains. Cellulose is not hydrophobic as such.

Depending on the charge of the dye molecule relative to the negatively charged surface of the cellulosic fiber, either repulsive or attractive electrostatic forces can arise when a dye molecule approaches the fiber. Cationic direct dyes as well as basic dyes have a high affinity towards the anionic charge on the fibers and any other anionic charges. The cationic direct dye attaches to the anionic charge, and if intermolecular forces occur the dye molecule is insolubilized on the fiber, resulting in very little migration of dye-on-the fiber [KS91]. Anionic direct dyes require a cationic shield to be applied, before they can attach the anionic charge and bond due to intermolecular forces. The affinity of anionic direct dyes to cellulose is a poorly understood phenomenon. Hydrogen bonding has been thought to give rise to substantivity, but there is evidence that cellulose is so strongly hydrogen bonded to water that preferential hydrogen bonding to amino, hydroxy or other groups present within direct dyes seems quite improbable [Asp97, §1.4.6]. The most likely cause of substantivity appears to be a combination of relatively weak

forces, such as van der Waals forces which contribute to the association of dye ions with one another in the form of aggregates, either in solution or at the fiber-water surface boundary [Asp97, §1.4.6]. The sorption of anionic direct dyes seems to depend strongly on the size of the cations used in shielding [Sho95]. Also dye molecules with the highest molecular weight tend to bind first to the fibers.

If sufficient energy is present and the dye on the fiber surface is mobile, it can diffuse into the fiber structure via pores. Longer exposure times, higher process temperatures, and greater degrees of refining increase the proportion of a dye adsorbed on the interior of fiber. This requires, that the pores of the fiber are large in comparison to the molecular dimensions of the dye, and that the pore network is accessible to the dye molecules [CBD<sup>+</sup>97]. Thus the diffusion process is strongly dependent on the number and size of pores in the fiber in fixed dyeing conditions. In the case of mechanically pulped fibers, the inner wall region is inaccessible, because lignin acts as an inhibitor for fiber swelling during beating and refining. In contrast, for chemically pulped fibers, more of the internal fiber wall surface becomes accessible to water and other materials during beating, refining and papermaking.

Colorant adsorption onto fibers, fines and fillers is a complex process since the solid structure is generally complex and is not well defined. Even though cellulose dyeing is the most important of all dyeing processes in terms of quality, it is perhaps the least well understood [Gil89, §2.6.7]. It may follow a Langmuir-type adsorption isotherm in isolated sites at low colorant concentrations, monolayer adsorption with molecular interaction at high concentration, or multilayer adsorption or dye aggregation [Bur89, §1.5.4] as shown in Figure 2.13. The coloring dynamic equilibrium can be expressed in simplified form as [Asp97, §1.6]:

$$r_{ads} = r_{des} \quad (2.2)$$

where  $r_{ads}$  is the rate of adsorption and  $r_{des}$  is the rate of desorption.

In the Langmuir adsorption model, a finite number of possible adsorption sites exist on the surface. All adsorption sites are equivalent (homogeneous), and adsorbed molecules are considered to be non-interacting and immobile. The adsorption process can thus be modelled as a second order reaction between molecules from the fluid and vacant adsorption sites, and desorption as a first order reaction. Let  $[S]_f$  be the concentration of dye on fiber when all adsorption sites are occupied, so that  $[S]_f - [D]_f$  is the concentration of free sites, then adsorption and desorption rates are:

$$\begin{aligned} r_{ads} &= k_{ads}[D]_s ([S]_f - [D]_f) \\ r_{des} &= k_{des}[D]_f \end{aligned} \quad (2.3)$$

where  $[D]_s$  is the concentration of dye in solution,  $[D]_f$  is the concentration of adsorbed dye on the fiber,  $k_{ads}$  is the adsorption rate constant and  $k_{des}$  is the desorption rate constant for the particular set of dyeing conditions. In principle  $[D]_f$  is the surface concentration (g/m<sup>2</sup>, etc.) of

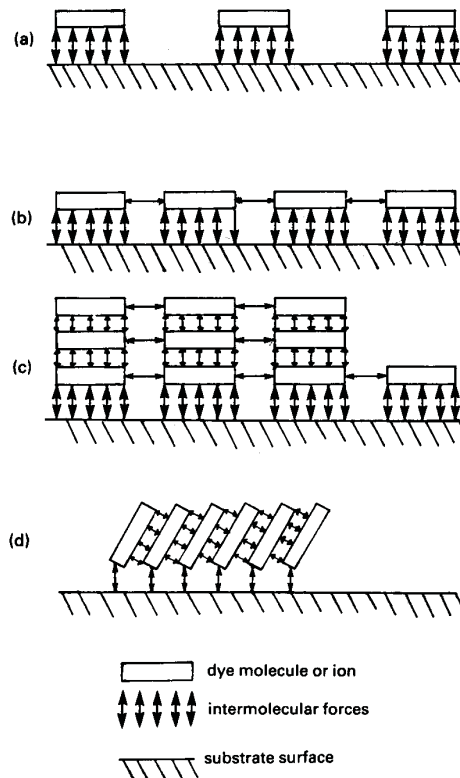


Figure 2.13: Different forms of adsorption on a surface: (a) Langmuir adsorption at low concentration, (b) molecular interaction at high concentration, (c) multilayer adsorption or dye aggregation, (d) non-Langmuir adsorption causing dye interaction and aggregation, [Bur89, §1.5.4].

dye on fiber. However, in cases where the specific surface area of the substrate is not known, but can be assumed to be constant, then volumetric or mass fraction concentrations ( $\text{kg}/\text{m}^3$  or  $\text{g}/\text{kg}$ , etc.) can be used instead. This is the case in this thesis, where dye on fiber concentrations are usually expressed as mass fractions ( $\text{g}/\text{kg}$ ). Setting the rates in Equation 2.3 to be equal and rearranging gives:

$$\frac{[D]_f}{[S]_f} = \frac{\frac{k_{ads}}{k_{des}}[D]_s}{1 + \frac{k_{ads}}{k_{des}}[D]_s} \quad (2.4)$$

where  $\frac{k_{ads}}{k_{des}}$  is the equilibrium constant  $b$  for the process. The rate constant of most chemical reactions follows an Arrhenius relation, which describes its temperature dependence [Zum98, §15.8]. The rate constants for the adsorption and desorption processes can be written as:

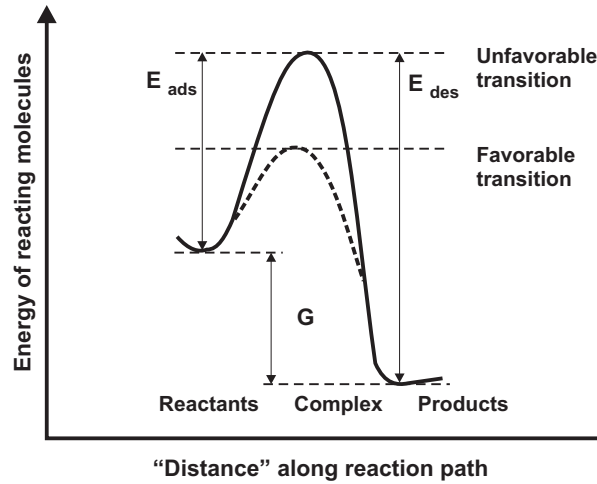


Figure 2.14: Schematic representation of energies involved in the transformation to products in an elementary reaction, after [Lev72, p.26].

$$\begin{aligned}
 k_{ads} &= A_{ads} \exp\left(-\frac{E_{ads}}{RT}\right) \\
 k_{des} &= A_{des} \exp\left(-\frac{E_{des}}{RT}\right)
 \end{aligned}
 \tag{2.5}$$

where  $E_{ads}$  and  $E_{des}$  are respectively the activation energies for adsorption and desorption,  $A_{ads}$  and  $A_{des}$  are the corresponding Arrhenius frequency factors,  $R$  is the universal gas constant, and  $T$  is the absolute temperature. The equilibrium constant  $b$  thus depends on the Gibbs free energy difference  $\Delta G$  for the adsorption process (see Figure 2.14):

$$b = \frac{A_{ads}}{A_{des}} \exp\left(-\frac{\Delta G}{RT}\right)
 \tag{2.6}$$

For adsorption of anionic dye onto anionic fibers the activation energy can be quite large, leading to poor adsorption rates. The presence of suitable cations catalyzes both adsorption and desorption by reducing the activation energy, and leads to much faster approach to equilibrium at the same temperature. This is illustrated schematically in Figure 2.14. The equilibrium constant is affected to a lesser extent.

There is no single isotherm which adequately describes all adsorption scenarios [Bur89, §1.5.4]. Various adsorption isotherms such as BET, Freundlich, and Langmuir have been used in dyeing studies. The BET isotherm is the most flexible, but has not been used much in dyeing studies [Gil89, §2.5], mainly due to the number of required parameters. The Freundlich isotherm does not have a limiting saturation value of dye on fiber. This cannot be physically justified

in stock dyeing. The Langmuir isotherm can be applied to most dyeing processes involving hydrophilic fibers [Gil89, §2.5], even though the fiber surfaces are commonly heterogeneous having adsorption sites at different potential energies and dye aggregation often occurs also by horizontal contact [Bur89, §1.5.4].

The simplest model describing the heterogeneity of solid surface is to assume that the surface is composed of several regions, each of which is homogeneous but need not be contiguous, and that adsorption onto different regions is described using different parameters for a common isotherm type [Do98, §6.2]. For example, if a Langmuir isotherm describes adsorption onto each region, then the composite isotherm is simply the summation of all the individual regional isotherms:

$$[D]_f = \sum_{j=1}^N \eta_j [D]_{f,j} = \sum_{j=1}^N \eta_j \frac{[S]_{f,j} b_j [D]_s}{1 + b_j [D]_s} \quad (2.7)$$

where the adsorption affinity constant  $b_j$  reflects the characteristics of homogeneous region  $j$ , and  $\eta_j$  denotes that region's fraction of the total number of adsorption sites.

## 2.5 Paper Coloring

Paper coloring falls into two categories: tinting (shading) and dyeing of paper. The aim of tinting paper is to achieve maximum whiteness for white paper grades. This can mean reducing or eliminating the yellowish hue caused by residual lignin in stock by adding blue dyes, pigments or FBAs, but more often tinting means shifting the shade of a white paper to an exact predetermined point in color space [Sch96]. All shades of copy paper all around the world aggregate along a straight line of which about 90 % lie in the blue-red quadrant of the CIE L\*a\*b\* color space [Sch96], Figure 2.15. Similarly the aim of paper coloring is to selectively reduce or increase the amount of reflected or emitted light in specific wavelength bands to reach a predetermined color of paper. This is commonly understood to be done only by using colorants, rather than by changing the amount of filler loading or stock blending.

A paper coloring system should be designed to meet the paper mill's specific requirements from both an operational perspective and product quality point of view. As a result, mills often rely on the consultation services of their colorant suppliers to optimize the coloration processes and in selecting the colorants to use.

### 2.5.1 Stock Coloring

In batch application the colorants are added in batches into the pulper or mixing chest. Usually liquid colorants are used, which allows pumping and metering colorants manually by batch, or using automatic or semi-automatic batch sequences. The advantages of batch application are: long contact time between dyes and fibers which allows use of dyes with lower substantivity,

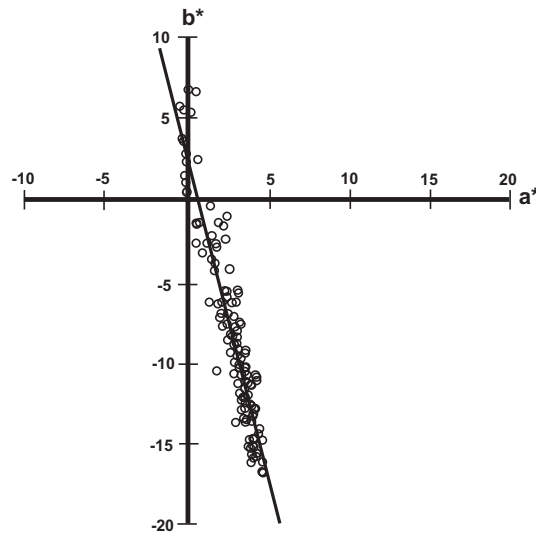


Figure 2.15: Color coordinates of white copy paper, after [Car98, Pamphlet Wp8006e].

deep shades are achievable and dye cost is lower for a given depth of coloring. The drawbacks are: long shade grade time, difficult to compensate for incorrect dye recipe, and closed loop color control is nearly impossible. Often, split stock dyeing is used for deep shade papers. Base dyeing is done in batches in the pulper and fine tuning of shade is done by continuous addition into the thick or thin stock, generally using the same dyes.

Continuous stock coloring of paper, especially within white and pastel shades, is increasing, as it offers benefits such as: quick shade changes, fast shade correction, minimum downtime for machine wash-up within color runs, and a closed loop color control with timely corrections. Its disadvantages are: significant capital expenditure for reliable and accurate colorant metering equipment, a need for good broke management, deep shades may not be attainable due to short contact time, high substantivity dyes are required, fixing agents may be required to achieve high dye-on-fiber and unwanted interactions with other additives may happen.

To control paper color, preferably one to three colorants are used simultaneously, optionally with FBA usage for white grade papers, to produce pure and bright shades and to minimize metamerism. Best controllability is reached, when the selected colorants have effects which are nearly orthogonal to each other in CIE  $a^*b^*$  subcolor space. This would give the largest attainable color gamut. Selection of colorants with effects which are nearly collinear in CIE  $a^*b^*$  subcolor space should be avoided. This may happen for example, if a yellow dye is to be used with a FBA.

Ideally, the total number of colorants used at the mill should be minimized. Good management of up to 12 colorants is much easier than 30. This is most important when automatic color control is to be used. The effects are seen as reduced tuning time and probably less need for manual intervention during color grade changes. Management of process waters is also easier

when fewer dyes are in use, since recirculation via pulpers, storage chests, and stock dilution involve large volumes and long residence times.

The colorants' addition order in relation to other chemical additives and fillers is important, as well as the rate of addition of each additive, and the residence time between addition points. Therefore, addition points of all wet end chemicals should be carefully selected to ensure the optimum efficiency of the individual components. In general, the order of addition of various wet end substrates may be as follows, but varies somewhat between mills and produced paper grades especially with dosage of fixing agents:

- Acid paper: Pulp - Filler - FBA - Dye - Pigment - Rosin Size - Alum - Fixing agent.
- Neutral or alkaline paper: Pulp - Filler - FBA - Dye - Pigment - Synthetic size - Cationic Polymers and Fixing agent.

In continuous coloration with a traditional white water system, the ideal addition point of dyes (especially anionic direct dyes with good affinity) and pigments is the suction side of the fan pump, Figure 2.16. If the affinity of dye for the fiber is poor, a longer contact time between fibers and dye is required. Then the addition point can be moved to a suitable location in the thick stock system, preferably not further down stream than the outlet of machine chest. Cationic direct dyes can be added into thin stock closer to the head box, because they do not suffer from retention problems, unlike pigments and anionic direct dyes with lower affinity [Car98]. The addition point of FBAs is often after the machine chest at the inlet of the stock pump to give longer contact time and to reduce unwanted reduction of FBA performance caused by other chemicals. In all cases a rapid thorough mixing of the colorants with the stock must be ensured to avoid mottling. Opinion is divided regarding the addition order when dyes of different types must be used in combination. Mill practice is to add first anionic dyes and then cationic dyes [Cib94] in continuous dyeing, or the exact opposite – first cationic dyes then anionic dyes [CD90, Cla97]. The latter order is thought to prevent possible reaction/precipitation, because complete dye exhaustion of cationic dyes occurs in less than three seconds [CD90]. Another opinion is that the dye with the best affinity should be added first [BD95]. In all cases, each dye group must be added at a different point into stock and sufficient time must be allowed for exhaustion of the first dye before adding the second dye.

For evenness in perceived color, colorant molecules must not only bond to cellulosic fibers and fines as discussed in Section 2.4, but also to fillers. Fillers such as titanium dioxide, kaolin clay, talc, calcium carbonate, aluminium trihydrate, silicas and plastic pigments, take on a wide variety of particle shapes, and their specific surface areas ( $m^2/g$ ) vary widely and are much higher than for fiber. It is very difficult to predict the magnitude and sign of surface charge that they will adopt when they are incorporated in papermaking systems [Sco96, §10]. Thus dyes have a varying substantivity for fillers, mainly via van der Waals forces and electrostatic forces. Preferably, the affinity of dyes on fillers should be tested for each stock application to minimize possible two-sidedness problems. The two-sidedness caused by fillers is often averted by the selection of another dye, use of retention aids, or changing the dye addition point in the process.

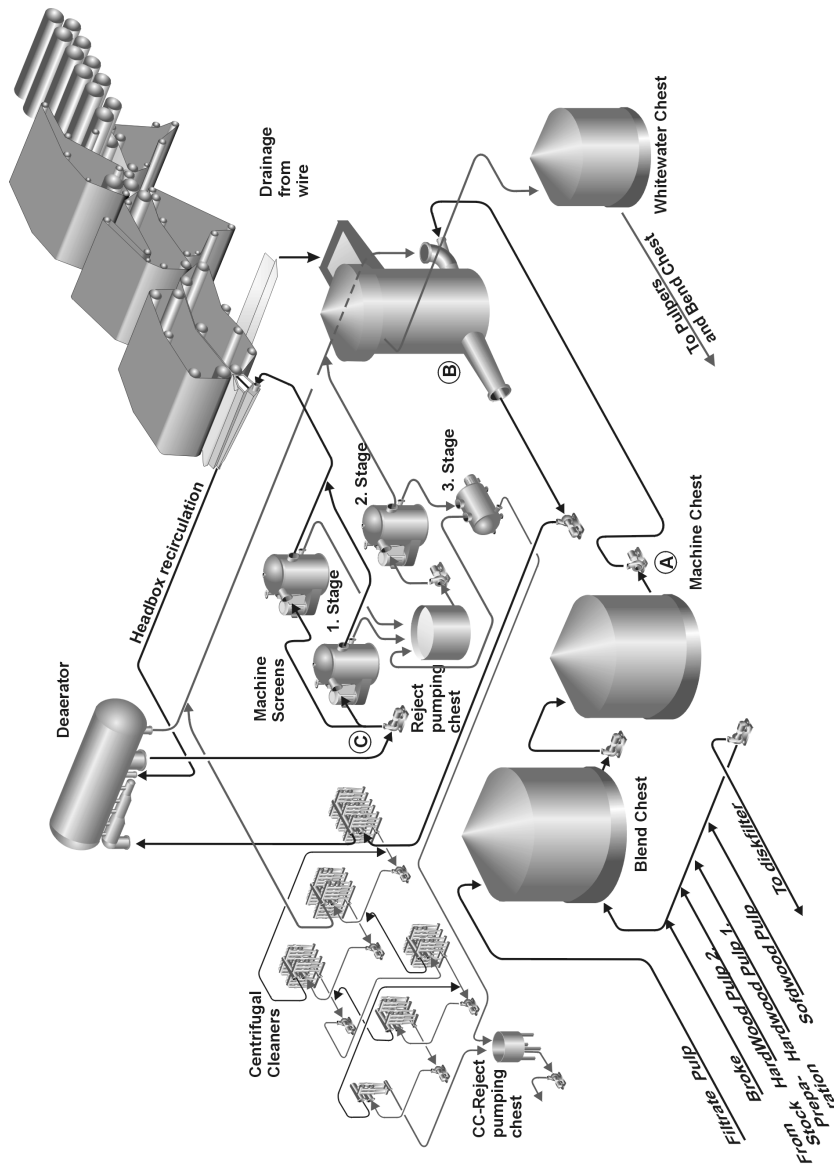


Figure 2.16: A traditional white water concept for a fine paper machine. For clarity, the saveall system, broke systems etc. are not shown. (A) location of a stock pump, (B) location of a fan pump, (C) location of a headbox feed pump.

Colorants are often diluted to suit performance of the metering equipment and fulfill the requirement of even coloring. There are some constraints concerning dilution of the dye, including pH and hardness of the dilution water and expected storage time in dilute form. Liquid FBAs are usually dosed at their delivered concentration. Often, the metered colorants are further diluted with carrying water(s) shortly before addition to stock, and the quality of these waters can affect the resulting paper color. Anionic direct dyes may sometimes be combined with acid dyes in the same solution, and basic dyes sometimes with cationic direct dyes. Even these combinations may be problematic: although the dyes have the same ionic character, reactions might be possible. Other combinations cause loss of dyes through precipitation.

For smooth tracking of colorant consumption, a good color controller contains master and slave setpoints for colorant dosage. The master setpoint defines the ratio of mass of pure colorant to total dry mass of production (or to mass of fiber, etc.). In principle, the required colorant dosage given as a ratio stays constant from one color grade run to the next and during basis weight and machine speed changes, when filler loading or stock quality is not changing. The slave setpoint and metered colorant dosage is calculated from the master setpoint, total dry mass and composition of production and applied dilution for a colorant. Also the colorant dosage ratio gives a uniform base for scaling amplitudes required in modelling paper coloring for a color controller.

For efficient coloring high retention of dye and pigment is essential. The dye retention is closely related to the retention of fines and fillers [Sco96, §2], and strongly depends on dyes' affinity at current conditions to used fibers, fines and fillers. When a dye is added to a stock, a coloring dynamic equilibrium is established between the dispersed fibers, fines, fillers and the suspending water, where the exposure time for adsorption onto fibers etc. prior to the next additive being introduced is short (5 s to 30 min). Variations in the coloring dynamic equilibrium (affinity) are seen often within few minutes at the reel, when dyes are applied at the inlet of the fan pump. The fine and filler retention cannot ever be perfect, due to for example headbox recirculation requirements and overflow from the wire pit. Thus a part of the colored fines and fillers ends up in short and long circulations of the white waters. This leads to several varying time domain responses of the colorants. If the equilibrium is disturbed, for instance by changing colorant or filler dosage or furnish quality, the new equilibrium may be reached after some time (some minutes to several hours) after the process change has finished depending on the design of white water system, and operation of broke and backwater systems. The design, terminology, instrumentation, and operating habits for these systems all vary between machine types and between geographic regions.

In Figure 2.17, the new Valmet OptiFeed white water system with a dilution headbox is depicted. For clarity, not all units of the white water system are shown. One of the aims of the new OptiFeed concept is to reduce grade change time by minimizing the blended stock volume. This fast blending process most likely will require use of cationic direct dyes or pigments to ensure colorless backwaters. As in a traditional white water concept, the first-pass filler and fine retention will dominate the dye and pigment retention, and challenges with the coloring kinetics

will continue.

The coloring kinetics of cellulose fibers has been studied under various conditions [HM98] and in the papermaking process [FWK95]. The latter reference clearly shows how sensitive the coloring results are for the adsorption time on fibers and all other process factors. Thus the key issue for the papermaker is to maintain the process conditions, chemical additive addition, filler load and stock quality as stable as possible during a colored paper run and to repeat those conditions as closely as possible the next time the same color grade is run. If changes are required, they should be introduced so that their effect on paper is slower than the achievable closed-loop response time of the colorants on paper. Hence their effect can be compensated by a color controller. As an example, oscillation can be introduced into the process if both the opacity control (manipulating a specific filler), and the color control (manipulating colorants), are both tightly tuned without modelling their cross effects. The correct approach is to have an opacity control which is less aggressive than the active color control. Based on the foregoing discussion, paper coloring is clearly a MIMO process, where the number of disturbances is generally higher than the number of controllable inputs (colorants) [SSK99c]. This thesis only studies the steady state modelling of coloring process at the equilibriums.

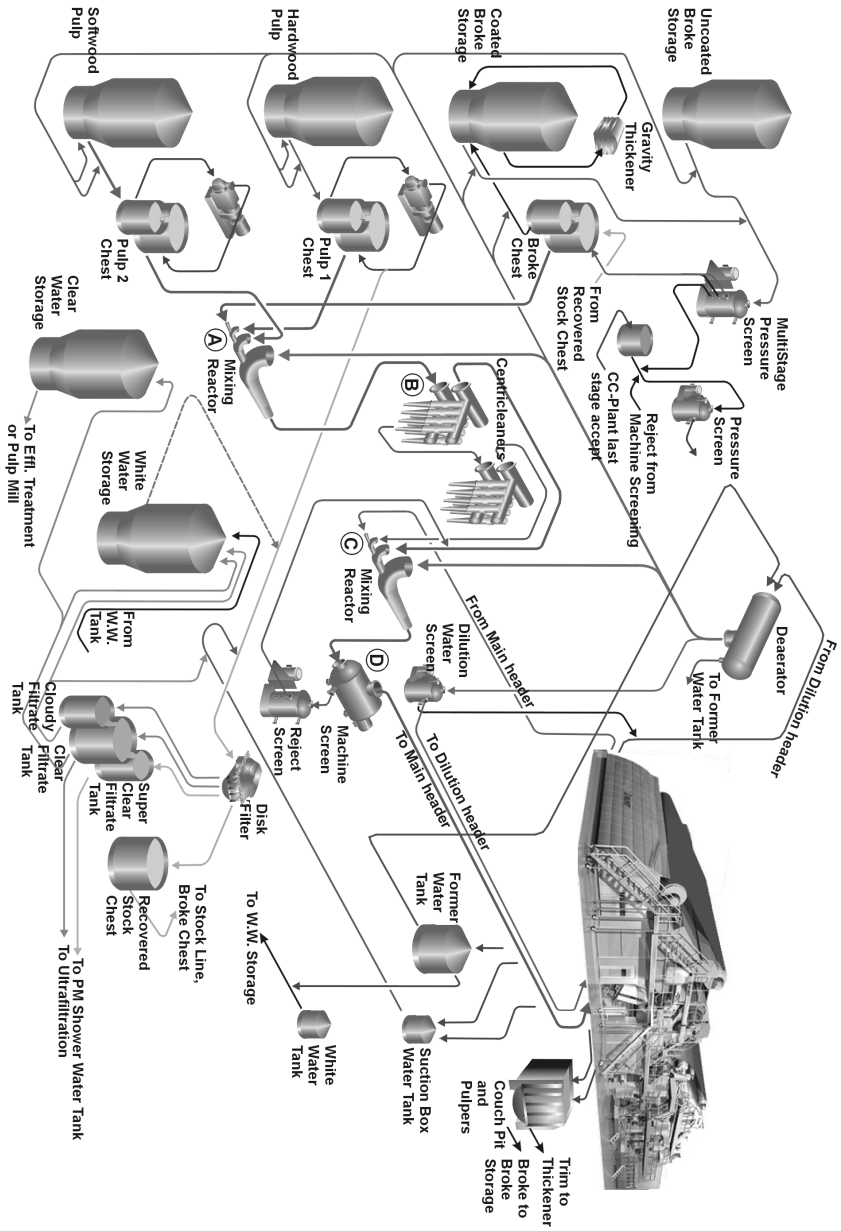


Figure 2.17: The new white water concept OptiFeed for coated fine paper with dilution headbox. Locations (A)-(D) represent preferred colorant addition locations. Courtesy of Valmet Stock Preparation.

## Chapter 3

# Color Measurement

It has been said that “to measure is to know”, to which must be added “...if you know what you are measuring” [Sha98]. The latter knowledge is sometimes lacking in measuring color. Therefore, the basis of physical colorimetry will be discussed in this chapter.

The perceived surface color of a specimen depends on three factors [Sin97]:

- the nature of the prevailing illumination under which the colored surface is viewed
- the interaction of the illuminating radiation with the colored species in the surface layers, particularly within the visible region
- the ability of the radiation that is transmitted, reflected, scattered and emitted from the colored surface to induce the sensation of color in the human eye/brain system

To transfer a visual process of deriving the attributes of color to an instrumental one, the CIE (La Commission Internationale de l'Éclairage) system of colorimetry was established in 1931. It attempts to simulate mathematically the perception of color and provide a standardized procedure for measuring and quantifying that perception [Mar98]. These colorimetric methods are for opaque matter or a pad of specimens of “infinite” thickness and are based on comparing the amount of light reflected from a specimen to that for the ideal diffusor under identical illuminating and viewing conditions.

### 3.1 Illuminating and Viewing conditions

CIE recommends four illuminating and viewing conditions to be used for diffusely reflecting non-fluorescent specimens [CIE86]:

- 45°/normal, (45/0)
- normal/45°, (0/45)

- diffuse/normal, (d/0)
- normal/diffuse, (0/d)

In the 45/0 condition, the specimen is illuminated by annular (continuous and uniform throughout the 360° of azimuth), circumferential (at regular intervals around the 360° azimuth) or uniplanar beams (one or two) whose effective axes are at an angle of  $45^\circ \pm 2^\circ$  from the normal to the specimen surface. The angle between the direction of viewing and the normal to specimen should not exceed  $10^\circ$ . The angle between the axis and any ray of an illumination beam should not exceed  $8^\circ$ , which restriction also applies in the viewing beam [CIE86]. For 0/45 the illumination requirements are interchanged with the viewing requirements and vice versa.

In the d/0 condition, the specimen is illuminated diffusely by an integrating sphere. The angle between the normal to the specimen and the axis of the viewing beam should not exceed  $10^\circ$ . The angle between the axis and any ray of the viewing beam should not exceed  $5^\circ$ . The integrating sphere may be of any diameter provided that total area of the ports does not exceed 10 % of the internal reflecting sphere area [CIE86]. For 0/d the illumination requirements are interchanged with the viewing requirements and vice versa.

ISO's requirements for the d/0 condition are different [ISO98a]. The internal diameter of an integrating sphere is 150 mm and the total area of the apertures and other non-reflecting area should not exceed 13 % of the area of the inner surface of the sphere, and only reflected rays within a cone whose vertex is in the test piece aperture and whose half-angle is not greater than  $4^\circ$  shall fall on the receptor. A gloss trap of non-reflective material subtending a half angle of  $15.5^\circ$  is placed around the receptor.

The first three listed illuminating and viewing conditions give values of reflectance factor,  $R(\lambda)$ , and the normal/diffuse condition gives the reflectance,  $\rho(\lambda)$ , when measuring diffusely reflecting specimens. In the case of fluorescent color measurement, it is not strictly valid to refer to a reflectance factor, but only to a radiance factor [Bat97].

The surface of a paper specimen often exhibits directionality and has a varying degree of texture and a relatively low gloss (except for some specialty papers). Based on these optical characteristics, specular component included or excluded conditions may be used for non-fluorescent specimens, because these conditions are relatively insensitive to polarization or sample directionality effects [Zwi98, §10]. However, for colorant formulations involving Kubelka-Munk or other turbid-medium theory either d/0 condition with specular component excluded or 45/0 condition may be used [Ric88].

The 45/0 condition with circumferential or annular illumination is commonly used in today's on-line color measurement instruments in the paper industry. However, most color measurement instruments in the paper mills' quality laboratories follow the d/0 condition or t/0 (total/normal). The condition t/0 includes all regularly reflected light (specular component included, SCI), while condition d/0 excludes it (specular component excluded, SCE). Due to differences in the gloss trap implementations in instruments equipped with an integrating sphere, the spread of measurement results under the specular component excluded condition is larger than when the specular component is included.

However, it should be noted, that results from instruments equipped with integrating spheres in either d/0 or t/0 conditions will differ from results using instruments with directional 45/0 geometry, and that these differences will be specimen-dependent.

For measurement of fluorescent specimens 45/0 or 0/45 conditions are required to minimize specimen-instrument interaction [AST95d]. Sphere instruments with d/0 condition produce erroneous results as the light in the sphere is contaminated and colored by the radiation emitted from the sample [Bat97]. If such an instrument is used for color measurement, it is possible to reduce the errors caused by self-illumination from a sample by making measurements using the smallest aperture available and making specular component excluded measurement. These requirements are commonly in conflict with currently used measurement standards and procedures. In all cases, a spectrophotometer with a light source that correctly simulates the desired standard illuminant is required.

## 3.2 Color stimulus

The perception of color can not be measured. However, the characteristic of the visual stimulus (spectral radiant exitance) by which an observer may distinguish color differences between two fields of view of the same size, shape, and structure, can be measured under unpolarized illumination as the spectral composition of the visual stimulus.

The physical colorimetry of non-fluorescent specimens can be understood as a special case of colorimetry of fluorescent specimens, in which the fluorescent emission approaches zero. The color of an opaque specimen is determined by the color stimulus function  $M(\lambda|S)$  which contains the combined information of reflected and luminescent radiation leaving the surface under illumination conditions  $S$ .

The measurement quantity of interest is most often the total radiance factor  $\beta_T(\lambda|S)$  under one or more specified illumination conditions  $S$  of arbitrary irradiation. It may be derived from knowledge of steady-state spectral radiant exitance (color stimulus function)  $M(\lambda|S)d\lambda$  detected in infinitesimal band  $d\lambda$  at wavelength  $\lambda$  from a non-self luminous specimen illuminated continuously from the same side as viewed using specified illuminating and viewing conditions with spectral irradiance  $S(\zeta)d\zeta$  of an illuminator  $S$  in infinitesimal bands  $d\zeta$  at each wavelength  $\zeta$ :

$$M(\lambda|S) d\lambda = \int_{\zeta=\zeta_0(\lambda)}^{\zeta=\lambda} \beta(\zeta, \lambda) d\lambda S(\zeta) d\zeta \quad (3.1)$$

where  $\beta(\zeta, \lambda)$  is the radiance transfer function from  $\zeta$  to  $\lambda$  [JW75, §2]. Note that for fluorescence  $\beta(\zeta, \lambda) = 0$  for  $\zeta > \lambda$ , always, and  $\beta(\zeta, \lambda) = 0$  for  $\zeta < \zeta_0(\lambda)$ , where  $\zeta_0(\lambda)$  is the minimum absorption wavelength for which a fluorescent emission occurs at  $\lambda$ . The radiance transfer function  $\beta(\zeta, \lambda)$  for a specimen varies as discussed in Section 2.2.3. It will also exhibit variation with illuminator intensity due to triplet effects if the illuminator is sufficiently energetic.

It is convenient to restate the steady-state spectral radiant exitance in Equation 3.1 in a slightly

different form as sum of the reflected spectral radiant exitance  $M_R(\lambda|S)$  and luminescent spectral radiant exitance  $M_L(\lambda|S)$ :

$$M(\lambda|S) d\lambda = M_R(\lambda|S) d\lambda + M_L(\lambda|S) d\lambda \quad (3.2)$$

This can be further restated to more closely resemble definitions used in current colorimetric practice, and which were largely developed for measurement of non-fluorescent specimens, but which are also used for fluorescent specimens:

$$M(\lambda|S)d\lambda = \beta_R(\lambda)S(\lambda) d\lambda + \int_{\zeta=\zeta_0(\lambda)}^{\zeta=\lambda-d\lambda} \beta(\zeta, \lambda) d\lambda S(\zeta) d\zeta \quad (3.3)$$

where  $\beta_R(\lambda) \equiv \beta(\lambda, \lambda)$  is the reflected radiance factor at wavelength  $\lambda$ , and is illuminator independent. In this form, the integral term contains the fluorescent effects and is clearly illuminator dependent for fluorescent samples, but is identically zero for all non-fluorescent samples. The illuminator  $S$  is understood to specify the relative spectral power distribution as well as the absolute power of the illumination used to irradiate a specimen.

The total radiance factor  $\beta_T(\lambda|S)$  and luminescent radiance factor  $\beta_L(\lambda|S)$  for the specimen irradiated by any illumination condition (illuminator)  $S$  with known spectral irradiance  $S(\lambda)d\lambda$  in infinitesimal bands  $d\lambda$  at each wavelength  $\lambda$  can be calculated based on Equation 3.4:

$$\beta_T(\lambda|S) = \frac{M(\lambda|S)d\lambda}{M_{\zeta=\lambda}(\lambda|S)_{PRD}d\lambda} = \beta_R(\lambda) + \frac{\int_{\zeta=\zeta_0(\lambda)}^{\zeta=\lambda-d\lambda} \beta(\zeta, \lambda) S(\zeta) d\zeta}{S(\lambda)} \quad (3.4)$$

Equation 3.4 encapsulates the difficulties involved in fluorescent color measurement.

### 3.3 Radiance Factors

There are two principal methods used to establish the radiance factors of a fluorescent specimen:

- a one-monochromator method, with polychromatic irradiation and monochromatic viewing (spectrophotometer)
- a two-monochromator method, involving monochromatic irradiation and monochromatic viewing (spectrofluorimeter).

The first method has an additional requirement, the illuminator of the instrument must closely approximate the desired CIE standard illuminant. The problem is, that the CIE standard illuminant  $D_{65}$  recommended for use in colorimetry of fluorescent specimens cannot easily be realized with sufficient accuracy as an illuminator. For colorimetry of non-fluorescent specimens this is not a limitation and the method gives results which correlate quite well with visual evaluations, as long as the illuminator contains adequate power at all visible wavelengths.

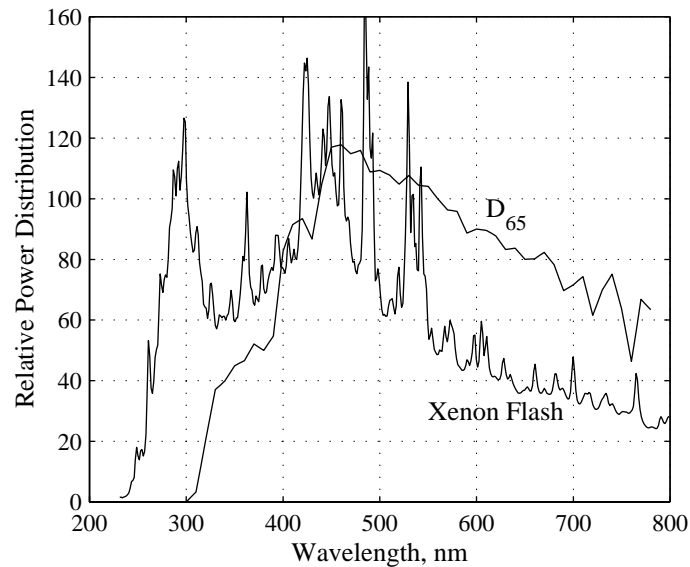


Figure 3.1: Relative spectral power distribution of  $D_{65}$  and typical discharge of a Xenon flash lamp [Kor00].

However, for colorimetry of fluorescent specimens the deviations in spectral power distribution of actual illuminators from the specified standard illuminant are major factors contributing to the poor reproducibility of measurements. Figure 3.1 shows the relative spectral power distribution of the standard illuminant  $D_{65}$  and a typical discharge of a Xenon flash lamp. Flash lamps exhibit considerable spectral power variation between discharges. Other major factors are color temperature variation between bulbs, bulb aging causing reduction in UV radiation, and efficiency of optical paths within instruments.

### 3.3.1 Spectrophotometer

Most commercial color measurement instruments are spectrophotometers, which employ the one-monochromator method (normally in viewing) with or without a variety of ad hoc extensions for fluorescent specimens. Many of these extensions for fluorescent specimens have become common practice, and some have been standardized, such as throttling the amount of UV in illumination by moving a UV cutoff filter across the light path based on for example ISO brightness under illumination with CIE standard illuminant C [Bri99]. Others are proprietary, such as algorithms using a known fluorescent standard with at least two levels of UV illumination [IHKM97, Alg87]. A common requirement for these method to work is, that the fluorescent standard must have the same excitation and emission properties as the fluorescent dyes existing in the fluorescent specimen to be measured.

Spectrophotometry uses relative measurements, and each wavelength band  $\delta\lambda$  is treated as

independent of the others, thus the method is suitable only for non-fluorescent specimens. A finite estimate of reflectance factor  $R(\lambda)$  is calculated for each wavelength band  $\delta\lambda$  of  $\lambda$  as the ratio of the reflected spectral radiant flux  $\Phi_R(\lambda|S)\delta\lambda$  of the specimen delimited by the given cone in that band to that in the same directions for the perfect reflecting diffuser  $\Phi_R(\lambda|S)_{PRD}\delta\lambda$  identically irradiated using the same rich light source  $S$ , which must contain adequate power at all measured wavelengths. Whereas there is no material surface which has the properties of the perfect reflecting diffuser, the reflectance factors of suitable materials ( $\text{MgO}$ ,  $\text{BaSO}_4$ , Spectralon) are calibrated as white standards in terms of the ideal uniform diffuser.

$$R(\lambda) = \frac{\Phi_R(\lambda|S)\delta\lambda}{\Phi_R(\lambda|S)_{PRD}\delta\lambda} = R(\lambda)_{Std-White} \frac{\Phi_R(\lambda|S)\delta\lambda}{\Phi_R(\lambda|S)_{Std-White}\delta\lambda} \quad (3.5)$$

where  $R(\lambda)_{Std-White}$  is the calibrated reflectance factor of the white standard.

This is a convenient relation for spectrophotometers, since only ratios of radiances in the same band are used, and hence absolute measurements are not required. Also, it is not necessary to know the exact spectral power distribution of the irradiance of the used illuminator, provided it is stable and adequate. Thus a convenient implementation of this would be:

$$R(\lambda) = R(\lambda)_{Std-Black} + (R(\lambda)_{Std-White} - R(\lambda)_{Std-Black}) \frac{\Phi_R(\lambda|S)\delta\lambda - \Phi_R(\lambda|S)_{Std-Black}\delta\lambda}{\Phi_R(\lambda|S)_{Std-White}\delta\lambda - \Phi_R(\lambda|S)_{Std-Black}\delta\lambda} \quad (3.6)$$

where  $\Phi_R(\lambda|S)_{Std-Black}$  is the reading recorded with the calibrated black reflectance standard  $R(\lambda)_{Std-Black}$  or a light trap for zero-scale,  $\Phi_R(\lambda|S)_{Std-White}$  is the reading recorded with the calibrated white standard  $R(\lambda)_{Std-White}$  for full-scale, and  $\Phi_R(\lambda|S)$  is the reading recorded with a specimen for wavelength band  $\delta\lambda$  of  $\lambda$ .

This procedure is also applied to fluorescent specimens, producing an apparent reflectance factor  $R'(\lambda|S)$ . This apparent reflectance factor is often treated as if it was the reflectance factor  $R(\lambda)$  without consideration of fluorescent effects. If  $R'(\lambda|S) \equiv R(\lambda)$  then:

$$R(\lambda)_{Std-White} \frac{\Phi(\lambda|S)\delta\lambda}{\Phi_R(\lambda|S)_{Std-White}\delta\lambda} \equiv R(\lambda)_{Std-White} \frac{\Phi_R(\lambda|S)\delta\lambda}{\Phi_R(\lambda|S)_{Std-White}\delta\lambda} \quad (3.7)$$

Clearly, this holds only for wavelengths for which fluorescent emission is negligible as seen from Equation 3.3, and such a condition is implicit in spectrophotometric color measurements. The spectrophotometrically measured apparent reflectance factor  $R'(\lambda|S)$  becomes dependent on the relative spectral power distribution of the irradiance of the used illuminator, especially the relative powers in the excitation and emission wavelength ranges of the fluor. For wavelengths in the emission band of the fluor, this apparent reflectance factor will exceed the reflectance factor by a variable systematic amount, which depends on the illuminator's spectral power distribution in both excitation and emission bands, as well as on the fluors' radiance transfer function

$\beta(\zeta, \lambda)$ . Thus spectrophotometers measure the combination of the reflectance factor with prevailing excitation-emission effects, and treat the total remitted light as if it were all reflected light. The problems of fluorescent colorimetry using the one-monochromator method are well studied [BS94, GT94, Bat97, SS99] and will not be further discussed here.

The discussion above is for an instrument with the perfect spectral responsivity function. Typically, only relative spectral responsivity is required, which is the product of the slit-scattering function  $f_\lambda(\mu)$  and the responsivity factor  $r^f(\lambda)$ . The latter one is equal to the product of the relative spectral responsivity of the detector and the spectral transmittance of the monochromator, and particularly at short wavelengths includes also the grating efficiency [Kos97, §4.6]. The slit-scattering function is largely responsible for the central shape of the spectral responsivity function and its magnitude in the wings [Kos97, §4.6]. In discussion below, the responsivity factor is assumed to be constant and independent of the wavelength. The slit-scattering function would be perfect, when the monochromator (dispersive element) has a rectangle shaped slit-scattering function  $f_\lambda(\mu)$  with unity amplitude, and finite narrow spectral bandpass  $\Delta\lambda = \delta\lambda$ , which is defined as the width in nanometers at half energy of the band of wavelengths transmitted by the dispersive element [AST95a]. Usually slit-scattering functions of grating and prism spectrometers are symmetrical and take shapes like triangular, trapezoid, diffraction profile or Gaussian [Mie82a, §I.3]. Rectangle and triangular shapes of the slit-scattering functions are shown in Figure 3.2. The spectral bandpass can not be infinitely narrow due to reduction in signal. For the rectangle shaped slit-scattering function with unity amplitude the reflectance factor  $R(\lambda_i)$  at wavelength  $\lambda_i$  is actually a mean value over the spectral bandpass  $\Delta\lambda$  [Sha00]:

$$R(\lambda_i) = \frac{1}{\Delta\lambda} \int_{\lambda - \frac{\Delta\lambda}{2}}^{\lambda + \frac{\Delta\lambda}{2}} \rho(\mu) d\mu \quad (3.8)$$

where  $\rho(\mu)$  is the measured reflectance at the sufficiently narrow spectral bandpass. Since the reflectance is normally a continuous function, some wavelength  $\mu_i$  must exist within the integration band  $[\lambda - \frac{\Delta\lambda}{2}, \lambda + \frac{\Delta\lambda}{2}]$ , such that  $R(\lambda_i) = \rho(\mu_i)$ .

Thus the slit-scattering function low-pass filters the measured reflectance factor so that the peaks are too broad and the valleys are too shallow. This spectral distortion is described mathematically by the convolution integral [Mie82a, §I.3], [Shu79]. The following replacement should take place in above equations, where  $\Phi_R(\lambda_j|S) \delta\lambda$  is replaced by its finite estimation or measurement  $\Psi_{S,\lambda_j}$ :

$$\Psi_{S,\lambda_j} \rightarrow \int_{-L}^{+L} f_\lambda(\mu) \Phi_R(\mu|S) d\mu = \int_{-L}^{+L} f_\lambda(\mu) \rho(\mu) S(\mu) d\mu \quad (3.9)$$

where  $f_\lambda(\mu)$  is the slit-scattering function, which varies relative to  $\lambda$ ,  $S(\mu)$  is the spectral irradiance of the illuminator, and  $\rho(\mu)$  is the measured reflectance with the sufficiently narrow spectral bandpass.

If the derivatives of the reflectance factor are small enough, this does not have a great effect. If the derivatives are large and the spectral bandpass is wide, the measured reflectance factor

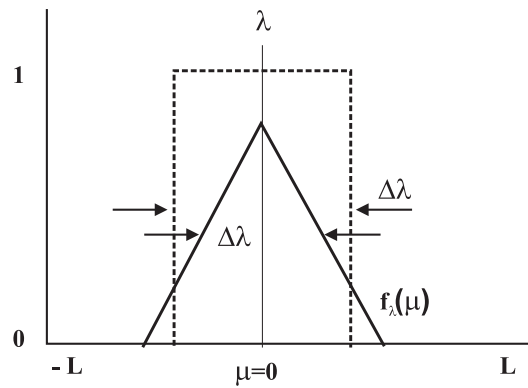


Figure 3.2: Perfect rectangular and triangular type slit-scattering functions.

looses sharpness of its peaks and valleys, which occurs at pastel and deep shade specimens and specimens containing FBAs and other fluorescent colorants. Let  $F$  denote the convolution operator corresponding to the slit scattering function  $f_\lambda(\mu)$ . Now Equation 3.5 can be rewritten as:

$$R(\lambda) = \frac{F^{-1} \Psi_{S,\lambda}}{F^{-1} \Psi_{S,\lambda_{PRD}}} \quad (3.10)$$

where  $F^{-1}$  is the deconvolution operator.

Shumaker has said in 1979, that exact deconvolution is not possible except by iterative refinement [Ole00]. In the publication [CIE86] it is stated, that the color stimulus function is required to be known at 5 nm wavelength intervals over the wavelength range 380 nm to 780 nm, but nothing is said about required spectral bandpass or deconvolution. Thus the measured results between commercial spectrophotometers are not usually in agreement.

### 3.3.2 Spectrofluorimeter

The two-monochromator method involves two separated monochromators, which provide monochromatic irradiation and monochromatic detection. In this method a specimen is irradiated with radiance of spectral energy  $S(\zeta)d\zeta$  in an infinitesimal band  $d\zeta$  at an incident wavelength  $\zeta$ . At the same time the steady-state spectral radiant exitance  $M(\lambda|S(\zeta)d\zeta)d\lambda$  of a specimen in an infinitesimal band  $d\lambda$  at emission wavelengths  $\lambda$  are measured. This process is repeated for each incident wavelength  $\zeta$  in the excitation spectrum covering at least the emission band characteristic of a fluorescent specimen.

The radiance transfer function  $\beta(\zeta, \lambda)$  is defined as the two-dimensional power distribution function of the radiant exitance  $M(\lambda|S(\zeta)d\zeta)d\lambda$  of the sample for given excitation and emission wavelengths, divided by the spectral radiant exitance  $M_{\zeta=\lambda}(\lambda|S(\zeta)d\zeta)_{PRD}d\lambda$  of a perfect

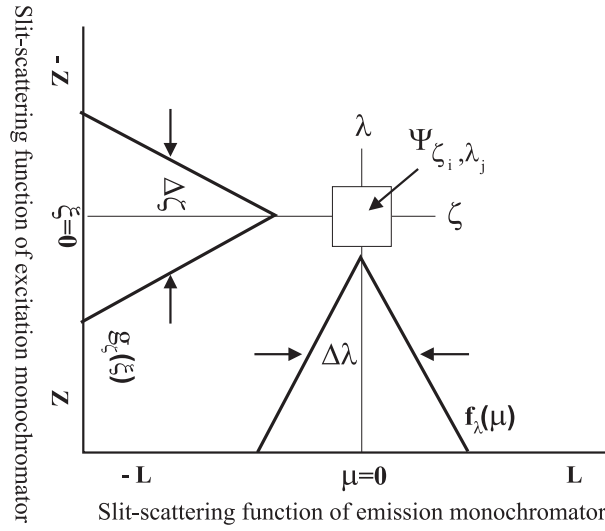


Figure 3.3: Effect of slit-scattering functions to measured finite estimate of steady-state radiant exitance  $\Psi_{\zeta_i, \lambda_j}$ .

reflecting diffuser, which is identically irradiated and viewed with infinitesimal bands  $d\zeta$  and  $d\lambda$  [Sha00], [WS82, §3.12.3]:

$$\beta(\zeta, \lambda) = \frac{M(\lambda|S(\zeta) d\zeta) d\lambda}{M_{\zeta=\lambda}(\lambda|S(\zeta) d\zeta)_{PRD} d\lambda} \quad (3.11)$$

since, from Equation 3.1

$$M(\lambda|S(\zeta) d\zeta) d\lambda = (S(\zeta)d\zeta) \beta(\zeta, \lambda)d\lambda \quad (3.12)$$

$$M_{\zeta=\lambda}(\lambda|S(\zeta) d\zeta)_{PRD} d\lambda = (S(\zeta)d\zeta) 1d\lambda \quad (3.13)$$

This ideal two-monochromator method can not be realized in practice. There are practical limits how narrow the bandpass  $\Delta\zeta$  of the incident wavelength  $\zeta$  can be to supply sufficient radiant energy for a specimen to remit adequate energy to the detector unit with a bandpass  $\Delta\lambda$  at wavelength  $\lambda$ , which is represented schematically in Figure 3.3. Also if power of the monochromatic irradiance  $S(\zeta)\delta\zeta$  at wavelength  $\zeta$  is insufficient, it reduces the sensitivity of the fluorescent emission measurement.

In practice  $M(\lambda_i|S(\zeta_j) d\zeta) d\lambda$  is replaced by its finite estimate of the radiant exitance  $\Phi_{\zeta_i, \lambda_j}$ , which can be derived from Equation 3.9, [Sha00]:

$$\Psi_{\zeta_i, \lambda_j} = \int_{-L}^L \int_{-Z}^Z f_\lambda(\mu) \beta(\zeta + \xi, \lambda + \mu) d\mu g_\zeta(\xi) S(\zeta + \xi) d\xi \quad (3.14)$$

where  $g_\zeta(\xi)$  and  $f_\lambda(\mu)$  are the slit-scattering functions varying relative to  $\zeta$  and  $\lambda$  of the excitation and the emission monochromators (see Figure 3.3).

Now the discrete form of radiance transfer function can be estimated. This quantity is a radiance transfer factor  $\mathbf{B}(\zeta, \lambda)$  and is also called a bispectral radiance factor [LJA97]. In the colorimetric meaning the radiance transfer factor is source independent [ZGN<sup>+</sup>97], if the used irradiance is sufficiently energetic in all excitation wavelengths. In practice, the convolution operations applied by the excitation and emission monochromators may lead to a source-dependency in measurement. Let  $G$  and  $F$  respectively be the operators containing the slit functions  $g_\zeta(\xi)$  and  $f_\lambda(\mu)$ . Then,  $\mathbf{B}(\zeta, \lambda)$  is the best estimate of  $\beta(\lambda, \zeta)$  over the region defined by the intersection of finite discrete excitation and emission wavelength bands  $\delta\zeta$  and  $\delta\lambda$  [Sha00]:

$$\mathbf{B}(\zeta, \lambda) = F^{-1} \Psi_{\zeta, \lambda} (GE)^{-1} \quad (3.15)$$

where  $E$  is a matrix, all columns equal to  $S(\zeta)$ . This forms a two dimensional matrix  $\mathbf{B}(\zeta, \lambda)$ , in which rows represent excitation wavelengths  $\zeta$  with bands  $\delta\zeta$  of the irradiance and columns represent emission wavelengths  $\lambda$  with bands  $\delta\lambda$  of reflected or emitted radiant exitance. The reflected radiance factor  $\beta_R(\lambda) = \mathbf{B}(\lambda, \lambda)$  appears on the diagonal of this matrix and is derived directly based on Equation 3.5, when  $\lambda = \zeta$ . The rest of the matrix shows the dependence of emitted flux on excitation and emission wavelengths.

The measured radiance transfer factor  $\mathbf{B}(\zeta, \lambda)$  of a fluorescent specimen, and its total radiance factor  $\beta_T(\lambda|S)$  and reflectance factor  $R(\lambda)$  are shown in Figure 2.7. The total radiance factor  $\beta_T(\lambda|S)$  can be calculated for the illuminant  $S$  with relative spectral distribution  $S(\lambda)$  as follows from the radiance transfer factor:

$$\beta_T(\lambda|S) = \frac{\sum_{\zeta=\zeta_0}^{\zeta} \mathbf{B}(\zeta, \lambda) S(\zeta) \delta\zeta}{S(\lambda) \delta\lambda} \quad (3.16)$$

There are still a few practical issues to be discussed relating to spectrofluorimeters. There do not exist suitable monochromatic light sources which cover the wavelength range of interest, which leads to use of polychromatic light sources, preferably continuous ones. Unfortunately, their spectral power distribution is not flat, and often it is not smooth. Especially, the spectral power distribution of the Xenon light source is very spiky. This radiation must be made monochromatic for each incident radiant wavelength  $\zeta$  with band  $\delta\zeta$ . The spikiness of the spectral power distribution of the used source with the fact of non-ideal monochromators with bandpasses  $\Delta\zeta$  and  $\Delta\lambda$ , makes central wavelength calibration between two monochromators very important. The goodness of this together with the used spectral bandpasses of the monochromators, algorithms used in deconvolution of measured radiances on the detector, and the methods and algorithms used to compensate time varying non-uniform spectral power distribution of the used source utilizing reference radiance detector, are all factors which can contribute to measurement variation among spectrofluorimeters.

The use of two-monochromator method will improve the color measurement of fluorescent papers [ZG95, ZGN<sup>+</sup>97, LJA97]. The method is old, but now these solutions are feasible or will become so in near future, as the first commercial instruments are available. However, the results would be more useful if agreed standards existed for this method, which were to be published by ASTM in April 2000.

### 3.4 Color Specification

Whereas spectrophotometric instruments measure color as a spectral quantity, it is perceived photopically by humans as a three-dimensional quantity consisting of a lightness attribute, and two chromatic attributes: hue and saturation. This has led ongoing research of the color appearance models such as CIECAM97 [LH98], especially the uniform three-dimensional color space ones, which would be important commercially as well as scientifically. So far, only approximations of the ideal uniform color space have been developed, giving limited visual uniformity. The paper industry uses mainly the CIE 1976 L\*a\*b\* opponent-color scale, and occasionally the Hunter Lab opponent-color scale. In principle, they give the possibility to transfer color specifications and tolerances of specimens between the papermaker and the customer in a compact form, with knowledge of the used standard illuminant, the field of view and the used illumination and viewing conditions. Unfortunately, reproducibility of color measurement is often not good enough due to differences between instruments, in wavelength resolution, measured wavelength range, illuminator spectral power distribution, geometry, sensitivity etc., often forcing use of specimen exchange to communicate the color specification. This is always the case with fluorescent specimens. The apparent reflectance factor is rarely used as a color target by itself. The measured apparent reflectance factors  $R'(\lambda|S)$  vary even more between commercial spectrophotometers and it is not the most compact form for transfer of information. However, within a single instrument or a specific model this method can be used, but it may not give the best perceived color matching. Thus the three dimensionless numbers (optionally with a target for another optical property) are preferred for specification of color.

Color spaces, such as CIE 1976 L\*a\*b\* or Hunter Lab, can be evaluated from the CIE 1931 standard colorimetric system  $(X, Y, Z)$  or the CIE 1964 supplementary standard colorimetric system  $(X_{10}, Y_{10}, Z_{10})$  which are evaluated from reflectance factor, transmittance factor or total radiance factor measurements. Auxiliary quantities, such as TAPPI or ISO brightness, are defined in terms of the reflectance factor measured under specific conditions. The formulae and methods for colorimetric and auxiliary quantity calculations are described in color literature and international standards [CIE86, CIE90, AST95c, ISO98b, TAP98].

The quantities of CIE 1976 (L\*a\*b\*) color space are defined as follows for photopic conditions, under which paper is most commonly consumed [CIE86]:

$$\begin{aligned}
L^* &= 116 \sqrt[3]{\frac{Y}{Y_n}} - 16 \\
a^* &= 500 \left( \sqrt[3]{\frac{X}{X_n}} - \sqrt[3]{\frac{Y}{Y_n}} \right) \\
b^* &= 200 \left( \sqrt[3]{\frac{Y}{Y_n}} - \sqrt[3]{\frac{Z}{Z_n}} \right)
\end{aligned} \tag{3.17}$$

where

$$\frac{X}{X_n}; \frac{Y}{Y_n}; \frac{Z}{Z_n} > 0.008856$$

where  $X_n$ ,  $Y_n$  and  $Z_n$  define the color of the normally white object-color stimulus, i.e. they are the tristimulus values of the used illuminant normalized such that  $Y_n = 100$ .

The CIE 1931 standard or 1964 supplementary standard colorimetric system, also called CIE tristimulus values for a  $2^\circ$  field of view ( $X, Y, Z$ ) or for a  $10^\circ$  field of view ( $X_{10}, Y_{10}, Z_{10}$ ), is evaluated from reflectance factor or transmittance factor for non-fluorescent specimens and from total radiance factor in a case of fluorescent specimens. When evaluating values for either CIE 1931 standard or 1964 supplementary standard colorimetric system, it is important to use the appropriate spectral quantity to guarantee correctness of the results. Otherwise, systematic errors with occasional large discrepancies may occur. Due to the uneven distribution of cones and relative spectral sensitivities of the three primary cone types in the human retina, an ideal colorimetric observer with color matching functions  $\bar{x}(\lambda)$ ,  $\bar{y}(\lambda)$ ,  $\bar{z}(\lambda)$  or  $\bar{x}_{10}(\lambda)$ ,  $\bar{y}_{10}(\lambda)$ ,  $\bar{z}_{10}(\lambda)$  corresponding to field of view subtending a  $2^\circ$  or  $10^\circ$  angle on the retina are approximated [Boy96, CIE86]. Tristimulus values ( $X, Y, Z$ ) or ( $X_{10}, Y_{10}, Z_{10}$ ) are evaluated using appropriate CIE color-matching functions and the color stimulus function [CIE86, AST95c]:

$$\begin{aligned}
X &= k \int_{380}^{780} \bar{x}(\lambda) M(\lambda|S) d\lambda = k \sum_i \bar{x}(\lambda_i) M(\lambda_i|S) \delta\lambda \\
Y &= k \int_{380}^{780} \bar{y}(\lambda) M(\lambda|S) d\lambda = k \sum_i \bar{y}(\lambda_i) M(\lambda_i|S) \delta\lambda \\
Z &= k \int_{380}^{780} \bar{z}(\lambda) M(\lambda|S) d\lambda = k \sum_i \bar{z}(\lambda_i) M(\lambda_i|S) \delta\lambda
\end{aligned} \tag{3.18}$$

The color stimulus function  $M(\lambda|S)$  is evaluated as  $R(\lambda)S(\lambda)$  for non-fluorescent specimens, or  $\beta_T(\lambda|S)S(\lambda)$  for fluorescent specimens. The constant  $k$  is a normalization factor to set  $Y = 100$  for the perfect diffuser with the illuminant  $S$  and  $\bar{x}(\lambda)$ ,  $\bar{y}(\lambda)$ , and  $\bar{z}(\lambda)$  are the colorimetric observer functions for the chosen field of view, also called CIE color-matching functions.

CIE recommends some standard illuminants for use in general colorimetry, which are defined by relative spectral power distributions [CIE86]:

- A with an absolute temperature 2856 K
- C with a correlated color temperature of about 6800 K
- D<sub>65</sub> with a correlated color temperature of about 6500 K, as the preferred member of a continuum of daylight illuminants

If colorimetric quantities are to be calculated for a fluorescent specimen based on spectrophotometric measurements, they can be calculated only for used illumination, otherwise gross errors can occur. Unfortunately, this is not the normal practice. The normalization factor  $k$  is evaluated for an illuminant, which preferably would match closely with the used illuminator in case of fluorescent color measurement done by spectrophotometers:

$$k = \frac{100}{\sum_{\lambda} \bar{y}(\lambda) S(\lambda) \delta\lambda} \quad (3.19)$$

When the color of the specimen is specified using three-dimensional quantities, it gives the possibility for metamerism to occur. Metamerism is the tendency for two specimens to match in perceived color under particular conditions of illumination and viewing, but to differ under another set of conditions. Illuminant metamerism can occur if the radiance factors of specimens differ, but their colorimetric values are the same. Metamerism can manifest itself in several ways and is discussed in [CIE86, SS99] among others.

### 3.5 Color Difference Formulas

The acceptability of a colored sample is often defined as maximum color difference from its target. The CIE 1976 total color difference,  $\Delta E_{ab}^*$ , is commonly used in paper industry and is defined as [CIE95]:

$$\Delta E_{ab}^* = \sqrt{(\Delta L^*)^2 + (\Delta a^*)^2 + (\Delta b^*)^2} \quad (3.20)$$

Generally color differences  $\Delta E_{ab}^*$  smaller than 0.5 are difficult to notice, but differences greater than unity can be seen even by the untrained eye.

A newer recommendation for the total color difference evaluation  $\Delta E_{94}^*$  has been promulgated by CIE [CIE95], but is not yet in common use. In the textile industry CMC(1:c) formula has been long in use, and it was utilized in the development of  $\Delta E_{94}^*$ . Also, the CIE 1976 chroma difference,  $\Delta C_{ab}^*$ , is used in the paper industry, and is given as [CIE95]:

$$\Delta C_{ab}^* = C_{ab,1}^* - C_{ab,2}^* = \sqrt{(\Delta a^*)^2 + (\Delta b^*)^2} \quad (3.21)$$

### 3.6 Accuracy

Color measurement is a multi-dimensional problem. Thus the absolute accuracy in colorimetry is less than for example in length and speed measurements. In practice the main sources for poor accuracy are use of dirty or aged working standard and/or unreliable reference reflectance and fluorescence standard. Today color measurement must be traceable. This means that working standards used to calibrate the instrument shall be periodically calibrated with ISO reference standard of level 3 (IR 3) in the instrument with which they will be used. IR 3 reference standard is distributed with reflectance factors accurately established using reference instruments.

Another major factor affecting measurement results achieved from high-white and pastel to deep shade papers is the spectral bandpass of the monochromator unit of the instrument, which was discussed earlier. There are still in use spectrophotometers in which the spectral bandpass of the monochromator unit is 20 nm or even more, whereas for newer ones it is commonly around 10 nm or less. If the goodness of the spectral bandpass correction varies between instruments, the measurements would similarly vary. As discussed earlier, a correction may be applied to calculate the true total radiance factor  $\beta_T(\lambda|S)$  from the measured  $\beta_T(\lambda|S)_{app}$  by deconvolution. In analytic spectroscopy a neat and simple form of this is given by [Mie82b, I.3]:

$$\beta_T(\lambda|S) = \beta_T(\lambda|S)_{app} + \frac{1}{12} \Delta\lambda^2 \frac{\partial^2 \beta_T(\lambda|S)}{\partial \lambda^2} \quad (3.22)$$

where fourth-order and higher terms of  $\Delta\lambda$  are negligible if the spectral bandpass is symmetric, and where  $\Delta\lambda$  is the spectral bandpass of the monochromator. The benefit of this method is that the exact form of the slit-scattering function does not need to be known, and the required second derivative of the  $\beta_T(\lambda|S)_{app}$  can be computed by numerical differentiation.

Other sources for poor accuracy are wavelength calibration errors, non-linear photometric scales, varying gloss-trap structures in instruments with integrating spheres, non-standard tables for color-matching functions and illuminants, use of abridged or truncated color stimulus functions, and varying spectral power distributions of illuminators used in color measurement on fluorescent specimens.

For non-fluorescent samples the absolute accuracy of spectrophotometers used in industrial laboratories relative to National Physical Laboratory in UK are given in Table 3.1 [VCO97], when the quantities of CIE 1976 ( $L^*a^*b^*$ ) color space are recalculated for the illuminant  $D_{65}$  and the CIE 1964 supplementary standard colorimetric system using method E308 from ASTM [AST95c]. As can be seen, most errors appear with chromatic specimens, especially with glossy ones.

For fluorescent samples the absolute accuracy of spectrophotometers is significantly worse, estimated for white fluorescent samples to be about  $\Delta E_{ab}^* = 0.8$  [SS99], when the instrument employs one of the ad hoc extensions for measuring fluorescent specimens and if this utility is used correctly with a traceable fluorescent standard to estimate the CIE 1976 ( $L^*a^*b^*$ ) color space for illuminant  $D_{65}$  and the CIE 1964 supplementary standard colorimetric system using method E308 from ASTM [AST95c].

Geometry	d/0	t/0	0/45
glossy yellow	0.60	0.25	0.23
matt yellow	0.37	0.32	-0.08
glossy white	0.00	0.05	0.03
mat white	0.01	0.05	-0.03

Table 3.1: Absolute accuracy to NPL as  $\Delta E_{ab}^*$  for spectrophotometers used in industrial laboratories [VCO97].

The main influence of the poor accuracy of colorimetry is that papermakers have to use unnecessarily tight deviation limit specifications for color, which often causes some production to be rejected unnecessarily as broke. If customer reclamations occur due to the paper color, the reasons should be defined precisely. They may be based on poor operation practice of the instrument, usage of a different standard illuminant or field of view or based on instrument differences, such as spectral range or bandwidth of the monochromator.



## Chapter 4

# Experimental Work

### 4.1 Colored Handsheets

To define a colorant model a number of colored handsheets at various concentrations of a colorant is usually required. Thus the experimental work involved many colored handsheets which were colored using anionic direct dyes and FBAs covering the gamut from bright fluorescent shades to nearly saturated shades. Also an aim of the experimental work was to produce handsheets which provide comparable color information to those provided by colorant suppliers. This information should be sufficient for off-line tuning of color controls.

The colorants used are listed in Tables 4.1 and 4.2. These classes of colorants were chosen, as they are the ones most used in wood-free fine and publishing papers, and perceived color is one of the main quality attributes for these paper grades.

The furnish may vary between color grades, especially in small papermills specialized in colored paper grades. The steady-state colorant model is known to be dependent on the furnish and its properties. To learn the main features of these dependencies, colored handsheets were made using three pulp blendings of which two were at different filler loadings. The produced colored handsheets can be divided into groups A, B, C and D sheets, based on the furnish type, sheet forming method, targeted basis weight and stock handling during the coloring. The methods used and properties of sheets in each group are discussed below.

#### Group A sheets

The group A sheets were made by the present author and others using refined and bleached softwood cellulose stock, obtained directly from a paper mill pulp line just before stock blending. The stock had been diluted with some clarified backwater which contained wet-end chemicals, but its fines and filler content was low. In total, six different batches of this pulp were used over a period of six months. The pH of the diluted and refined stock was adjusted to be near neutral using NaOH and diluted to a consistency of about 2 % using tap water. The target

C.I. Direct Red 239	Pergasol Red 2G Powder
C.I. Direct Yellow 169	Pergasol Yellow RN Liquid and Powder
C.I. Direct Yellow 157	Pergasol Yellow 6G Liquid
C.I. Direct Black 168	Pergasol Black N Liquid
C.I. Direct Blue 199	Pergasol Turquoise R Liquid and Powder
C.I. Direct Blue 281	Durazol Blue GD Liquid
C.I. Direct Violet 51	Levacell Violet BBN (40 %) Liquid
C.I. Direct Yellow 131	Fastusol Yellow 14L Liquid
C.I. Fluorescent Brightener 154	Tinopal UP Liquid
C.I. Fluorescent Brightener 230	Leucophor AP Liquid
C.I. Fluorescent Brightener 336	Tinopal ABP Liquid and ABP-X h.c.

Table 4.1: Colorants used in the group A and D sheets.

dry weight for the handsheets (16.5 cm by 16.5 cm) was 5-6 g, (equivalent to a basis weight exceeding 200 g/m<sup>2</sup>). These sheets were made using a sheet former, which was not equipped with draining water recycling. The anionic direct dyes and FBAs used are listed in Table 4.1. The colorant suppliers selected these particular colorants for the desired colorant classes, but omitted fluorescent dyes from the selection. No explanation was forthcoming for this omission.

The group A sheets were produced as described here. The liquid colorants were diluted using deionized water to make working solutions of 10 g/l, 1 g/l and 0.01 g/l. The measured mass of powder colorants were first mixed with 90 °C deionized water to make solutions of 10 g/l and further diluted as liquid ones.

The metered, diluted colorant solution was added into the beaker and further diluted using tap water to a final volume of 100 ml in each case. After that a constant volume of agitated stock (200ml) – the amount for a single sheet – was measured from a stock batch and dosed into a beaker with manual agitation. A batch of beakers containing colored stock was kept at least 30 min in the 60°C water bath with intermittent agitation, so that dye adsorption would effectively reach its equilibrium. After that colored stock was formed into sheets using a sheet former using tap water starting typically from lower dye concentration towards higher one. This progression in dye concentrations could, in principle, be a source of systematic error. However, the residuum after cleaning the sheet former would be negligible compared to the higher dye amount in the next sheet. A greater risk of significant contamination would exist if the sheets were made in random concentration sequence. The sheets were dried on a drum dryer between drying sheets made from cotton fibers. The drying stage took several hours, drum temperature being 80°C in each case. For each coloring batch, at least one uncolored reference sheet was produced. For some batches, uncolored reference sheets were made both at the beginning and at the end of the batch. Thus, for each stock there were several reference sheets made during test colorings. Later each sheet was weighed, and colorant ratio was calculated as dosed pure colorant to dry solid of sheet, having units of kg/T.

In the group A sheets, some batches of stock from the paper mill contained an unquantified but significant amount of FBA. The amount of FBA would be constant within a pulp batch, but its effective excitation and emission properties may vary dramatically depending on the colorant added as discussed earlier in Section 2.2.3.

The sheets were stored in sets within their original drying sheets and sealed in air tight plastic bags. These bags were packed in cardboard boxes and stored at room temperature in a dark closet.

The color of a paper sheet is nearly always two-sided. Thus it is important to establish a suitable measurement procedure. Each handsheet was cut into smaller samples, to provide enough samples to form an opaque stack from the minimum number of handsheets. The top side of paper was always measured, the stack of sheet contained a specific number of sheets, the defined number of measurements were made at different locations on the surface, and the instrument was calibrated at the start of each batch of measurements.

The non-fluorescent samples were measured with a Minolta CM-3700d spectrophotometer. Generally, four reflectance factor measurements per sample were made from stacks of four sheets formed from the two identically colored sheets, using black cavity as backing. The fluorescent samples were measured with Labsphere's BFC-450 spectrofluorimeter. Generally, only a single radiance transfer factor measurement per sample was made from two identically colored samples piled on top of each others. Due to the very long measurement time with the BFC-450, it was not practical to repeat most measurements.

### Group B and C sheets

The group B and C handsheets represent an extended set of colored handsheets supplied by a colorant supplier for off-line tuning of a color controller, as a part of the commissioning of an optimizing color controller at a paper mill. The supplier's procedure was described as follows. The stock is not heated during coloring, but it is mixed continuously. The handsheets are usually formed by floating a mold in water and pouring metered colored stock onto its surface, but sometimes using a sheet former. The mold is jiggled, causing water to break up the stock, and allowing it to spread to even thickness. The sheets are dried between drying sheets. The basis weight of the groups B and C sheets was about 120 g/m<sup>2</sup>, and they were colored using colorants listed in Table 4.2.

Each sheet was colored using only a single colorant. The supplied information contained the name of the used colorant and the amount of colorant as kg/T. These data were supplied without the mass balances and other measurements from which they were derived. Their reliability and accuracy is therefore not known.

The group B sheets were made using a furnish containing mixed bleached hardwood, kraft softwood, short cotton fibers, neutral sizing agent with 0 %, 5 %, 10 % and 16 % of retained chalk.

The group C sheets were made using furnish containing bleached hardwood, kraft softwood, short cotton fibers, neutral sizing agent and 0 %, 5 %, 10 % and 14 % of retained precipitated calcium carbonate, PCC.

C.I. Direct Red 81	Carta Red EB Liquid
C.I. Direct Blue 199	Carta Turquoise FBL Liquid
C.I. Direct Blue 267	Cartasol Blue 3RF Liquid
C.I. Direct Violet 35	Cartasol Brilliant Violet 5BF Liquid
C.I. Direct Yellow 148.1	Cartasol Yellow 5GFN Liquid
C.I. Direct Yellow 133	Cartasol Yellow RF Liquid
C.I. Fluorescent Brightener 28	Leucophor AL Liquid
C.I. Fluorescent Brightener 321	Leucophor HWL Liquid

Table 4.2: Colorants used in the groups B and C coloring sheets.

These sheets were stored in sealed black air tight plastic bags, which were packed in a cardboard box and stored at room temperature in the dark closet.

All sheets were measured with both CM-3700d and BFC-450. Four radiance factor measurements per sample were made with CM-3700d using stacks of four sheets, with a black cavity as backing. Only a single radiance transfer factor measurement per sample was made with BFC-450 from the stack of four colored sheets.

#### Group D sheets

A smaller group of D sheets were made later using refined and bleached pine cellulose stock, picked up directly from a board mill pulp line before stock blending. The stock had been diluted with some clarified backwater which contained wet-end chemicals, but its fines and filler content were low. The intended basis weight of the sheets was  $80 \text{ g/m}^2$  to enable determination of Kubelka-Munk scattering coefficients from single sheet and stack reflectance factor measurements. To reduce sheet weight variations, now 13.5 % stock consistency was used, and 15 g of this was weighed for each test coloring to produce round sheet with diameter of 180 mm (basis weight of  $80 \text{ g/m}^2$ ). This set contained also dyeings with a fluorescent yellow, Fastusol Yellow 14L Liquid.

Colorants were prepared as in the group A sheets. The metered amounts of colorants were dosed into the beaker containing 400 ml of deionized water (pH 7 and conductivity  $0.74 \mu\text{S}$ ). Next the pre-weighed amount of stock was added and agitated, after which the total volume was increased to 600 ml. A batch of beakers containing colored stock was kept at least 45 min in the  $60 \text{ }^\circ\text{C}$  water bath with intermittent agitation. The coloring equilibrium was reached at total volume of 600 ml and pH 5. After that colored stock was diluted with 2.4 liters of tap water (pH 7.8 and conductivity  $165 \mu\text{S}$ ), short vigorous mixing was applied and the volume was poured into the sheet former pre-charged with one liter of tap water to cover up the wire. The sheet was formed and all backwater was collected, from which a sample of 250 ml was taken to be used to analyze the amount of colorant in solution. The sheet forming progressed from lower dye concentrations towards higher one, as before. The sheets were dried on a drum dryer at about  $70 \text{ }^\circ\text{C}$  between drying sheets made from cotton fibers.

Generally, four reflectance factor measurements per sample were made using the single sheet visually judged to have the most even formation and using stacks of twelve sheets formed from two similarly colored samples. In both cases, the CM-3700d was used with a black cavity as backing.

The amount of dye adsorbed on or entrained in the fibers and solids was determined by estimating the amount remaining dissolved in the backwater. This estimation was based on the Beer-Lambert law, which states that “the absorption of light in passage through any medium is proportional to the number of absorbing entities in its path” [DS89, §11.2]. For a non-scattering medium, the light path through a medium has length equal to the thickness of the medium. Thus:

$$A(\lambda) = \varepsilon(\lambda)c = \log \frac{\Phi_T(\lambda|S)_{Std}}{\Phi_T(\lambda|S)} = \log \frac{1}{T(\lambda)} \quad (4.1)$$

where  $A(\lambda)$  is the spectral absorbance at each wavelength,  $\varepsilon(\lambda)$  is the extinction coefficient (also called spectral absorption coefficient) of the colorant contained in a clear solution in the used cell,  $c$  is the concentration of the colorant,  $\Phi_T(\lambda|S)_{Std}$  is the intensity of light passing through the reference cell filled with the solvent (in this case deionized water),  $\Phi_T(\lambda|S)$  is the intensity of light passing through the sample cell, and  $T(\lambda)$  is the total transmittance.

The extinction coefficient  $\varepsilon(\lambda)$  of each dye can be obtained from transmittance measurements using standard dye solutions of known concentration. The dye concentration in the backwater is then estimated from its transmittance at the wavelength of maximum absorption. By allowing for the dilution during sheet-forming, the final concentration of dye in the backwater can be calculated. Since the backwaters contained some fines, the samples were allowed to settle through sedimentation, requiring a few days to produce a visually clear supernatant solution. The amount of dye-on-fiber was determined in this way for sheets dyed with Pergasol Yellow RN Powder and Pergasol Turquoise R Powder, which are shown in Figure 5.1.

## 4.2 Measurements

Due to problems of fluorescent color measurement as discussed in Chapter 3, two color measurement instruments were used: Minolta’s spectrophotometer CM-3700d with d/8 geometry, 28 mm/25.4 mm aperture with specular component excluded, and Labsphere’s BFC-450 Bispectral Fluorescence Colorimeter (spectrofluorimeter) with annular 45/0 geometry having 2° illumination aperture and 1° viewing aperture. No modifications were made to the instruments by the present author.

For various reasons (mainly defects with BFC-450, which required repeated modification by its manufacturer), the measurements of the A, B, and C groups of colored handsheets were made from a half year to two years after the sheets were made. The group D sheets were made after the instrument problems were addressed, so that they were measured promptly after being made. Thus the group A, B and C sheets were exposed to aging. The aging affected all sheets, especially the FBA containing sheets, reducing emitted radiant flux. However, the effect should

be consistent within each set of the colored sheets due to the common storage conditions, and thus the sheets are applicable for this study.

There are several requirements for the color measurement instruments used in colorant formulation. A selected instrument must have good short and long term repeatability (closeness of the agreement between the results of successive measurements of the same measurand carried out under the same conditions of measurement [TK94]). The amount of measurement uncertainty which is acceptable depends, of course, on the requirement for colorimetric accuracy of measurement (closeness of the agreement between the result of a measurement and the value of the measurand [TK94]), which is application dependent. Long term repeatability can be maintained by regular calibration of the instrument using traceable IR 3 reference standards. The detection wavelength range should cover the near-UV and visible bands, and the spectral bandpass of the monochromator unit of the instrument should be sufficiently narrow to allow identification of spectral features. In practice, since absorption and emission spectra are reasonably smooth, a spectral bandpass of 5 to 10 nm suffices for most applications. Also the photometric linearity of the detection unit can not be ignored. If several instruments are utilized in colorant formulation, then measurement reproducibility, (closeness of the agreement between the results of successive measurements of the same measurand carried out under the changed conditions of measurement [TK94], here a change of a measurement instrument) is a critical issue. In practice, due to problems of reproducibility in spectrophotometers and spectrofluorimeters the same instrument (or at least the same instrument model) must be used whenever measurements are to be compared or communicated.

### 4.2.1 Used Instruments

#### CM-3700d

Minolta's CM-3700d is a dual-beam spectrophotometer, which is equipped with a pulsed Xenon light source, a 6-inch barium sulfate coated integrating sphere and a gloss trap. Its wavelength range is 360 nm to 740 nm with spectral bandpass approximately 14 nm. Measured reflectance factors are reported at 10 nm wavelength pitch. Its specified photometric resolution is stated to be 0.001 % (0.002 as  $R(\lambda)$ ), and reflectance factor repeatability (30 measurements at 10 s interval) as standard deviation for white calibration tile as  $\Delta E_{ab}^*$  of 0.01 and for black tile from BCRA Series of 0.05 [Min95]. The amount of UV included in the illumination can be throttled by moving a UV cutoff filter across the light path based on for example the CIE Whiteness D65/10° reading of the fluorescent standard. The measurement software can average several measurements on different locations of the sample to form a measurement.

The total transmittance factor of either a liquid solution in a cuvette or a thin sheet of substrate can be measured with this instrument. This requires a transmittance calibration, where a reference is placed on the light path between the illuminating integrating sphere and the unit containing the diffraction grating and the detector. Later the reference is replaced with a sample to be analyzed.

**BFC-450**

Labsphere's BFC-450 instrument uses a continuous 150W Xenon lamp, whose radiance is passed through a grating and slit monochromator and then split as monochromatic irradiance onto a specimen and to the internal reference photodetector. The radiation reflected and emitted from the specimen is dispersed via polychromator and detected using an array detector. The excitation range is from 300 nm to 780 nm with about 10 nm spectral bandpass, and detection range is from 380 nm to 780 nm with about 4.5 nm spectral bandpass. The measured values forming a matrix are reported at 10 nm wavelength pitch. The measurement repeatability is specified as standard deviation of  $\Delta E_{ab}^*$ . For a non-fluorescent white Spectralon this is stated to be 0.03, for a weakly fluorescent specimen 0.10 and for a strongly fluorescent specimen 0.30 [Lab97]. The measurement time per sample is in the range 10 to 15 minutes, depending on the set integration time for each excitation band. The sample is held in place with a ring shaped clamp, and in later modifications with a solid clamp. This instrument is not suitable for transmittance measurements.

BFC-450 produces a measurement file containing radiance transfer factor  $\mathbf{B}(\lambda, \zeta)$  normalized to the used irradiance and the perfect white diffuser. The columns on this file represent monochromatic illumination at different wavelengths from 300 nm to 780 nm, and the rows the amount of detected normalized light from 380 nm to 780 nm. Thus the size of the matrix with 10 nm nominal band width is (41,49). Elements in diagonal  $(i, i + 8)$  represent the reflected radiance factor  $\beta_R(\lambda)$ .

**4.2.2 Measurement Uncertainty**

Measurements are subject to imperfections. Some of these are due to random effects (type A), while others are due to the practical limits to which correction can be made for systematic effects (type B), such as offsets of a measuring instruments, drift in its characteristics between calibrations or the uncertainty of the value of a reference standard. In the first case (type A), evaluation of uncertainty by the statistical analysis of series of observations is used. The standard uncertainty  $u(x_i)$  to be associated with the input estimate  $x_i$  being the sample mean from  $n$  independent observations  $X_{i,k}$  of an input quantity  $X_i$  obtained under the same conditions of measurement is defined as [TK94, Bel99]:

$$u(x_i) = \sqrt{\frac{1}{n-1} \sum_{k=1}^n (X_{i,k} - \bar{X}_i)^2} \quad (4.2)$$

In cases of systematic effect (type B), a different evaluation of uncertainty is used. Now the standard uncertainty  $u(x_i)$  to be associated with  $x_i$  is the positive square root of the variance of the distribution of input quantity  $X_i$ , whose value is estimated from an assumed rectangular probability distribution of lower limit  $a_-$  and upper limit  $a_+$  [TK94]:

$$u(x_i) = \frac{(a_+ + a_-) / 2}{\sqrt{3}} \quad (4.3)$$

The combined standard uncertainty  $u_c(x_i)$  from all the individual aspects can be calculated as square root of the sum-of-the-squares [TK94]:

$$u_c(x_i) = \sqrt{\sum_{i=1}^m u_i(x_i)^2} \quad (4.4)$$

The radiance factor measurements clearly contain imperfections originating from both random effects, such as variation of flash lamp spectral power distribution between flashes and directionality of radiation, and systematic effects, such as drift in lamp and detector characteristics between calibrations, non-homogeneous reflectance properties of the sphere, and calibration uncertainty. Due to problems of reproducibility (here a change of a measuring instrument), the colorant modelling should be performed with the same measurement instrument, where it is desired to be used for colorant formulation. Thus the most interesting property is repeatability (closeness of the agreement between the results of successive measurements of the same measurand carried out under the same conditions of measurement [TK94]). Therefore the calibration uncertainty can be excluded from the uncertainty analysis. The statistical analysis of measurement uncertainty is based on Equation 4.2, without quantification of individual contributions to uncertainty.

Since the standard uncertainty of radiance factor measurements is wavelength dependent, using mean values to compare measurement and coloring uncertainties, a usage of a ‘nominal’ standard uncertainty would be helpful. This ‘nominal’ standard uncertainty is defined to describe the mean of the standard uncertainty on the selected wavelength band, typically at the maximum absorption and emission band of a colorant.

### CM-3700d

A non-fluorescent white Spectralon was measured sixty times during twenty minutes with the same settings as for the colored handsheets, 28 mm/25.4 mm aperture with specular component excluded, using CM-3700d. The used optical-grade Spectralon is hydrophobic and thermally stable to 350 °C, and is highly lambertian over its effective spectral range [Lab96, p.8]. In Figure 4.1 the mean reflectance factor  $R(\lambda)$  of these sixty repeated measurements and the standard uncertainty (excluding accuracy of measurement) based on Equation 4.2 is shown. A ‘nominal’ standard uncertainty over whole measured wavelength range is estimated to be  $8.3 \cdot 10^{-5}$  as  $R(\lambda)$ . A small increase of the standard uncertainty in blue end of the detection band can be explained with lower signal-to-noise, due to reduction in grating efficiency and spectral responsiveness of the detector.

Figure 4.2 shows the mean reflectance factor  $R(\lambda)$  of forty repeated measurements of the group C sheet colored with 2 kg/T of Cartasol Blue 3RF Liquid and the standard uncertainty. A

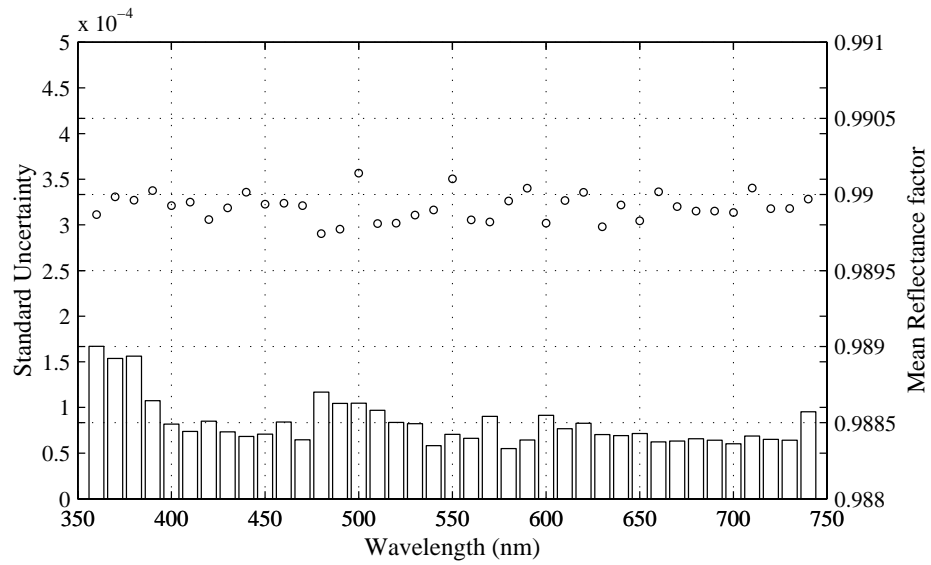


Figure 4.1: The mean reflectance factor  $R(\lambda)$  of sixty repeated measurements of white Spectralon and the standard uncertainty with CM-3700d.

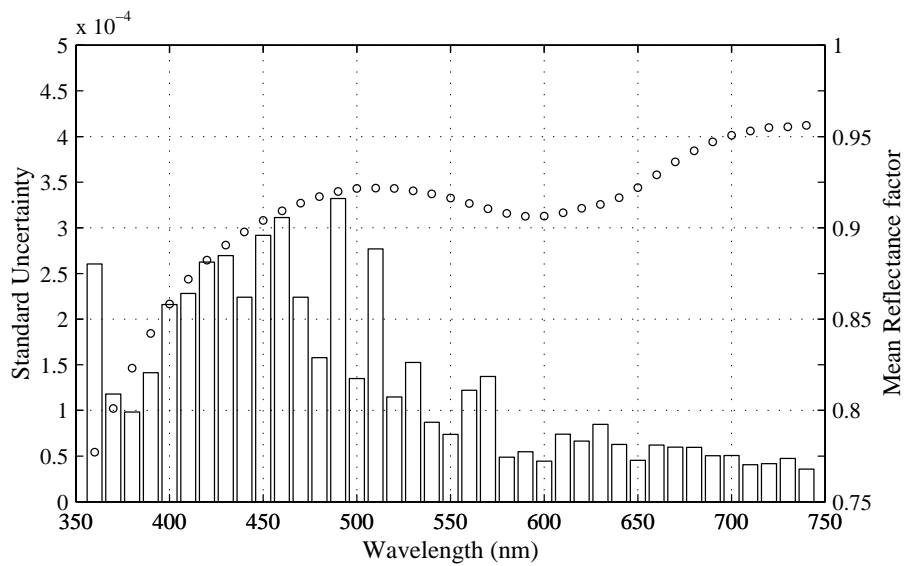


Figure 4.2: The mean reflectance factor  $R(\lambda)$  of forty repeated measurements of the group C sheet colored with 2 kg/T of Cartasol Blue 3RF Liquid and the standard uncertainty with CM-3700d.

‘nominal’ standard uncertainty of wavelength range 390-470 nm is estimated to be  $2.4 \cdot 10^{-4}$  as  $R(\lambda)$ . The increased standard uncertainty of measurements may be caused by non-homogeneous reflection properties of the sphere, local variation of the discharge of the Xenon flash, and non-lambertian sample.

Figure 4.3 shows the mean transmittance factor  $T(\lambda)$  of twenty repeated measurements of a cuvette containing deionized water and the standard uncertainty (excluding accuracy of measurement) based on Equation 4.2. A ‘nominal’ standard uncertainty over whole measured wavelength range is estimated to be  $4.3 \cdot 10^{-5}$  as  $T(\lambda)$ .

In Figure 4.4 the effect of relocating the same cuvette containing deionized water twenty-five times is shown for the mean transmittance factor  $T(\lambda)$  and the standard uncertainty. A ‘nominal’ standard uncertainty of reproducibility of results of measurements is now estimated to be  $2.8 \cdot 10^{-4}$  as  $T(\lambda)$ . The major source for the increase of the uncertainty of measurement is probably the change of angle of the cuvette relative to the light path, but other factors, such as nonuniformity in the cuvette surface may also contribute.

Based on these analyses, the CM-3700d is suitable for colorant modelling. Its uncertainty of measurements (especially in terms of repeatability) based on standard uncertainty multiplied by a coverage factor  $k = 2$ , providing a level of confidence of approximately 95 %, of reflectance and transmittance factor is below the level of 0.001 as  $R(\lambda)$  or  $T(\lambda)$ .

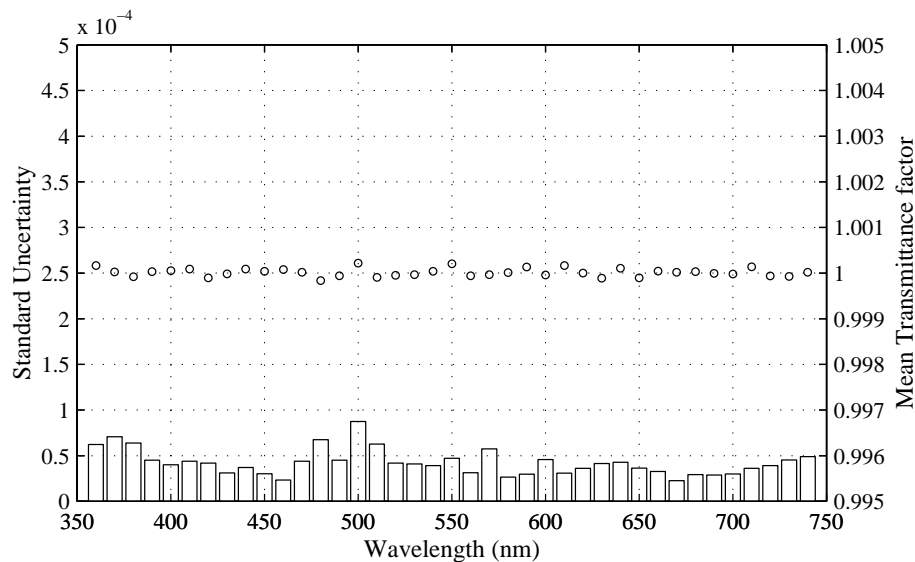


Figure 4.3: The mean transmittance factor  $T(\lambda)$  of twenty repeated measurements of cuvette containing deionized water and the standard uncertainty with CM-3700d.

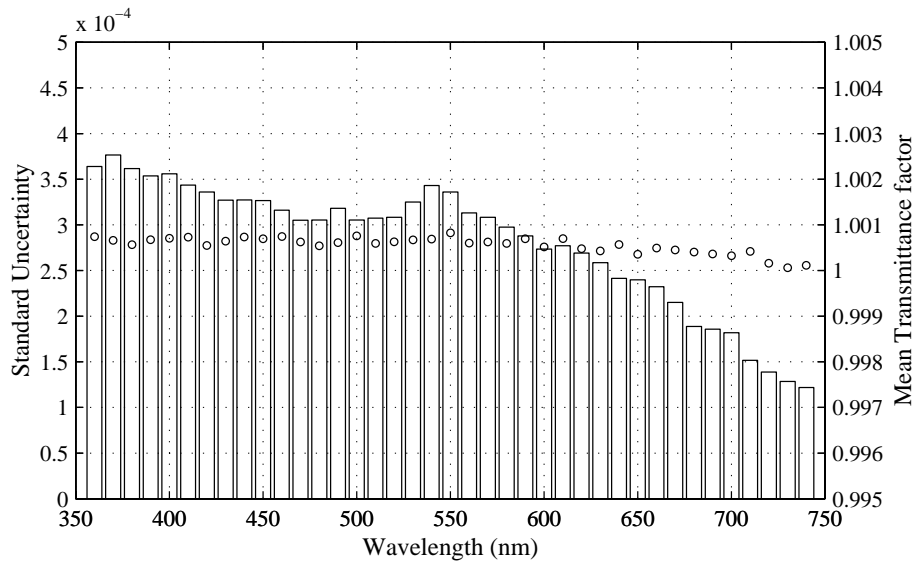


Figure 4.4: The mean transmittance factor  $T(\lambda)$  of twenty-five repeated measurements of relocated cuvette containing deionized water and the standard uncertainty with CM-3700d.

### BFC-450

Serious problems were discovered with the BFC-450 during measurement of the handsheets. Due to the severity of the problems, the instrument was not used again until after significant modifications by the manufacturer. The modifications were made in several stages, and the repeatability results presented here were made after all of the modifications, at the time when most handsheet measurements were made.

The measured reflectance factors  $R(\lambda)$  tended to contain spikiness in their shape, which was thought to originate partly from spiky reflectance of the white reflectance standard. One source of this was the method used to transfer the calibrated reflectance factor of the measured standard from 1 nm pitch to 10 nm pitch.

In case of a fluorescent specimen, luminescent radiance energy is distributed in the area below the reflectance diagonal, due to the fact that fluorescent emission occurs at longer wavelengths than excitation. This leads to a problem, because most of the detector array is measuring “dark current” signal. The signal to noise ratio is good in channels measuring reflected light, and is acceptable in channels detecting emitted light near the emission maximum of a strong fluor. The signal to noise ratio is poor for emission from weak fluors, and away from the emission maximum of strong fluors.

Based on the nature of fluorescence, the values above the reflectance diagonal contain only detector noise and can be set directly zero. Theoretically the first upper off-diagonal and the first bottom off-diagonal for a non-fluorescent sample should be zero. After analyzing the data, this

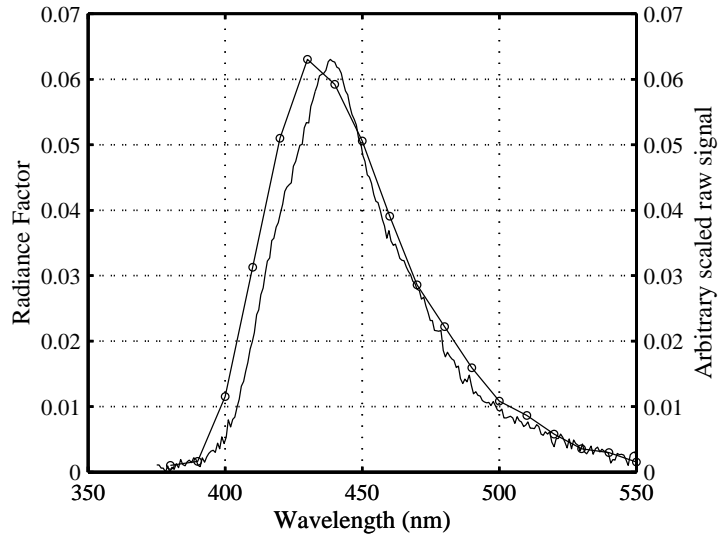


Figure 4.5: Arbitrary scaled raw detector reading and radiance transfer factor measurement of emission of a fluor excited by monochromatic irradiance of 360 nm.

was not the case. This problem originates from the differences in monochromator and detector spectral bandpasses of 10 nm and 4.5 nm, and may also be influenced by the goodness of both monochromators' wavelength calibration, the method for spectral bandpass corrections, and the method used to sample data at 10 nm pitch.

An example of difficulties in changing data sampling rate is given in Figure 4.5, where the raw detector reading and the radiance transfer factor measurement of emission of a fluor excited by monochromatic irradiance of 360 nm are shown. As can be seen the wavelength of the peak emission is significantly different between the two. In this case the raw detector reading gave better peak wavelength matching to the measurement values given at 5 nm pitch by NRC [Vaa99].

The small amplitude noise in the bottom corner of the matrix where no emitted light exist and thus can not be detected has a significant effect on luminescent radiant factor  $\beta_L(\lambda|S)$  if it is not cleaned out. The noise contains also negative values, which are theoretically impossible. This noise must be validated using a method which relies on the smoothness of molecular fluorescent emission. Such a method was developed by the current author. Thus, the validity of values below a noise threshold is judged using values in neighboring elements, and is retained only if at least one neighbor exceeds a larger threshold value:

$$\begin{aligned}
 & \text{IF } \mathbf{B}(i, j) < db_1 \\
 & \text{AND all } \mathbf{B}(i', j') < db_2 \\
 & \text{AND all } \mathbf{B}(i'', j'') < db_3 \\
 & \text{THEN } \mathbf{B}(i, j) = 0
 \end{aligned} \tag{4.5}$$

where  $db_1$ ,  $db_2$  and  $db_3$  are deadband factors with default values of 0.004, 0.005 and 0.0075, and  $(i', j')$  are from the set of eight nearest neighbours  $\{(i, j \pm 1); (i \pm 1, j); (i \pm 1, j \pm 1)\}$  and  $(i'', j'')$  are from the set of sixteen second nearest neighbours  $\{(i, j \pm 2); (i \pm 2, j); (i \pm 1, j \pm 2); (i \pm 2, j \pm 1); (i \pm 2, j \pm 2)\}$ .

A white fluorescent Spectralon doped with fluors having emission peak at 430 nm and 460 nm was measured ten times during five hours using BFC-450. In Figure 4.6 the mean of the reflectance factor (the diagonal  $\mathbf{B}(\lambda, \lambda)$ ) of the repeated measurements of the white fluorescent Spectralon and the standard uncertainty calculated using Equation 4.2 is shown. A ‘nominal’ standard uncertainty over whole measured wavelength range is estimated to be 0.0018 as  $R(\lambda)$ . The uncertainty of the commercial two-monochromator method instrument is clearly worse than the dual-beam spectrophotometer. Part of this may be due to drift in spectral power distribution of the illumination between calibrations or thermal effects. However, the implemented internal reference photodetector should compensate a possible drift in SPD.

In Figure 4.7 the mean of the total radiance factor  $\beta_T(\lambda|D_{65})$  calculated for  $D_{65}$  of the same ten measurements and the standard uncertainty is shown. A ‘nominal’ standard uncertainty over whole measured wavelength range is now estimated to be 0.0083 as  $\beta_T(\lambda|D_{65})$ .

In Figure 4.8 the mean of the total radiance factor  $\beta_T(\lambda|D_{65})$  calculated for  $D_{65}$  of the same ten *validated* measurements using Equation 4.5 and the standard uncertainty is shown. A ‘nominal’ standard uncertainty over whole measured wavelength range is now estimated to be

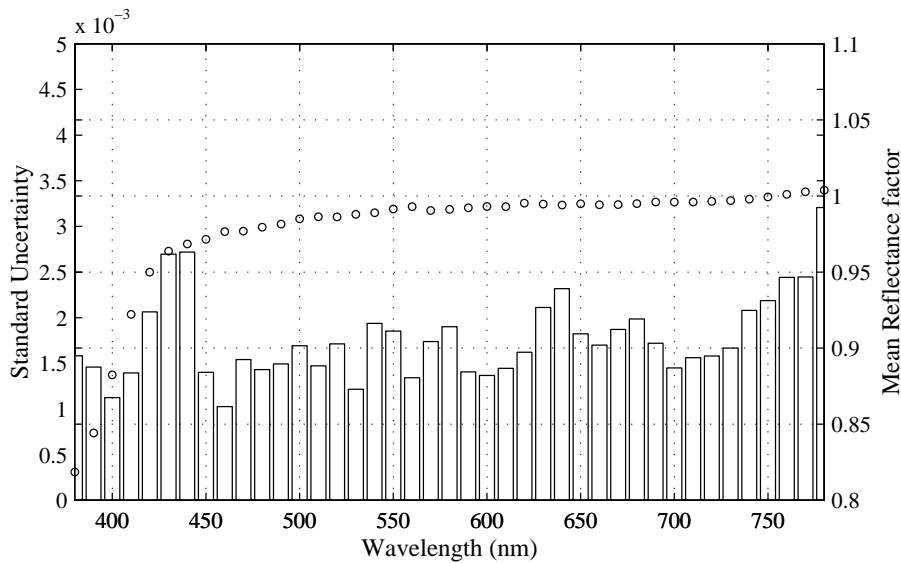


Figure 4.6: The mean reflectance factor  $R(\lambda)$  of ten repeated measurements during five hours of a white fluorescent Spectralon having emission peak at 430 nm and 460 nm and the standard uncertainty with BFC-450.

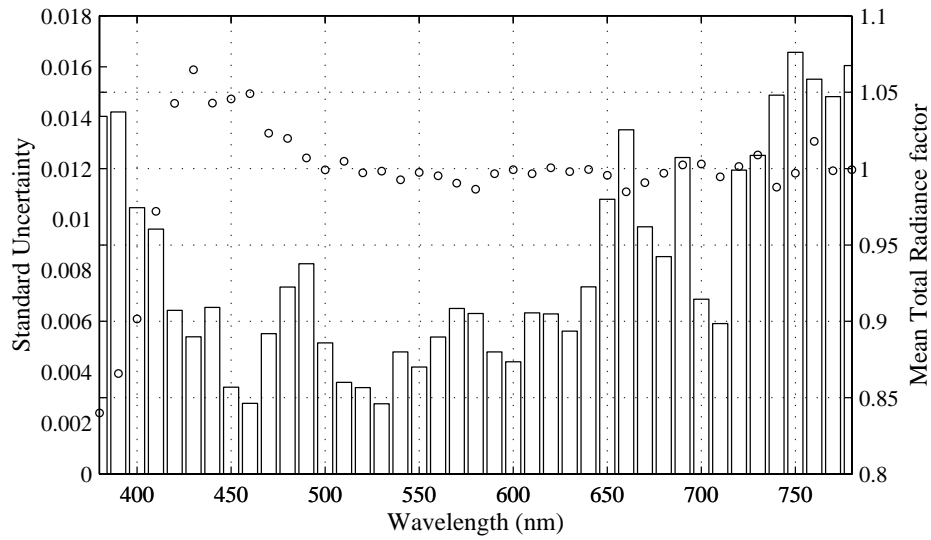


Figure 4.7: The mean total radiance factor  $\beta_T(\lambda|D_{65})$  of ten repeated measurements during five hours of a white fluorescent Spectralon having emission peak at 430 nm and 460 nm and the standard uncertainty with BFC-450.

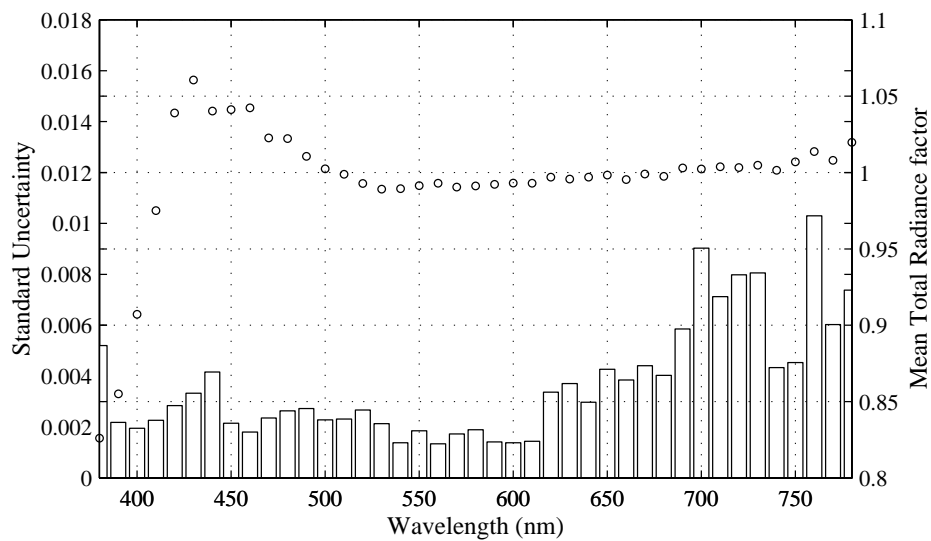


Figure 4.8: The mean total radiance factor  $\beta_T(\lambda|D_{65})$  of ten *validated* measurements during five hours of a white fluorescent Spectralon having emission peak at 430 nm and 460 nm and the standard uncertainty with BFC-450.

0.0037 as  $\beta_T(\lambda|D_{65})$ . The validation significantly reduces the standard uncertainty.

Based on these analyses, the BFC-450 has to be improved before it would be suitable for commercial colorant modelling. Its uncertainty of measurements (especially in terms of repeatability) based on standard uncertainty multiplied by a coverage factor  $k = 2$ , providing a level of confidence of approximately 95 %, of total radiance factor is well above the level of 0.001 as  $\beta_T(\lambda|D_{65})$ , being 0.017. The discussion of improvements and open issues with the manufacture is ongoing. However, BFC-450 can be used for research purposes to analyze excitation and emission properties, being the only commercial instrument available to measure radiance transfer factors.

### Measurement Comparison

In Figure 4.9 two non-fluorescent and two fluorescent handsheets from the group C sheets were measured with CM-3700d and BFC-450 to compare the linearity of their photometric scales and calibration uncertainty. The difference in measurements of non-fluorescent handsheets is small, but significant. In subfigure (B) the emission peak of the fluor (Leucophor AP) locates at 430 nm when measured using BFC-450, while it locates at 440 nm with CM-3700d. This may be explained by reference to the illuminator, and its effect to the total radiance factors on the emission band of the fluor, and also reference to the spectral bandpass and deconvolution. The calculated  $\Delta E_{ab}^*$  for the measurements of weak fluor is 7.4 and 12.8 for strong fluor calculated for  $D_{65}$  and 1964 supplementary colorimetric system. These unacceptably large differences are common in apparent reflectance measurements produced by spectrophotometers.

## 4.3 Coloring Method Analysis

The coloring variation appearing in the colored sheets can be divided into systematic and random effects. Errors in colorant dilutions will have similar systematic effects on all sheets in the batch of colored sheets where it is used. Variation in stock properties and processing will similarly affect whole batches systematically, as discussed in Section 2.2.

Random variations can be minimized only by developing good working practices and having a careful and thorough worker [Ran97]. Random variations have four main causes which are discussed here.

### Colorant dosage

Dosage errors can occur while measuring colorants, and these tend to be more significant at higher colorant concentrations and when metering small volumes. To minimize this, precision volumetric pipettes were used in coloring the group A and D sheets. The standard solutions were prepared using precision scales or precision volumetric pipettes, and diluted into precision volumetric flasks.

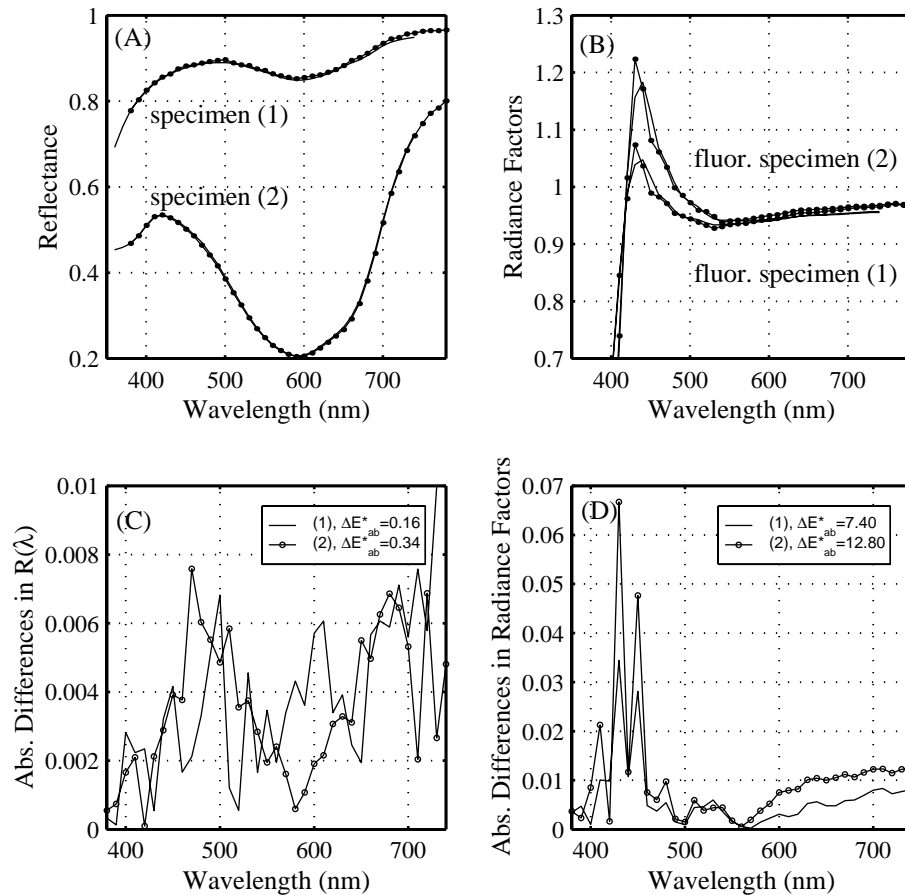


Figure 4.9: (A)-(B) Four handsheets from the group C sheets measured with CM-3700d (solid with dots) and BFC-450 (solid).

(C)-(D) Absolute radiance factor error between the instruments.

Errors in relative concentrations of diluted working colorant solutions would be noticeable as outliers from the fitted regression line.

Also, improper washing of beakers and pipettes, especially after FBA usage, may cause colorant contamination and interaction to take place. Glassware was cleaned using thorough water flushing only, without soap. Forming wires were stored in alcohol and thoroughly flushed with water before use. Pulp processing equipment (beaters, sheet formers, etc.) were flushed with water with light scrubbing with nylon brush.

### Stock dosage

The homogeneity of dosed stock to be colored is critical. Variations in total surface area, as well as in distribution of fibers, fillers and fines in the dosed stocks would affect the coloring isotherm.

A considerable source of color variation in the group A sheets was caused by the variation of dry solids in the dosed constant volume of diluted stock due to consistency variation of the stock. In this case, the diluted stock (2 %) was agitated, but variation in the number and size of flocs in the constant volume of the dosed stock can be seen as varying dry weight of a sheet. Also flocs easily adhere to a measuring beaker, especially on the lip. The variation of sheet weights in group A is below 9 %, typically about 4-5 %.

An improved method was tested with the group D sheets. Now the consistency of stock was 13.5 % and a constant mass of it was weighted, and it was diluted in the beaker with constant volume of deionized water. The variation of sheet weights reduced to typically about 2.5 %, possibly including some fine retention variation.

The group B and C sheets were formed using the mold in water method, where some fibers and flocks may escape with drainage water. Also sheet edges were cut, thus quantitative estimates of this error for these sheets is not available.

### Dyebath

Dyeing conditions should not vary between batches, especially the dyebath temperature and exposure time. This ensures that all dyeings approach adsorption equilibrium to the same degree. Other factors affecting the adsorption rate, such as presence of cations and agitation to prevent local exhaustion of the dye solution, are also important. Agitation ensures that the dye solution adequately penetrates large fiber flocs; otherwise they may not be colored thoroughly and the measured color will vary locally.

### Sheet forming

The cleanliness of the sheet former is an important issue. A small amount of previously colored fibers can ruin the effort. Figure 4.10 contains a real example of improper washing (most likely the mold and basin) in the group B sheets, where an undyed reference sheet was probably contaminated by previously used colorants. The lack of a reliable undyed reference sheet reduced the usability of this whole dyeing set.

The uniformity of coloration is largely determined by sheet formation. An even distribution of fibers, fines and filler in the sheet is required with constant filler and fines content from sheet to sheet. In addition, the affinity of a colorant for each major component of the sheet should not be very different. If scattering coefficients are to be determined, good formation is required.

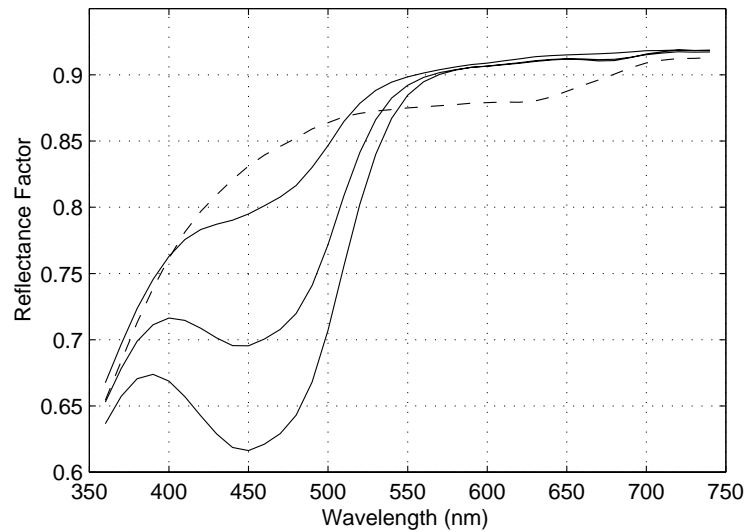


Figure 4.10: Result of improper washing on undyed colored handsheet (dashed line) compared to dyed ones (solid line) in group B sheets.

### 4.3.1 Coloring Uncertainty

The colorings contain imperfections originating from both random and systematic effects, as discussed above. Here the most interesting property is the reproducibility of the colorings. Since this has to be defined based on the radiance factor measurements of the measurands (colored handsheets), the reproducibility [TK94] of results of measurements, in means of varying the measurement location within a measurand, should be defined. This reproducibility of results of the measurements would vary depending on such as the surface roughness, variation in transmitted radiation due to opacity of the stack, and the sensitivity of the measurement instrument to directionality of fibers, if not compensated by adopting a suitable measurement procedure. The implication of opacity variation is that several identically colored sheets must be made to provide sufficient layers to make an opaque stack, in which the number of sheets needed to form an effectively opaque stack depends on the furnish, especially the amount and types of filler and the type and processing of fiber.

The analysis of the reproducibility of the colorings is simplified and would be based on Equation 4.2. Further more, the uncertainties of colorings and measurements are assumed to be independent and both based on random variation. So that the ‘nominal’ standard uncertainty of the colorings  $u_n(R(\lambda)_{col})$  would be the difference of the ‘nominal total’ standard uncertainty  $u_n(R(\lambda)_{tot})$ , which includes coloring uncertainties and all measurement uncertainties, and the ‘nominal’ standard uncertainty of measurements  $u_n(R(\lambda)_{mea})$ , which includes all measurement uncertainties:

$$u_n(R(\lambda)_{col}) = u_n(R(\lambda)_{tot}) - u_n(R(\lambda)_{mea}) \quad (4.6)$$

A view will be taken, what is the total effect of all random variations in coloration on quantities of interest, based on two sets of repeated colorings.

#### Absorbance analysis

To define dye-on-fiber, the transmittance of backwater samples was measured. To study the general variability in colorings, a set of undyed sheets and a set of equally-dyed sheets were made. The dyed sheets were all dyed with 10 ml of 0.2g/l Pergasol Yellow RN Powder equal to 1 kg/T. Figure 4.11 shows the absorbance variation in undyed backwaters at wavelength 410 nm (absorption maximum) of dyed backwaters dyed with 1 kg/T Pergasol Yellow RN Powder. These samples are for the backwaters from the sheet former; the corresponding absorbance of the final dyebath solution would be 6.67 times higher, due to dilution. The backwater samples were not clear. They contained some fines, which absorbed light at the blue end of the spectrum. Since it was not possible to centrifuge the samples, the samples were allowed to settle for two days, during which most of the fines sedimented to the bottom. A sample was taken by pipetting from the clear solution without disturbing the sediment. A method of filtration through a paper filter was rejected, due its potential for adsorption of dyes from backwaters. This base level of absorbance caused by fines was taken into account when the amount of dye-on-fiber was defined.

The estimated dye-on-fiber from a nominal dose of 1 kg/T of Pergasol Yellow RN Powder was 0.90, 0.79, 0.90, 0.89, 0.90, 0.86, 0.89, and 0.89 kg/T for these colored sheets. The second coloring seems anomalous, with unknown cause. The standard uncertainty of estimated dye-on-fiber is 0.014 as kg/T excluding the second coloring.

#### Reflectance analysis

In Figure 4.12 the mean reflectance factor of measurements of eighteen uncolored sheets and the standard uncertainty is shown. These reflectance factor measurements were made using CM-3700d at four different locations on each of eighteen uncolored sheets belonging to the group A sheets. These sheets were formed in two batches from the same batch of stock, between which several batches of colored sheets were made. A 'nominal' standard uncertainty of wavelengths 500-600 nm is estimated to be 0.0015 as  $R(\lambda)$ . This estimate includes the repeatability and reproducibility uncertainties of the measurements, and it also includes uncertainties caused by variation of surface texture of the samples. Some of this uncertainty is caused by the fact that the sheet former cannot be completely cleaned between batches. This estimate would be now taken as the 'nominal' standard uncertainty of measurement  $u_n(R(\lambda)_{mea})$ , and it is approximately below the photometric resolution of most spectrophotometers.

In Figure 4.13 the mean reflectance factor of measurements of eighteen colored sheets with a nominal 2.7 kg/T Levacell Violet BBN belonging to the group A sheets and the 'total' standard

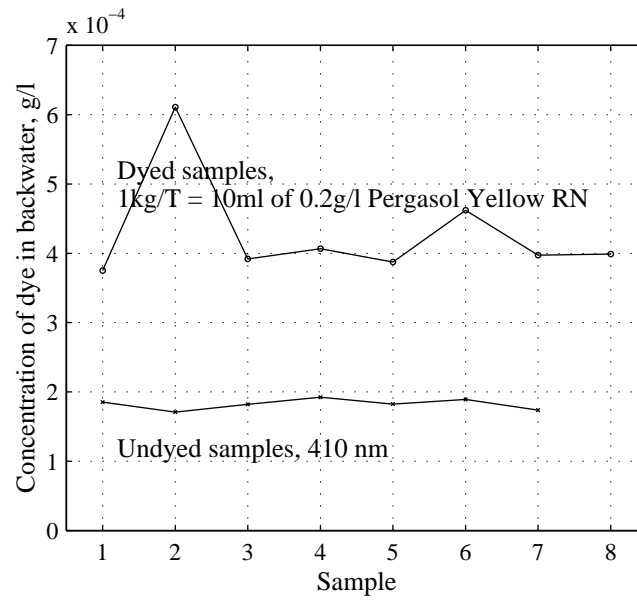


Figure 4.11: The absorbance variation in dyed (1 kg/T Pergasol Yellow RN Powder) and undyed backwaters at wavelengths 410 nm (absorption maximum).

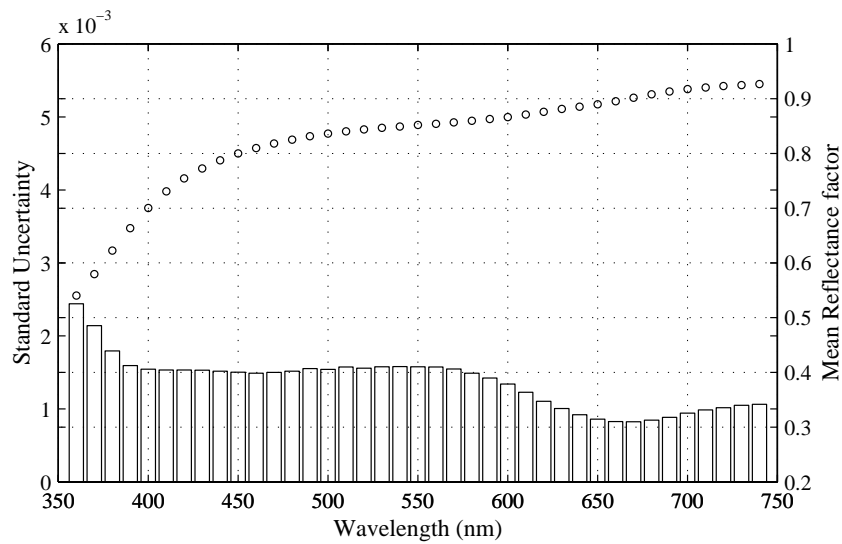


Figure 4.12: The mean reflectance factor  $R(\lambda)$  of measurements of 18 uncolored sheets belonging to the group A sheets and the standard uncertainty measured with CM-3700d.

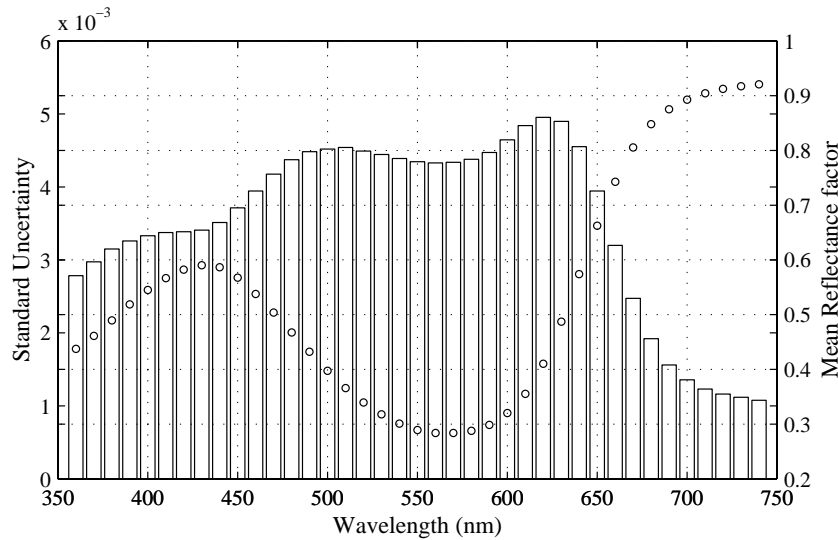


Figure 4.13: The mean reflectance factor  $R(\lambda)$  of measurements of 18 colored sheets colored with nominal 2.7 kg/T Levacell Violet BBN belonging to the group A sheets and the ‘total’ standard uncertainty measured with CM-3700d.

uncertainty is shown. For each beaker 20 ml of 1.0 g/l Levacell Violet BBN was dosed. This produced a deep shade of violet. In addition to the above sources of variation, the effect of dry weight differences between sheets and possibly unevenness of coloring increased the ‘nominal total’ standard uncertainty  $u_n(R(\lambda)_{tot})$  of wavelengths 500-600 nm to be 0.0044 as  $R(\lambda)$ . Thus the estimate of ‘nominal’ coloring standard uncertainty  $u_n(R(\lambda)_{col})$  of wavelengths 500-600 nm would be 0.0029 as  $R(\lambda)$ , based on Equation 4.6.

In Figure 4.14 the mean reflectance factor of 32 measurements made from eight colored sheets (four measurements per sheet) belonging to the group D sheets colored with 1 kg/T Pergasol Yellow RN Powder and the ‘total’ standard uncertainty is shown. The ‘nominal total’ standard uncertainty  $u_n(R(\lambda)_{tot})$  of wavelengths 390-470 nm is calculated to be 0.0079 as  $R(\lambda)$ . The ‘nominal’ standard uncertainty of wavelengths 390-470 nm for undyed group D sheets is estimated to be 0.0029 as  $R(\lambda)$ . Thus the estimate of ‘nominal’ coloring standard uncertainty  $u_n(R(\lambda)_{col})$  would be 0.0050 as  $R(\lambda)$ , based on Equation 4.6. The observed coloring variation is greater than in the case of the colored group A sheets, even though the dry weight variation between group D sheets are smaller. Possibly the colorant dosage and homogeneity of the stock in terms of total surface area plays a more important role. A better explanation would be, that here the stack was formed from twelve sheets of two equal 80 g/m<sup>2</sup> colorings, whereas in the earlier case from four sheets of two equal 200+ g/m<sup>2</sup> colorings. The layered structure of 24 sheets is less consolidated and contains more air space layers, and may exhibit greater cumulative variation in formation.

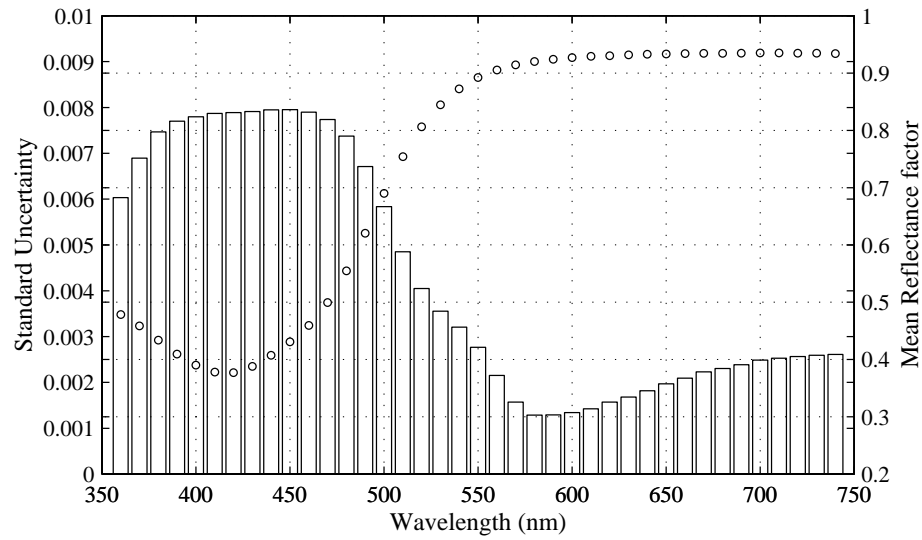


Figure 4.14: The mean reflectance factor  $R(\lambda)$  of measurements of eight colored sheets colored with 1 kg/T Pergasol Yellow RN Powder belonging to the group D sheets and the 'total' standard uncertainty measured with CM-3700d.

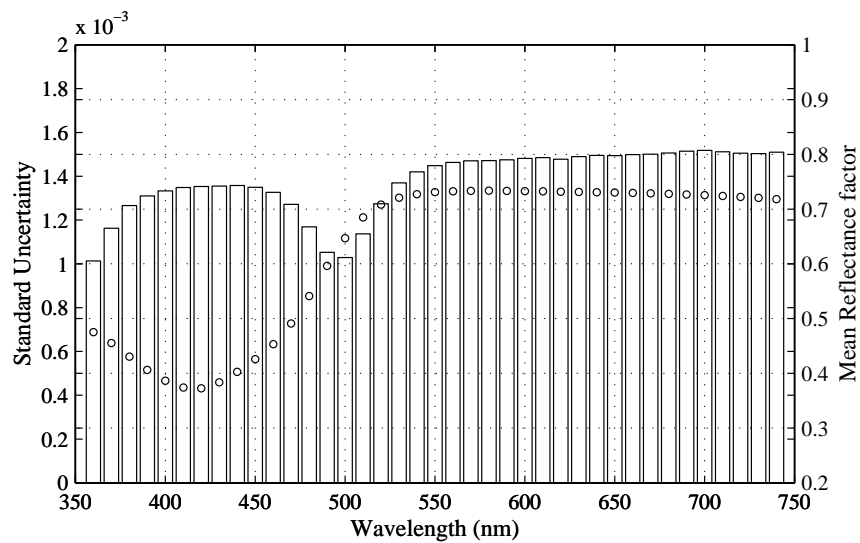


Figure 4.15: The mean reflectance factor  $R(\lambda)$  of single sheet measurements of eight colored sheets colored with 1 kg/T Pergasol Yellow RN Powder belonging to the group D sheets and the 'total' standard uncertainty measured with CM-3700d.

The mean and the ‘total’ standard uncertainty of the single sheet reflectance measurements for the same sheets (80 g/m<sup>2</sup>) with black cavity as backing are shown in Figure 4.15. The ‘nominal total’ standard uncertainty  $u_n(R(\lambda)_{tot})$  of wavelengths 390-470 nm is calculated to be 0.0075 as  $R(\lambda)$  for the single sheet measurements. The increased variability in wavelengths greater than 500 nm is probably caused by variation in sheet formation.

### Scattering analysis

In paper coloring applications, the Kubelka-Munk scattering coefficients  $S(\lambda)$  are of interest and can be calculated for a non-fluorescent sheet based on reflectance factors of the sheet over a backing of zero reflectance  $R_0(\lambda)$ , the reflectance of an infinitely thick pile of sheets  $R_\infty(\lambda)$  and the grammage  $w$  of the sheet [Kub48]:

$$S(\lambda) = \frac{1000}{w b(\lambda)} \operatorname{arccoth} \left( \frac{1 - a(\lambda) R_0(\lambda)}{b(\lambda) R_0(\lambda)} \right) \quad (4.7)$$

where

$$b(\lambda) = 0.5 \left( \frac{1}{R_\infty(\lambda)} - R_\infty(\lambda) \right) \quad (4.8)$$

and where

$$a(\lambda) = 0.5 \left( \frac{1}{R_\infty(\lambda)} + R_\infty(\lambda) \right) \quad (4.9)$$

For FBA containing papers, the measurement must be made using a cut-off filter to eliminate all FBA effects in spectrophotometric measurement or a spectrofluorimetric measurement should be used. Unfortunately this method is suitable only for translucent sheets.

Similarly, the specific absorption coefficients  $K(\lambda)$  can be calculated from the same measurements:

$$K(\lambda) = \frac{1000}{w} \frac{a(\lambda) - 1}{b(\lambda)} \operatorname{arccoth} \left( \frac{1 - a(\lambda) R_0(\lambda)}{b(\lambda) R_0(\lambda)} \right) \quad (4.10)$$

In Figure 4.16 the mean of the scattering coefficient  $S(\lambda)$  and ‘total’ standard uncertainty is calculated for the same sheets as shown in Figures 4.14 and 4.15 having ‘total nominal’ standard uncertainty of wavelengths 390-470 nm 1.13 as  $S(\lambda)$ .

### 4.3.2 Conclusions

The coloring uncertainty based on standard uncertainty multiplied by a coverage factor  $k = 2$ , providing a level of confidence of approximately 95 %, of reflectance factor has been estimated

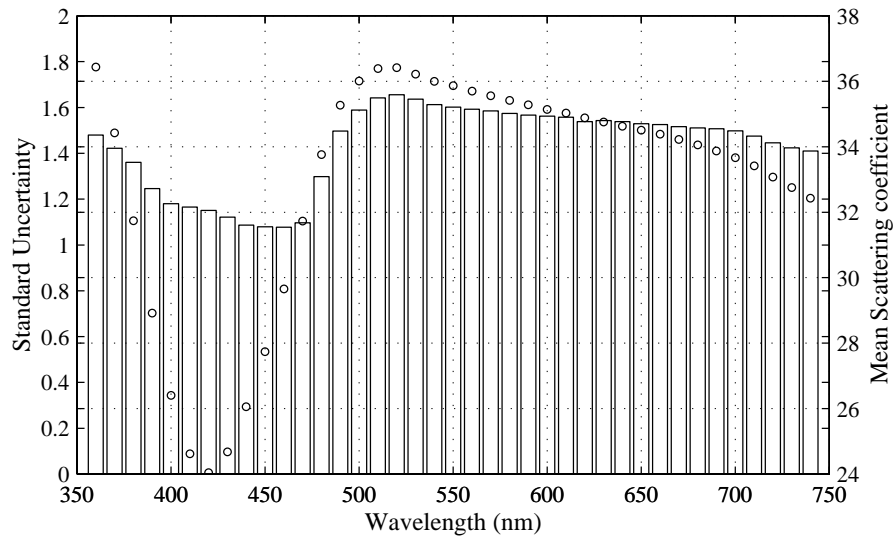


Figure 4.16: The mean scattering coefficient  $S(\lambda)$  of 8 colored sheets colored with 1 kg/T Pergasol Yellow RN Powder belonging to the group D sheets and the ‘total’ standard uncertainty measured with CM-3700d.

to be 0.01 as  $R(\lambda)$  using the stack measurements. Variation of most properties in handsheets tends to be higher than in machine-made sheets. The maximum accuracy that can be obtained in preparing textile dyeings is about 0.025 unit of  $R(\lambda)$  [Ste69, §3-2]. Considering that in textile dyeing yarn or fabric is dyed while in papermaking loose fibers, fines and fillers are dyed, then subsequently formed into a sheet, the results achieved are acceptable.

The surface texture effect in measurements was shortly studied. The approximately random distribution of surface fiber orientations means that directional variations in reflectivity and hence reflectance factor are small. Effects on reflectance due to surface nonuniformity are minimized under conditions of diffuse illumination with specular component excluded, but are still significant. The uncertainty of measurements of undyed sheets based on standard uncertainty multiplied by a coverage factor  $k = 2$ , providing a level of confidence of approximately 95 %, of reflectance factor has been estimated to be 0.005 as  $R(\lambda)$  using the stack measurements.

There is, of course, a more philosophical question relating to the experimental work: do the colored handsheets represent the stock coloring process at the paper mill, especially at low colorant concentrations in the sheets. They may, if they are made from the same stock as used at the mill, but depth of color may be lower at lowest colorants’ dosage. This may result from different dilution levels of the colorants, whereas at the mill the colorants often are diluted only to a single concentration, at which they are metered into the stock.

## Chapter 5

# Colorant Modelling

Paper colorant models may be grouped as phenomenological models, physical chemistry models, or ad hoc data fitting models. A general requirement for a steady-state paper colorant model, which describes the relation between total radiance factor of the colored substrate and increasing concentration of colorant(s) in the dye bath, is that the model should be linear and additive [McL86, §12]. Linearity implies that change in the modelled quantity of a colored material is proportional to the amount of colorant added to the substrate. Additivity implies that the change in the modelled quantity of a colored material when two or more colorants are added to the substrate is equal to the sum of the changes caused by the addition of the same amounts of single colorants to the substrate. In addition to linearity and additivity, the model should contain the minimum number of parameters to minimize the number of colored handsheets or on-line tuning tests needed for parameter identification, and it should be robust and simple. Robustness implies that model predictions should change uniformly with variation of parameter values, and that small parameter changes should not lead to large changes in modelled behaviour.

A tour of adsorption isotherm analysis will first be taken. To understand the requirements for and use of the colorant models, a short tour of color control algorithms will also be taken, before studying phenomenological theory and models, and some of their extensions.

### 5.1 Adsorption isotherm analysis

The amount of dye-on-fiber was determined based on backwater analyses for sheets dyed with Pergasol Yellow RN Powder and Pergasol Turquoise R Powder, which are shown in Figure 5.1. In this Figure the dye-on-fiber is modelled based on a monolayer Langmuir isotherm at the dyes' absorption maxima having the saturation value of  $[S]_f = 10.6 \text{ kg/T}$  and the adsorption equilibrium constant of  $b = 124.1 \text{ L/mg}$  for the Yellow dye, and respectively  $[S]_f = 5.4 \text{ kg/T}$  and  $b = 112.8 \text{ L/mg}$  for the Turquoise dye. The saturation value of a dye is estimated from fitting  $\frac{[D]_f}{[D]_s}$  versus  $[D]_f$  as shown in subfigure (B), which is more sensitive than reciprocal plots. The goodness of a fit as the root-mean-square residual for the Yellow dye is 0.136 and for the Tur-

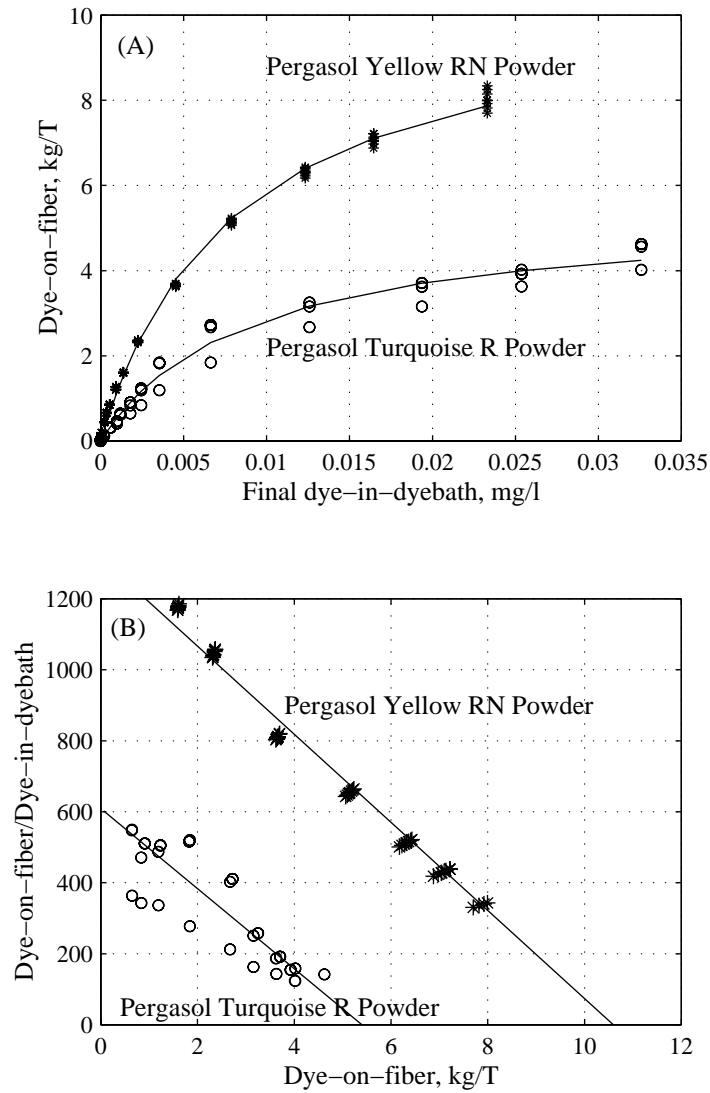


Figure 5.1: (A) The ratio of dye-on-fiber to final dye-in-dyebath for Pergasol Yellow RN Powder and Pergasol Turquoise R Powder in coloring conditions used for the group D sheets, and their estimated Langmuir isotherm based model, (solid).

(B)  $\frac{[D]_f}{[D]_s}$  versus  $[D]_f$  plot of the colorings and their estimate to define  $[S]_f$ .

quiose dye 0.199. If the coloring follows a Langmuir isotherm a straight line should be obtained whose intercept on the  $[D]_f$  axis is the saturation value of dye on-the-fiber  $[S]_f$ . In this case, it is hard to distinguish non-linearity originating due to coloring errors from the possibility that coloring does not follow a Langmuir isotherm. Moreover, the amount of dye-on-fiber depends

on surface area of fiber, which changes with refining and pulping processes as well as with fiber type.

Since direct anionic dyes have a high tendency to form aggregates, a multilayer model of Langmuir isotherm was constructed with the following assumptions:

- the first adsorbed layer of molecules appears as a homogeneous surface for adsorption of a second layer of molecules, and consistently for the subsequent layers  $j$  and  $j + 1$
- excitation energy and energy of adsorption for adsorption onto the second layer differ from those of the first layer; for the second and the subsequent layers these energies are assumed to be the same
- the saturation concentration for the second and subsequent layer is equal to the concentration of the layer immediately beneath, (i.e. the saturation concentration for layer  $j$  is  $[D_{j-1}]_f$ )

Note that this model assumes that a  $j$  layer molecule is as likely to adsorb onto an isolated  $j - 1$  layer molecule as onto a cluster of  $j - 1$  layer molecules, which may not be physically realistic. It thus may overestimate the extent of the  $j$  layer at low concentrations of the  $j - 1$  layer. However, the  $j$  layer will be small under these conditions, so the error is not significant. Adsorption of  $j$  layer onto  $j - 1$  layer can be modelled as follows:

$$r_{ads,j} = k_{ads,j}[D]_s([D_{j-1}]_f - [D_j]_f) \quad (5.1)$$

$$r_{des,j} = k_{des,j}([D_j]_f - [D_{j+1}]_f) \quad (5.2)$$

where  $[D_j]_f$  is the surface concentration of the  $j^{\text{th}}$  adsorbed layer and  $[D_{j+1}]_f$  is the surface concentration of the  $(j + 1)^{\text{th}}$  adsorbed layer, and where  $[D_0]_f = [S]_f$ , see Figure 5.2.

Equating rates of adsorption and desorption for a layer  $j$  at equilibrium and rearranging, the fractional saturation of adsorbed dye on a layer  $j$  is obtained:

$$\frac{[D_j]_f}{[D_{j-1}]_f} = \frac{\frac{[D_{j+1}]_f}{[D_{j-1}]_f} + b_j[D]_s}{1 + b_j[D]_s} \quad (5.3)$$

where  $b_j = \frac{k_{ads,j}}{k_{des,j}}$ . Rearranging gives:

$$\frac{[D_j]_f}{[D_{j-1}]_f} = \frac{\frac{b_j[D]_s}{1+b_j[D]_s}}{1 - \frac{1}{1+b_j[D]_s} \frac{[D_{j+1}]_f}{[D_j]_f}} \quad (5.4)$$

The fractional saturation of adsorbed dye on the top layer  $n$  is:

$$\frac{[D_n]_f}{[D_{n-1}]_f} = \frac{b_2[D]_s}{1 + b_2[D]_s} \quad (5.5)$$

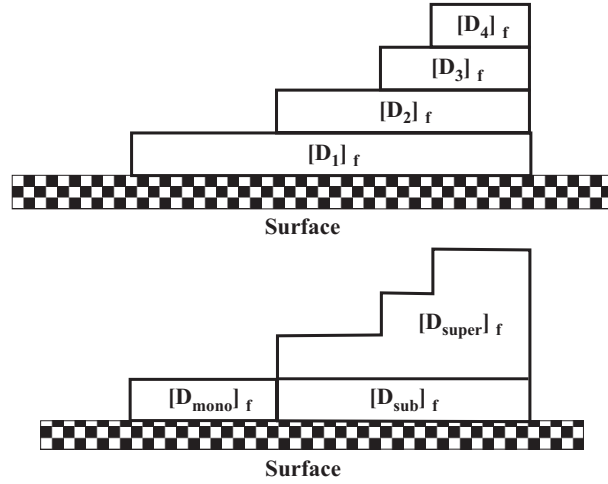


Figure 5.2: The first adsorbed layer  $[D_1]_f$  and the subsequent layers  $[D_2]_f$ ,  $[D_3]_f$  etc. form regions with monolayer coverage  $[D_{mono}]_f$  and multilayer coverage  $[D_{multi}]_f$ , where the multilayer is composed of sublayer  $[D_{sub}]_f$  and superlayer  $[D_{super}]_f$ .

since  $\frac{[D_{n+1}]_f}{[D_n]_f} = 0$ , and our earlier assumptions imply that  $b_2 = b_3 = \dots = b_n$ .  
For the first layer:

$$\frac{[D_1]_f}{[S]_f} = \frac{\frac{[D_2]_f}{[S]_f} + b_1[D]_s}{1 + b_1[D]_s} \quad (5.6)$$

The total surface concentration of adsorbed dye is thus:

$$[D_{total}]_f = \sum_{j=1}^{j=n} [D_j]_f = [D_1]_f \left( 1 + \frac{[D_2]_f}{[D_1]_f} \left( 1 + \dots \left( 1 + \frac{[D_n]_f}{[D_{n-1}]_f} \right) \right) \right) \quad (5.7)$$

while the multilayer surface concentration is:

$$[D_{multi}]_f = 2[D_2]_f + \sum_{j=3}^{j=n} [D_j]_f \quad (5.8)$$

The superlayer surface concentration (all layers not in contact with the substrate) is:

$$[D_{super}]_f = \sum_{j=2}^{j=n} [D_j]_f \quad (5.9)$$

and the monolayer surface concentration (in contact only with the substrate) is:

$$[D_{mono}]_f = [D_1]_f - [D_2]_f \quad (5.10)$$

and the sublayer surface concentration (in contact with the substrate and with the superlayer) is:

$$[D_{sub}]_f = [D_2]_f \quad (5.11)$$

This multilayer model of Langmuir isotherm with infinite number of layers is equivalent to the BET isotherm [Do98, §3.3].

The result of fitting Pergasol Yellow RN Powder data to the five-layer model of Langmuir isotherm is shown in Figure 5.3. The monolayer saturation value was  $[S]_f = 7.94$  kg/T, and adsorbed masses have been normalized to saturated monolayer equivalents. The adsorption equilibrium constants were  $b_1 = 185.8$  L/mg and  $b_2 = 7.460$  L/mg. The goodness of a fit for the Yellow as the root-mean-square residual is now 0.014.

The result of fitting Pergasol Turquoise R Powder data to the five-layer model is shown in Figure 5.4. The monolayer saturation value was  $[S]_f = 4.33$  kg/T, and adsorbed masses have been normalized to saturated monolayer equivalents. The adsorption equilibrium constants were  $b_1 = 152.5$  L/mg and  $b_2 = 4.653$  L/mg. The goodness of a fit for the Turquoise as the root-mean-square residual is now 0.045. The saturation value appears lower than for Yellow, because the Turquoise dye molecule has two chromophores it is substantially larger than the Yellow dye molecule.

The adsorption behavior of Yellow and Turquoise dyes is quite similar, expect for a scale factor, which represents the accessibility of the surface to the molecule and geometric issues relating to the arrangement of molecules on the surface.

Based on the results shown in Figures 5.1, 5.3 and 5.4 the anionic direct dyes' adsorption process on cellulosic fibers in conditions of handsheet making can be modelled well enough using Langmuir isotherm. This result will be used later in developing a new colorant model.

## 5.2 Importance of Colorant Modelling

The function of color control is to minimize specified color errors by governing the available colorants' dosage. Traditionally, Kubelka-Munk based colorant formulation algorithms [KM31, McD97b] have also been used for on-line color control in the paper industry [CMS96, She99], despite their limitations, of which the neglect of fluorescence is the most serious. In the optimizing color controller, an approach was taken in 1993 to control paper coloring directly in total radiance factor domain, using a non-linearized colorant response model, and to regulate the colorants' dosage to minimize for example CIE  $L^* a^* b^*$  errors for a particular standard illuminant and field of view, optionally also including a brightness error in the optimization [SS97, SS98a, SS98b]. This gave the benefit of better color control for brilliant white papers than the traditional methods [TSS99]. A question arose, whether this was because of the colorant responses in this algorithm.

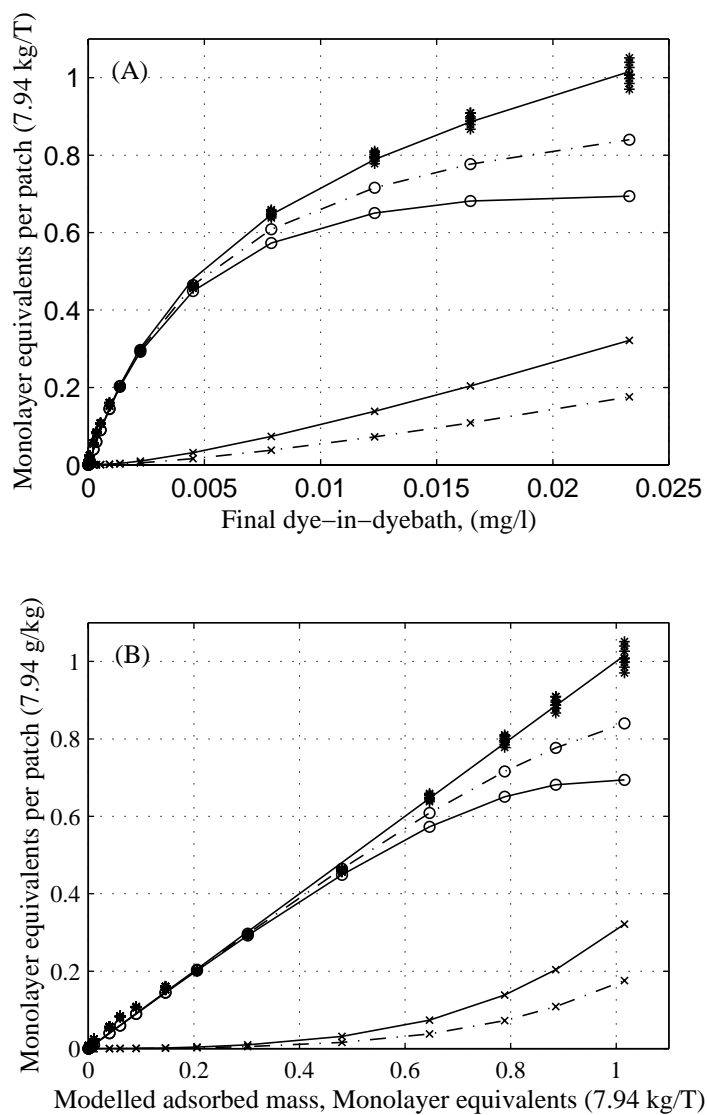


Figure 5.3: Measured and modelled adsorption isotherms for Pergasol Yellow RN Powder, using a five-layer adsorption model. \*=measured values, the uppermost curve is the overall fit to the measurement, dash lines indicate the modelled individual layers, o=first layer  $[D_1]_f$ , x=superlayer  $[D_{super}]_f$ , solid lines indicate monolayer and multilayer concentrations, o=monolayer  $[D_{mono}]_f$ , x=multilayer  $[D_{multi}]_f$ .

(A) Adsorption breakdown versus dye-in-dyebath.

(B) Adsorption breakdown versus total modelled amount adsorbed.

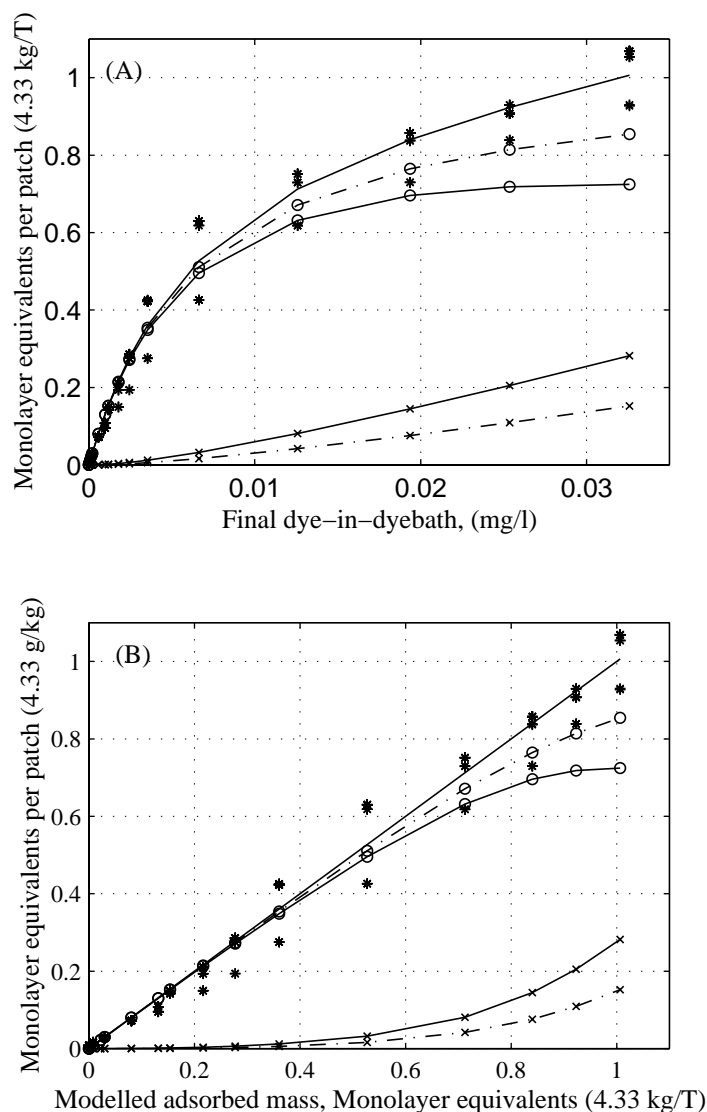


Figure 5.4: Measured and modelled adsorption isotherms for Pergasol Turquoise R Powder, using a five-layer adsorption model. \*=measured values, the uppermost curve is the overall fit to the measurement, dash lines indicate the modelled individual layers, o=first layer  $[D_1]_f$ , x=superlayer  $[D_{super}]_f$ , solid lines indicate monolayer and multilayer concentrations, o=monolayer  $[D_{mono}]_f$ , x=multilayer  $[D_{multi}]_f$ .

(A) Adsorption breakdown versus dye-in-dyebath.

(B) Adsorption breakdown versus total modelled amount adsorbed.

### 5.2.1 Colorant Formulation with Dyes

Colorant formulation is understood to be based on phenomenological theory in turbid media, which explains how the radiance of light incident on a layer is affected by absorption and scattering, either using a many-flux model or a two-flux version of the many-flux model. Many-flux theory is the most generalized of the phenomenological theory, but has only theoretical value [Völ95, §3.1.2]. It utilizes a three-dimensional solid angle coordinate system having position coordinate  $z$  and fixed solid angles  $\Omega$  to describe the angular distribution of the radiation. The four-flux and two-flux theories have practical significance and the two-flux model is the most used phenomenological theory. The Kubelka-Munk two-flux model provides a two constant and a single constant version, of which the latter approach [KM31, McD97a] is widely used in the paper industry, even though real colorants do not respond ideally in the way suggested by the phenomenological theory [Hof89]. This model is described in Section 5.3.3.

#### Spectrophotometric matching

The basic approach in colorant formulation via spectrophotometric matching is to use the least-squares technique over all wavelengths to minimize the sums of the square of the residuals for each wavelength to be at a minimum using constrained optimization [McD97b]. This matching is done in the ratio  $\frac{K(\lambda)}{S(\lambda)}$  base, which utilizes the benefit of Kubelka-Munk absorption and scattering coefficients both to be linear and additive to a first approximation [McL86, §12]. If the change in absorption caused by a dye concentration in the dyebath is modelled using a wavelength dependent absorption coefficient  $a_j(\lambda)$  of dye  $j$ , then the objective to be minimized is:

$$\min \sum_{\lambda=380}^{780} \left( \left( \frac{K_t(\lambda)}{S_t(\lambda)} - \frac{K_s(\lambda)}{S_s(\lambda)} \right) - \sum_{j=1}^n a_j(\lambda) c_j \right)^2 \quad (5.12)$$

where the ratio  $\frac{K_t(\lambda)}{S_t(\lambda)}$  is the target, the ratio  $\frac{K_s(\lambda)}{S_s(\lambda)}$  is for the base substrate, and  $c_j$  is the dye concentration in the dyebath of dye  $j$ .

If the same dyes and substrate are used to produce new colors, non-metameric matches are possible using spectrophotometric matching. If different dyes or substrates with different reflectance factor are used, in general only a colorimetric match can be supplied. The latter case is the reality in papermaking.

#### Colorimetric matching

In the case of colorimetric color matching in color formulation, typically tristimulus errors are minimized. This requires and is generally limited to three dyes, but can be extended up to  $3N$  dyes if minimization is done using measurements obtained with  $N$  illuminants which are linearly independent in the visual wavelength range (and with  $3N$  colorimetric targets as a consequence):

$$\min \left( \left( \begin{bmatrix} X_t \\ Y_t \\ Z_t \end{bmatrix} - \begin{bmatrix} X_s \\ Y_s \\ Z_s \end{bmatrix} \right) - \begin{bmatrix} \frac{\partial X}{\partial c_j} \\ \frac{\partial Y}{\partial c_j} \\ \frac{\partial Z}{\partial c_j} \end{bmatrix} \Delta c_j \right)^2 \quad (5.13)$$

where  $X_t$   $Y_t$   $Z_t$  are CIE tristimulus targets,  $X_s$   $Y_s$   $Z_s$  are CIE tristimulus values of the base substrate,  $c_j$  is concentration of dye  $j$  and a process model [McD97b, Che95]

$$\begin{bmatrix} \frac{\partial X}{\partial c_j} \\ \frac{\partial Y}{\partial c_j} \\ \frac{\partial Z}{\partial c_j} \end{bmatrix} = \sum_{\lambda=380}^{780} \left( S(\lambda) \begin{bmatrix} \bar{x}(\lambda) \\ \bar{y}(\lambda) \\ \bar{z}(\lambda) \end{bmatrix} \begin{pmatrix} \frac{\partial R(\lambda)}{\partial \frac{K(\lambda)}{S(\lambda)}} \\ \frac{\partial \frac{K(\lambda)}{S(\lambda)}}{\partial c_j} \end{pmatrix} \right) \quad (5.14)$$

in which

$$\begin{pmatrix} \frac{\partial R(\lambda)}{\partial \frac{K(\lambda)}{S(\lambda)}} \end{pmatrix} = \frac{2R(\lambda)^2}{R(\lambda)^2 - 1} \quad (5.15)$$

and

$$\begin{pmatrix} \frac{\partial \frac{K(\lambda)}{S(\lambda)}}{\partial c_j} \end{pmatrix} = a_j(\lambda) \quad (5.16)$$

where  $a_j(\lambda)$  is the wavelength dependent absorption coefficient of dye  $j$ ,  $R(\lambda)$  is either the target reflectance factor  $R(\lambda)_t$ , if it exists or the calculated reflectance factor  $R(\lambda)_k$  based on corresponding dye concentrations of the current recipe at the end of each iteration.

The value of  $\frac{\partial R(\lambda)}{\partial \frac{K(\lambda)}{S(\lambda)}}$  varies according to the magnitude of the reflectance factor and therefore applies only over a relatively small reflectance range. The least-squares optimization can use a constant process model for minor adjustments, but should adapt the process model at each step in the optimization for larger adjustments.

Thus in the case of color control of fluorescent paper, the reflectance factor  $R(\lambda)$  has to be separated from the total radiance factor  $\beta_T(\lambda|S)$  measurement, and the color control would be done in base of reflectance factor and the usage of fluorescent brightening agents (FBAs) would be controlled based on measurement of a fluorescence index. This concept leads to the situation, where color is controlled under illumination conditions which differ from those of its intended use by the consumer.

The optimization can be easily extended to combine minimization of both reflectance and colorimetric errors. This would require use of both a  $\frac{K_t(\lambda)}{S_t(\lambda)}$  target together with a three dimensional colorimetric target. Unfortunately, the desired  $\frac{K_t(\lambda)}{S_t(\lambda)}$  target may be unreachable, especially if the stock composition or quality changes.

## 5.2.2 Optimizing Color Controller

The optimizing color controller minimizes a quadratic objective function formed from the total radiance factor error using specified illuminant  $S$  and/or colorimetric error in a defined color space using a radiance factor based algorithm. The general form is described in [SS98b, SS97] and only the principal form of this objective function to be minimized is discussed here:

$$\min (\alpha_{\beta_T(\lambda|S)} P_{\beta_T(\lambda|S)} + \alpha_{XYZ(S,k)} P_{XYZ(S,k)}) \quad (5.17)$$

where  $\alpha_{\beta_T(\lambda|S)}$  is the weighting factor for the total radiance factor objective  $P_{\beta_T(\lambda|S)}$ , where the specimen is irradiated with the illuminant  $S$ .  $P_{XYZ(S,k)}$  is the objective for CIE tristimulus values, evaluated from the total radiance factor using illuminant  $S$  and field of view  $k$ , with weighting factor  $\alpha_{XYZ(S,k)}$ . The objective can also contain terms for deviation from targets in CIELAB or Hunter Lab opponent-color scales, and those objective terms are the most important for paper mills. It can also contain other terms, such as cost of each dye, and so forth. All scalar weighting factors are non-negative. The objective function  $P$ , is minimized using a Newton type method, modified for constrained optimization in simple convex regions.

Here, only the CIE tristimulus objective  $P_{XYZ(S,k)}$ , its gradient  $\nabla P_{XYZ(S,k)}$ , and Hessian  $\nabla\nabla P_{XYZ(S,k)}$  are given:

$$P_{XYZ(S,k)} = w_X \Delta X^2(S, k) + w_Y \Delta Y^2(S, k) + w_Z \Delta Z^2(S, k) \quad (5.18)$$

where  $\Delta X(S, k)$  is CIE tristimulus X error with illuminant  $S$  and field of view  $k$ , correspondingly for  $\Delta Y(S, K)$  and  $\Delta Z(S, k)$ .

$$\nabla P_{XYZ(S,k)} = w_X \nabla X(S, k) + w_Y \nabla Y(S, k) + w_Z \nabla Z(S, k) \quad (5.19)$$

where

$$\begin{bmatrix} \nabla X(S, k) \\ \nabla Y(S, k) \\ \nabla Z(S, k) \end{bmatrix} = \begin{bmatrix} 2\Delta X(S, k) \nabla \beta_T^t(\lambda|S) \bar{x}(\lambda) S(\lambda) \\ 2\Delta Y(S, k) \nabla \beta_T^t(\lambda|S) \bar{y}(\lambda) S(\lambda) \\ 2\Delta Z(S, k) \nabla \beta_T^t(\lambda|S) \bar{z}(\lambda) S(\lambda) \end{bmatrix} \quad (5.20)$$

in which the normalized total radiance factor response,  $\nabla \beta_T(\lambda|S)$ , for each colorant at the specific concentration  $c$  at steady state, where each response is normalized to the ratio of mass of pure colorant to mass of dry solids of the sheet:

$$\nabla \beta_T(\lambda|S) = \frac{\partial \beta_T(\lambda|S)}{\partial c} \cong \frac{\Delta \beta_T(\lambda|S)}{\Delta c} \quad (5.21)$$

and

$$\nabla\nabla P_{XYZ(S,k)} = w_X \nabla\nabla X(S,k) + w_Y \nabla\nabla Y(S,k) + w_Z \nabla\nabla Z(S,k) \quad (5.22)$$

where

$$\begin{bmatrix} \nabla\nabla X(S,k) \\ \nabla\nabla Y(S,k) \\ \nabla\nabla Z(S,k) \end{bmatrix} = \begin{bmatrix} 2 [\nabla\beta_T^t(\lambda|S) \bar{x}(\lambda) S(\lambda)] [\nabla\beta_T^t(\lambda|S) \bar{x}(\lambda) S(\lambda)]^t \\ 2 [\nabla\beta_T^t(\lambda|S) \bar{y}(\lambda) S(\lambda)] [\nabla\beta_T^t(\lambda|S) \bar{y}(\lambda) S(\lambda)]^t \\ 2 [\nabla\beta_T^t(\lambda|S) \bar{z}(\lambda) S(\lambda)] [\nabla\beta_T^t(\lambda|S) \bar{z}(\lambda) S(\lambda)]^t \end{bmatrix} + \begin{bmatrix} 2 \Delta X(S,k) \nabla\nabla\beta_T^t(\lambda|S) \bar{x}(\lambda) S(\lambda) \\ 2 \Delta Y(S,k) \nabla\nabla\beta_T^t(\lambda|S) \bar{y}(\lambda) S(\lambda) \\ 2 \Delta Z(S,k) \nabla\nabla\beta_T^t(\lambda|S) \bar{z}(\lambda) S(\lambda) \end{bmatrix} \quad (5.23)$$

where the latter summing term containing  $\nabla\nabla\beta_T^t(\lambda|S)$  is ignored, being negligible over a broad range for non-interacting or weakly-interacting colorants.

In practice, usually only a single response per colorant is required to cover white shade grades where only small variations in dosage of this colorant exist, and other process conditions are generally constant. Often colorant responses are defined using on-line tuning tests only. Clearly, if the same colorant is used with white and pastel shades then a second colorant response is required. As stated earlier, the motivation of this research was to develop currently used static dye and FBA responses into dynamic ones.

The benefit of this approach is, that color matching can be made based on total radiance factor measurement using specified illuminator(s), which approximates closely standard illuminant(s), and taking proper account of fluorescence. Use of more than one illuminant in the measurement and control allows illuminant and illuminator metamerism to be minimized.

The effect of a colorant in color coordinate systems such as CIELAB can be calculated from its normalized total radiance factor response and the measured total radiance factor of the sheet. Thus, a process model for these color spaces can be formulated in terms of total radiance factor [SS97, SS98b].

### 5.3 Two-Flux Model

The two-flux theory is a phenomenological model which describes how the diffuse radiance of light incident on a layer is affected by isotropic absorption and scattering. It models diffuse radiances  $\Phi_z^+(\lambda)$  and  $\Phi_z^-(\lambda)$  respectively travelling inside a plane-parallel light-scattering specimen towards its unilluminated and its illuminated surface, Figure 5.5. The absorption  $K(\lambda)$  and scattering  $S(\lambda)$  coefficients are deemed to be intrinsic properties of the material, but tell us little of actual absorption and scattering mechanisms [SB72].

Let  $z$  be the position coordinate from the illuminated surface,  $\Phi_0^+(\lambda)$  the diffuse incident radiance of light at wavelength  $\lambda$  on the illuminated surface and  $\Phi_0^-(\lambda)$  the diffuse radiance of light

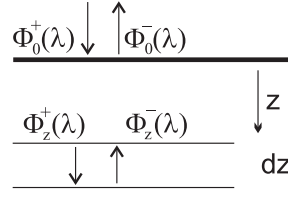


Figure 5.5: Diffuse radiances  $\Phi_z^+(\lambda)$ ,  $\Phi_z^-(\lambda)$  inside a layer.

at wavelength  $\lambda$  exiting the illuminated surface. The decrease in the amount of individual radiances as the light traverses the short distance  $dz$  in the non-fluorescent specimen by absorption is modelled using Lambert's law, and is  $-K(\lambda)\Phi_z^+(\lambda)dz$ . If scattering is present,  $\Phi_z^+(\lambda)$  also loses  $-S(\lambda)\Phi_z^+(\lambda)dz$  scattered forward and  $-S(\lambda)\Phi_z^-(\lambda)dz$  scattered backward, where  $S(\lambda)$  is a scattering coefficient. Now, the model for two-flux system [KM31] based on assumptions of ideally diffuse radiation distribution on the irradiation side of specimen and in the interior of the layer, and continuity in refractive index [Völ95, §3.3.1] can be written as:

$$\frac{d\Phi_z^+(\lambda)}{dz} = -(K(\lambda) + S(\lambda))\Phi_z^+(\lambda) + S(\lambda)\Phi_z^-(\lambda) \quad (5.24)$$

$$\frac{d\Phi_z^-(\lambda)}{dz} = (K(\lambda) + S(\lambda))\Phi_z^-(\lambda) - S(\lambda)\Phi_z^+(\lambda) \quad (5.25)$$

By differentiating Equation 5.24, substituting  $\frac{d\Phi_z^+(\lambda)}{dz}$  from Equation 5.24 and  $\frac{d\Phi_z^-(\lambda)}{dz}$  from Equation 5.25, one obtains:

$$\frac{d^2\Phi_z^+(\lambda)}{dz^2} = (K(\lambda)^2 + 2K(\lambda)S(\lambda))\Phi_z^+(\lambda) \quad (5.26)$$

This differential equation has a solution:

$$\Phi_z^+(\lambda) = \Phi_0^+(\lambda) \exp^{-z\sqrt{K(\lambda)^2 + 2K(\lambda)S(\lambda)}} \quad (5.27)$$

By differentiating this and substituting it back to Equation 5.24,  $\Phi_z^-(\lambda)$  can be now solved. The amount of radiance at the distance  $z$  from the surface travelling towards the surface is hence:

$$\Phi_z^-(\lambda) = \Phi_0^+(\lambda) \left( 1 + \frac{K(\lambda)}{S(\lambda)} - \frac{\sqrt{K(\lambda)^2 + 2K(\lambda)S(\lambda)}}{S(\lambda)} \right) \exp^{-z\sqrt{K(\lambda)^2 + 2K(\lambda)S(\lambda)}} \quad (5.28)$$

Since the standard Kubelka-Munk theory does not take account of fluorescence, it only addresses reflected radiance factors, which are defined as ratio of the diffuse flux reflected from

the specimen to the diffuse incident flux under the same geometric and spectral conditions of measurement. Thus let  $z$  be zero and the specimen infinitely thick, then reflectance factor at the surface for a sample of infinite thickness having continuity in refractive index is:

$$R(\lambda) = \frac{\Phi_0^-(\lambda)}{\Phi_0^+(\lambda)} = 1 + \frac{K(\lambda)}{S(\lambda)} - \sqrt{\left(\frac{K(\lambda)}{S(\lambda)} + 1\right)^2 - 1} \quad (5.29)$$

However, a discontinuity in refractive index is usually present at the surface of the medium. Thus the reflectance factors measured at the surface of a sample can differ greatly from the reflectance factors measured prevailing in the interior of the layer under study [Völ95, §3.3.1]. The phenomenological analysis requires the reflectance factors measured at the surface of a sample be converted to the corresponding internal quantities. This is known as the surface reflection correction and is discussed further in Section 5.3.1.

The ratio of the substrate's absorption and scattering coefficients, the basic Kubelka-Munk formula, can be solved from Equation 5.29:

$$\frac{K(\lambda)}{S(\lambda)} = \frac{(1 - R(\lambda))^2}{2R(\lambda)} \quad (5.30)$$

where  $R(\lambda)$  is the reflectance factor in the interior of the layer under study. In Figure 5.6, in the subfigure (A) the  $\frac{K(\lambda)}{S(\lambda)}$  is shown as function of  $R(\lambda)$ .

### Error sensitivity

The error sensitivity of Equation 5.30 for the measurement errors can be calculated. For an error  $\Delta R(\lambda)$  in  $R(\lambda)$ , the resulting error in  $\frac{K(\lambda)}{S(\lambda)}$  is:

$$\Delta \left( \frac{K(\lambda)}{S(\lambda)} \right) = \frac{\partial \frac{K(\lambda)}{S(\lambda)}}{\partial R(\lambda)} \Delta R(\lambda) = \frac{R(\lambda)^2 - 1}{2R(\lambda)^2} \Delta R(\lambda) \quad (5.31)$$

Thus, even with a reasonably small error in  $R(\lambda)$ , errors in  $\frac{K(\lambda)}{S(\lambda)}$  can be quite large when  $R(\lambda)$  is small, as can be seen in the subfigure (B) in Figure 5.6.

The relative error in  $\frac{K(\lambda)}{S(\lambda)}$  for an error  $\Delta R(\lambda)$  is:

$$\Delta \log \left( \frac{K(\lambda)}{S(\lambda)} \right) = \frac{1}{\frac{K(\lambda)}{S(\lambda)}} \frac{\partial \frac{K(\lambda)}{S(\lambda)}}{\partial R(\lambda)} \Delta R(\lambda) = \frac{R(\lambda) + 1}{R(\lambda)(R(\lambda) - 1)} \Delta R(\lambda) \quad (5.32)$$

Clearly, the relative error in  $\frac{K(\lambda)}{S(\lambda)}$  will be large if  $R(\lambda)$  is near zero or near unity (i.e. when  $\frac{K(\lambda)}{S(\lambda)}$  is large or small). This relation is plotted in Figure 5.6 in the subfigure (C). Völz has made a similar evaluation including Saunderson correction for a change in refractive index [Völ95, §3.3.2].

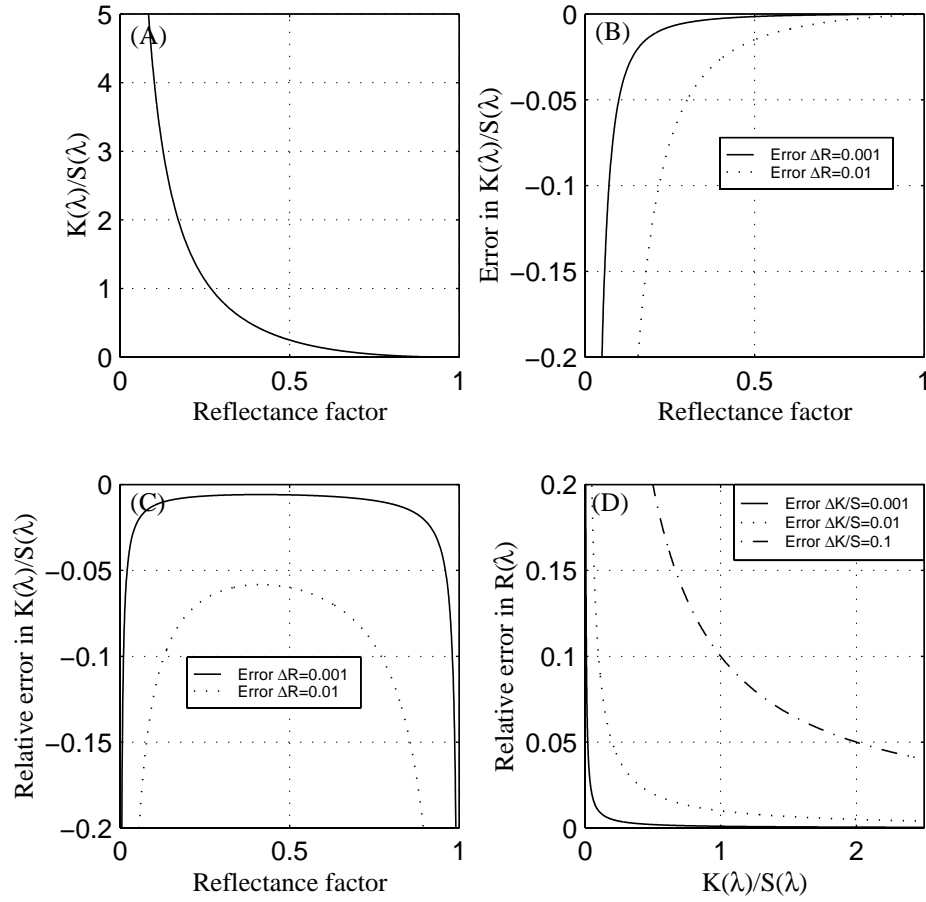


Figure 5.6: (A)  $\frac{K(\lambda)}{S(\lambda)}$  as function of  $R(\lambda)$ .

(B) The error in  $\frac{K(\lambda)}{S(\lambda)}$  for  $R(\lambda)$  error of 0.001 and 0.01 based on Equation 5.31.

(C) The relative error in  $\frac{K(\lambda)}{S(\lambda)}$  for  $R(\lambda)$  error of 0.001 and 0.01 based on Equation 5.32.

(D) The relative error in  $R(\lambda)$  for  $\frac{K(\lambda)}{S(\lambda)}$  error of 0.001, 0.01 and 0.1 based on Equation 5.33.

The error sensitivity for the relation 5.29 can also be calculated. For an error  $\Delta \left( \frac{K(\lambda)}{S(\lambda)} \right)$  in  $\frac{K(\lambda)}{S(\lambda)}$ , the resulting error in  $R(\lambda)$  is:

$$\Delta R(\lambda) = \frac{\partial R(\lambda)}{\partial \frac{K(\lambda)}{S(\lambda)}} \Delta \left( \frac{K(\lambda)}{S(\lambda)} \right) = \left( 1 - \frac{\frac{K(\lambda)}{S(\lambda)} + 1}{\sqrt{\left( \frac{K(\lambda)}{S(\lambda)} + 1 \right)^2 - 1}} \right) \Delta \left( \frac{K(\lambda)}{S(\lambda)} \right) \quad (5.33)$$

Thus, large errors in  $R(\lambda)$  will occur when  $\frac{K(\lambda)}{S(\lambda)}$  is near zero (i.e. when  $R(\lambda)$  is near unity). This relation is plotted in Figure 5.6 in the subfigure (D). In fact, errors in  $\frac{K(\lambda)}{S(\lambda)}$  will be numer-

ically amplified as errors in  $R(\lambda)$  whenever  $\frac{K(\lambda)}{S(\lambda)} < \frac{2-\sqrt{3}}{\sqrt{3}} \approx 0.1547$ , which occurs with many samples in this study.

### 5.3.1 Surface Reflection Correction

Kubelka [Kub48] assumed in the derivations of the Kubelka-Munk theory, that the turbid material forms a plane layer of constant, generally finite, thickness, being infinitely extended, and with optical inhomogeneities incomparably smaller than the thickness of the specimen and uniformly distributed in the material. Moreover, the medium of the material is assumed to be the same as the medium the light comes out of (generally air.)

The continuity of refractive index requires that the host medium containing the scattering particles must be the same as that from which the radiation impinges on the surface of the layer, so that no additional reflection loss occurs at the surface because of a refractive index difference [Kor69, §IV.c]. “In practice then, only particles embedded in air, such as powders, paper, textiles, etc., fulfill these conditions. Suspensions in liquids, colloidal dispersions, etc., will only be capable of treatment by these equations when additional corrections are introduced for the surface reflection loss” [Kor69, §IV.c].

As a material, paper is a stochastic and planar network of fibers, since the fibers are much longer than the thickness of the paper sheet. The voids ignored in the two-dimensional approximation give paper its opaque, bulky, and stiff structure [NKP98], and paper is anisotropic. Based on Kortüm’s above statement, the fiber network is understood as “independent” scattering particles uniformly distributed in the air. The surface structure of uncoated paper and textile samples is indefinable. Thus the surface reflection correction is frequently neglected [Kue75, §3], and was not applied for paper samples in this study.

Experimentally, the surface (specular) reflection may be determined by dyeing the substrate with increasing concentrations of a strongly absorbing dye until the reflectance factor at the wavelength of the maximum absorption becomes independent of the dye concentration. This limiting value of the reflectance factor  $r_0(\lambda)$  is considered to be the surface (specular) reflectance factor measure at that instrument under the prevailing measurement conditions [Kue75, §3]. Pineo correction for textiles uses  $R(\lambda) - r_0(\lambda)$  instead of measured  $R(\lambda)$  [McL86, §12].

For samples with a macroscopically plane surface (paint and plastic samples, also coated paper) the surface reflection correction (Saunderson correction) should be applied to the measured reflectance factor, which is for 0/t and t/0 measuring geometries [Völ95, §3.1.3]:

$$R_*(\lambda) = \frac{R(\lambda) - r_0(\lambda)}{1 - r_0(\lambda) - r_2(\lambda)(1 - R(\lambda))} \quad (5.34)$$

where  $R_*(\lambda)$  is the Saunderson corrected reflectance of the layer under study,  $R(\lambda)$  is the measured reflectance factor at the surface,  $r_0(\lambda)$  is the specular reflectance and  $r_2(\lambda)$  is the internal reflection. If the measurement is performed under specular exclusion conditions, then  $R(\lambda)$  must be replaced by  $R(\lambda) + r_0(\lambda)$ . For refractive index  $n(\lambda) = 1.5$ , values of  $r_0(\lambda) = 0.04$  and  $r_2(\lambda) = 0.596$  are given, when  $\lambda = 550$  nm [Völ95, §3.1.3].

### 5.3.2 Interdependence of the Coefficients

Traditionally the Kubelka-Munk scattering coefficient of dyed paper has been assumed to be totally independent of absorption process. Foote [Foo39] reported this dependency first, and this phenomenon is called either the Foote effect or the NAM anomaly.

A study made by dyeing low basis weight filter papers with a basic dye (crystal violet), showed empirically that there was a linear relationship between  $S_c(\lambda)$  and  $K_c(\lambda)$  assuming that  $K_s(\lambda)$  is negligible [KJ97]:

$$S_c(\lambda) = S_s(\lambda) - \tau K_c(\lambda) \quad (5.35)$$

where  $S_c(\lambda)$  and  $S_s(\lambda)$  are the scattering coefficients of dyed and undyed papers,  $K_c(\lambda)$  is the absorption coefficient of dyed paper, and  $\tau$  is the proportionality factor for the optical constants of the fibers, estimated in this case as 0.273.  $\tau$  may be valid only for a band of wavelengths near the absorption maximum.

To date, there are three explanations for the NAM anomaly [KJ97]. The first attributes the effect to nonuniform spatial distribution of absorption and scattering sites in the sheet of paper. The second attributes the effect to the failure of dyed fibers to meet the criterion of absorbing power within a given volume fraction of the material being small compared with the scattering power in Kubelka-Munk theory. The third is that the internal reflectance constitutes the greatest portion of the total reflectance of the fiber wall, and thus its attenuation within the cell wall caused by chromophore absorption is viewed as the principal cause of the NAM anomaly [KJ97].

However, scattering and absorption are not mutually independent processes [BH98, §1.1]. They are dependent on the optical constants of the material – refractive index  $n(\lambda)$  and absorption index  $\kappa(\lambda)$ , which are determined by the molecular electronic configuration of the substrate. For real pigments that exhibit absorption peaks of finite breadth, the refractive index behaves in an anomalous way on the absorption band and nearby it. The rule is that the refractive index drops abruptly on the rising edge of the absorption and rises abruptly on the falling edge, as seen in Figure 5.7. This behaviour can be modelled using quantities of the complex refractive index and the complex dielectric function [BH98, §9]. The real part of the complex dielectric constant is a function of real and imaginary parts of the complex refractive index:

$$\epsilon' = n(\lambda)^2 - \kappa(\lambda)^2 \quad (5.36)$$

It is also the function of the plasma frequency  $\omega_p^2$  which later can be deemed to be a constant  $A$  describing the amplitude of the absorptivity maximum at frequency  $\omega_0$  and the width at half-maximum  $\gamma$ , thus:

$$\epsilon' = 1 + \frac{\omega_p^2 (\omega_0^2 - \omega^2)}{(\omega_0^2 - \omega^2) + \gamma^2 \omega^2} \quad (5.37)$$

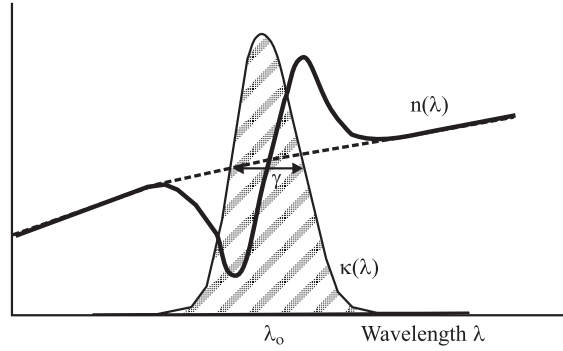


Figure 5.7: Absorption and anomalous refractive index, after [Völ95, §5.2.4].

Now after some modifications and change from frequency to wavelength, one obtains for the real part of the complex refractive index:

$$n(\lambda) = 1 + \kappa(\lambda)^2 + \frac{A(\lambda^2 - \lambda_0^2)}{(\lambda^2 - \lambda_0^2) + \gamma^2 \lambda_0^2} \quad (5.38)$$

Since scattering is directly dependent on the refractive index, this characteristic may well lead to pronounced color effects. This behavior virtually guarantees that  $\tau$  in Equation 5.35 is wavelength dependent:

$$S_c(\lambda) = S_s(\lambda) - \tau(\lambda)K_c(\lambda) \quad (5.39)$$

Thus, at each wavelength  $\lambda$ , the Kubelka-Munk scattering coefficient  $S(\lambda)$  is dependent on the refractive index  $n(\lambda)$ , which in turn depends on the absorption index  $\kappa(\lambda)$  [Völ95, §5.2.4], which determines also the Kubelka-Munk absorption coefficient  $K(\lambda)$ . Thus,  $S(\lambda)$ , which is the empirical measure of the scattering power of the material, and  $K(\lambda)$ , which is the empirical measure of its absorbing power, must be considered to be interdependent.

However, care must be taken to distinguish between changes in scattering that arise from the fiber bonding and those that are results of chromophores.

### 5.3.3 Single Constant Kubelka-Munk Model

The Kubelka-Munk model assumes that the absorption and scattering coefficients of a colored substrate  $K_c(\lambda)$  and  $S_c(\lambda)$  are to a first approximation both linear and additive [McL86, §12]:

$$\frac{K_c(\lambda)}{S_c(\lambda)} = \frac{\sum_{j=1}^n c_j K_j(\lambda)}{\sum_{j=1}^n c_j S_j(\lambda)} \quad (5.40)$$

where  $c_j$  is concentration of the  $j^{\text{th}}$  component, and  $S_j(\lambda)$  and  $K_j(\lambda)$  are the  $j^{\text{th}}$  component's scattering and absorption coefficients, and where  $\frac{K(\lambda)}{S(\lambda)}$  is a function of reflectance factor, usually as given in Equation 5.30. In the case where one component (the substrate) dominates the mixture, and all other components have small  $c_j$ , then an approximation is often made:

$$\frac{K_c(\lambda)}{S_c(\lambda)} = \frac{\sum_{j=1}^n c_j K_j(\lambda) + K_s(\lambda)}{\sum_{j=1}^n c_j S_j(\lambda) + S_s(\lambda)} \quad (5.41)$$

where  $S_s(\lambda)$  and  $K_s(\lambda)$  are the scattering and absorption coefficients of the uncolored substrate.

It is often assumed that the dyes are dissolved in the fibers, fines and fillers and therefore have no scattering power of their own, unlike pigments. This assumption implies that scattering of light is only from the furnish particles, and thus Equation 5.41 simplifies to:

$$\frac{K_c(\lambda)}{S_s(\lambda)} = \frac{\sum_{j=1}^n c_j K_j(\lambda) + K_s(\lambda)}{S_s(\lambda)} \quad (5.42)$$

As discussed above, Equation 5.42 contains an error, because coloring with dyes affects the scattering coefficient  $S(\lambda)$  of the colored furnish at the colorant's absorption band. Thus now  $S_s(\lambda)$  should be replaced by  $S_c(\lambda)$  in Equation 5.42.

Equation 5.42 simplifies further in case of a single dye, and gives the concept of linearization of  $\frac{K(\lambda)}{S(\lambda)}$  of the colored substrate related to dye concentration in the dyebath by the means of a constant wavelength dependent coefficient  $a_j(\lambda)$  of dye  $j$ .

$$\frac{K_c(\lambda)}{S_c(\lambda)} = a_j(\lambda)c_j + \frac{K_s(\lambda)}{S_s(\lambda)} \quad (5.43)$$

where [McD97b]

$$a_j(\lambda) \equiv \frac{K_j(\lambda)}{S_s(\lambda)} = \frac{\partial \frac{K(\lambda)}{S(\lambda)}}{\partial c_j} \quad (5.44)$$

The linearity of the one-constant Kubelka-Munk function, Equation 5.43, frequently only applies at low dye concentrations [McD97b]. This is understandable from Equation 5.39, which implies validity of Equation 5.43 is restricted to cases where:

$$S_s(\lambda) \gg \tau(\lambda)K_c(\lambda) \quad (5.45)$$

Nonlinear deviations can occur for other reasons, and some exemplary forms are shown in Figure 5.8. These deviations are stated to be due to: nonlinear dye uptake and incomplete dye penetration as discussed earlier, and deficiencies in the Kubelka-Munk model to take account of the specularly reflected light from the surface of the sample. Two commonly used practical

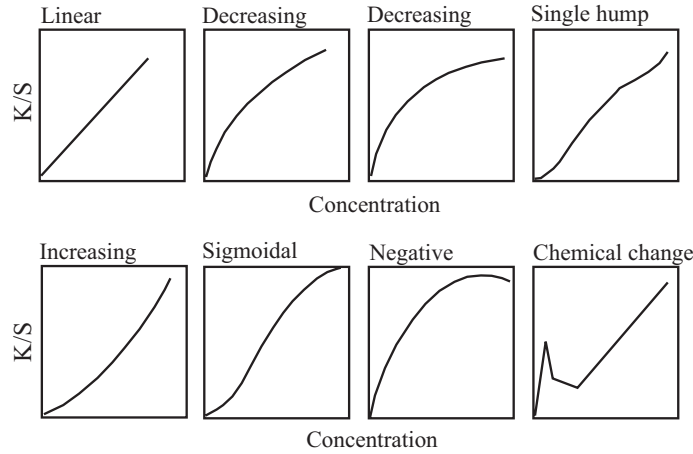


Figure 5.8: Non-linear  $\frac{K_c(\lambda)}{S_c(\lambda)}$  behavior, after [Hof89, McD97b].

approaches to this linearity problem are: use of overall best-fit absorption coefficients and use of simple best-polynomial fit to individual concentration-dependent coefficients.

The overall best-fit wavelength dependent absorption coefficient  $a_j(\lambda)$  is defined based on measurements of a set of colored handsheets produced typically at six different concentrations using a curve fitting technique such as least-squares regression [McD97b]:

$$\min \sum_{k=1}^m \left( \left( \frac{K_c(\lambda)}{S_c(\lambda)} \right)_k - \frac{K_s(\lambda)}{S_s(\lambda)} - a_j(\lambda) c_{jk} \right)^2 \quad (5.46)$$

where  $m$  is the number of measured calibration dyeings for dye  $j$ .

In practice, this solution giving  $a_j(\lambda)$  tends to be biased towards higher dye concentrations, where  $\frac{K_c(\lambda)}{S_c(\lambda)}$  values are larger commonly giving greater absolute errors [McD97b]. Thus the errors may be scaled in the least-squares fit instead:

$$\min \sum_{k=1}^m \left( \frac{\left( \frac{K_c(\lambda)}{S_c(\lambda)} \right)_k - \frac{K_s(\lambda)}{S_s(\lambda)} - a_j(\lambda) c_{jk}}{\left( \frac{K_c(\lambda)}{S_c(\lambda)} \right)_k} \right)^2 \quad (5.47)$$

However, the selection of the method to use should be based on what the expected error bounds would be. The expected error bounds for  $\frac{K_c(\lambda)}{S_c(\lambda)}$  consist of measurement and coloring errors. As shown in the subfigure (B) on Figure 5.6 based on Equation 5.31, the expected measurement error bound is large when  $R(\lambda)$  is small. This happens with dyes even at low concentration, if their absorption band is narrow, as well as for dyes with broader absorption bands at higher concentration. The estimated coloring errors would be expected to be greatest at high concentration, where adsorption may not be complete. Small errors may occur at very low concentrations due to random variation in coloration results.

Colorant modelling forms a two-dimensional optimization problem, where optimization relative to concentration is dominant, but the smoothness of absorptivity relative to wavelength must be kept as a fitting constraint.

### Linearity study

The absorbance  $A(\lambda)$  behaviour of the anionic direct dyes in a diluted solution is commonly linear versus concentration as individual dyes. An example of this behaviour is given in Figure 5.9, which shows the measured absorbance maxima of Pergasol Yellow RN Powder at 410 nm in several concentrations prepared with deionized water.

This linear behaviour is less common for the ratio of  $\frac{K_c(\lambda)}{S_c(\lambda)}$  versus dye-on-fiber. Figure 5.10 shows the ratio  $\frac{K_c(\lambda)}{S_c(\lambda)}$  at each dye's maximum absorption wavelength versus dye-on-fiber for Car-tasol Yellow RF Liquid in the group B and C sheets, and for Pergasol Yellow RN Powder and Per-gasol

Turquoise R Powder in the group D sheets. The Turquoise dyeings show clear non-linearity, while the other dyeings show a linear relation. The linear behaviour of the ratio  $\frac{K_c(\lambda) - K_s(\lambda)}{S_c(\lambda) - S_s(\lambda)}$  versus dye-on-fiber would require a relation, being:

$$K_c(\lambda, [D_f]) - K_s(\lambda) = a(\lambda) [D_f] (S_c(\lambda, [D_f]) - S_s(\lambda)) \quad (5.48)$$

when  $\frac{K_c(\lambda) - K_s(\lambda)}{S_c(\lambda) - S_s(\lambda)} = a(\lambda) [D_f]$ . Note that  $K_s(\lambda)$  is often negligible.

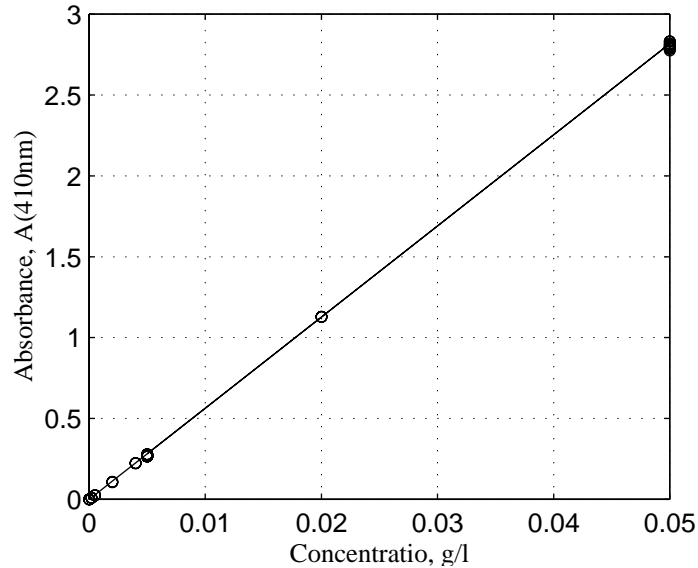


Figure 5.9: Measured maximum absorbances at 410 nm of Pergasol Yellow RN Powder in several concentrations prepared with deionized water.

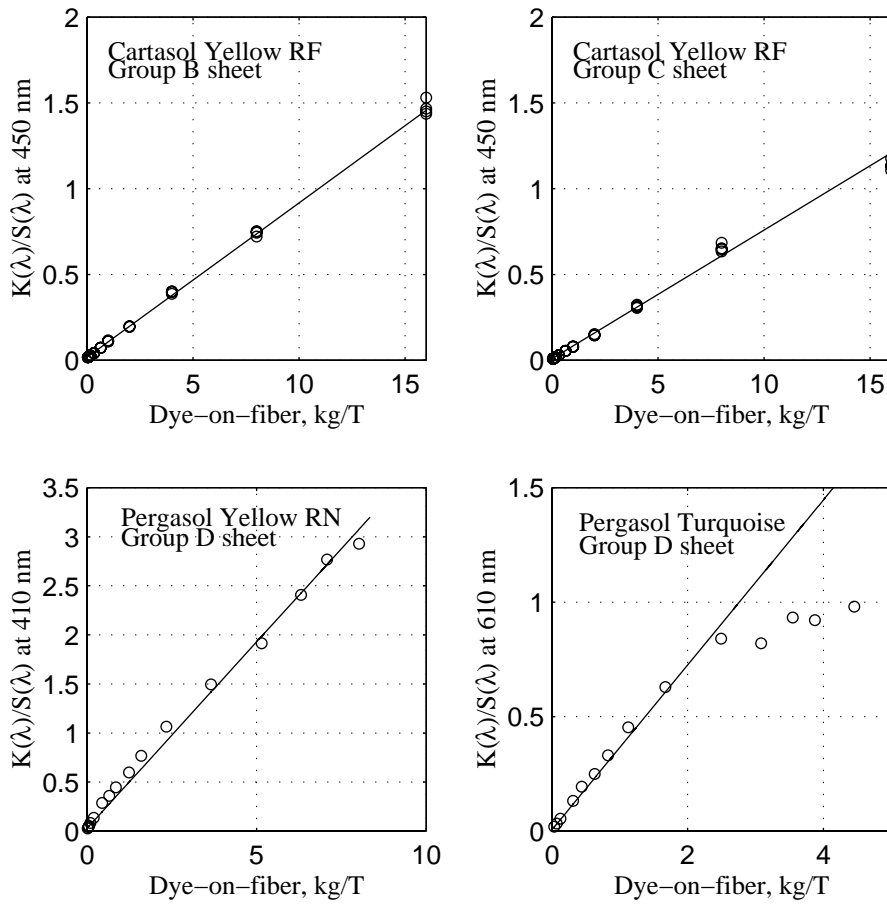


Figure 5.10:  $\frac{K_c(\lambda)}{S_c(\lambda)}$  at each dyes' maximum absorption wavelength versus dye-on-fiber for Cartasol Yellow RF Liquid in the group B and C sheets, and for Pergasol Yellow RN Powder and Pergasol Turquoise R Powder in the group D sheets.

Figure 5.11 shows the absorption coefficients  $K_c(\lambda)$  at each dye's maximum absorption wavelength versus dye-on-fiber for Cartasol Yellow RF Liquid in the group B and C sheets, and for Pergasol Yellow RN Powder and Pergasol Turquoise R Powder in the group D sheets. As can be observed, the absorption coefficient behaviour at maximum absorption wavelength of each dye is similar, being linear only at small amount of dye-on-fiber where also the adsorption process of dye-on-fiber is linear. As a very rough estimate, the total surface for 2 g of furnish could be about  $6 \text{ m}^2$  for group B sheets, about  $8.3 \text{ m}^2$  for group C sheets and below  $4 \text{ m}^2$  for group D sheets. The specific surface is seen to influence the relation between dye-on-fiber and  $K_c(\lambda)$ .

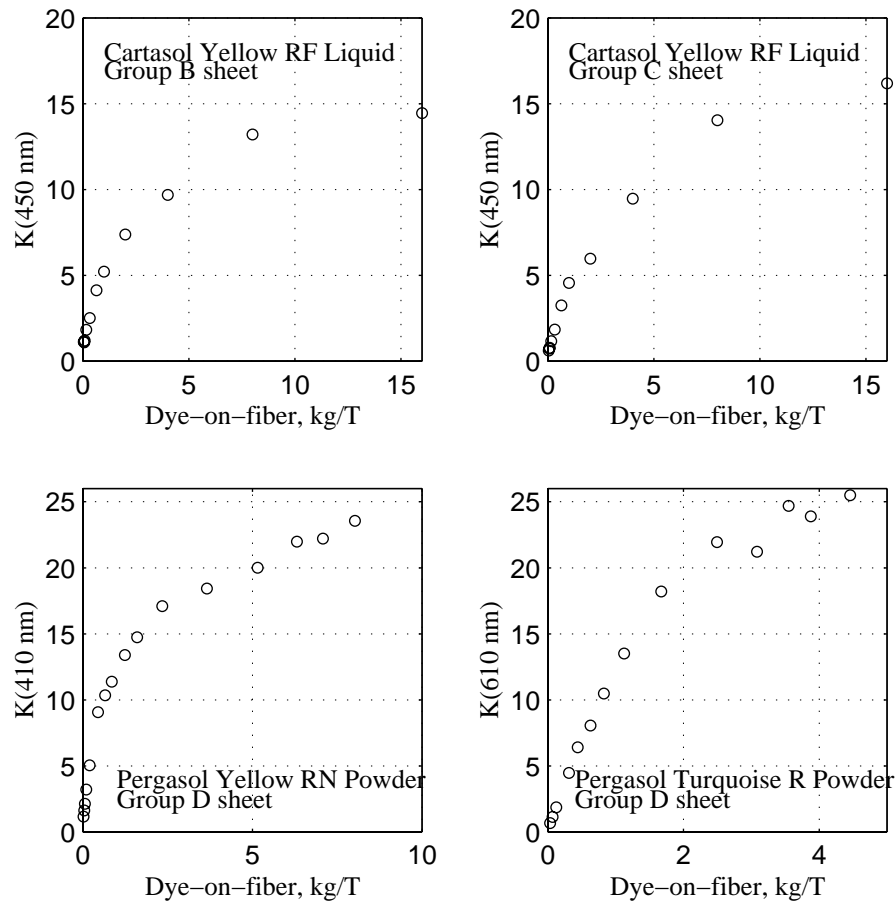


Figure 5.11:  $K_c(\lambda)$  at each dyes' maximum absorption wavelength versus dye-on-fiber for Cartasol Yellow RF Liquid in the group B and C sheets, and for Pergasol Yellow RN Powder and Pergasol Turquoise R Powder in the group D sheets.

In spite of differences in actual dye-on-fiber between colorings (approximately 8 kg/T for Yellow and 4.4 kg/T for Turquoise on dry masses of about 2 g, from doses of 15 kg/T in a 600 ml dyebath), the maximum value of the absorption coefficient  $K(\lambda)$  of each coloring seems to be related to the extinction coefficient of the dye. The extinction coefficients are at the wavelength of maximum absorption  $28.1 \text{ l g}^{-1} \text{ cm}^{-1}$  for Yellow, and  $28.6 \text{ l g}^{-1} \text{ cm}^{-1}$  for Turquoise.

Figure 5.12 shows the scattering behavior at each dye's maximum absorption wavelength (where the effect on scattering is greatest) for the dyes Cartasol Yellow RF Liquid in group B and C sheets, and Pergasol Yellow RN Powder and Pergasol Turquoise R Powder in group D sheets. Clearly, the change in scattering coefficient  $S_c(\lambda)$  depends strongly on the properties of the furnish, especially its total specific surface area, which correlates with the amount of scattering in undyed paper. When the furnish contains fillers in addition to fibers and fines,

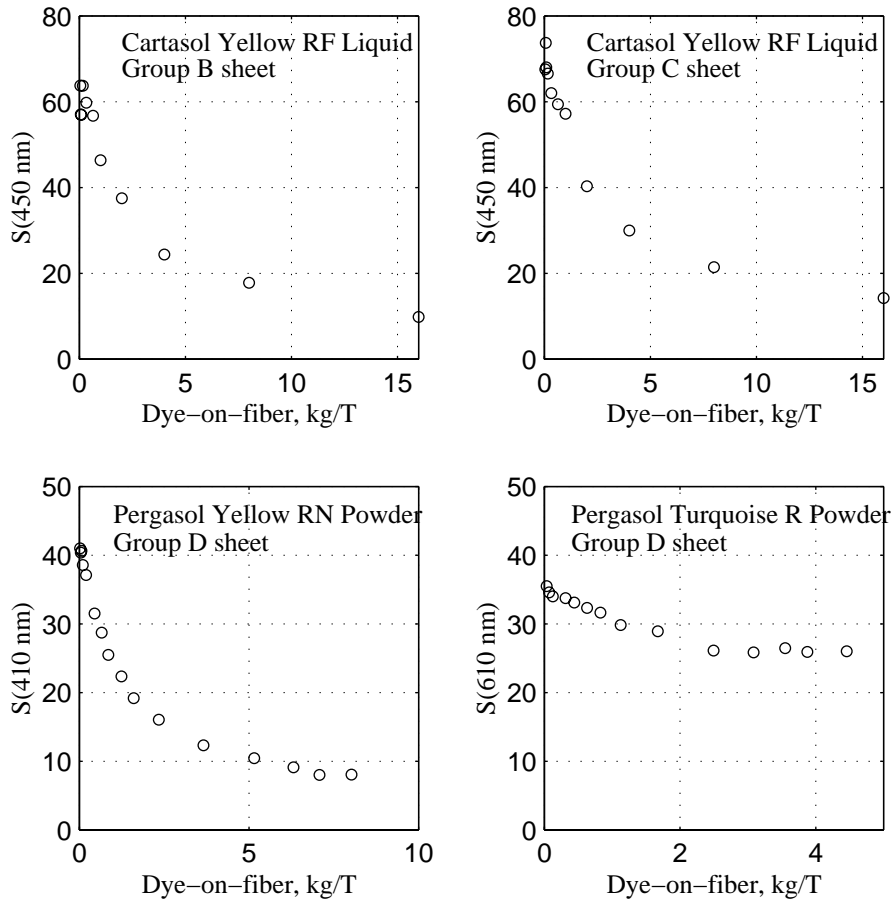


Figure 5.12:  $S_c(\lambda)$  at each dyes' maximum absorption wavelength versus dye-on-fiber for Cartasol Yellow RF Liquid in the group B and C sheets, and for Pergasol Yellow RN Powder and Pergasol Turquoise R Powder in the group D sheets.

more dye-on-fiber may be required to compensate for the difference in the optical path lengths, Section 2.2.2.

The change in scattering  $S(\lambda)$  caused by dyeing is significantly smaller with Pergasol Turquoise R Powder than in the case of Yellow. The smaller dye-on-fiber rate could be explained since the molecule size of Pergasol Turquoise R Powder is too large (two chromophores in the molecule instead of one) to enter into the pores of the used fibers and thence to the lumen, or if it can enter into the pores its mobility therein is poor. Thus adsorbed dye molecules and aggregates in these dyeings with Turquoise are located more on the surface of the fiber.

An example illustrating both absorption band broadening and scattering band broadening is given in Figure 5.13, which contains calculated absorption coefficients  $K_c(\lambda)$  in subfigure (A) and scattering coefficients  $S_c(\lambda)$  in subfigure (C) for the group D sheets colored with Pergasol

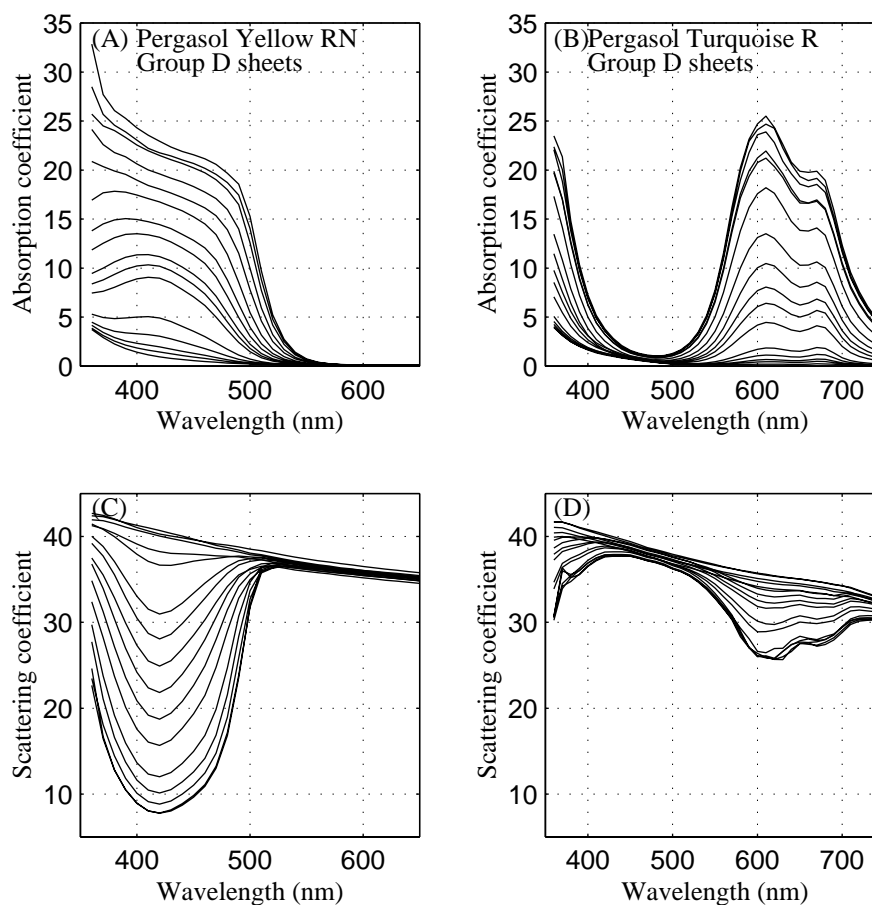


Figure 5.13: (A) Calculated  $K_c(\lambda)$  of the group D sheets colored with Pergasol Yellow RN Powder.

(B) Calculated  $K_c(\lambda)$  of the group D sheets colored with Pergasol Turquoise R Powder.

(C) Calculated  $S_c(\lambda)$  of the Yellow colorings.

(D) Calculated  $S_c(\lambda)$  of the Turquoise colorings.

Yellow RN Powder, and calculated  $K_c(\lambda)$  in subfigure (B) and  $S_c(\lambda)$  in subfigure (D) for the set of colorings from the group D sheets colored with Turquoise R Powder. As can be seen, the absorption band broadening is a common feature for anionic direct dyes, either via colorant interactions or aggregation or via other mechanisms in which the substrate may also participate. The broadening causes the proportionality constant  $\tau(\lambda)$  used in Equation 5.39 to become concentration dependent, so that relations such as given in Equations 5.35 and 5.39 are of limited use. The two-flux equations can be solved in various ways leading to several formulae used to calculate  $S(\lambda)$  and  $K(\lambda)$  from the measured reflectance factors. Here their calculations are based on Equations 4.7 and 4.10.

Based on observations of several dyeings including those in Figures 5.10, 5.11 and 5.12, the absorption and scattering coefficients of dyed paper are not linear versus increasing dye-on-fiber, except at very low dye concentrations. The absorption behavior between different dyes in various furnishes is similar, while the scattering behavior varies greatly. This would suggest that the major origin for non-linear behavior of the ratio of  $\frac{K_c(\lambda) - K_s(\lambda)}{S_c(\lambda) - S_s(\lambda)}$  in paper dyeing is how the scattering at the absorption band of the dye is affected by the dyeing. There are two requirements for this ratio to be linear:

- in the whole range of dye-on-fiber of interest there must be a sufficient amount of adsorption sites available for dye molecules
- a relation such as given in Equation 5.48 must be approximately valid

A plausible hypothesis of the effect of fiber dyeing on the absorption and scattering coefficients is, that it is mainly result of the change in specular reflectance on the fiber surfaces also within the sheet at the wavelengths corresponding to the absorption band of the dye, which is caused by the change in refractive index of colored fibers. This effect is greatest at large angles of incidence from normal [Kor69, §II.f]. This is based on the assumption, that dyes do not dissolve as such into cell walls, but they are adsorbed on the surface of fibers, pores and lumen walls. Furthermore, the narrower scattering band broadening compared to the absorption band, may be because aggregated dye molecules cause higher light absorption than single-layer molecule adsorption [Koo90] and the number of aggregated molecules in the lumen is smaller than on the surface of the fiber, causing local refractive indexes of a fiber to vary. This conjecture is consistent with models which ascribe most scattering by fibers to the lumen.

### Additivity study

In mixtures of anionic direct dyes, non-additive spectral characteristics are quite common [Sch95]. Figure 5.14 shows the calculated and measured absorbances for mixtures of 1.0 mg Pergasol Yellow RN Powder and 1.0 mg Pergasol Turquoise R Powder in 500 ml of deionized water, and respectively 0.3 mg Yellow and 0.1 mg Turquoise in 500 ml of deionized water. Even in deionized water with pH 7.0 and conductivity of  $0.74 \mu\text{S}$  these dyes are non-additive in absorbance.

Whereas  $\frac{K_c(\lambda)}{S_c(\lambda)}$  behaviour of the substrate dyed with the anionic direct dyes is often linear versus concentration as individual dyes, this does not necessarily hold for dyeing with mixed dyes. Figure 5.15 illustrates additivity behavior in mixed dyeing for  $\frac{K_c(\lambda)}{S_c(\lambda)}$ . In subfigure (A) dyeings as individual dyes 0.19 kg/T on fiber of Pergasol Yellow RN Powder and 1.24 kg/T on fiber of Pergasol Turquoise R Powder are shown as solid line and their equal mixture dyeing is also shown utilizing the same furnish, all belonging to the group D sheets. In subfigure (C) the wavelength dependent absorption coefficient  $a(\lambda)$  was defined over the dosage range of 0.5-2 kg/T for both Yellow dye and Turquoise dye based on  $\frac{K(\lambda)}{S(\lambda)}$  measurements of group D sheet dyeings as individual dyes. The solid line represents modelled additivity for 0.19 kg/T on fiber of Yellow dye with 1.24 kg/T on fiber of Turquoise dye and for 1.6 kg/T with 0.31 kg/T, while

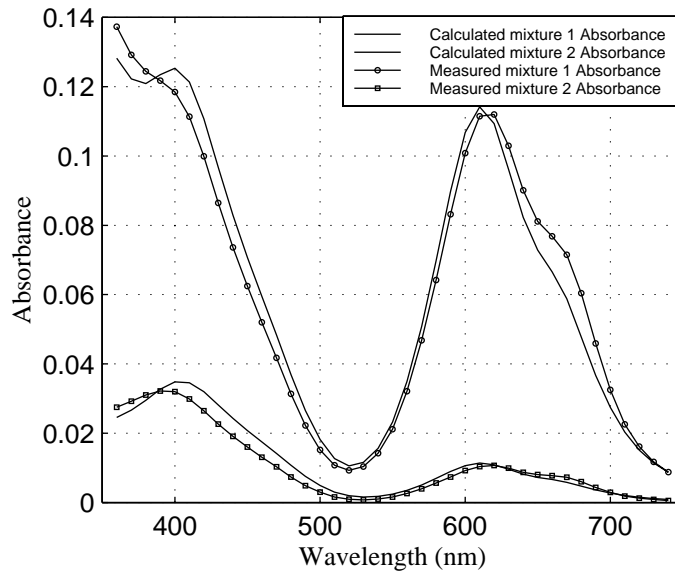


Figure 5.14: Calculated and measured absorbances  $A(\lambda)$  for mixtures of 1.0 mg Pergasol Yellow RN Powder and 1.0 mg Pergasol Turquoise R Powder in 500 ml of deionized water (mixture 1), and respectively 0.3 mg and 0.1 mg of them in 500 ml of deionized water (mixture 2).

the line with dots represents measured results for those dye mixtures. In subfigure (B), dyeings as individual dyes 0.44 kg/T on fiber of Yellow dye and 0.31 kg/T on fiber of Turquoise dye are shown as solid line and their equal mixture dyeing is also shown, all belonging to the group D sheets. In subfigure (D) the solid line represents modelled additivity for the mixture dyeing given in (B). It is interesting to observe an increase in  $\frac{K(\lambda)}{S(\lambda)}$  of dye mixtures in these dyeing conditions, and that absorption properties of Turquoise dye change as the dye-on-fiber increases. Foote [Foo39] observed that in dyeing with basic dyes, the calculated  $\frac{K(\lambda)}{S(\lambda)}$  values of the mixture dyeing were greater than the observed values. This obviously is true at high concentration of dye-on-fiber, due to limited amount of suitable adsorption sites.

One of the major sources for non-additivity is colorant interactions, causing changes in the spectral characteristic of the dyes and changes in exhaustion of each component due to the presence of the other [Sch95]. The severity of colorant interactions is greatly affected by hardness of used water, in addition to the state of the wet end chemical balance.

At present, the standard practice is to produce sets of colored handsheets so that each sheet is colored using only a single colorant. This ignores the potential effect of colorant interactions, which can be significant as shown earlier, and thus lead to erroneous color control tuning. The colored handsheets made for pretuning of any color control should be made using the same colorant mixtures at similar dosage levels to those intended in final coloring, varying a single colorant's concentration in the dyebath at the time when the others' ones are constant. In this

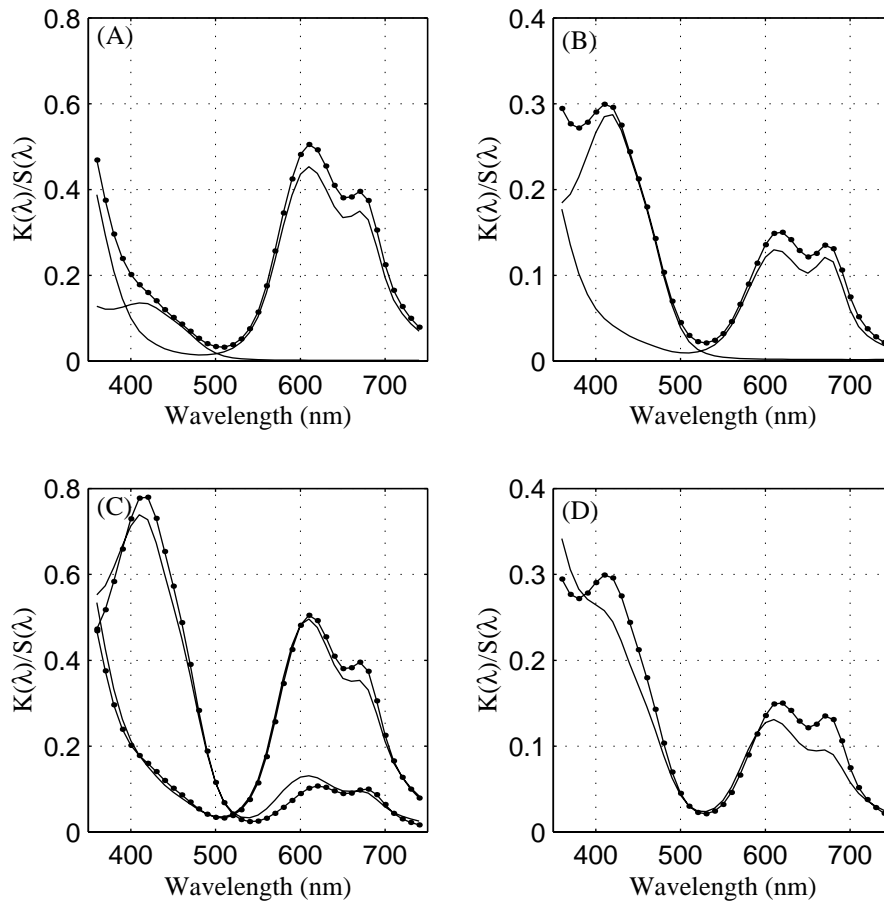


Figure 5.15: All dyeings from the group D sheets with amount of dye-on-fiber. (A) Measured  $\frac{K(\lambda)}{S(\lambda)}$  of as individual dyes (solid lines) 0.19 kg/T of Pergasol Yellow RN Powder and 1.24 kg/T of Pergasol Turquoise R Powder and their mixture dyeing.

(B) Measured  $\frac{K(\lambda)}{S(\lambda)}$  of as individual dyes (solid lines) 0.44 kg/T of Yellow dye and 0.31 kg/T of Turquoise dye and their mixture dyeing.

(C) Calculated (solid line) and measured  $\frac{K(\lambda)}{S(\lambda)}$  based on dye mixtures of 0.19 kg/T Yellow dye and 1.24 kg/T Turquoise dye, and respectively 1.6 kg/T and 0.31 kg/T.

(D) Calculated (solid line) and measured  $\frac{K(\lambda)}{S(\lambda)}$  based on dye mixtures of 0.44 kg/T Yellow dye and 0.31 kg/T Turquoise dye.

way the model for the coloring process derived from colored handsheets would be closer to the real coloring process at the mill, where the same class of colorants are metered into carrier water shortly before addition to stock, especially if the mill's furnish(es) is used to make the handsheets.

## 5.4 Absorption Band Broadening and Non-Linear Extension to Kubelka-Munk Model

An adsorbed colorant molecule on a fiber or on any solid absorbs electromagnetic radiation as discrete quantities according to the characteristics of the colorant molecule. This unites the adsorption and the absorption processes. Thus the change of the absorption coefficient  $K_c(\lambda) - K_s(\lambda)$  at the wavelength of the colorant's absorption maximum caused by the dyeing of the substrate should have the same characteristics as its adsorption isotherm. In other words, the probability of a photon to be absorbed within a optical path typical for the substrate by the adsorbed dye molecules increases as the fraction of the area covered by the adsorbed dye molecules to the total area of the solid increases. The effect of absorbed photons versus dye-on-fiber varies in measured different properties, since the process of light scattering and absorption to produce the diffuse and specular reflectance in paper is very complicated. As discussed earlier the scattering also changes if the absorption changes, since  $K(\lambda)$  and  $S(\lambda)$  are interdependent.

The published literature contains models for dyed fiber blending, filler and pigment blending etc. The most suitable base model for modelling the behavior of the absorption and the scattering coefficient versus increasing dye concentration is to utilize the model for the absorption  $K_{fs}(\lambda)$  and the scattering  $S_{fs}(\lambda)$  coefficient for a filled sheet by a increasing filler published originally by van der Akker [MJA94]:

$$S_{fs}(\lambda) = S_s(\lambda) + (S_f(\lambda) - S_s(\lambda)) x \quad (5.49)$$

$$K_{fs}(\lambda) = K_s(\lambda) + (K_f(\lambda) - K_s(\lambda)) x \quad (5.50)$$

where  $x$  is the weight fraction of the filler,  $S_s(\lambda)$  and  $K_s(\lambda)$  are the scattering and absorption coefficients for the pulp, and  $S_f(\lambda)$  and  $K_f(\lambda)$  are the scattering and absorption coefficients for the filler.

In the case of furnish dyeing, the weight fraction of the filler is now replaced by the probability function, which describes the probability of a photon to be fully absorbed within its optical path by the adsorbed dye molecules, and the coefficients of the filler are replaced by the wavelength dependent coefficients describing the probability of photons with different energy levels to be absorbed by the adsorbed dye molecules. Now a linear approximation describing the absorption  $K_c(\lambda)$  and scattering  $S_c(\lambda)$  coefficient at concentration of  $[D_{total}]_f$  of dye-on-fiber can be formed as:

$$K_c(\lambda) = K_s(\lambda) + K_1(\lambda) \frac{q [D_{total}]_f}{1 + q [D_{total}]_f} \quad (5.51)$$

$$S_c(\lambda) = S_s(\lambda) + S_1(\lambda) \frac{q [D_{total}]_f}{1 + q [D_{total}]_f} \quad (5.52)$$

where  $K_s(\lambda)$  and  $S_s(\lambda)$  are the absorption and scattering coefficients of the base substrate,  $K_1(\lambda) = K_\infty(\lambda) - K_s(\lambda)$  and  $S_1(\lambda) = S_\infty(\lambda) - S_s(\lambda)$ , where  $K_\infty(\lambda)$  and  $S_\infty(\lambda)$  are the absorption and scattering coefficients of the colored substrate at the adsorption maximum,  $q$  is the probability constant of the photon absorption process,  $[D_{total}]_f$  is the amount of dye-on-fiber including all layers.

This models assumes that the shape of the absorption band would stay constant relative to amount of dye-on-fiber.

Anionic direct dyes have a high tendency to aggregate, leading to absorption band broadening. This is clearly noticeable in the absorption coefficients of Pergasol Yellow RN Powder, shown in Figure 5.13. Absorption band broadening is due to interaction between adsorbed molecules. Dye molecules adsorbed in close proximity on the surface, and especially those adsorbed as a superlayer above the first layer of adsorbate, will have additional modes of vibrational relaxation available. These molecules will therefore have wider absorption bands. In the case of the superlayer molecules, new vibrational relaxation modes and consequent absorption band broadening will also occur for the subjacent adsorbate molecules. The surface concentration of superlayer adsorbate  $[D_{super}]_f$  (using the adsorption model above) can be taken as a suitable proxy measure of the amount of adsorbed dye molecules which are interacting with other adsorbed dye molecules. This proxy concentration will be used to model broadening phenomena in absorption and scattering.

Note that the adsorbed colorant molecules can be divided into distinct populations, for instance: (i) monolayer, bound only to the substrate, (ii) superlayer, bound only to other adsorbed colorant molecules, (iii) sublayer, bound both to the substrate and to superlayer molecules. The second and third populations in combination form the multilayer. The electronic energy levels and allowed vibrational modes may differ among these populations. In principle, the sublayer and superlayer may contribute differently to broadening phenomena. However, since the third and subsequent layers are much smaller than the second for most of the dyeings,  $[D_{super}]_f \cong [D_{sub}]_f$ , so that  $[D_{multi}]_f \cong 2[D_{super}]_f$ , since  $[D_{sub}]_f = [D_{multi}]_f - [D_{super}]_f = [D_2]_f$ . In other words, the effects of superlayer and sublayer are largely collinear in the dyeings, and cannot be reliably distinguished. Therefore, superlayer  $[D_{super}]_f$ , sublayer  $[D_{sub}]_f$ , and multilayer  $[D_{multi}]_f$  modelled concentrations are equally suitable for use as proxies for modelling broadening phenomena, and models of broadening based thereon would be essentially identical.

To take the absorption band broadening into account, an additional term is required in the model given in Equations 5.51 and 5.52:

$$K_c(\lambda) = K_s(\lambda) + K_1(\lambda) \frac{q [D_{total}]_f}{1 + q [D_{total}]_f} + K_2(\lambda) \frac{p [D_{super}]_f}{1 + p [D_{super}]_f} \quad (5.53)$$

$$S_c(\lambda) = S_s(\lambda) + S_1(\lambda) \frac{q [D_{total}]_f}{1 + q [D_{total}]_f} + S_2(\lambda) \frac{p [D_{super}]_f}{1 + p [D_{super}]_f} \quad (5.54)$$

where  $K_2(\lambda) = K_{\infty,a}(\lambda) - K_s(\lambda)$  and  $S_2(\lambda) = S_{\infty,a}(\lambda) - S_s(\lambda)$ ,  $K_{\infty,a}(\lambda)$  includes the absorption band broadening effect on the absorption coefficient at the adsorption maximum, and

respectively for  $S_{\infty,a}(\lambda)$ , and  $p$  is the probability constant of the photon to be absorbed by the dye molecules in the superlayer  $[D_{super}]_f$ .

Figure 5.16 contains the measured and modelled (solid line) absorption and scattering coefficients of the group D sheets dyed with Pergasol Yellow RN Powder based on Equations 5.53 and 5.54, where  $K_s(\lambda)$  and  $S_s(\lambda)$  are constant and identified based on measurements of undyed sheets in subfigures (A) and (B). The subfigures (C) and (D) contains the measured coefficient  $K_s(\lambda)$  and  $S_s(\lambda)$  of the undyed sheet, which were used in the model and the modelled coefficients  $K_1(\lambda)$ ,  $K_2(\lambda)$ ,  $S_1(\lambda)$  and  $S_2(\lambda)$ .  $[D_{total}]_f$ ,  $[D_1]_f$ , and  $[D_{super}]_f$  are shown in Figure 5.3 for the Yellow. The goodness of a fit of absorption coefficients as root-mean-square residual over effective wavelengths 360-600 nm is 0.267, and for scattering coefficients 0.392.

The model based on Equations 5.53 and 5.54 was also applied to the group D sheets dyed with Pergasol Turquoise R Powder. A model for  $K_c(\lambda)$  versus dye-on-fiber existed like for Yellow dyeings, including small broadening effect. However, a model for  $S_c(\lambda)$  failed. A reason for this is, the change in  $S_c(\lambda)$  was not continuous relative to the dye-on-fiber because the Turquoise dye molecules are too large to enter the lumen. The dyeing caused only change in the scattering due to fiber surface adsorption of dye molecules, but it did not have a significant effect on the major scattering process, which takes place in the lumen of the fiber.

The disadvantage of this model estimated using error minimization optimization is, that several single sheet and stack measurements of dyeings at several concentrations are required to find the statistically meaningful core data, due to noisiness of the calculated scattering coefficients of the colored handsheets caused by the local formation variation in the low basis weight sheets. Also it is reasonable to ask when these calculated scattering and absorption coefficients are actually valid, especially in terms of difference between reflectance factor measurement of a single sheet and a stack. There exist functional data analysis methods (including extensions to principal component analysis), which may reduce the number of required dyeings, and would speed up the cumbersome optimization [SSK99a, SSK99b]. Utilization of these advanced methods is left for future work.

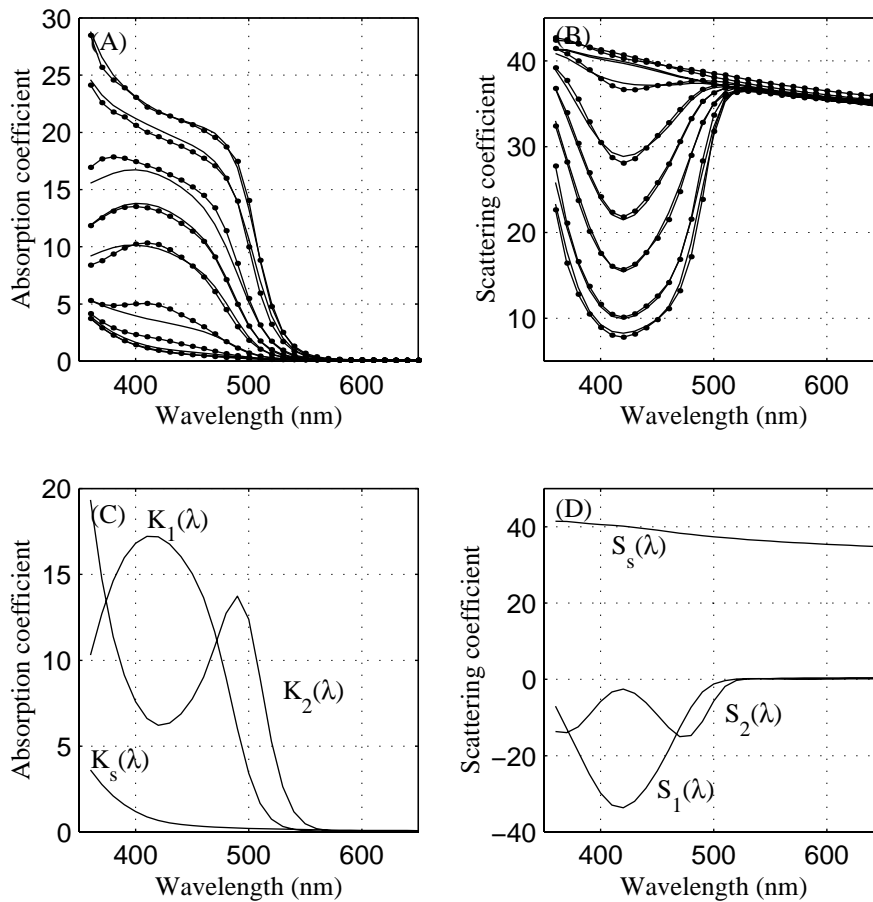


Figure 5.16: A model for the group D sheets dyed with Pergasol Yellow RN Powder based on Equations 5.53 and 5.54. (A) Measured and modelled (solid line)  $K_c(\lambda)$ .

(B) Measured and modelled (solid line)  $S_c(\lambda)$ .

(C)  $K_s(\lambda)$  and modelled  $K_1(\lambda)$  and  $K_2(\lambda)$  for the model in (A), when  $q = 2.37$  and  $p = 2.50$ .

(D)  $S_s(\lambda)$  and modelled  $S_1(\lambda)$  and  $S_2(\lambda)$  for the model in (B), when  $q = 1.05$  and  $p = 4.12$ .

## 5.5 Two-Flux Model with Fluorescence

Phenomenological theory does not include fluorescence. However the required extension can be made. In paper, fluorescence is a complicated phenomenon. In Figure 5.17 the behavior of a fluorescent brightening agent, Tinopal ABP-X h.c, in group D sheets is shown. Subfigure (A) shows the measured radiance transfer factors  $B(370, \lambda)$  with excitation 370 nm at increasing concentration of Tinopal ABP-X h.c in group D sheets versus wavelength. In subfigure (B) the measured radiance transfer factors  $B(370, 430)$  versus estimated dye-on-fiber, defined at 370 nm rather than at the wavelength of the absorption maximum, are shown. The actual dye-on-fiber

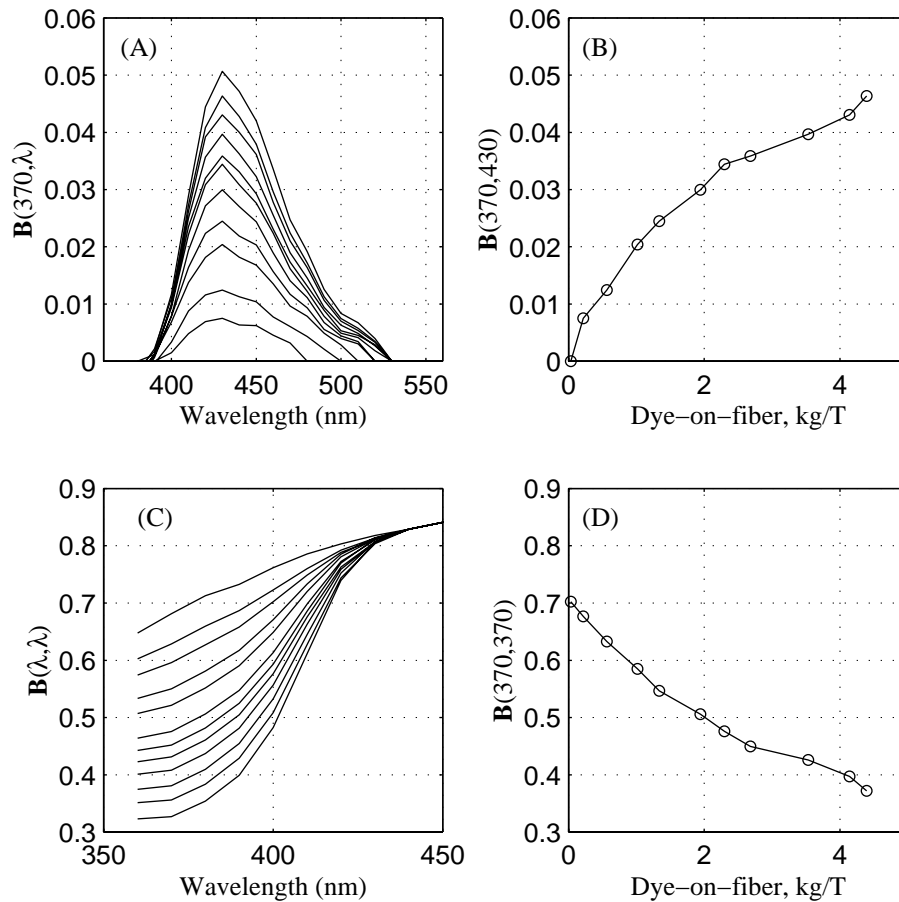


Figure 5.17: (A) Measured radiance transfer factors  $B(370, \lambda)$  with excitation 370 nm at increasing concentration of Tinopal ABP-X h.c in group D sheets versus wavelength. (B) Measured radiance transfer factors  $B(370, 430)$  with excitation 370 nm and emission at 430 nm versus initial dye-on-fiber, kg/T. (C) Measured radiance transfer factors  $B(\lambda, \lambda)$  at the excitation band of Tinopal ABP-X h.c in group D sheets versus wavelength. (D) Measured radiance transfer factors  $B(370, 370)$  versus estimated dye-on-fiber, kg/T.

was difficult to define, because CM-3700 can not reliably measure below 370 nm. As can be seen the relation of emission to dye-on-fiber is not a linear process, like the reduction in  $B(370, 370)$  versus dye-on-fiber at the excitation band of the FBA in subfigure (D). In subfigure (C)  $B(\lambda, \lambda)$  is shown at the measured excitation band of the FBA. The partial lack of the measurement at the excitation band of a FBA is a serious limitation. The excitation and emission bands of fluorescent dyes (daylight fluors) is mostly in the visible band of spectrum, thus a fluorescent yellow is used later.

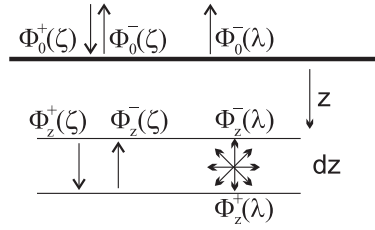


Figure 5.18: Diffuse radiances  $\Phi^+(\zeta)$ ,  $\Phi^-(\zeta)$  and emitted radiances  $\Phi^+(\lambda)$ ,  $\Phi^-(\lambda)$  inside a layer.

The fluorescent radiance is generated at varying depths within the paper sheet depending on the scattering properties of the substrate and absorption properties of both colorant and substrate, after which it may be further scattered or absorbed before reaching the surface of the paper. The excitation band  $\zeta_1 < \zeta < \zeta_2$  of a fluorescent colorant can be modelled using original two-flux theory, but an extension is required for the emission band  $\lambda_1 < \lambda < \lambda_2$  of the fluorescent colorant. In the wavelength band where the colorant fluoresces, both radiances of light  $\Phi_z^+$  and  $\Phi_z^-$  discussed in Section 5.3 are augmented by fluorescence as shown in Figure 5.18. Thus Equations 5.24 and 5.25 become [Bon86]:

$$\frac{d\Phi_z^+(\lambda)}{dz} = -(K(\lambda) + S(\lambda))\Phi_z^+(\lambda) + S(\lambda)\Phi_z^-(\lambda) + f_z(\zeta, \lambda)/2 \quad (5.55)$$

$$\frac{d\Phi_z^-(\lambda)}{dz} = (K(\lambda) + S(\lambda))\Phi_z^-(\lambda) - S(\lambda)\Phi_z^+(\lambda) - f_z(\zeta, \lambda)/2 \quad (5.56)$$

The factor  $1/2$  arises for fluorescence  $f_z(\zeta, \lambda)$  at depth  $z$  because it is assumed to be isotropic. It is assumed, that the quantum efficiency is independent of concentration and scattering coefficient  $S(\zeta)$  to be unaffected by the presence of fluorescent dye at the irradiating wavelength. Note, at that time it was commonly believed, that  $K(\lambda)$  and  $S(\lambda)$  are independent.

The radiance of fluorescent light  $f_z(\zeta, \lambda)$  produced in an infinitesimal layer at depth  $z$ , is given by:

$$f_z(\zeta, \lambda) = \int_{\zeta < \lambda} K_F(\zeta) Q(\zeta, \lambda) (\Phi_z^-(\zeta) + \Phi_z^+(\zeta)) d\zeta \quad (5.57)$$

where  $K_F(\zeta) = K_c(\zeta) - K_s(\zeta)$  is the effective absorption coefficient of colored sample, calculated as difference of colored and uncolored samples,  $Q(\zeta, \lambda)$  is the quantum yield of fluorescence per unit emission wavelength  $\lambda$ , and the last term in brackets describes the radiance available for absorption by the fluorescent colorant per unit wavelength per unit depth at a wavelength  $\zeta$  and depth  $z$  within the sample and is the sum of Equations 5.27 and 5.28 now at wavelength  $\zeta$ . For brevity, let  $B(\zeta)$  represent  $\sqrt{K(\zeta)^2 + 2K(\zeta)S(\zeta)}$ , then:

$$f_z(\zeta, \lambda) = \int_{\zeta < \lambda} K_F(\zeta) Q(\zeta, \lambda) \Phi_0^+(\zeta) \left( 2 + \frac{K(\zeta)}{S(\zeta)} - \frac{B(\zeta)}{S(\zeta)} \right) \exp^{-zB(\zeta)} d\zeta \quad (5.58)$$

This set of equations can be solved under various illumination conditions, of which some are discussed in following sections.

### 5.5.1 Extended Kubelka-Munk Model for Fluorescence, Polychromatic Illumination

Bonham has solved Equations 5.55 and 5.56 for polychromatic illumination [Bon86]. The reference also contains a detailed derivation. The model is based on following assumptions:

- Fluorescence is isotropic so that half of light is emitted in each direction
- $S(\lambda)$  is independent of wavelength, thus only the ratio of  $\frac{K(\lambda)}{S}$  is necessary
- The absorption (excitation) and emission spectra of a fluorescent dye do not overlap (for mathematical convenience)
- The emission spectrum obtained should not depend on the dye concentration, being an intrinsic property of the dye molecule
- The total quantum yield  $Q$ , obtained by integrating the emission spectrum, should be reasonably high, but less than 100 %

The main result gives an explicit relation between the measured total radiance factor, diffuse absorption and scattering coefficients of uncolored and colored sample, colorant's quantum yield of fluorescence and the incident radiance:

$$\beta_T(\lambda | S) = \left( 1 + \frac{K(\lambda)}{S(\lambda)} - \frac{B(\lambda)}{S(\lambda)} \right) + \frac{Q(\lambda)}{2 \Phi_0^+(\lambda)} \int_{\zeta < \lambda} \frac{K_F(\zeta) \Phi_0^+(\zeta)}{B(\lambda) + B(\zeta)} \left( 2 + \frac{K(\lambda)}{S(\lambda)} - \frac{B(\lambda)}{S(\lambda)} \right) \left( 2 + \frac{K(\zeta)}{S(\zeta)} - \frac{B(\zeta)}{S(\zeta)} \right) \delta\zeta \quad (5.59)$$

where  $B(\zeta) = \sqrt{K(\zeta)^2 + 2K(\zeta)S(\zeta)}$  and  $B(\lambda) = \sqrt{K(\lambda)^2 + 2K(\lambda)S(\lambda)}$ .

In calculations, the nominal spectral power distribution supplied by the manufacturer of the spectrophotometer used in the study was used as irradiance  $\Phi_0^+$  on the sample.

The model has been verified by Bonham for daylight fluorescent colorants absorbing and emitting in visible band. However, results obtained are dependent on the used illumination, and are not transferable between instruments.

Here Bonham's model is used for Fastusol Yellow 14L Liquid measured with Minolta CM-3700d. Calculation of  $\frac{K(\lambda)}{S(\lambda)}$  is also applied for the total radiance factors greater than unity, and CIE standard illuminant  $D_{65}$  is used as irradiance on the sample.

In Figure 5.19 the calculated quantum efficiency  $Q(510)$  at emission of 510 nm versus dye-on-fiber, kg/T, of Fastusol Yellow 14L in group D sheets is shown. In subfigure (B) the calculated quantum efficiency  $Q(\lambda)$  is shown at several concentrations versus wavelength. Here, the calculated quantum efficiency is clearly dependent on the amount of dye-on-fiber. The measured scattering coefficient of the undyed sheets is used.

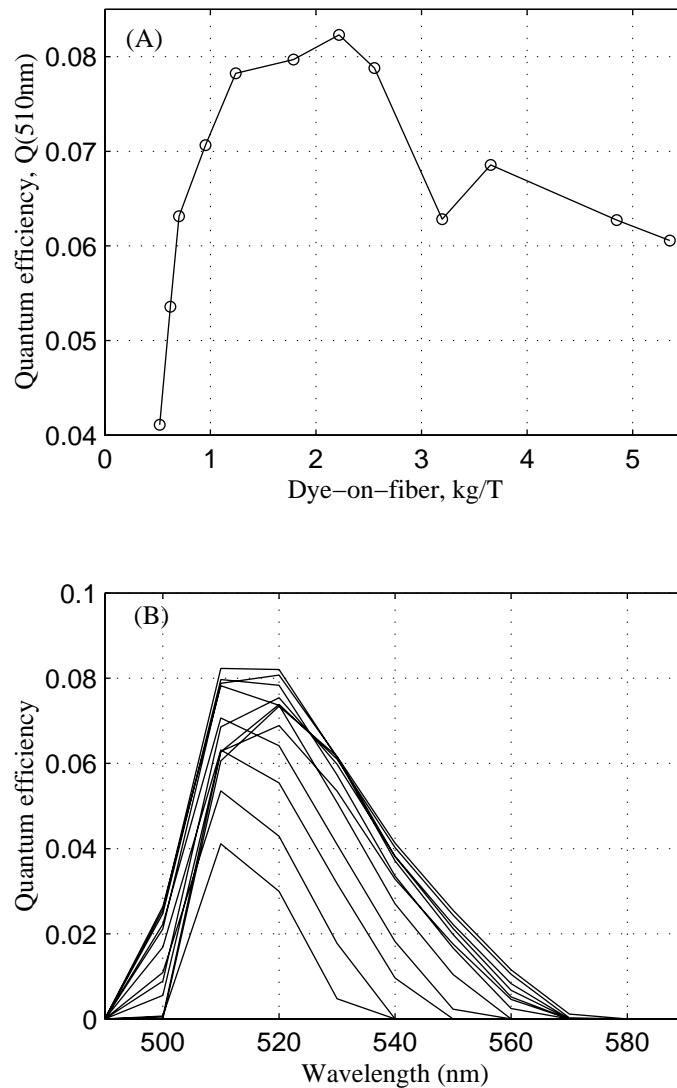


Figure 5.19: (A) Calculated quantum efficiency  $Q(510)$  at emission of 510 nm versus dye-on-fiber, kg/T, of Fastusol Yellow 14L in group D sheets.

(B) Calculated quantum efficiency  $Q(\lambda)$  at several concentration versus wavelength.

In Figure 5.20 the apparent reflectance factor  $R'(\lambda|D_{65})$  measured with Minolta CM-3700d of Fastusol Yellow 14L in group D sheets are shown at various concentrations versus wavelength. In subfigure (B) the modelled  $R'(\lambda|D_{65})$  are shown at the same concentrations. As can be seen, that goodness of the model is not great, the root-mean-square residual being 0.0165 over wavelength band of 500-630 nm.

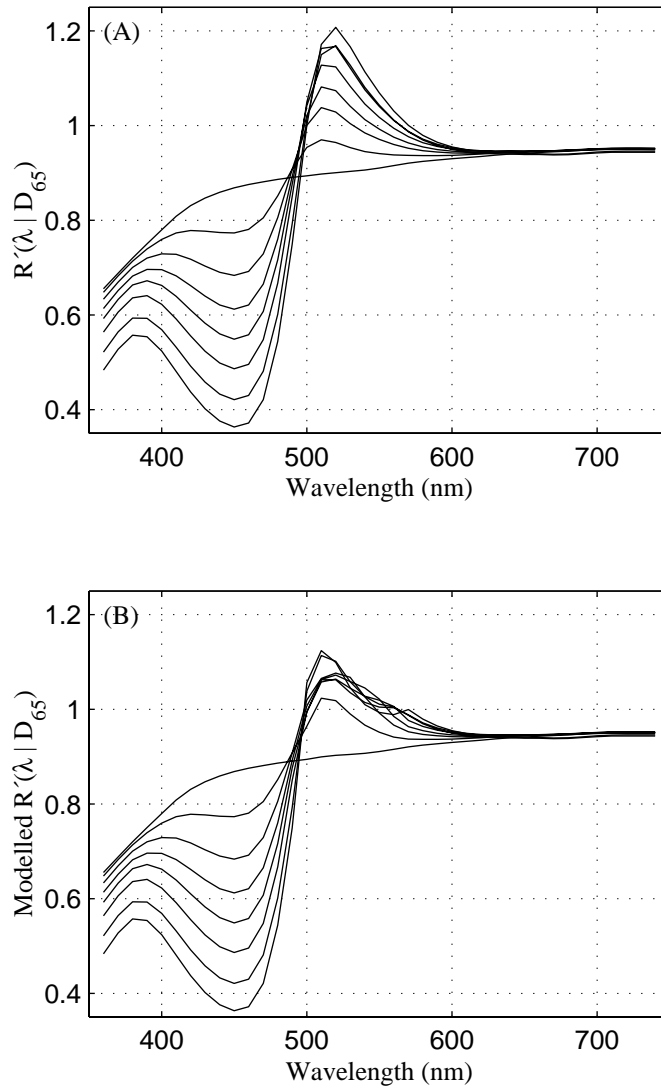


Figure 5.20: (A) Apparent reflectance factors  $R'(\lambda|D_{65})$  measured with Minolta CM-3700d of Fastusol Yellow 14L in group D sheets at various concentrations versus wavelength. (B) Modelled apparent reflectance factors  $R'(\lambda|D_{65})$  at the same concentrations as in (A).

### 5.5.2 Extended Kubelka-Munk Model for Fluorescence, Monochromatic Illumination

The extended Kubelka-Munk model for fluorescence using monochromatic illumination developed by the current author is based on the following assumptions:

- Fluorescence is isotropic
- The excitation and emission spectra of a fluorescent dye do not overlap (for mathematical convenience)
- The quantum yields of optically thick fluorescent samples do not depend on concentration, after the effects of aggregation are removed
- The emitted radiant flux  $M(\lambda|S(\zeta)d\zeta)d\lambda$  is dependent on the absorption and scattering coefficients at the excitation and emission wavelengths.

Equations 5.55 and 5.56 will now be solved for monochromatic illumination to be utilized with two-monochromator measurements.

By differentiating Equation 5.55, substituting right hand sides of Equation 5.55 and 5.56 to it, one obtains:

$$\frac{d^2\Phi_z^+(\lambda)}{dz^2} = B(\lambda)^2 \Phi_z^+(\lambda) - \frac{2S(\lambda) + K(\lambda) + B(\lambda)}{2} W(\zeta, \lambda) \quad (5.60)$$

where

$$W(\zeta, \lambda) = \int_{\zeta < \lambda} K_F(\zeta) \left( 2 + \frac{K(\zeta)}{S(\zeta)} - \frac{B(\zeta)}{S(\zeta)} \right) Q(\zeta, \lambda) \Phi_0^+(\zeta) \exp^{-zB(\zeta)} d\zeta \quad (5.61)$$

This differential equation has a solution:

$$\Phi_z^+(\lambda) = \frac{(2S(\lambda) + K(\lambda) + B(\lambda)) W(\zeta, \lambda)}{2(B(\zeta)^2 - B(\lambda)^2)} \left( \exp^{-zB(\lambda)} - \exp^{-zB(\zeta)} \right) \quad (5.62)$$

By differentiating this, requiring that  $B(\lambda) \neq B(\zeta)$ , and substituting back to Equation 5.55 and assuming the illumination is monochromatic, the amount of radiance  $\Phi_z^-(\lambda)$  travelling towards the illuminated surface is hence:

$$\begin{aligned} \Phi_z^-(\lambda) = & -\frac{K_F(\zeta)Q(\zeta, \lambda)}{2S(\lambda)} \left( 2 + \frac{K(\zeta)}{S(\zeta)} - \frac{B(\zeta)}{S(\zeta)} \right) \Phi_0^+(\zeta) \exp^{-zB(\zeta)} + \\ & \left( \left( 1 + \frac{K(\lambda)}{S(\lambda)} - \frac{B(\lambda)}{S(\lambda)} \right) \exp^{-zB(\lambda)} - \left( 1 + \frac{K(\lambda)}{S(\lambda)} - \frac{B(\zeta)}{S(\lambda)} \right) \exp^{-zB(\zeta)} \right) * \\ & \frac{(2S(\lambda) + K(\lambda) + B(\lambda)) W(\zeta, \lambda) \Phi_0^+(\lambda)}{2(B(\zeta)^2 - B(\lambda)^2)} \quad (5.63) \end{aligned}$$

This can be further reorganized and by setting  $z = 0$  the amount of fluorescent radiance at the surface is hence:

$$\Phi_0^-(\lambda) = \Phi_0^+(\zeta) \frac{K_F(\zeta)Q(\zeta, \lambda)}{2(B(\zeta) + B(\lambda))} \left(2 + \frac{K(\zeta)}{S(\zeta)} - \frac{B(\zeta)}{S(\zeta)}\right) \left(2 + \frac{K(\lambda)}{S(\lambda)} - \frac{B(\lambda)}{S(\lambda)}\right) \quad (5.64)$$

Taking account the definition of radiance transfer factor, the radiance transfer factor for emission band of fluorescence  $\lambda > \zeta$  is hence:

$$\frac{\Phi_0^-(\lambda)}{\Phi_0^+(\zeta)} = \frac{K_F(\zeta)Q(\zeta, \lambda)}{2(B(\zeta) + B(\lambda))} \left(2 + \frac{K(\zeta)}{S(\zeta)} - \frac{B(\zeta)}{S(\zeta)}\right) \left(2 + \frac{K(\lambda)}{S(\lambda)} - \frac{B(\lambda)}{S(\lambda)}\right) \quad (5.65)$$

where  $B(\zeta) = \sqrt{K(\zeta)^2 + 2K(\zeta)S(\zeta)}$  and  $B(\lambda) = \sqrt{K(\lambda)^2 + 2K(\lambda)S(\lambda)}$ .

Equation 5.65 is the main result. From this equation the  $Q(\zeta, \lambda)$  can be solved, and be estimated based on a set of colored handsheets, which are measured with a spectrofluorimeter producing measurement matrix of  $\mathbf{B}(\zeta, \lambda)$ . The undyed and dyed substrate's absorption and scattering coefficients can be calculated from diagonal values of radiance transfer factor,  $\mathbf{B}(\lambda, \lambda)$ . Due to limitations of the measurement band of spectrofluorimeter, results for part of the absorption band are shown in Figure 5.21. In subfigure (A) calculated quantum efficiency  $Q(\zeta, 430)$  at emission of 430 nm with excitations of 360 nm, 370 nm and 380 nm are shown versus dye-on-fiber, kg/T, of Tinopal ABP-X h.c in group D sheets. Taking into account the poor repeatability of the used spectrofluorimeter and only single measurement per concentration, the quantum efficiency  $Q(\zeta, 430)$  can not be said to depend on the amount of dye-on-fiber. In the model  $Q(\zeta, \lambda)$  values would be based on average values being  $Q(360, 430) = 0.095$ ,  $Q(370, 430) = 0.089$ ,  $Q(380, 430) = 0.087$  and similarly determined for the rest of the elements of  $Q(\zeta, \lambda)$ . Received results are in agreement with measurable location of maximum absorption at wavelength of 360 nm. In subfigure (B) is shown the total quantum efficiency calculated over the emission band with excitations of 360 nm, 370 nm and 380 nm. In these results no clear dependence on concentration can be perceived. In subfigures (C) and (D)  $Q(360, \lambda)$  and  $Q(380, \lambda)$  are shown at various concentration versus wavelength.

In Figure 5.22 modelled  $\mathbf{B}(370, \lambda)$  at various concentrations versus wavelength are shown in subfigure (A). As can be seen, the modelling error is within the repeatability of the BFC-450.

In Figure 5.23 calculated quantum efficiency  $Q(\zeta, 510)$  at emission of 510 nm with excitations of 440 nm, 450 nm and 460 nm versus dye-on-fiber, kg/T, of Fastusol Yellow 14L in group D sheets is shown in (A). Subfigure (B) contains calculated total quantum efficiency  $Q_T(\zeta)$  over the emission band with excitations of 440 nm, 450 nm and 460 nm versus dye-on-fiber, kg/T, and subfigures (C) and (D) show calculated  $Q(440, \lambda)$  and  $Q(460, \lambda)$  at several concentrations versus wavelength. As in the case of Tinopal ABP-X h.c, these results do not show any clear dependence of quantum efficiency on the amount of dye-on-fiber, when the poor repeatability of BFC-450 and only two measurements per concentration are taken into account.

Figure 5.24 shows the total radiance factors  $\beta_T(\lambda|D_{65})$  measured with BFC-450 of Fastusol Yellow 14L in group D sheets at various concentrations versus wavelength. In subfigure (B)

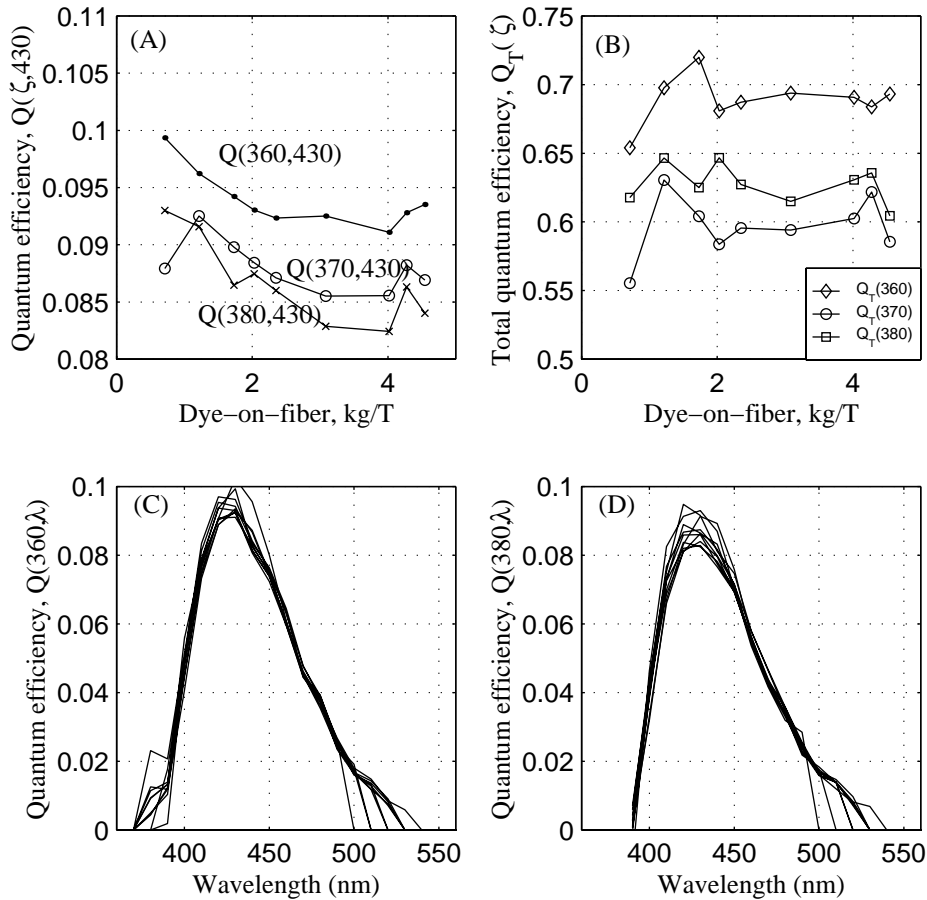


Figure 5.21: (A) Calculated quantum efficiency  $Q(\zeta, 430)$  at emission of 430 nm with excitations of 360 nm, 370 nm and 380 nm versus dye-on-fiber, kg/T, of Tinopal ABP-X h.c in group D sheets.

(B) Calculated total quantum efficiency  $Q_T(\zeta)$  over the emission band with excitations of 360 nm, 370 nm and 380 nm versus dye-on-fiber, kg/T.

(C) Calculated  $Q(360, \lambda)$  at several concentration versus wavelength.

(D) Calculated  $Q(380, \lambda)$  at several concentration versus wavelength.

the modelled  $\beta_T(\lambda|D_{65})$  at the same concentrations are shown. As can be seen, the fit is better than in Figure 5.20, and the rms residual of the model is now 0.0071 over wavelength band of 500-630 nm.

The total radiance factor estimate of a fluorescent dye at given dosage can now be calculated in various illumination conditions:

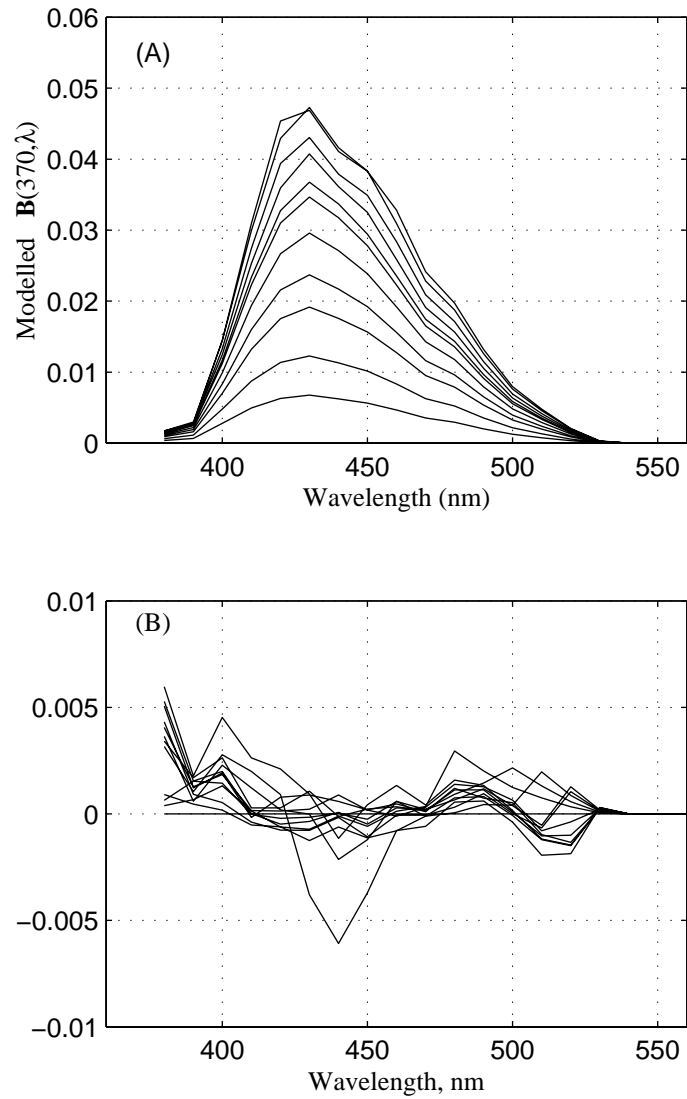


Figure 5.22: (A) Modelled  $B(370, \lambda)$  at various concentrations versus wavelength, compare with Figure 5.17.

(B) Error in modelled  $B(370, \lambda)$  versus measured ones at various concentrations.

$$\beta_T(\lambda|S) = \left(1 + \frac{K(\lambda)}{S(\lambda)} - \frac{B(\lambda)}{S(\lambda)}\right) + \frac{\sum_{\zeta_0}^{\zeta < \lambda} \frac{K_F(\zeta)Q(\zeta, \lambda)}{2(B(\zeta) + B(\lambda))} \left(2 + \frac{K(\zeta)}{S(\zeta)} - \frac{B(\zeta)}{S(\zeta)}\right) \left(2 + \frac{K(\lambda)}{S(\lambda)} - \frac{B(\lambda)}{S(\lambda)}\right) S(\zeta)\delta\zeta}{S(\lambda)\delta\lambda} \quad (5.66)$$

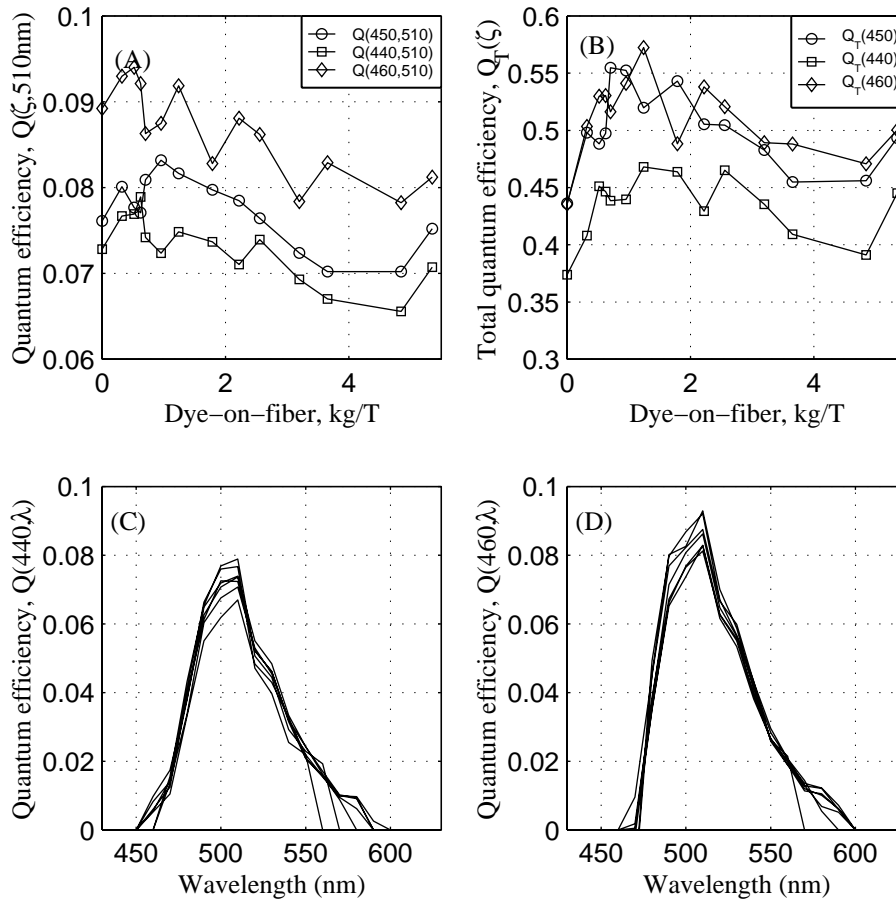


Figure 5.23: (A) Calculated quantum efficiency  $Q(\zeta, 510)$  at emission of 510 nm with excitations of 440 nm, 450 nm and 460 nm versus dye-on-fiber, kg/T, of Fastusol Yellow 14L in group D sheets.

(B) Calculated total quantum efficiency  $Q_T(\zeta)$  over the emission band with excitations of 440 nm, 450 nm and 460 nm versus dye-on-fiber, kg/T.

(C) Calculated  $Q(440, \lambda)$  at several concentration versus wavelength.

(D) Calculated  $Q(460, \lambda)$  at several concentration versus wavelength.

This method allows estimation of fluorescent emission at known process conditions combined with the traditional single constant Kubelka-Munk method in the absorption band of the fluorescent dyes. It thus gives a base for calculation of total radiance factors of a fluorescent dye in various illumination conditions, so that illuminator metamerism can be evaluated in advance or minimized through control.

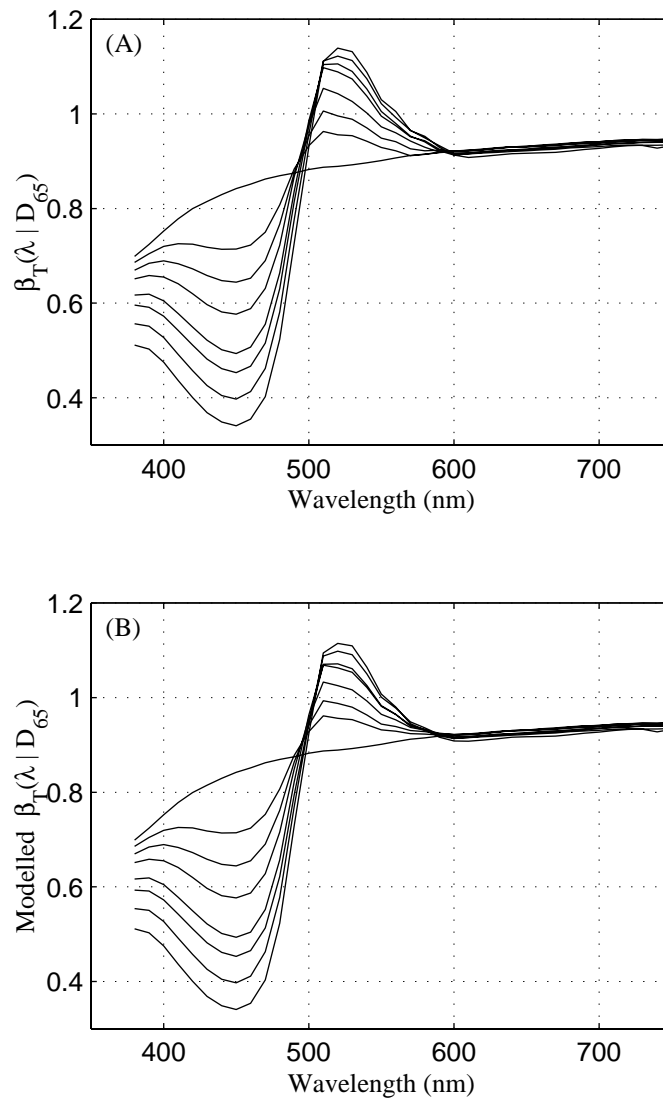


Figure 5.24: (A) Total radiance factors  $\beta_T(\lambda | D_{65})$  measured with BFC-450 of Fastusol Yellow 14L in group D sheets at various concentrations versus wavelength.

(B) Modelled total radiance factors  $\beta_T(\lambda | D_{65})$  at the same concentrations as in (A).

## 5.6 Absorption Band Broadening and Non-Linear Total Radiance Factor Model

Traditionally, the definition of wavelength dependent absorption coefficient  $\frac{\partial \frac{K(\lambda)}{S(\lambda)}}{\partial c} = a(\lambda)$  is based on reflectance factor measurement of stacked sheets at known concentrations of dye-on-fiber, containing no more information than is used in defining colorant response  $\frac{\partial \beta_T(\lambda|S)}{\partial c}$  in the optimizing color controller. The change in reflectance factor by increasing dye-on-fiber is a function of light absorption and scattering in the sheet by absorbing dye molecules. Thus it can be assumed that a model describing the probability of a photon to be absorbed within an optical path typical for the substrate by the adsorbed dye molecules, such as discussed in Section 5.4, could also be applied not only for changes effected in absorption coefficient by dyeing, but also for reflectance factor and total radiance factor at the absorption band of dyes and at the excitation band of fluorescent dyes.

In Equation 5.29 the reflectance factor  $R(\lambda)$  is defined as function of  $K(\lambda)$  and  $S(\lambda)$ . This relation can be expressed also in the form of binomial series, where  $p_0 = 0.5$  and for  $i \geq 1$ ,  $p_i = p_{i-1} \left( \frac{2i-1}{2i+2} \right)$ :

$$\begin{aligned} R(\lambda) &= 1 + \frac{K(\lambda)}{S(\lambda)} - \sqrt{\left( \frac{K(\lambda)}{S(\lambda)} + 1 \right)^2 - 1} \\ &= \sum_{i=0}^{\infty} p_i \left( \frac{S(\lambda)}{K(\lambda) + S(\lambda)} \right)^{2i+1} \end{aligned} \quad (5.67)$$

By differentiating Equation 5.67, one obtains:

$$\partial R(\lambda)_c = \sum_{i=0}^{\infty} p_i \left( \frac{S_c(\lambda)}{K_c(\lambda) + S_c(\lambda)} \right)^{2i} \frac{K_c(\lambda) \partial S_c(\lambda) - S_c(\lambda) \partial K_c(\lambda)}{(K_c(\lambda) + S_c(\lambda))^2} \quad (5.68)$$

The interest here is to apply derivatives of Equations 5.51 and 5.52 relative to  $f = \frac{q [D_{total}]_f}{1+q [D_{total}]_f}$ , which are:

$$\frac{\partial K_c(\lambda)}{\partial f} = K_{\infty}(\lambda) - K_s(\lambda) \quad (5.69)$$

$$\frac{\partial S_c(\lambda)}{\partial f} = S_{\infty}(\lambda) - S_s(\lambda) \quad (5.70)$$

By differentiating Equation 5.67 relative to  $f = \frac{q [D_{total}]_f}{1+q [D_{total}]_f}$ , one obtains:

$$\begin{aligned} \frac{\partial R(\lambda)_c}{\partial f} &= \sum_{i=0}^{\infty} p_i \left( \frac{S_c(\lambda)}{K_c(\lambda) + S_c(\lambda)} \right)^{2i} \\ &\quad \frac{K_c(\lambda) (S_{\infty}(\lambda) - S_s(\lambda)) - S_c(\lambda) (K_{\infty}(\lambda) - K_s(\lambda))}{(K_c(\lambda) + S_c(\lambda))^2} \end{aligned} \quad (5.71)$$

The binomial coefficients for the first three terms of  $p_i$  are  $\frac{1}{2}$ ,  $\frac{1}{8}$  and  $\frac{1}{16}$ . If only the first term is taken into account as first approximation, then the derivative simplifies to:

$$\frac{\partial R(\lambda)}{\partial f} = S_c(\lambda) \left( \frac{K_c(\lambda)S_\infty(\lambda) - S_c(\lambda)K_\infty(\lambda)}{2(K_c(\lambda) + S_c(\lambda))^3} + \frac{S_c(\lambda)K_s(\lambda) - K_c(\lambda)S_s(\lambda)}{2(K_c(\lambda) + S_c(\lambda))^3} \right) \quad (5.72)$$

Utilizing only the first term and differentiating it at  $f = 0$ , further on assuming  $K_s(\lambda)$  being small and thus can be ignored:

$$\begin{aligned} \left. \frac{\partial R(\lambda)_c}{\partial f} \right|_{f=0} &= S_s(\lambda) \left( \frac{K_s(\lambda)S_\infty(\lambda) - S_s(\lambda)K_\infty(\lambda)}{2(K_s(\lambda) + S_s(\lambda))^3} + \frac{K_s(\lambda)S_s(\lambda) - S_s(\lambda)K_s(\lambda)}{2(K_s(\lambda) + S_s(\lambda))^3} \right) \\ &\doteq \frac{-K_\infty(\lambda)}{2S_s(\lambda)} \end{aligned} \quad (5.73)$$

The reflectance factor model for the colored substrate can be modelled now as:

$$R(\lambda)_c = R(\lambda)_s + \frac{\partial R(\lambda)_c}{\partial f} \Delta f \quad (5.74)$$

Knowing that the substrate is uncolored and thus  $[D_{total}]_f = 0$ , assuming  $K_s(\lambda)$  is small, and assuming the first term can be doubled to model the rest of summations (note,  $\sum_{i=0}^{\infty} p_i = 2p_0$ ), the reflectance factor of colored substrate can be estimated to be:

$$\begin{aligned} R(\lambda)_c &= R(\lambda)_s + \left. \frac{\partial R(\lambda)_c}{\partial f} \right|_{f=0} f \\ &\doteq R(\lambda)_s - \frac{-K_\infty(\lambda)}{S_s(\lambda)} \frac{q [D_{total}]_f}{1 + q [D_{total}]_f} \end{aligned} \quad (5.75)$$

As can be seen, the reflectance factor of the colored substrate caused by increasing concentration of dye-on-fiber is function of the absorption coefficient. The term  $\frac{-K_\infty(\lambda)}{S_s(\lambda)}$  can be conceived as change in the reflectance factors.

Thus one can write, as a first approximation:

$$R(\lambda)_c = R(\lambda)_s + R(\lambda)_1 \frac{q [D_{total}]_f}{1 + q [D_{total}]_f} \quad (5.76)$$

where  $R(\lambda)_s$  is reflectance factor of the undyed substrate,  $R(\lambda)_1 = R(\lambda)_\infty - R(\lambda)_s$ , where  $R(\lambda)_\infty$  describes the reflectance of the colored substrate at the adsorption maximum,  $[D_{total}]_f$  is the concentration of dye-on-fiber, and  $q$  is the probability constant of the photon absorption process.

The reasons for the absorption band broadening and basis for modelling it were discussed in Section 5.4. Thus the absorption band broadening typical for anionic direct dyes can be taken into account as:

$$R(\lambda)_c = R(\lambda)_s + R(\lambda)_1 \frac{q [D_{total}]_f}{1 + q [D_{total}]_f} + R(\lambda)_2 \frac{p [D_{super}]_f}{1 + p [D_{super}]_f} \quad (5.77)$$

where  $R(\lambda)_2 = R(\lambda)_{\infty,a} - R(\lambda)_s$  and  $R(\lambda)_{\infty,a}$  models the absorption band broadening effect to the reflectance factor at the described adsorption maximum, and  $p$  is the probability constant of a photon to be absorbed by the dye molecules in the superlayer  $[D_{super}]_f$ .

In Figure 5.25 the measured and modelled (solid line)  $R(\lambda)$  of the group D sheets dyed with Pergasol Yellow RN Powder based on a model given in Equation 5.77 are shown in subfigure (A). Subfigure (B) contains  $R(\lambda)_s$  and modelled  $R(\lambda)_1$  and  $R(\lambda)_2$  for the model in (A), when  $q = 2.89$  and  $p = 6.17$ . The goodness of a fit as the root-mean-square residual over wavelength band 360-600 nm is 0.003.

Typical modelling error is similar to the observed color variability in the colored handsheets. The benefits of this model compared to absorption and scattering coefficient models are, that only reflectance factor measurements from stacked sheets are required, and colorings at about four dosage levels including undyed sheet are sufficient to characterize coloring for each main furnish type. Also the error minimizing optimization is simple and converges quickly.

A similar derivation most likely can be done also for extended two-flux model with fluorescence to obtain total radiance factor model, which is left here for further research. A model for fluorescent dyes including FBAs in their excitation band would be based on the reflectance factor model of non-fluorescent dyes, because the absorption of ultraviolet and visible light does not differ in respect to the mechanism of light absorption by colorants [Zol91, §2.3]. In the emission band of fluorescent dyes an illumination dependent term is needed. By knowing that  $\beta_T(\lambda|S) = R(\lambda) + \beta_L(\lambda|S)$ , and assuming that the quantum yield of optically thick fluorescent samples do not depend on the concentration, after the effects of aggregation are removed, a following model may be formed for the total radiance factor of the colored substrate:

$$\beta_T(\lambda|S)_c = R(\lambda)_s + R(\lambda)_1 \frac{q [D_{total}]_f}{1 + q [D_{total}]_f} + \beta_L(\lambda|S)_s + \beta_L(\lambda|S)_1 \frac{q [D_{total}]_f}{1 + q [D_{total}]_f} \quad (5.78)$$

where  $\beta_L(\lambda|S)_s$  is the luminescent radiance factor of the substrate, and  $\beta_L(\lambda|S)_1 = \beta_L(\lambda|S)_{\infty*} - \beta_L(\lambda|S)_s$ , where  $\beta_L(\lambda|S)_{\infty*}$  describes maximum luminescence at some high concentration (not necessarily at the adsorption maximum, if greening occurs). The probability constant  $q$  must be the same for both excitation and emission band, from the definition of the quantum yield. However, emission is dependent on the light absorption.

This is a useful model, when measurements of  $R(\lambda)$  and  $\beta_L(\lambda|S)$  are available at few concentrations and they can be used in the objective function to be minimized. However, in the case of spectrophotometric measurements only  $R'(\lambda|S)$  is available, which is an approximation of  $\beta_T(\lambda|S)$ . In this case a simpler model may be applied:

$$\beta_T(\lambda|S)_c = \beta_T(\lambda|S)_s + \beta_T(\lambda|S)_1 \frac{q [D_{total}]_f}{1 + q [D_{total}]_f} \quad (5.79)$$

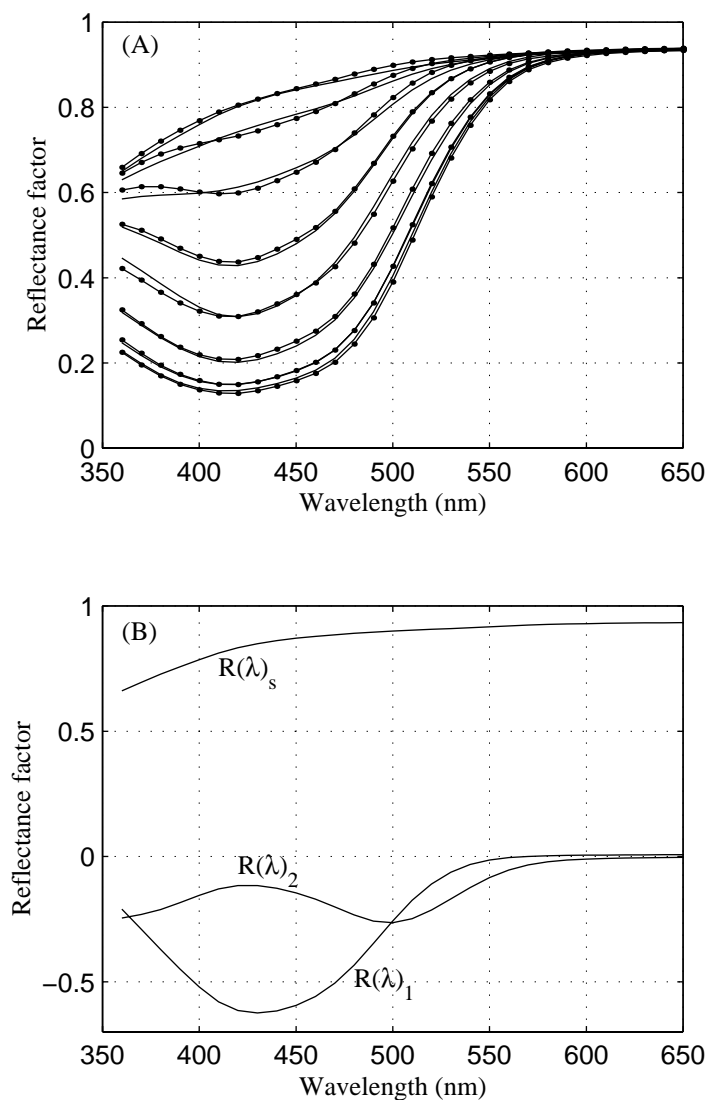


Figure 5.25: (A) Measured and modelled (solid line)  $R(\lambda)$  of the group D sheets dyed with Pergasol Yellow RN Powder based on a model given in Equation 5.77.

(B)  $R(\lambda)_s$ , and modelled  $R(\lambda)_1$  and  $R(\lambda)_2$ , when  $q = 2.89$  and  $p = 6.17$ .

where  $\beta_T(\lambda|S)_s$  is the total radiance factor of the substrate, and  $\beta_T(\lambda|S)_1 = \beta_T(\lambda|S)_{\infty*} - \beta_T(\lambda|S)_s$ , where  $\beta_T(\lambda|S)_{\infty*}$  describes maximum total radiance factor at some high concentration (not necessarily at the adsorption maximum, if greening exist).

This model may have more inaccuracy in the wavelength band, where both excitation and emission band of a fluorescent dye overlap, but contains the same benefits as the reflectance factor model. If absorption band broadening in the excitation band of the fluorescent dye and

greening effect is to be taken into account, then an additional term is required as in:

$$\beta_T(\lambda|S)_c = \beta_T(\lambda|S)_s + \beta_T(\lambda|S)_1 \frac{q [D_{total}]_f}{1 + q [D_{total}]_f} + \beta_T(\lambda|S)_2 \frac{p [D_{super}]_f}{1 + p [D_{super}]_f} \quad (5.80)$$

where  $\beta_T(\lambda|S)_2 = \beta_T(\lambda|S)_{\infty*,a} - \beta_T(\lambda|S)_s$  and where  $\beta_T(\lambda|S)_{\infty*,a}$  models both the absorption band broadening and the greening effect to the total radiance factor at some high concentration (not necessarily at the adsorption maximum, if greening occurs).

It is a good practice to define maximum dosage limits for fluorescent dyes for on-line color controllers to prevent possible over dosing, and thus greening.

In Figure 5.26 the measured and modelled (solid line)  $R'(\lambda|D_{65})$  of the group D sheets dyed with Tinopal ABP-X h.c based on Equation 5.79 are shown in subfigure (A). Subfigure (B) contains  $R'(\lambda|D_{65})_s$  and modelled  $R'(\lambda|D_{65})_1$ , when  $q = 0.232$ . The goodness of the model as root-mean-square residual over wavelength band 360-550 nm is 0.0019. Note, models in Figure 5.26 and 5.27 are based on an estimate of dye-on-fiber  $[D_{total}]_f$  defined at 370 nm, not at the wavelength of the absorption maximum of the FBA. For the same colorings the model based on Equation 5.80 was defined and results are shown in Figure 5.27. Now subfigure (B) contains  $R'(\lambda|D_{65})_s$  and modelled  $R'(\lambda|D_{65})_1$  and  $R'(\lambda|D_{65})_2$ , when  $q = 0.425$  and  $p = 0.0984$ . The goodness of this model as root-mean-square residual over wavelength band 360-550 nm is 0.0018.

In Figure 5.28 the measured and modelled (solid line)  $R'(\lambda|D_{65})$  of the group D sheets dyed with Fastusol Yellow 14L Liquid based on Equation 5.79 are shown in subfigure (A). Subfigure (B) contains  $R'(\lambda|D_{65})_s$  and modelled  $R'(\lambda|D_{65})_1$ , when  $q = 0.677$ . The goodness of the model as root-mean-square residual over wavelength band 360-650 nm is 0.0115. For the same colorings the model based on Equation 5.80 was defined and results are shown in Figure 5.27. Now subfigure (B) contains  $R'(\lambda|D_{65})_s$  and modelled  $R'(\lambda|D_{65})_1$  and  $R'(\lambda|D_{65})_2$ , when  $q = 1.128$  and  $p = 0.228$ . The goodness of this model as root-mean-square residual over wavelength band 360-650 nm is 0.0038. As can be seen, the combined model taking account both absorption band broadening in the excitation band of the fluorescent dye and noticeable 'greening' effect utilizing the superlayer surface concentration gives a significantly better fit.

Typically, the modelling error is somewhat higher than the observed color variability in the colored handsheets, especially where absorption and emission band overlap. The benefits of this total radiance factor model is, that only total radiance factor or apparent reflectance factor measurements from stacked sheets are required. Also colorings at about four dosage levels including undyed sheet are sufficient to characterize coloring for each main furnish type. The major disadvantage is, that the model is dependent on the used illumination conditions.

The presented models for reflectance factor and total radiance factor are not affected by the error sensitivity existing in the Kubelka-Munk based models, discussed in Section 5.3. Thus they are more suitable to model coloring process at very low dye-on-fiber rate.

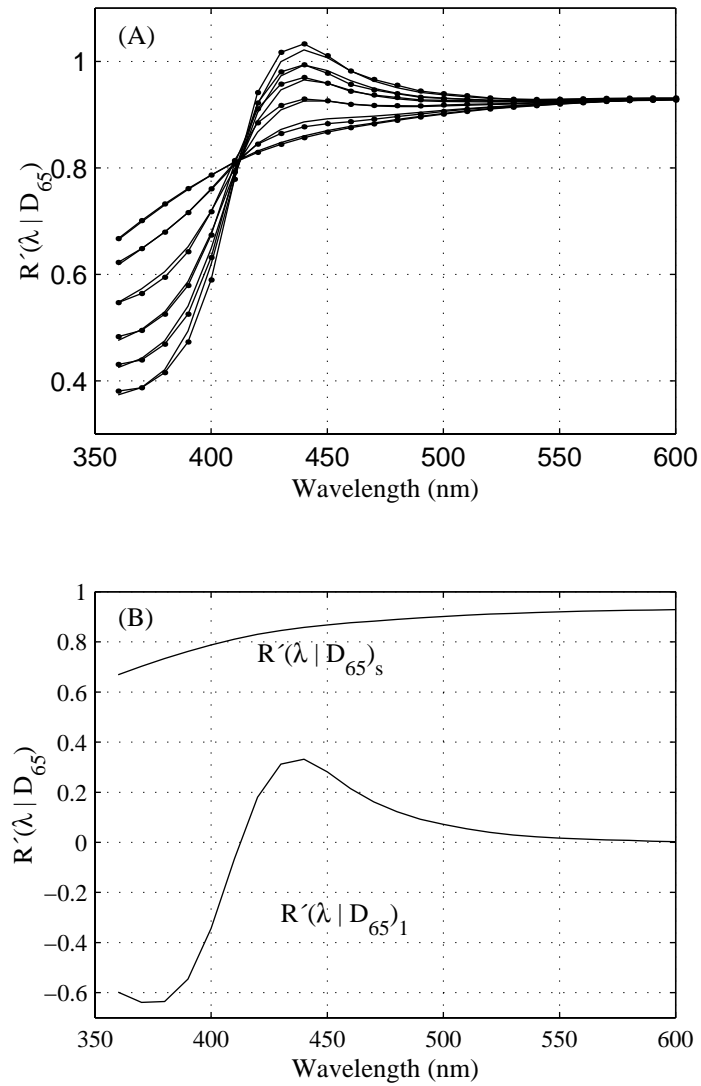


Figure 5.26: (A) Measured and modelled (solid line)  $R'(\lambda | D_{65})_s$  of the group D sheets dyed with Tinopal ABP-X h.c based on Equation 5.79.

(B)  $R'(\lambda | D_{65})_s$  and modelled  $R'(\lambda | D_{65})_1$  for the model in (A), when  $q = 0.232$ .

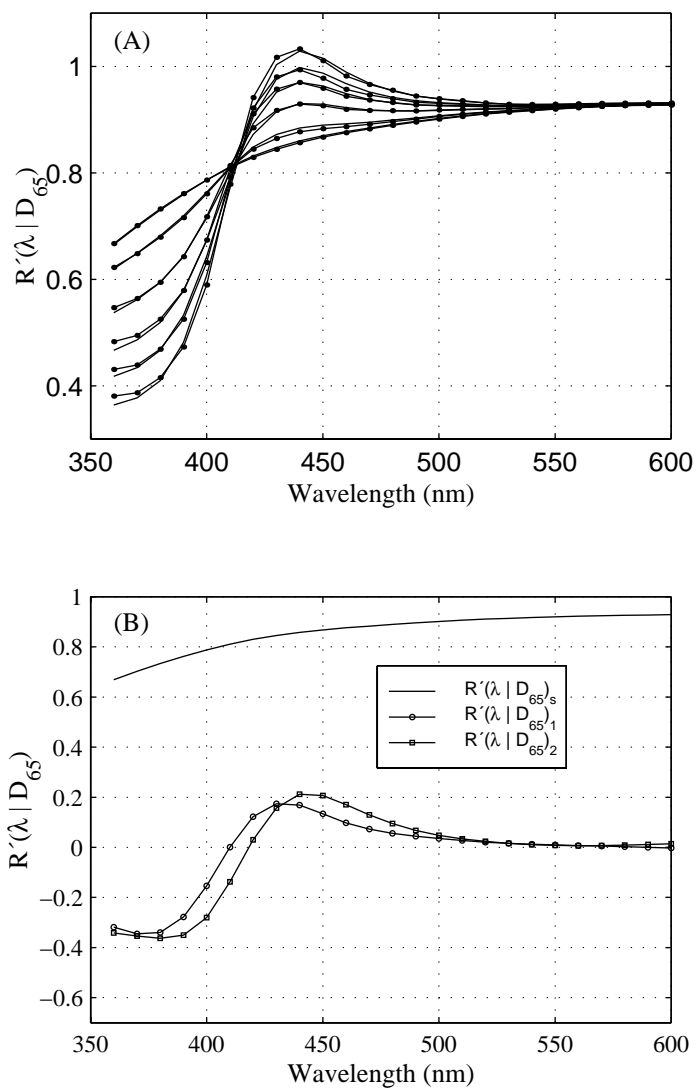


Figure 5.27: (A) Measured and modelled (solid line)  $R'(\lambda | D_{65})_s$  of the group D sheets dyed with Tinopal ABP-X h.c based on Equation 5.80.

(B)  $R'(\lambda | D_{65})_s$ , modelled  $R'(\lambda | D_{65})_1$  and  $R'(\lambda | D_{65})_2$  for the model in (A), when  $q = 0.425$  and  $p = 0.0984$ .

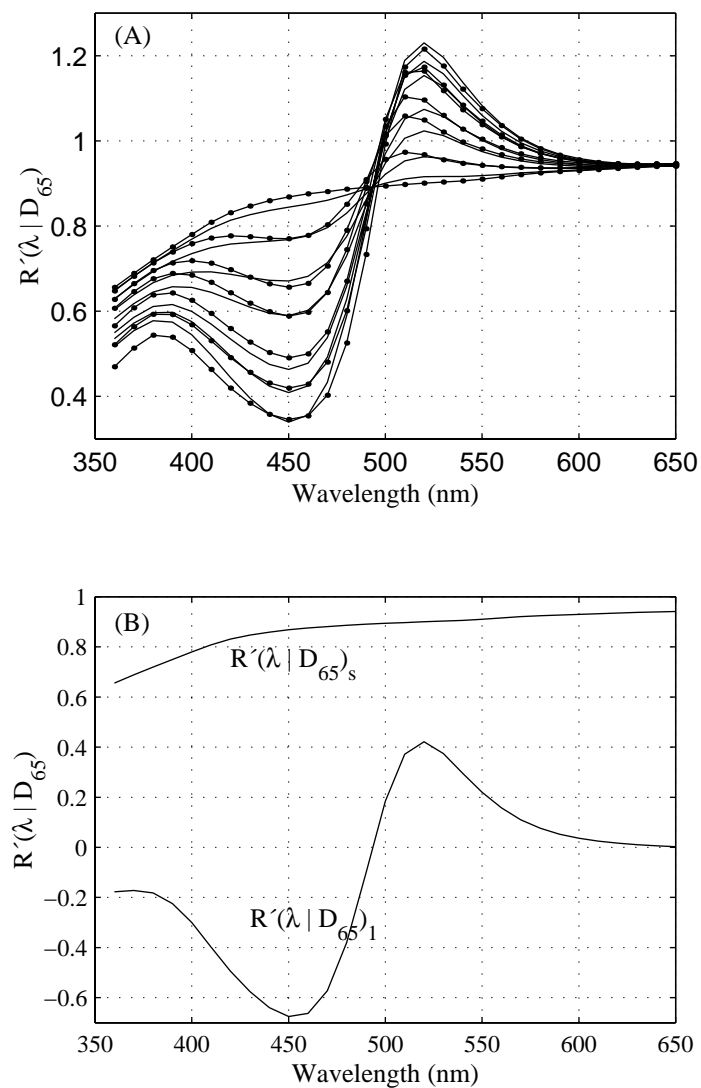


Figure 5.28: (A) Measured and modelled (solid line)  $R'(\lambda | D_{65})_s$  of the group D sheets dyed with Fastusol Yellow 14L Liquid based on Equation 5.79.

(B)  $R'(\lambda | D_{65})_s$  and modelled  $R'(\lambda | D_{65})_1$  for the model in (A), when  $q = 0.677$ .

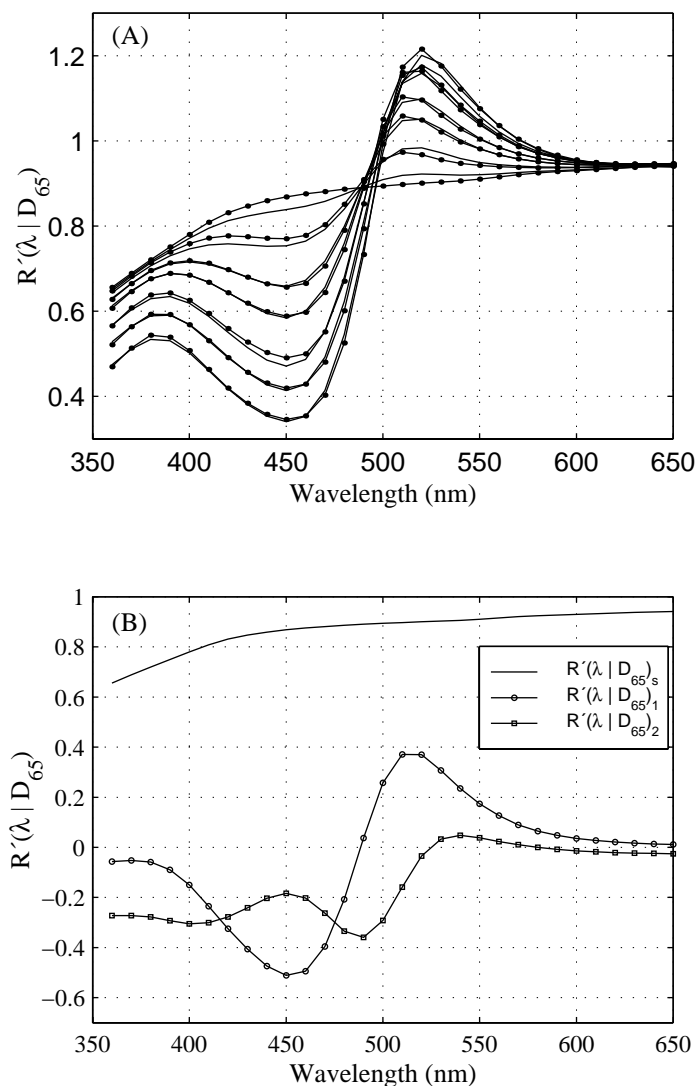


Figure 5.29: (A) Measured and modelled (solid line)  $R'(\lambda|D_{65})_s$  of the group D sheets dyed with Fastusol Yellow 14L Liquid based on Equation 5.80.

(B)  $R'(\lambda|D_{65})_s$ , modelled  $R'(\lambda|D_{65})_1$  and  $R'(\lambda|D_{65})_2$  for the model in (A), when  $q = 1.128$  and  $p = 0.228$ .

## 5.7 Colorant Responses

Color control algorithms based on reflectance factor colorant models require the use of  $\frac{\partial R(\lambda)}{\partial c}$  to minimize color error in color coordinates. As discussed in Section 5.2.1, the dye response used in the colorimetric colorant formulation is separated to the product  $\frac{\partial R(\lambda)}{\partial \frac{K(\lambda)}{S(\lambda)}} \frac{\partial \frac{K(\lambda)}{S(\lambda)}}{\partial c}$ . The value of  $\frac{\partial R(\lambda)}{\partial \frac{K(\lambda)}{S(\lambda)}}$  varies according to the magnitude of the reflectance factor and therefore applies only over a relatively small reflectance range as can be seen in Figure 5.30, leading  $\frac{\partial R(\lambda)}{\partial c} = \frac{2R(\lambda)^2}{R(\lambda)^2 - 1} a(\lambda)$  to be non-linear, while  $\frac{\partial \frac{K(\lambda)}{S(\lambda)}}{\partial c} = a(\lambda)$  is often linear over a wide range of concentrations. Thus the use of the colorimetric colorant formulation essentially nullifies the benefits of linearity in a single constant Kubelka-Munk colorant model.

In the optimizing color controller the colorant response  $\frac{\partial \beta_T(\lambda|S)}{\partial c} \simeq \frac{\Delta \beta_T(\lambda|S)}{\Delta c}$  is used directly, as discussed in Section 5.2.2.

Based on the developed reflectance factor model in Equation 5.77, its differential is:

$$\frac{\partial R(\lambda)_c}{\partial [D_{total}]_f} = R(\lambda)_1 \frac{q}{(1 + q [D_{total}]_f)^2} + R(\lambda)_2 \frac{p}{(1 + p [D_{super}]_f)^2} \frac{\partial [D_{super}]_f}{\partial [D_{total}]_f} \quad (5.81)$$

The first term in Equation 5.81 gives the differential for the reflectance factor model given in Equation 5.76. The same format also applies for the total radiance factor model given in Equation 5.80. The numerical derivative of these is used here. An analytic derivative is possible,

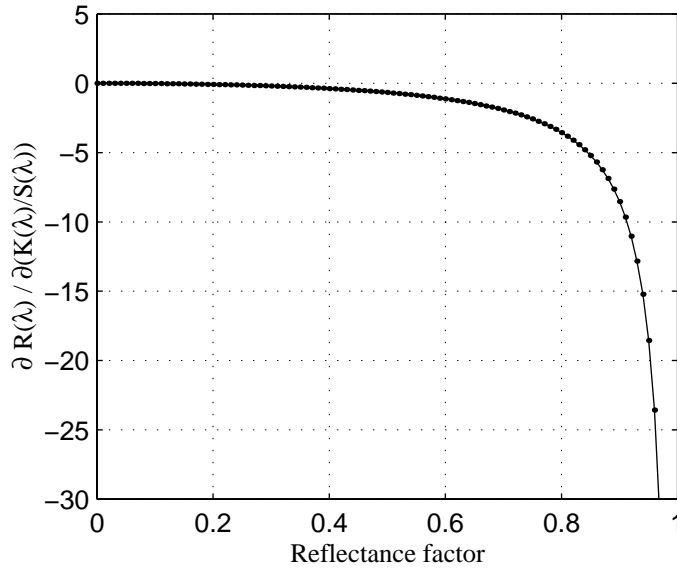


Figure 5.30:  $\frac{\partial R(\lambda)}{\partial \frac{K(\lambda)}{S(\lambda)}}$  as function of  $R(\lambda)$ .

but gives little benefit, and is left for the interested readers.

Figure 5.31 shows calculated  $\frac{\partial R(\lambda)}{\partial c}$  responses as given above at the wavelength of maximum absorption used in the colorimetric colorant formulation and in the optimizing color controller (solid line), based on the defined model for Pergasol Yellow RN Powder from the group D sheets, shown in Figure 5.25. The dye responses are equal at moderate dye dosage levels (1-4 kg/T), but the  $\frac{\partial R(\lambda)}{\partial \frac{K(\lambda)}{S(\lambda)}} \frac{\partial \frac{K(\lambda)}{S(\lambda)}}{\partial c}$  shows greater colorant response than the  $\frac{\partial R(\lambda)}{\partial c}$  at low dye dosage, and smaller one at high dosage. This smaller response of  $\frac{\partial R(\lambda)}{\partial \frac{K(\lambda)}{S(\lambda)}} \frac{\partial \frac{K(\lambda)}{S(\lambda)}}{\partial c}$  originates from  $\frac{K(\lambda)}{S(\lambda)}$  being insensitive when  $R(\lambda)$  approaches unity, as discussed in Section 5.3. This gave a first part of the answer for the question of reasons for better color control for brilliant white papers, when the optimizing color controller is applied. A second part of the answer is given from non-linearities in the colorant response models and color process uncertainties leading to a strong requirement for robustness and good constraint handling in the color control algorithm, especially for brilliant white and white shade paper grades.

As have been seen,  $\frac{\partial R(\lambda)}{\partial c}$  of the dyes is not linear relative to the colorant concentration on fiber. Based on this, linearity of the colorant model is not a requirement when a colorimetric matching algorithm utilizing a reflectance factor based colorant model is applied. Instead, the best colorant model should be used.

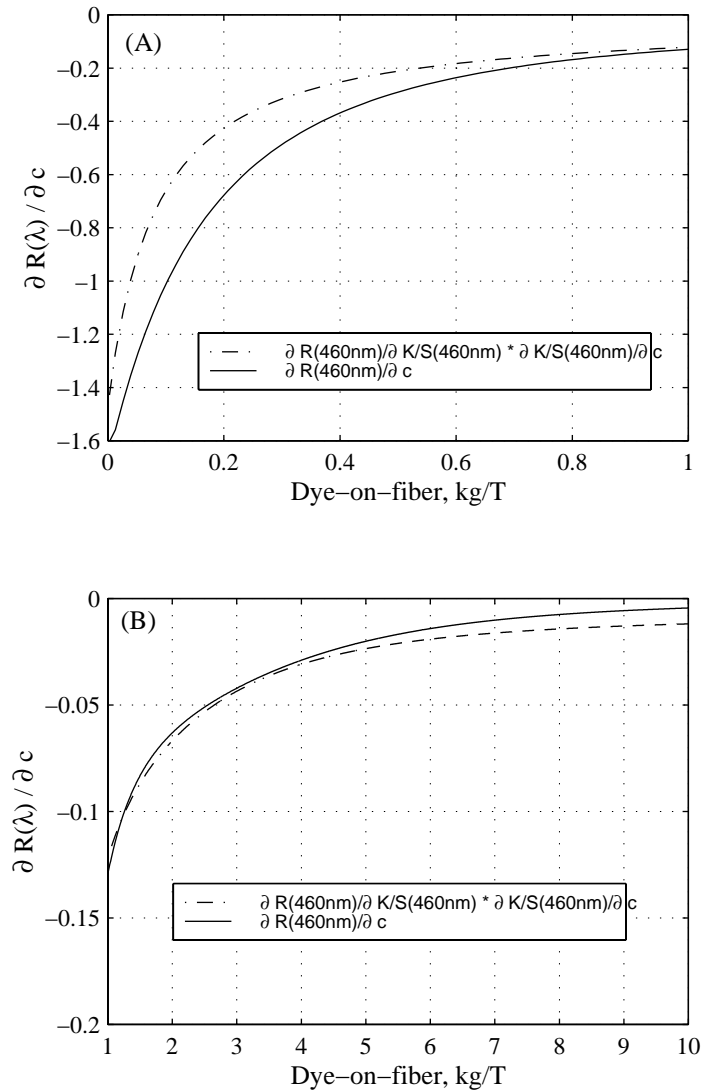


Figure 5.31: (A)-(B)  $\frac{\partial R(\lambda)}{\partial c}$  responses at the wavelength of maximum absorption, 460 nm, used in the colorimetric colorant formulation and in the optimizing color controller (solid line) are calculated based on the defined model in Figure 5.25 for Pergasol Yellow RN Powder from the group D sheets.

## Chapter 6

# Conclusions

The main intention of this research was to improve the colorant response model in the optimizing color controller. This meant a study of traditionally used models such as, a single constant Kubelka-Munk model, which ignores the fluorescence.

The linearity study of  $K(\lambda)$  and  $S(\lambda)$  of colored handsheets dyed with individual and mixtures of anionic direct dyes and FBAs showed, that neither of them is linear versus dye-on-fiber, which agrees with the fact, that the adsorption process of a colorant follows often Langmuir-type adsorption isotherm. However, under some conditions their ratio  $\frac{K(\lambda)}{S(\lambda)}$  is linear versus dye-on-fiber. This requires a relation to exist between affected change in scattering and absorption by the dyeing.

The knowledge of Langmuir-type adsorption isotherm process was utilized in the development of a model for  $K_c(\lambda)$  and  $S_c(\lambda)$  as a function of dye-on-fiber. Especially anionic direct dyes has great tendency to aggregate and interact, which leads to absorption band broadening. In this research, the surface concentration of superlayer absorbate was taken as a suitable proxy to measure the amount of adsorbed dye molecules which are interacting with other adsorbed dye molecules. A single constant Kubelka-Munk model does not address absorption band broadening, but only gives an average fit.

Based on the same knowledge of the adsorption isotherm process, a reflectance factor and total radiance factor model was also derived for non-fluorescent and fluorescent dyes. The latter gives an illuminant dependent model. Notwithstanding of their non-phenomenological base, these models give a simple and powerful tool for colorant modelling at a steady-state of stock coloring, where the optical properties of the produced paper from the used furnish cannot be measured prior to its coloring. Any colorant model would be only better or worse approximation at each process conditions.

To have a tool for illuminator metamerism minimization, which is important for the papermakers at high fluorescence levels, an extended single constant Kubelka-Munk model with fluorescence for monochromatic illumination based on radiance transfer factors utilizing a spectrofluorimeter was developed. Based on the model, total radiance factor at varying dosage levels

of fluorescent dyes and under several illumination conditions can be calculated. Thus, the best spectral colorimetric match under varying illumination conditions may be perceived.

The study of colorant responses showed, that there is not an argument why Kubelka-Munk based colorant models or colorant formulation should be preferred in the on-line paper coloring. Instead, the best colorant model should be used in the robust color control algorithm containing good constraint handling. Also an improvement would be received in pretuning of on-line color controls, when handsheets made for pretuning of a color control is made using the same colorant mixture as intended in final coloring, especially if the mill's furnish(es) is used.

#### **Further work and research**

One of the key further works is to improve the described model for the absorption band broadening and greening effect for fluorescent dyes and non-fluorescent dyes, and test it for on-line paper coloring.

In colorant modelling, statistically optimal methods of functional data analysis (such as principal component analysis and its extensions) should be used to provide the core information of the change of measured properties versus dye-on-fiber.

Fluorescent color measurement still requires research in both theoretical investigations and applying the theory in measurement instruments. Spectrofluorimeters intended for colorimetry are now commercially available, but the measured results are not at the level required in colorimetry. Especially, the measurement band must be extended to cover the excitation band of the fluors used in the paper and textile industries, in addition to the visual band.

Further development of illuminant independent models for emission of fluorescent dyes including FBAs in radiance transfer factor base, without including phenomenological models, based on stack sheet measurements should also be evaluated.

# Bibliography

- [AB77] D.H. Alman and F.W. Billmeyer, Jr. “New method for the colorimetric measurement of opaque fluorescent samples”. *Color Research and Application*, 2(1):19–25, 1977.
- [Alg87] M.J. Alguard. Color sensor. United States Patent 4,699,510, October 1987.
- [All73] E. Allen. “Separation of the spectral radiance factor curve of fluorescent substances into reflected and fluoresced components”. *Applied Optics*, 12(2):289–293, February 1973.
- [Asp97] J.R. Aspland. *Textile Dyeing and Coloration*. American Association of Textile Chemists and Colorists, Research Triangle Park, USA, 1997.
- [AST95a] ASTM. “E 1164 - 94, Standard practice for obtaining spectrophotometric data for object-color evaluation”. In *ASTM Standards on Color and Appearance Measurement*, pages 392–398. American Society for Testing and Materials, Philadelphia, 5<sup>th</sup> edition, 1995.
- [AST95b] ASTM. “E 284 - 95a, Standard terminology of appearance”. In *ASTM Standards on Color and Appearance Measurement*, pages 235–252. American Society for Testing and Materials, Philadelphia, 5<sup>th</sup> edition, 1995.
- [AST95c] ASTM. “E 308 - 95, Standard practice for computing the colors of objects by using the CIE system”. In *ASTM Standards on Color and Appearance Measurement*, pages 253–283. American Society for Testing and Materials, Philadelphia, 5<sup>th</sup> edition, 1995.
- [AST95d] ASTM. “E 991 - 90, Standard practice for color measurement of fluorescent specimens”. In *ASTM Standards on Color and Appearance Measurement*, pages 389–391. American Society for Testing and Materials, Philadelphia, 5<sup>th</sup> edition, 1995.
- [Bat97] D.R. Battle. “The measurement of colour”. In R. McDonald, editor, *Colour Physics for Industry*, chapter 2, pages 57–80. Society of Dyers and Colourists, Bradford, UK, 2<sup>nd</sup> edition, 1997.

- [BC80] F.W. Billmeyer, Jr. and T-F. Chong. "Calculation of the spectral radiance factors of luminescence samples". *Color Research and Application*, 5(3):156–168, 1980.
- [BD95] W.J. Bartz and M.E. Darroch. "Alkyl ketene dimer sizing reversion and efficiency in papers filled with calcium carbonate". In *Notes of 1995 TAPPI Dyes, Fillers & Pigments Short Course, 26-28 April, 1995, Chicago, USA*, pages 425–435. TAPPI, 1995.
- [Bel99] S. Bell. *A Beginner's Guide to Uncertainty of Measurement*. National Physical Laboratory, Teddington, UK, 1999.
- [BH98] C.F. Bohren and D.R. Huffman. *Absorption and Scattering of Light by Small Particles*. John Wiley, New York, 1983, Paperback 1998.
- [Bie96] C.J. Biermann. *Handbook of Pulping and Papermaking*. Academic Press, San Diego, USA, 2<sup>nd</sup> edition, 1996.
- [Bon86] J.S. Bonham. "Fluorescence and Kubelka-Munk theory". *Color Research and Application*, 11(3):223–230, 1986.
- [Boy96] R.M. Boynton. "History and current status of a physiologically based system of photometry and colorimetry". *Journal of the Optical Society of America*, 13(8):1609–1621, August 1996.
- [Bri99] J.A. Bristow. "ISO brightness – a more complete definition". *Tappi Journal*, 82(10):54–56, October 1999.
- [BS94] A. Berger-Schunn. *A Practical Color Measurement – A Primer for the Beginner – A Reminder for the Expert*. John Wiley, New York, 1994.
- [Bur89] B.C. Burdett. "Physical chemistry essential to dyeing theory". In A. Johnson, editor, *The Theory of Coloration of Textiles*, chapter 1, pages 1–96. Society of Dyers and Colourists, Bradford, UK, 2<sup>nd</sup> edition, 1989.
- [Bur95] J.A. Burt. "Factors that influence dyeing & colorant selection criteria". In *Notes of 1995 TAPPI Dyes, Fillers & Pigments Short Course, 26-28 April, 1995, Chicago, USA*, pages 283–289. TAPPI, 1995.
- [Car98] Ciba Consumer Care. Tinopal – The Absolute White, 1998.
- [CBD<sup>+</sup>97] E. Cleve, E. Bach, U. Denter, H. Duffner, and E. Schollmeyer. "New mathematical model for determining time-dependent adsorption and diffusion of dyes into fibers through dye sorption curves in combination shades. Part I: Mathematical fundamentals". *Textile Research Journal*, 67(10):701–706, 1997.

- [CD90] R. Cobden and R. Davenport. "Coloring and tinting of paper under neutral/alkaline conditions". In *Notes of 1990 TAPPI Neutral-Alkaline Papermaking Short Course, 16-18 October, 1990, Orlando, USA*, pages 113–118. TAPPI, 1990.
- [CG88] Ciba-Geigy. MC Seminar Davos 1988, 1988.
- [Che95] S-C. Chen. "Color control system for paper machines". In *Proceedings of TAPPI 1995 Process Control Conference, 1995, USA*, pages 3–9. TAPPI, 1995.
- [Cib94] Ciba. Pergasol liquid direct dyes. Technical Information Leaflet, 1994. Edition 1994.
- [CIE86] CIE. Publ. No 15.2, Colorimetry, 1986. 2<sup>nd</sup> edition.
- [CIE87] CIE. Publ. No 17.4, International lighting vocabulary, 1987. 3<sup>rd</sup> edition.
- [CIE90] CIE. Publ. No 76, Intercomparison on measurement of (total) spectral radiance factor of luminescent specimens, 1988, reprint 1990.
- [CIE95] CIE. Publ. No 116-95, Industrial colour difference evaluation, 1995.
- [Cla97] Clariant. Cartasol blue 3RF liquid. Technical Information Leaflet, 1997. PA.100.E16.97.
- [CMS96] S-C. Chen, T. Murphy, and R. Subbarayan. "A color measurement and control system for paper-making processes". In *Proceedings of the 1996 IEEE International Conference on Control Applications, 15-18 September, 1996, Dearborn, USA*, pages 136–142. IEEE, 1996.
- [Dea79] J.A. Dean, editor. *Lange's Handbook of Chemistry*. McCraw-Hill, New York, 12<sup>th</sup> edition, 1979.
- [Do98] D.D. Do. *Adsorption Analysis: Equilibria and Kinetics*, volume 2 of *Chemical Engineering*. Imperial College Press, 1998.
- [DS89] D.G. Duff and R.S. Sinclar. *Giles's Laboratory Course in Dyeing*. Society of Dyers and Colourists, 4<sup>th</sup> edition, 1989.
- [Foo39] W.J. Foote. "An investigation of the fundamental scattering and absorption coefficients of dyed handsheets". *Technical Association Papers (TAPPI)*, XXII:397–404, 1939.
- [Fun80] R.A. Funk. *A New Method for Characterizing Fluorescent Colorants for Match Prediction*. Dissertation for doctor of philosophy, Graduate School of Clemson University, May 1980.

- [FWK95] W. Falkenberg, E. Wenderoth, and S. Kleemann. "Aufziehverhalten von anionischen Direktfarbstoffen". *Wochenblatt für Papierfabrikation*, 123(23/24):1104–1111, 1995.
- [Gan77] E. Ganz. "Problems in fluorescence in colorant formulation". *Color Research and Application*, 2(2):81–84, 1977.
- [GC77] F. Grum and L. Costa. "Color evaluation by fluorescence measurement without the need for multiple illumination sources". *Tappi*, 60(8):119–121, August 1977.
- [Gil89] C.H. Giles. "Dye-fibre bonds and their investigation". In A. Johnson, editor, *The Theory of Coloration of Textiles*, chapter 2, pages 97–168. Society of Dyers and Colourists, Bradford, UK, 2<sup>nd</sup> edition, 1989.
- [Gru80] F. Grum. "Colorimetry of fluorescent materials". In F. Grum and C.J. Bartleson, editors, *Optical Radiation Measurement, Vol. 2 Color Measurement*, chapter 6, pages 235–288. Academic Press, New York, 1980.
- [GT94] D. Gundlach and H. Terstiege. "Problems in measurement of fluorescent materials". *Color Research and Application*, 19(6):427–436, 1994.
- [HH87] R.S. Hunter and R.W. Harold. *The Measurement of Appearance*. John Wiley, New York, 2<sup>rd</sup> edition, 1987.
- [Hin99] C. Hindley. Paper colouring. Private communication, September 1999. Ciba Specialty Chemicals UK, Consumer Care Chemicals.
- [HM98] Y.S. Ho and G. McKay. "Kinetic models for the sorption of dye from aqueous solution by wood". *Transactions of Institution of Chemical Engineers*, 76(Part B):183–191, May 1998.
- [Hof89] P.H. Hoffenberg. "A mathematical model and algorithm for commercial color matching software based on single-constant Kubelka-Munk theory". In *Proceeding of American Association of Textile Chemists and Colorists Annual Conference, 1989, Philadelphia, USA*, pages 208–217. AATCC, 1989.
- [IIKM97] K. Imura, K. Imai, T. Kawabata, and M. Makino. Measuring apparatus for measuring an optical property of a fluorescent sample. United States Patent 5,636,015, June 1997.
- [ISO98a] ISO. "2469:1994, Paper, board and pulps – Measurement of diffuse reflectance factor". In *ISO Standard Handbook – Paper, board and pulps*, pages 165–172. The International Organization for Standardization, Genève, 1998.
- [ISO98b] ISO. "2470:1977, Paper, board – Measurement of diffuse blue reflectance factor (ISO brightness)". In *ISO Standard Handbook – Paper, board and pulps*, pages 173–176. The International Organization for Standardization, Genève, 1998.

- [Jok98] O. Jokinen. FBA usage. Private communication, 21.9.1998. Ciba Specialty Chemicals Finland Oyj, Consumer Care Chemicals.
- [JW75] D.B. Judd and G. Wyszecki. *Color in Business, Science and Industry*. Wiley Series in Pure and Applied Optics. John Wiley & Sons, New York, USA, 3<sup>rd</sup> edition, 1975.
- [Kau57] W. Kauzmann. *Quantum Chemistry – An Introduction*. Academic Press, New York, 1957.
- [KJ97] A.A. Koukoulas and B.D. Jordan. “Effect of strong absorption on the Kubelka-Munk scattering coefficient”. *Journal of Pulp and Paper Science*, 23(5):J224–J232, May 1997.
- [KM31] P. Kubelka and F. Munk. “Ein Beitrag zur Optik der Farbanstriche”. *Zeitschrift für technische Physik*, 12(IIa):593–601, 1931.
- [Koo90] I.P.L. Kool. “Use of dyes in the production of paper”. In *Notes of 1990 TAPPI Dyes, Fillers & Pigments Short Course, 25-27 April, 1990, Atlanta, USA*, pages 13–18. TAPPI, 1990.
- [Kor69] G. Kortüm. *Reflectance Spectroscopy: Principles, Methods, Applications*. Springer-Verlag, Berlin-Heidelberg, 1969.
- [Kor00] A. Korhonen. An example of SPD of Xenon flash lamp, Hamamatsu L4633. Private communication, 09.03.2000. Hamatsu Photonics Norden AB, Sweden.
- [Kos97] H.J. Kostkowski. *Reliable Spectroradiometry*. Spectroradiometry Consulting, Maryland, USA, 1997.
- [KS91] I.P.L. Kool and E.L. Strom. “The causes and control of two-sidedness in a dyed paper sheet”. In *Proceedings of TAPPI 1991 Papermakers Conference, 8-10 April, 1991, Seattle, USA*, pages 85–91. TAPPI, 1991.
- [Kub48] P. Kubelka. “New contributions to the optics of intensely light-scattering materials: Part I”. *Journal of the Optical Society of America*, 38(5):448–457, May 1948.
- [Kue75] R.G. Kuehni. *Computer Colorant Formulation*. Lexington Books, D.C. Heath and Company, Lexington, USA, 1975.
- [Kwo90] R.A. Kwoka. “Strategies for cost effective optical performance”. In *Notes of 1990 TAPPI Dyes, Fillers & Pigments Short Course, 25-27 April, 1990, Atlanta, USA*, pages 21–29. TAPPI, 1990.
- [Lab96] Labsphere. Diffuse reflectance coatings and materials. Catalog, 962-7.5K, 1996.
- [Lab97] Labsphere. The BFC-450 Bispectral Fluorescence Colorimeter. Datasheet, 9712.5K, 1997.

- [Lat81] S. Latawiec. “The overlooked aspects of coloring the paper”. In *Preprints of the 67<sup>th</sup> Annual Meeting of the Technical Section of the CPPA, 29-30 January, 1981, Montreal, Canada*, volume A, pages A51–A54. Canadian Pulp and Paper Association, 1981.
- [Les97] M. Leskelä. *Simulation of Particle Packing for Modelling the Light Scattering Characteristics of Paper*. Dissertation for doctor of philosophy, Helsinki University of Technology, October 1997.
- [Lev72] O. Levenspiel. *Chemical Reaction Engineering*. John Wiley & Sons, New York, 2<sup>nd</sup> edition, 1972.
- [LH98] M.R. Luo and R.W.G. Hunt. “The structure of the CIE 1997 colour appearance model (CIECAM97s)”. *Color Research and Application*, 23(3):138–146, June 1998.
- [Lin92] T. Lindström. “Electrokinetics of the papermaking industry”. In J.C. Roberts, editor, *Paper Chemistry*, chapter 3, pages 25–43. Blackie Academic & Professional, Glasgow, 1991, reprint 1992.
- [LJA97] J. Leland, N. Johnson, and A. Arecchi. “Principles of bispectral fluorescence colorimetry”. In Angelo V. Arecchi, editor, *Photometric Engineering of Sources and Systems, 29-30 July 1997, San Diego, USA*, volume 3140, pages 76–87. The International Society for Optical Engineering (SPIE), July 1997.
- [LK95] C.G. Landes and L. Kroll. *Paper Coating Additives*. TAPPI Press, Atlanta, GA, 1995.
- [LL93] M. Leskelä and P. Luner. “Light scattering and relative bonded area: simulation of the effect of fiber collapse”. *Paperi ja Puu*, 75(8):601–605, 1993.
- [LOG65] R.B. Love, S. Oglesby, and I. Gailey. “The relation between dye concentration and reflectance – Amendments to the Kubelka-Munk equation”. *Journal of the Society of Dyers and Colourists*, 81:609–614, December 1965.
- [Mar98] R.T. Marcus. “The measurement of color”. In K. Nassau, editor, *Color for Science, Art and Technology*, chapter 2, pages 31–96. Elsevier, Amsterdam, 1998.
- [McC94] W.R. McCluney. *Introduction to Radiometry and Photometry*. Artech House, Norwood, USA, 1994.
- [McD97a] R. McDonald, editor. *Colour Physics for Industry*. Society of Dyers and Colourists, 2<sup>nd</sup> edition, 1997.
- [McD97b] R. McDonald. “Recipe prediction for textiles”. In R. McDonald, editor, *Colour Physics for Industry*, chapter 5, pages 209–291. Society of Dyers and Colourists, Bradford, UK, 2<sup>nd</sup> edition, 1997.

- [McK76] D.B. McKay. *Practical Recipe-Prediction Procedures Including the Use of Fluorescent Dyes*. Thesis for doctor of philosophy, University of Bradford, July 1976.
- [McK81] D. McKay. "Fluorescent recipe prediction theory". In *SDC Symposium, 1981, Nottingham*. Society of Dyers and Colourists, 1981.
- [McL86] K. McLaren. *The Colour Science of Dyes and Pigments*. Adam Hilger, Bristol, 2<sup>nd</sup> edition, 1986.
- [Mer90] A. Mercer. "Fluorescent brightening agents". In J. Shore, editor, *Colorants and Auxiliaries: Organic Chemistry and Application Properties*, volume 2 Auxiliaries, chapter 11, pages 470–511. Society of Dyers and Colourists, Bradford, 1990.
- [Mer94] *Merriam-Webster's Collegiate Dictionary*. Merriam-Webster, 4<sup>th</sup> edition, 1994.
- [Mie82a] K.D. Mielenz, editor. *Measurement of Photoluminescence*, volume 3 of *Optical Radiation Measurements*. Academic Press, 1982.
- [Mie82b] K.D. Mielenz. "Photoluminescence spectrometry". In K.D. Mielenz, editor, *Measurement of Photoluminescence*, volume 3 of *Optical Radiation Measurements*, chapter 1, pages 2–87. Academic Press, 1982.
- [Min95] Minolta. Spectrophotometer CM-3700d. Datasheet, 9242-4851-31, 1995.
- [MJA94] S.R. Middleton, Desmeules J., and Scallan A.M. "The Kubelka-Munk coefficients of fillers". *Journal of Pulp and Paper Science*, 20(8):J231–J235, 1994.
- [Mur92] S.G. Murray. "Dyes and fluorescent whitening agents for paper". In J.C. Roberts, editor, *Paper Chemistry*, chapter 9, pages 132–161. Blackie Academic & Professional, Glasgow, 1991, reprint 1992.
- [Nev95] P. Nevell. "Cellulose: structure, properties and behaviour in the dyeing process". In J. Shore, editor, *Cellulosics Dyeing*, chapter 1, pages 1–80. Society of Dyers and Colourists, Bradford, 1995.
- [NKP98] K. Niskanen, I. Kajanto, and P. Pakarinen. "Paper structure". In J. Gullichsen and H. Paulapuro, editors, *Paper Physics*, volume 16, chapter 1, pages 14–53. The Finnish Paper Engineer's Association and TAPPI, Helsinki, Finland, 1998.
- [Ole00] C. Oleari. "Spectral-reflectance-factor deconvolution and colorimetric calculations by local power expansion". *Color Research and Application*, 25(3):176–185, June 2000.
- [PC73] R.H. Perry and C.H. Chilton, editors. *Chemical Engineers Handbook*. McGraw-Hill, 5<sup>th</sup> edition, 1973.

- [Pue96] C. Puebla. "Predicting whiteness from first principles. A further step towards recipeing white paper". In *29<sup>th</sup> Pulp and Paper Annual Meeting, 4-8 November, 1996, Sao Paulo, Brazil*, pages 629–636. ABTCP, 1996.
- [Ran97] D.L. Randall. "Preparation and evaluation of calibration dyeings for computer color matching". In *Color Technology in the Textile Industry*, chapter 8, pages 72–77. American Association of Textile Chemists and Colorists, 2<sup>nd</sup> edition, 1997.
- [Ric88] D.C. Rich. "The effect of measuring geometry on computer color matching". *Color Research and Application*, 13(2):113–118, April 1988.
- [SB72] A.M. Scallan and J. Borch. "An interpretation of paper reflectance based upon morphology". *TAPPI*, 55(4):583–588, 1972.
- [Sch95] W. Schlenker. "Combination dyeing with anionic direct dyes". In *Proceedings of Tissue World 95 Conference, 14-16 March, 1995, Nice, France*, pages Session 6: Auxiliary components, 12pp. Pulp and Paper International, 1995.
- [Sch96] W. Schleinker. "Tinting white paper to achieve maximum whiteness". In B. Attwood, editor, *World Pulp & Paper Technology*, pages 39–40. Sterling Publications, 1996.
- [Sco96] W.E. Scott. *Principles of Wet End Chemistry*. TAPPI Press, Atlanta, USA, 2<sup>nd</sup> edition, 1996.
- [SDC96] *Colour Index International, CD-rom*. Society of Dyers and Colourists, Bradford, UK, 3<sup>rd</sup> edition, 1996.
- [Sha98] J. Shakespeare. "Tutorial: Fibre orientation angle profiles - process principles and cross-machine control". In *Proceedings of TAPPI 1998 Process Control, Electrical & Information Conference, 16-19 March, 1998, Vancouver, Canada*, pages 593–636. TAPPI, 1998.
- [Sha00] J. Shakespeare. Properties of dispersive element. Private communication, February 2000. Neles Paper Automation, Finland.
- [She99] R.P. Shead. "Next generation colour change control: its strategy and results". In *Proceedings of PITA Annual Conference – Engineering Solutions for Process Improvement, 14-16 September, 1999, Manchester, UK*, pages 29–36. PITA, 1999.
- [She00] R.P. Shead. "Next generation colour control: its strategy and results". In *Proceedings of Pulp and Paper 2000, 11-12 April, 2000, Czech Republic*, page 21pp., 2000.
- [Sho90] J. Shore, editor. *Colorants and Auxiliaries – Organic Chemistry and Application Properties*, volume 1 Colorants. Society of Dyers and Colourists, Bradford, 1990.

- [Sho95] J. Shore. "Dyeing with direct dyes". In J. Shore, editor, *Cellulosics Dyeing*, chapter 3, pages 152–188. Society of Dyers and Colourists, Bradford, 1995.
- [Shu79] J.B. Shumaker. "Deconvolution". In F.E. Nicodemus, editor, *Self-study manual on optical radiation measurements: Part 1 - Concepts*, NBS TN 910-4, chapter 8, pages 35–90. National Bureau of Standards, Washington, DC, 1979.
- [Sim72] F.T. Simon. "The two-mode method for measurement and formulation with fluorescent colorants". *Journal of Color & Appearance*, 1(4):5–11, 1972.
- [Sin97] R.S. Sinclair. "Light, light sources and light interactions". In R. McDonald, editor, *Colour Physics for Industry*, chapter 1, pages 1–56. Society of Dyers and Colourists, Bradford, UK, 2<sup>nd</sup> edition, 1997.
- [Smi97] K.J. Smith. "Colour-order systems, colour spaces, colour difference and colour scales". In R. McDonald, editor, *Colour Physics for Industry*, chapter 4, pages 121–208. Society of Dyers and Colourists, Bradford, UK, 2<sup>nd</sup> edition, 1997.
- [SS97] J. Shakespeare and T. Shakespeare. "An optimizing color controller". In *Proceedings of TAPPI 1997 Process Control, Electrical & Information Conference and ISA PUPID 37<sup>th</sup> Annual Symposium, 10-13 March, 1997, Birmingham, USA*, pages 127–135. TAPPI, 1997.
- [SS98a] J. Shakespeare and T. Shakespeare. "An optimizing color controller". *Tappi Journal*, 81(9):171–179, September 1998.
- [SS98b] T. Shakespeare and J. Shakespeare. "Advanced colour control through reflectance optimization". In *Proceedings of the 2<sup>nd</sup> Economy and Ecology in Papermaking Technology Conference, 1-5 June, 1998, Helsinki, Finland*, pages 183–194. KCL & PI, 1998.
- [SS99] T. Shakespeare and J. Shakespeare. "Problems in colour measurement of fluorescent paper grades". *Analytica Chimica Acta*, 380(2-3):227–242, 1999.
- [SSK99a] J. Shakespeare, T. Shakespeare, and A. Kaunonen. "Functional data analysis in paper machines, part 1 – theory". In *Proceedings of TAPPI 1999 International Engineering Conference, 12-16 September, 1999, Anaheim, USA*, pages 555–562. TAPPI, 1999.
- [SSK99b] J. Shakespeare, T. Shakespeare, and A. Kaunonen. "Functional data analysis in paper machines, part 2 – applications". In *Proceedings of TAPPI 1999 International Engineering Conference, 12-16 September, 1999, Anaheim, USA*, pages 563–569. TAPPI, 1999.
- [SSK99c] T. Shakespeare, J. Shakespeare, and A. Kaunonen. "Approaches in modelling the paper coloring process". In *Proceedings of TAPPI 1999 International Engineering Conference, 12-16 September, 1999, Anaheim, USA*, pages 525–534. TAPPI, 1999.

- [Ste69] E.I. Stearns. *The Practice of Absorption Spectrophotometry*. John Wiley, New York, 1969.
- [Sum89] H.H. Sumner. "Thermodynamics of dye sorption". In A. Johnson, editor, *The Theory of Coloration of Textiles*, chapter 4, pages 255–372. Society of Dyers and Colourists, Bradford, UK, 2<sup>nd</sup> edition, 1989.
- [Suz67] H. Suzuki. *Electronic Absorption Spectra and Geometry of Organic Molecules*. Academic Press, New York, 1967.
- [TAP98] TAPPI. "T 452-om 98, Brightness of pulp, paper and paperboard (Directional reflectance at 457 nm)". In *1998-1999 TAPPI Test Methods*. TAPPI, Atlanta, GA, 1998.
- [TK94] B.N. Taylor and C.E. Kuyatt. *Guidelines for Evaluating and Expressing the Uncertainty of NIST Measurement Results*. TN 1297. National Institute of Standards and Technology, Washington, 1994 edition, 1994.
- [TSS99] M. Toivonen, T. Shakespeare, and J. Shakespeare. "Optimal control of paper colour". In *Proceedings of PITA Annual Conference – Engineering Solutions for Process Improvement, 14-16 September, 1999, Manchester, UK*, pages 37–43. PITA, 1999.
- [Vaa99] J. Vaarasalo. Emission peak of a fluorescent sample. Private communication, November 1999. KCL, Finland.
- [VCO97] J.F. Verrill, P.J. Clarke, and J. O'Halloran. "Study of colorimetric errors on industrial instruments". In *Study of Improved Methods for Absolute Colorimetry*, volume 5<sup>th</sup> Report of *NPL Report COEM 2*. National Physical Laboratory, Middlesex, UK, 1997.
- [Völ95] H.G. Völz. *Industrial Color Testing: Fundamentals and Techniques*. Verlagsgesellschaft, Weinheim, Germany, 1995.
- [WS82] F. Wyszecki and W.S. Stiles. *Color Science: Concepts and Methods, Quantitative Data and Formulae*. John Wiley, New York, 2<sup>nd</sup> edition, 1982.
- [WW99] C.E. Wayne and R.P. Wayne. *Photochemistry*, volume 39 of *Oxford Chemistry Primers*. Oxford University Press, New York, 1996, reprinted with corrections 1999.
- [ZG95] J.C. Zwinkels and D.S. Gignac. "Development of a new reference spectrofluorimeter". In C. Burgess and D.G. Jones, editors, *Spectrophotometry, Luminescence and Colour; Science and Compliance*, volume 6 of *Analytical Spectroscopy Library*, pages 97–110. Elsevier, Amsterdam, 1995.
- [ZGN<sup>+</sup>97] J.C. Zwinkels, D.S. Gignac, M. Nevins, I. Powell, and A. Bewsher. "Design and testing of a two-monochromator reference spectrofluorimeter for high-accuracy total radiance factor measurements". *Applied Optics*, 36(4):892–902, February 1997.

- 
- [Zol91] H. Zollinger. *Color Chemistry – Syntheses, Properties and Applications of Organic Dyes and Pigments*. VCH, Weinheim, 2<sup>nd</sup> edition, 1991.
- [Zum98] S.S. Zumdahl. *Chemical Principles*. Houghton Mifflin, Boston, 3<sup>rd</sup> edition, 1998.
- [Zwi98] J.C. Zwinkels, editor. *Summary of 23 Lectures of Photometry, Radiometry and Colorimetry, 1-3 April, 1998, Ottawa*. National Research Council Canada, Ottawa, 1998.

281. Cameron, Frank, Low-order Runge-Kutta Methods for Differential-Algebraic Equations. 1999. 159 s.
282. Saarinen, Kari, On Filtering, Analysis, and Display of Digital Color and Radar Images. 1999. 190 s.
283. Gustafsson, Jouni, Electronics for Cyclotron Ion Beam Diagnostics and Control. 1999. 102 s.
284. Rusu, Corneliu, Several Approaches to Cost Function Adaptation and Phase Approximation. 2000. 179 s.
285. Koivisto, Pertti, Training-Based Design of Soft Morphological Filters: Methods and Criteria. 2000. 216 s.
286. Melnik, Vladimir, Nonlinear Locally Adaptive Techniques for Image Filtering and Restoration in Mixed Noise Environments. 2000. 234 s.
287. Alajääski, Jarkko, Tietokoneopetukseen liittyvän osaamisen ja vaikuttavuuden kehittyminen informaatioteknologiaan perustuvassa opetusympäristössä – opettajien itsearviointiin perustuva tutkimus Rauman normaalikoulussa. 2000. 187 s.
288. Öktem, Ruşen, Transform Domain Algorithms for Image Compression and Denoising. 2000. 142 s.
289. Hynynen, Ari, Yhdyskuntasuunnittelun paikallinen potentiaali. 2000. 169 s.
290. Saari, Seppo, Tuottavuuden mittaaminen osana kannattavuuden mittausta teollisuusyrityksessä: Mittausmenetelmien vertaileva tutkimus. 2000. 164 s.
291. Lappalainen, Markku, Strategic Development of Information Services in Building Product Export. 2000. 153 s.
292. Labounets-Rundblad, Ekaterina, Fast Fourier-Clifford Transforms Design and Applications in Invariant Image Recognition. 2000. 194 s.
293. Viljamaa, Pauli, Fuzzy Gain Scheduling and Tuning of Multivariable Fuzzy Control—Methods of Fuzzy Computing in Control Systems. 2000. 189 s.
294. Kolinummi, Pasi, Hardware Implementation and Applications of Scalable Parallel Computer. 2000. 250 s.
295. Salmela, Petri, Neural Networks in Speech Recognition. 2000. 254 s.
296. Kuulusa, Mika, DSP Processor Core-Based Wireless System Design. 2000. 156 s.
297. Peltonen, Sari, Output Distributional Influence Function. 2000. 125 s.
298. Laurila, Kari, Robust Speech Recognition Methods for Voice Dialing. 2000. 165 s.
299. Viik, Jari, Diagnostic Properties of Exercise Electrocardiographic Leads and Variables in the Detection of Coronary Artery Disease. 2000. 134 s.
300. Ahola, Erkki, Matrix Methods for Analysis and Grouping of Product or Concept Data. 2000. 130 s.
301. Shodjaeifar, Farnak, Preparation and Characterization of Zirconia Microfiltration Membranes. 2000. 172 s.
302. Laarne, Päivi, Implementation of a Realistic Conductivity Model for the Head. 2000. 109 s.
303. Wang, Haifeng, Advanced Multiuser Receiver for CDMA Communications. 2000. 140 s.
304. Shakespeare, Tarja, Colorant Modelling for On-Line Paper Coloring: Evaluations of Models and an Extension to Kubelka-Munk Model. 147 s. 2000.

**Tampereen teknillinen korkeakoulu**  
**PL 527**  
**33101 Tampere**

**Tampere University of Technology**  
**P. O. B. 527**  
**FIN-33101 Tampere Finland**

**ISBN 952-15-0474-9**  
**ISSN 0356-4940**